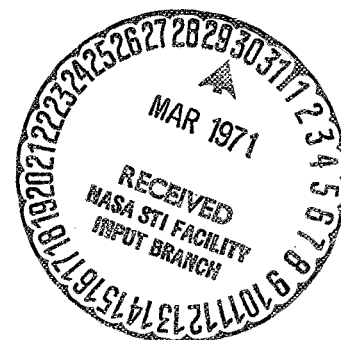*T-71-18734*

N71-20476

NASA CR-111822

CASE FILE COPY

ISOLATION CHARACTERISTICS OF

SPACE TELESCOPE SUSPENSION SYSTEMS

FEBRUARY 19, 1971

FINAL TECHNICAL REPORT

SPACE DIVISION ◆ **CHRYSLER CORPORATION**

ISOLATION CHARACTERISTICS OF SPACE TELESCOPE SUSPENSION SYSTEMS

By Vincent Spear, Norman Ockman and Roger Keefe

Distribution of this report is provided in the interest of information exchange. Responsibility for the contents resides in the author or organization that prepared it.

TABLE OF CONTENTS

SYMBOLS

a_1, a_2, a_3	outputs from accelerometers #1, #2 and #3 respectively. See Section 4.2.2.
A_n	height of the N'th peak of displacement or acceleration in a damped oscillatory response
c	distance measured parallel to the Y'-axis from the center of the air platform to its center of mass, meters. See Section 4.2.2.
D	gain of feedback amplifiers in magnetic suspension system
g	gravitational acceleration = 9.80 m/sec^2
I	moment of inertia, kg-m^2
I_b	moment of inertia of the air platform about its center of geometry.
I_o	moment of inertia of the air platform about its center of mass
J	instantaneous current through magnetic suspension coil, amperes
J_o	steady state current through magnetic suspension coil, amperes
K	spring constant, newtons/meter. (This parameter is also described in units of pounds/inch for identification of the different springs used in the test.)
K_r	radial spring constant at suspension point
K_t	tangential spring constant at suspension point
M	mass, kg
p	ratio of amplitides of successive peaks for an oscillatory waveform.
R	radius of the air platform. Approximately 44.5 cms.

T	period of oscillation, seconds
T_o	period of oscillation for zero damping
TR_x	ratio of platform displacement in the X-direction to shaker displacement
TR_θ	ratio of platform rotation to shaker displacement
W_1, W_2, W_3	arrangements of added weights. See Figure 3.4-1.
X, Y	rectangular Cartesian coordinates with axes set fixed to shaker frame. Shaker motion is along the X-axis.
X', Y'	rectangular Cartesian coordinates with axes set fixed to air platform. See Section 4.2.2.
x_b, y_b	coordinates of the geometric center of the platform in the X, Y system.
$\overline{X}'$, $\overline{Y}'$	coordinates of the platform center of mass in the X', Y' system.
X_I	shaker displacement, meters
X_{out}, Y_{out}, θ_{out}	platform displacements and rotation
$\ddot{X}_{IN}$	shaker acceleration, g's
$\ddot{X}_{out}$, $\ddot{Y}_{out}$, $\ddot{\theta}_{out}$	platform accelerations in translation and rotation
z	damping ratio,
β	damping constant, kg/sec
β_c	critical damping constant, kg/sec
γ	β/M , sec^{-1}
γ_c	β_c/M
δ	logarithmic decrement
μ	inertial X-coordinate of the platform center, meters
θ	rotational displacement of the air platform
ω	angular frequency, radians/second
ω_o	resonant angular frequency

1.0 ABSTRACT

Tests are performed to compare the isolation effectiveness of several candidate suspension systems for space telescopes. Spring, hysteresis, and magnetic systems are tested. A 250-kilogram air bearing platform, which simulates the telescope, is attached to a hydraulic shaker by means of the test suspension systems. The shaker arm is moved in a straight line in several disturbance modes, including sinusoidal, ramp and step functions, and the resultant acceleration and displacement of the air bearing are recorded. Sinusoidal frequencies from .01 to 1.0 Hz are used. The effective spring constants range from .175 to 8.76 newtons/meter.

All systems are tested to determine the effects of variations in platform moment of inertia and moment arm of the applied force.

The spring suspension system consists of four pairs of springs spaced equally around the platform. Acceleration transfer ratios (air-bearing acceleration/shaker acceleration) from .0001 to .001 are obtained at a driving frequency of 1 Hz. Resonance frequency for the system is approximately .01 to .03 Hz, dependent on the value of spring constant for the particular system.

A hysteresis damping suspension system with an effective spring constant equal to that of one of the spring suspension systems is tested to observe the effects of damping. For small amplitude disturbances the system performs as expected, with noticeable damping. However, at larger displacements, design problems in the instrument appear which preclude normal operation.

A passive magnetic suspension system of effective spring constant comparable to that of the other systems is tested. This system also has the capability for electronic damping. The system response is non-linear with the damping applied. Damping ratios analogous to those of a linear system are obtained which range in value in value from 0 to 0.1.

2.0 INTRODUCTION

One of the space scientific programs proposed for post-Apollo applications is the large orbital telescope, or space observatory. Such a space observatory will carry out observations much as its earth-based counterpart, but above the obscuration of the earth's atmosphere. The advantages of space astronomy - an increased spectral range and higher resolution - are so attractive that the eventual deployment of such an observatory is a virtual certainty.

However, to fully use the theoretical resolving power of a space telescope, perhaps as low as 0.01 arc-sec, the telescope must be stabilized in attitude to a corresponding precision. To achieve this level of stability, the physical disturbances transmitted to the telescope during operation must be very small. For an unmanned telescope in synchronous orbit this is no problem; the natural space environment is practically disturbance free and the control system can handle the small internal disturbances. But for a manned telescope, the disturbance environment caused by man's dynamic movements and increased spacecraft complexity creates a serious stabilization problem, even at synchronous orbit.

The key to meeting the precise stabilization requirements is to isolate the telescope from the disturbances created by the manned spacecraft to which it is attached.

The purpose of this study has been to perform comparative tests of three types of candidate suspension systems and to use the results of the tests to determine the characteristics and relative effectiveness of the systems.

The analytical and experimental work described in this report was sponsored by the Langley Research Center of the National Aeronautical and Space Administration under contract NAS1-9674.

2

3.0 TEST DESCRIPTION

3.1 MAJOR EQUIPMENT

The facility used to perform the tests consisting of the following major apparatus.

(1) A 35" diameter air bearing with self-contained air supply.

(2) A granite micro-flat table on which the air bearing moves essentially without friction.

(3) An independent simulated spacecraft structure mounted on slip tables and connected to a hydraulic shaker. The structure is also referred to in the report as the shaker frame.

(4) A hydraulic shaker which can be programmed to follow an electronic waveform with a frequency range from 0.01 Hz to 20 Hz.

(5) A Systron-Donner Model 80 analogue computer which was used for several different applications.
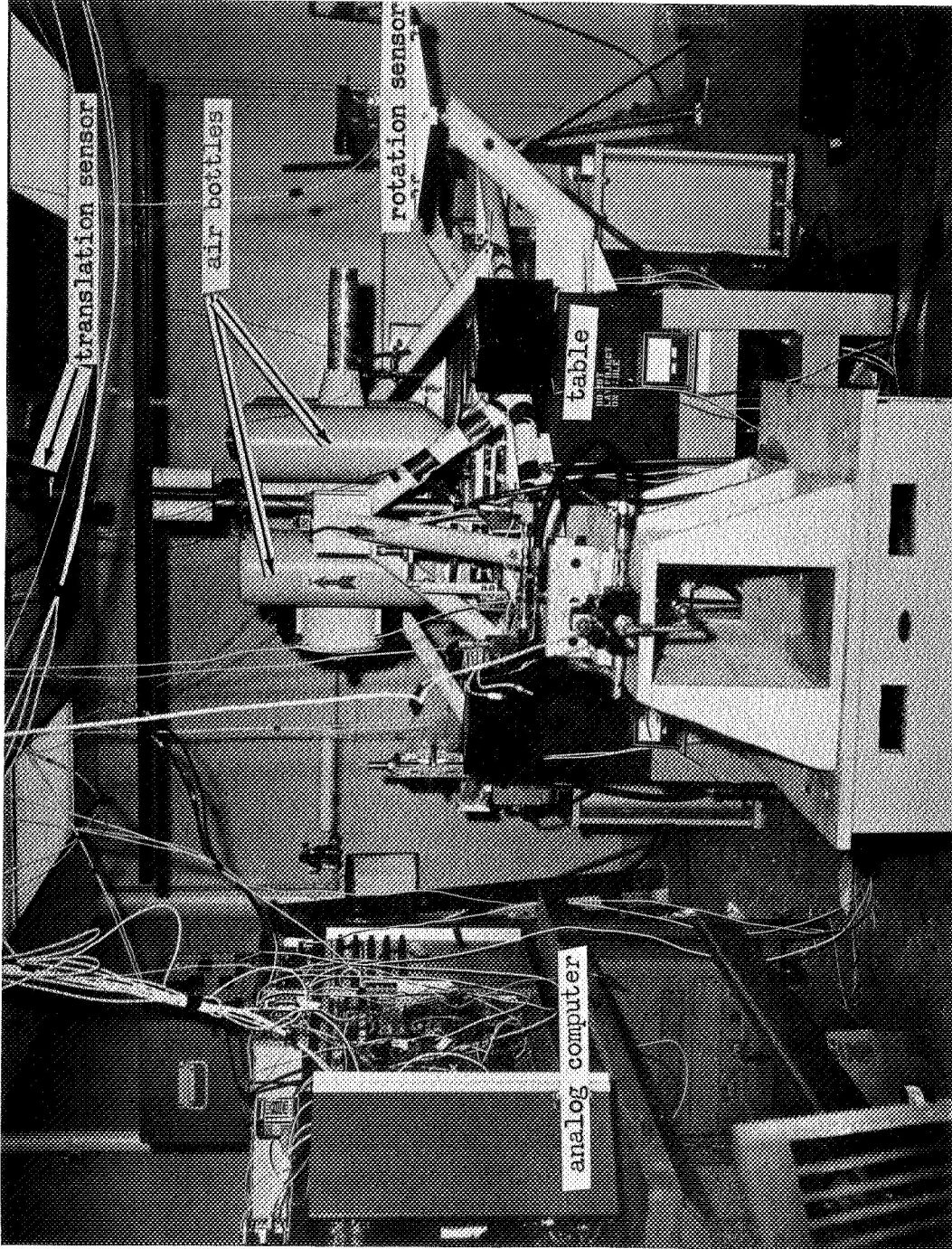
The entire facility is shown in Figure 3.1-1.

3

translation sensor

rotation sensor

air bottle

table

analog computer

Figure 3.1-1 Isolation Test Facility

4

3.2 INSTRUMENTATION

3.2.1 Location on platform.

The location of the sensors and accelerometers described in this section is shown in Figure 3.2-1. Figure 3.2-2 is a photograph of the three accelerometers, viewed toward the west. Accelerometer #2 is in the foreground, with #1 and #3 on the left and right-hand sides, respectively. The displacement sensors are shown in Figure 3.1-1.

3.2.2 Shaker Signal Circuit.

The electrical disturbance signals and zero position signals to the hydraulic shaker were fed into a servo amplifier (one of the amplifiers in the analog computer). This amplifier operated a solenoid valve in the hydraulic line of the shaker mechanism, so that the shaker responded to a signal applied to the servo amplifier.

The fidelity with which the shaker followed the electrical waveform was verified by applying square electrical impulses to the amplifier and recording the actual physical motion of the shaker. The rise times recorded from the shaker displacements were much shorter than the time constants of any of the accelerometer electronics or any time constant involved in the entire test. Therefore, the shaker movement is considered to be an exact reproduction of the electrical input signal.

Sine wave signals for the transfer function curves were obtained from a Hewlett Packard model 202A Low Frequency Function Generator. This instrument was the source of all sine and square wave disturbance inputs.

Step function inputs were obtained by simply switching a DC voltage across the input of the servo amplifier. No problems with contact bounce were observed.

Ramp functions were obtained from one of the integrating amplifiers of the analog computer.

A series of positive and negative going pulses was also used as a disturbance signal. The time line for these pulses is shown in Figure 3.2-3.

These pulses were obtained by switching two DC voltages (one for each pulse) into the servo amplifier by means of two relays. The signals to the relays were obtained from the digital section of the computer by using the digital clock and a number of gating and flip-flop circuits to trigger the relays. All step and pulse responses of the shaker were found to correspond exactly to the desired input signal. No significant edge trailing, nor rise times were seen.

3.2.3 Translation Sensor.

The position of the air bearing was measured by means of an optical system incorporating a United Detector Technology, SC/25 two axis position sensor. This solid state device produces two electrical signals proportional to the X and Y position of a light spot focused on the surface of the detector.
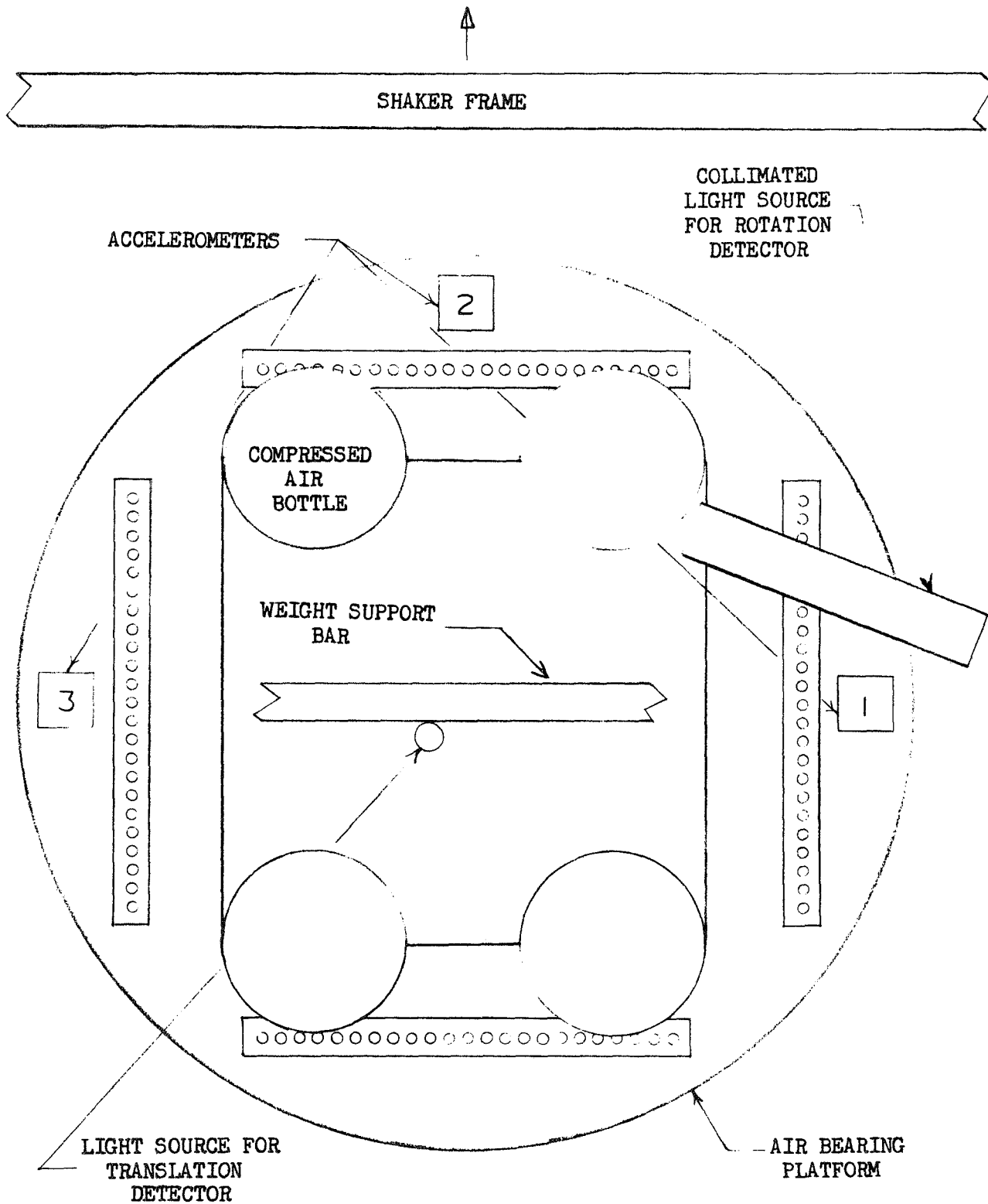
5

SHAKER FRAME

COLLIMATED
LIGHT SOURCE
FOR ROTATION
DETECTOR

ACCELEROMETERS

2

COMPRESSED
AIR
BOTTLE

WEIGHT SUPPORT
BAR

3

1

LIGHT SOURCE FOR
TRANSLATION
DETECTOR

AIR BEARING
PLATFORM

Figure 3.2-1 Diagram of air bearing platform

air bearing

accelerometer #2

shaker frame
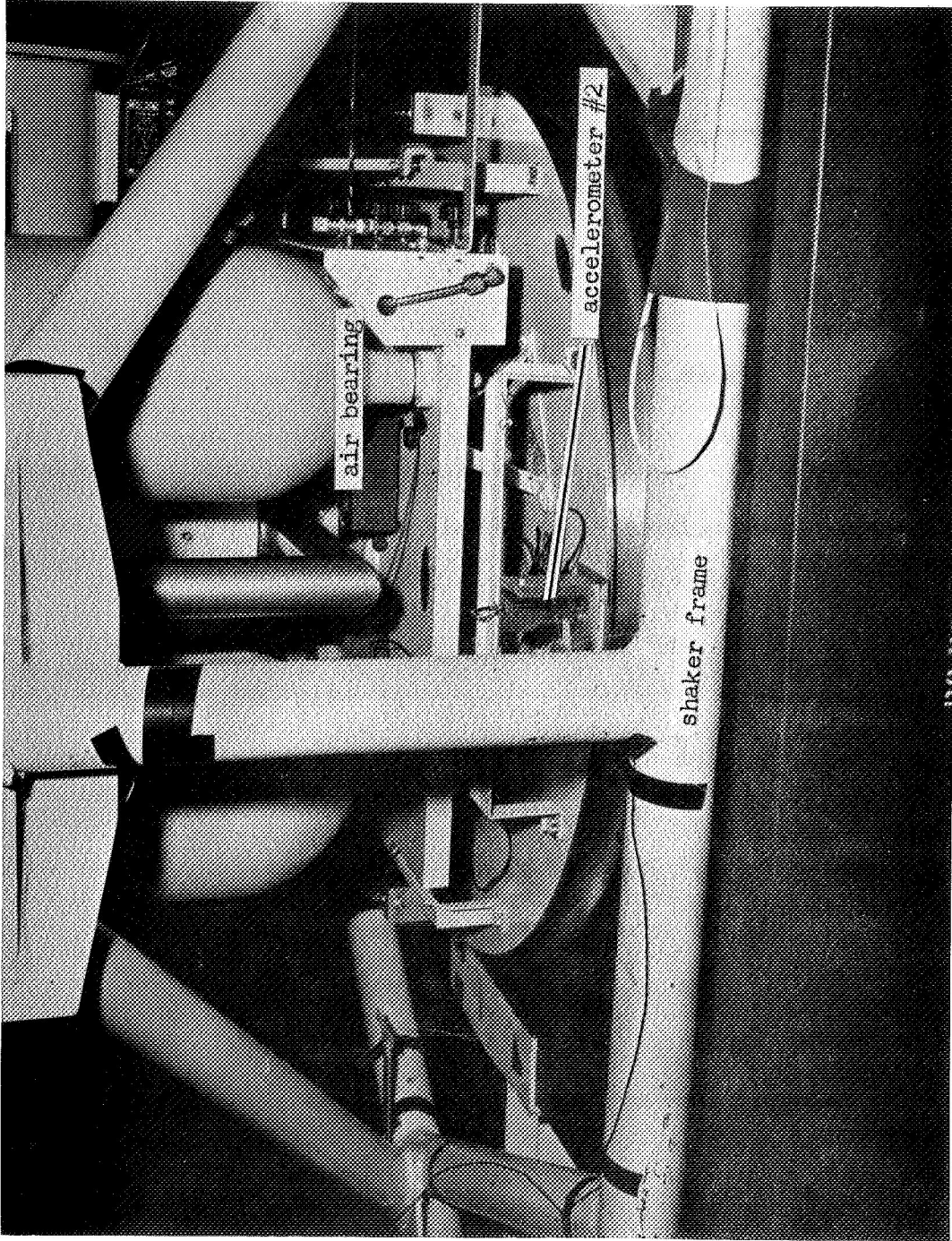
Figure 3.2-2, Air Bearing Viewed Toward the West

7

```
0.25 in.  ┐      ┌──┐                                                8.88    9.88
          │      │  │                                                 ┌────────────
          ├──────┘  └──────────────────────────────────────────────┐ │
          │.51    1.51              Time (seconds)                  │ │
-0.25 in. ┤                                                         └─┘
          │
```
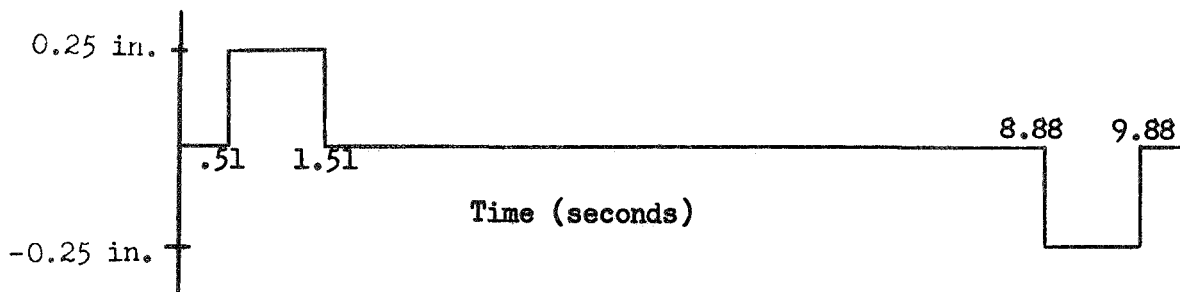
Figure 3.2-3   Pulse time line base

A lens was mounted in front of the detector and the combination mounted on the ceiling of the test cell. A small light source was mounted near the center of the air bearing to indicate the horizontal location of the bearing. By focusing this light on the detector surface, the translation of the bearing was presented on the detector, and electrical signals were obtained proportional to the X and Y positions of the bearing. These signals were amplified and fed into the Brown recorder.

Figures 3.2-4 and 3.2-5 show the translation detector system without the cardboard tube which enclosed the lamp and detector to minimize stray light effects.

The translation sensors were calibrated directly against platform motion each day, so that their accuracy was limited only by the accuracy with which the measuring scale and the Brown recorder scale could be read, or approximately 0.5 millimeters for translations of less than 1 centimeter, and up to 1.5 millimeter at full range of approximately 5 centimeters.

For relatively large displacements some cross talk was found between the X and Y channels, i.e., a large X displacement would produce a small signal in the Y channel. However, this was noted only for bearing displacements greater than a centimeter.

3.2.4   Rotation Sensor

Rotational position of the bearing was determined in a manner similar to that for the X and Y positions. A collimated light source was mounted on the

8

bearing. On the floor next to the bearing was mounted an optical telescope gunsight (Edmund Scientific No. 70,774) of approximately 5.375 inches focal length. A United Detector Technology (also Model SC/25) X-Y position detector was mounted in the focal plane of the gunsight.
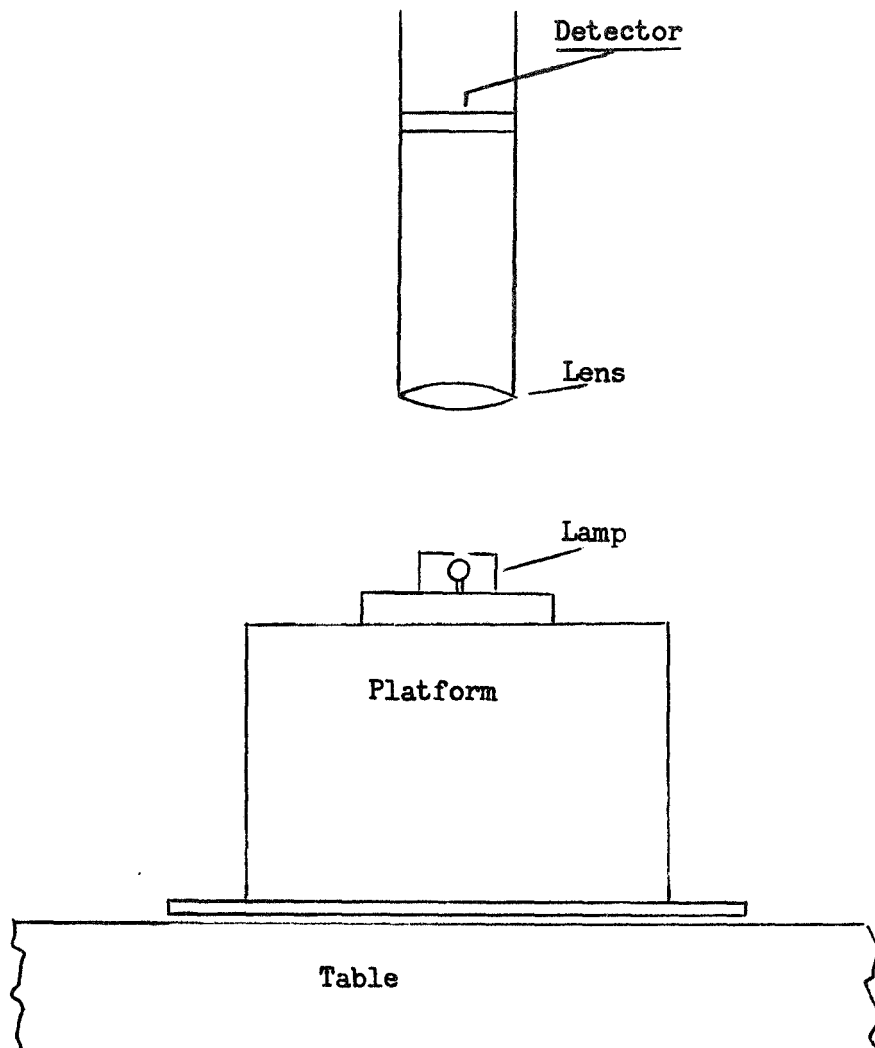

Figure 3.2-4 Translation sensor

Collimated light from the bearing was directed into the telescope. Rotation of the air bearing changed the incident angle of the collimated beam with respect to the axis of the gunsight, causing the spot at the focal plane to move across the detector and creating an electrical signal proportional to rotational angle. (Only one axis of the X-Y detector was used.) Figures 3.2-6 and 3.2-7 show this system.
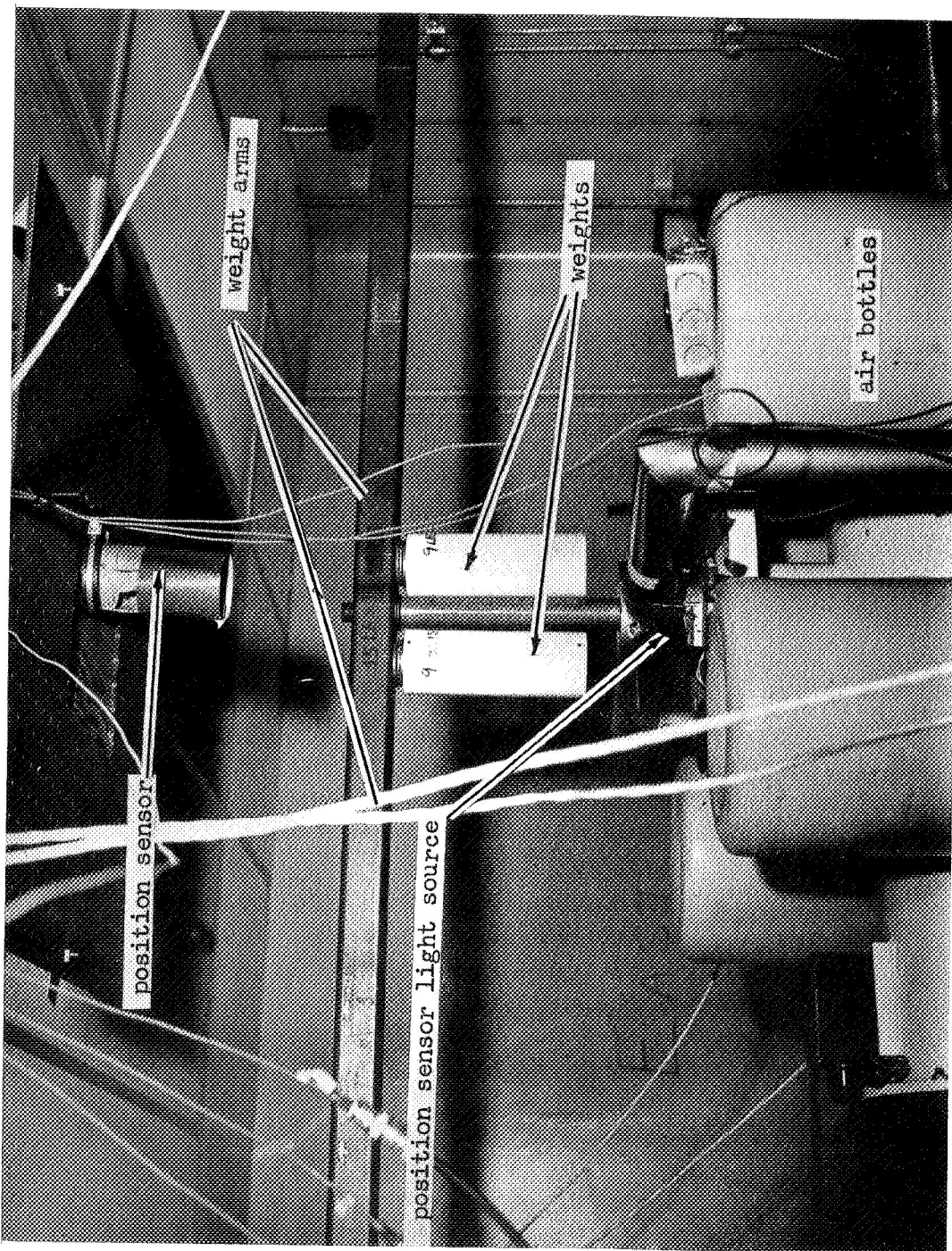
9

Figure 3.2-5 Position Sensor

weight arms

weights

air bottles

position sensor
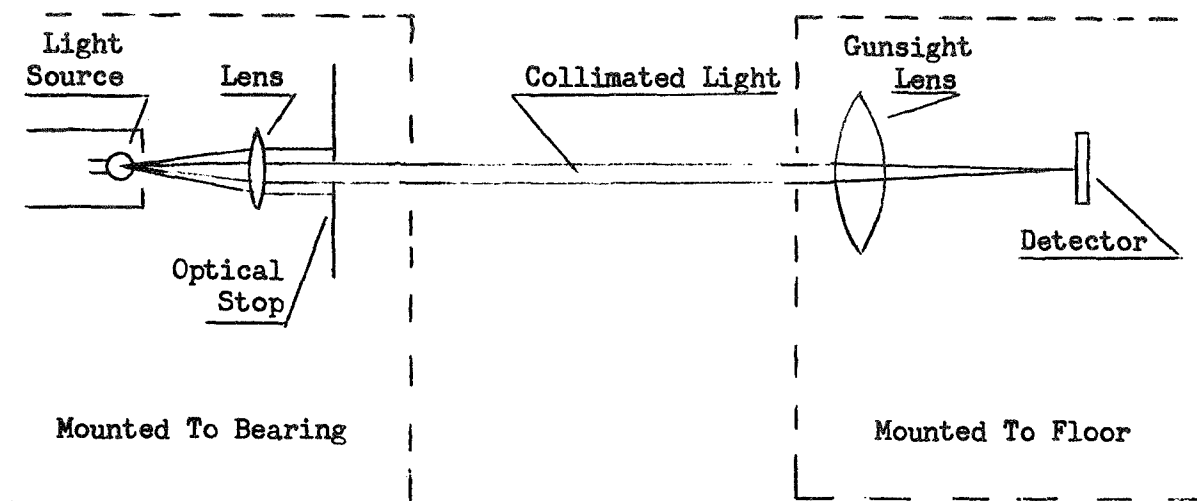
position sensor light source

Figure 3.2-6 Rotation sensor

Since the light bulb on the bearing was not a true point source, the incident beam on the telescope was not perfectly collimated, and there was some sensitivity of the detector to linear displacements greater than 0.5 centimeter. That is, for platform displacements greater than 0.5 centimeter, the output from this detector is a function of bearing translation as well as rotation.

Accuracy of this sensor was approximately 2 minutes of arc for conditions of zero or small X-displacement of the platform.

3.2.5 Accelerometer Computer Circuits.

The acceleration of the air bearing was measured by means of three Accumetric Corporation accelerometers mounted on the bearing as shown in Figures 3.2-1 and 3.2-2. These instruments are of the self-generating non-forcebalance type. Their frequency response is flat within $\pm$ 2% from 0.016 to 10 Hz. A closeup view of accelerometer #2 is shown in Figure 3.3-2.

Relationship of Accelerometer Readings to X, Y and θ.

rotation sensor light source

shaker frame
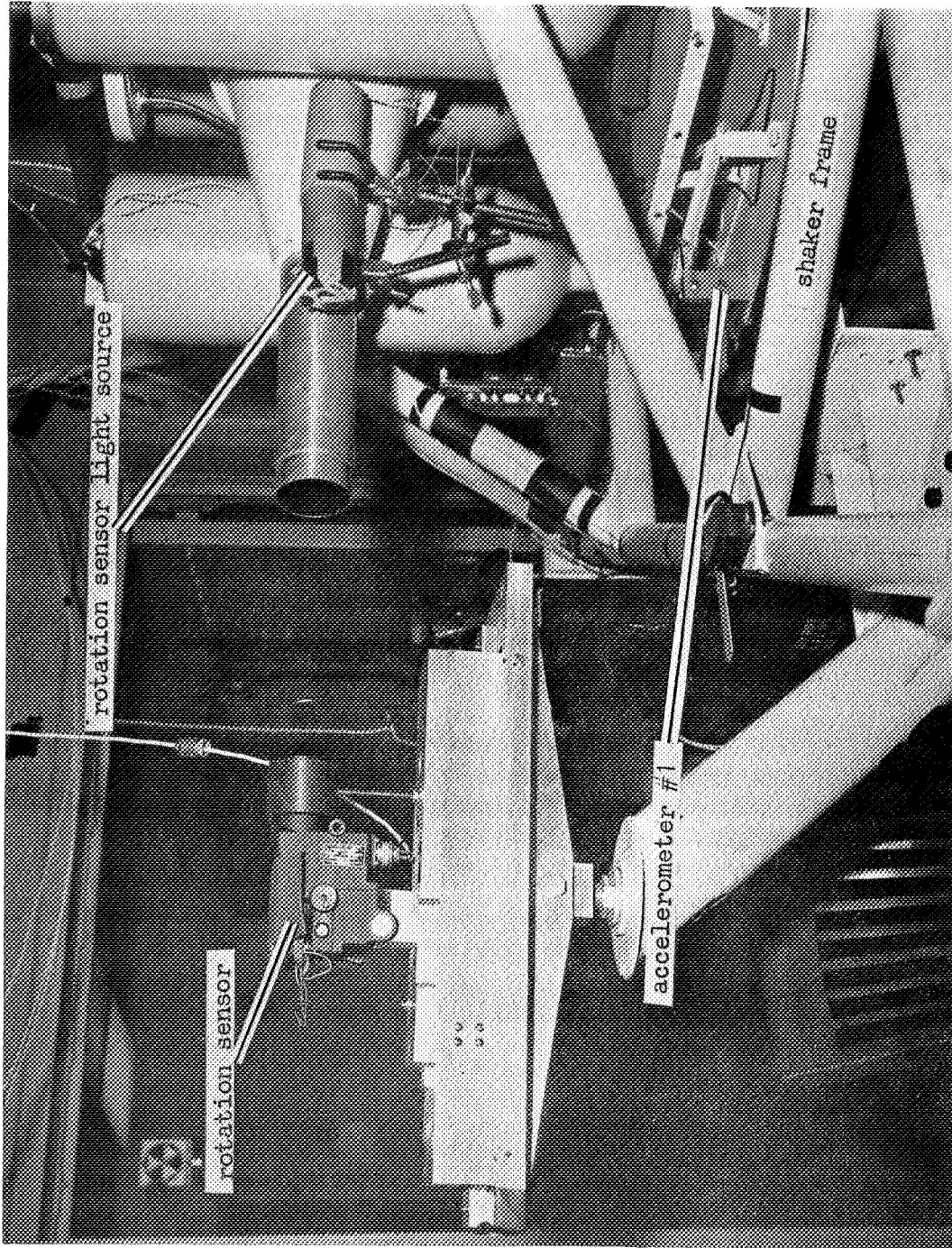
rotation sensor

accelerometer #1

Figure 3.2-7 Rotation Sensor

12

With the accelerometers positioned as shown in Figure 3.2-1, there is an interaction between the translational and rotational measurements for each accelerometer. That is, both rotational and translational accelerations will be measured without separation. In order to remove this ambiguity, the outputs of the three individual accelerometers were combined as described in the following paragraphs.

Assigning a positive X direction from West to East and positive Y direction from South to North, the accelerometers were positioned so that instruments 1 and 3 measured acceleration in the positive X direction and instrument 2 measured acceleration in the positive Y direction. Then calling a_1, a_2, a_3 the outputs from accelerometers #1, #2, #3 respectively, the following equations apply:

$$(1) \quad a_1 = \ddot{X} + R\ddot{\theta}$$

$$(2) \quad a_2 = \ddot{Y} + R\ddot{\theta}$$

$$(3) \quad a_3 = \ddot{X} - R\ddot{\theta}$$

where R is the distance from the axis of rotation of the bearing to the accelerometers (this distance is the same for all three accelerometers) and θ is the angular acceleration of the bearing with counterclockwise rotation assigned as positive.

Then, adding equations (1) and (3) above, we obtain:

$$(4) \quad \ddot{X} = \frac{a_1 + a_3}{2}$$

Subtracting equations (1) and (3), we obtain:

$$(5) \quad \ddot{\theta} = \frac{a_1 - a_3}{2R}$$

And substituting equation (5) in equation (2)

$$(6) \quad \ddot{Y} = a_2 - \frac{(a_1 - a_3)}{2}$$

The individual outputs from the accelerometers were processed as described in the following section and combined to provide, except for constant multipliers, the terms specified in equations (4), (5) and (6). These final signals were applied to a Brush Company recorder and appear on the first three tracks of the output data tape.

Actually, the input signals to the first three tracks are:

$$(1) \quad k_1\, a_1 + k_2\, a_2$$

$$(2) \quad k_3\, a_3 - k_1\, a_1$$

13

$$(3) \quad \frac{k_1 \, a_1 - k_3 \, a_3}{2} - k_2 \, a_2$$

where k_1, k_2, k_3 are the gains for the three accelerometer filter amplifiers described in the next section.

For input setting of 0.1 volts/division on the Brush recorder, the following calibration applies:

$$(\overset{..}{X}) - 1 \text{ division} = 2.22 \times 10^{-6} g$$

$$(\overset{..}{Y}) - 1 \text{ division} = 4.44 \times 10^{-6} g$$

$$(\overset{..}{\theta}) - 1 \text{ division} = 10.8 \ \overline{\sec}/\sec^2$$

Ancillary Electronic Circuitry for Accelerometers

It was discovered that a ground vibration of approximately 15 Hz was being transmitted through the table to the accelerometers from other equipment located within the plant. To simplify the data analysis a low pass filter was inserted in the output of each accelerometer. The filters incorporated three operational amplifiers in the analog computer, and were designed for cutoff frequency of 3.2 Hz. The response of the filters was essentially flat out to a frequency of 0.3 Hz and was down less than 10 percent at 1.0 Hz. Correction factors for the response falloff were applied to the readings for 0.5, 0.7 and 1.0 Hz. With the filters the ground noise was reduced to the level of the internal noise of the accelerometers.

The outputs of the accelerometers were then combined in the analog computer to give the values of $\overset{..}{X}$, $\overset{..}{Y}$ and $\overset{..}{\theta}$ on the Brown Recorder.

14

3.3 SUSPENSION SYSTEMS

3.3.1 Spring System.

The springs used in this test were simple helical springs arranged in pairs at each of four suspension points as shown in Figures 3.3-1 and 3.3-2. In order to determine the effect of force constant, three spring systems were tested, with the springs having force constant values of 0.01, 0.005 and 0.001 pounds/inch, respectively. The included angle between each pair of springs was approximately 82 degrees.

Twelve springs were wound in our laboratory for each spring constant value, and from these, eight were selected whose spring constants were most nearly equal. In all cases the eight selected values were within two percent of the average value and the average value was within two percent of the selected spring constant. Each spring was attached to the air platform by clips as shown in Figure 3.3-2. The other end of the spring was tied to a small length of string that passed through a hole in a strip which was rigidly attached to the shaker frame. The string was then run under the head of a small bolt. The tension in each spring could then be adjusted by loosening this bolt and pulling the string until the desired spring tension (or length) was obtained and then tightening the bolt head over the string.

3.3.2 Hysteresis System.

The test set-up for the hysteresis suspension system is shown in Figures 3.3-3 and 3.3-4. A more detailed description of the construction and theory of the hysteresis system is presented in Appendix A of this report.

The effective force constant of each hysteresis system was measured to be 0.02 pounds per inch. The systems were placed at the North and West suspension points of the bearing, and were opposed by pairs of 0.01 pounds per inch springs at the South and East suspension points. The springs were connected in parallel.

Each hysteresis system was attached by a string which wrapped around the circumference of the hysteresis disc and connected to the platform. The attachment point on the platform was raised above the spring system attachment point to the same height as the plane of the hysteresis disc.

Tension was adjusted on the springs and hysteresis system to center the bearing with respect to the shaker. Care was taken to provide sufficient tension on the string from the hysteresis disc so that the string did not go slack when shaker motion was in the direction of the hysteresis system. This was particularly necessary for the system attached along the axis of shaker motion. Although this technique worked successfully for gradual motions, there was string "slap" associated with rapid shaker motion such as the step functions and the higher frequency sine waves, approximately 0.5 Hz and higher.

In a separate test of the hysteresis system characteristics, there appeared to be a frictional type of damping in addition to the hysteresis damping from the magnets. This friction is probably due to the torsion wire rubbing against the teflon insert, 'T', as shown in Appendix A.
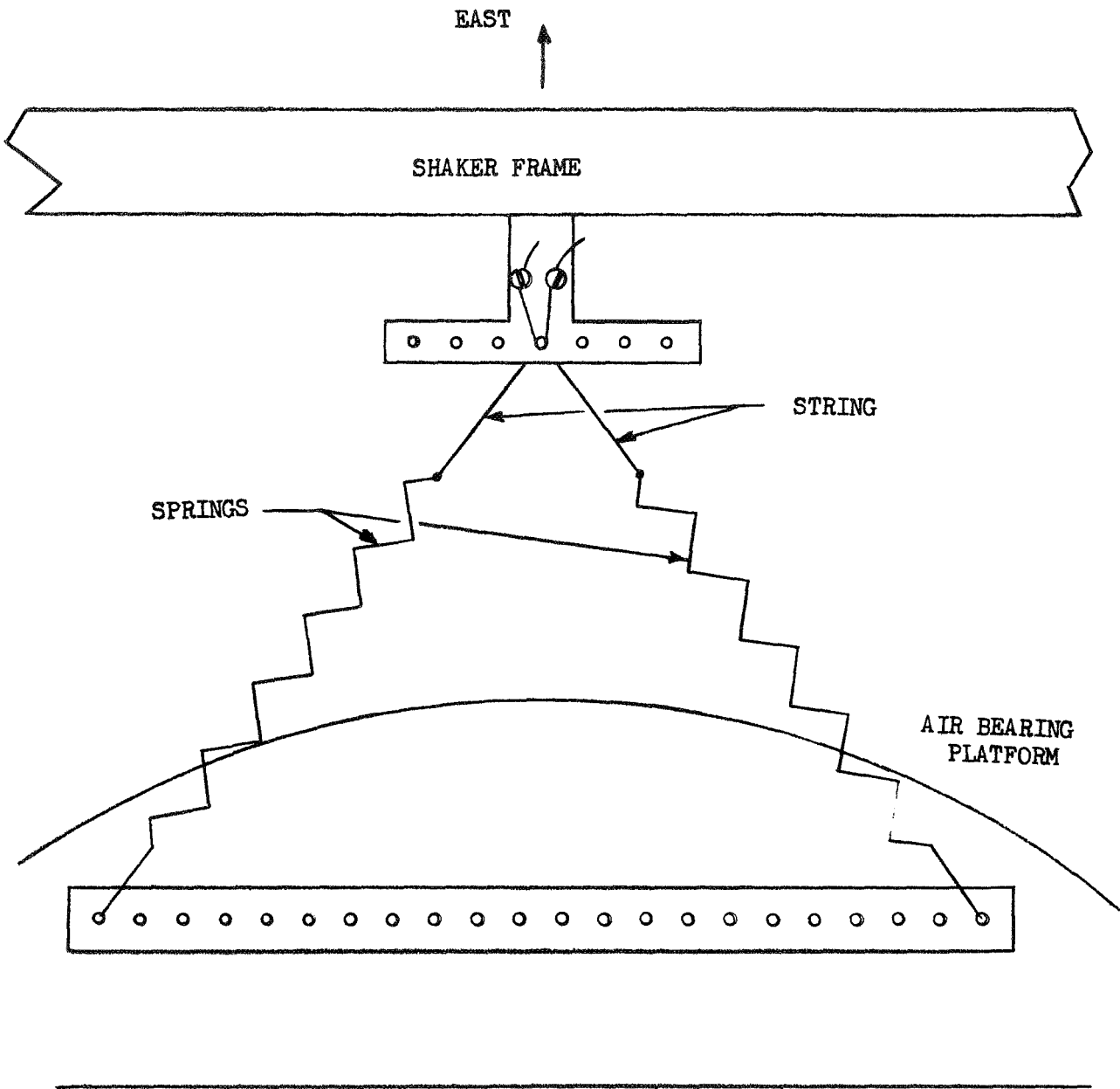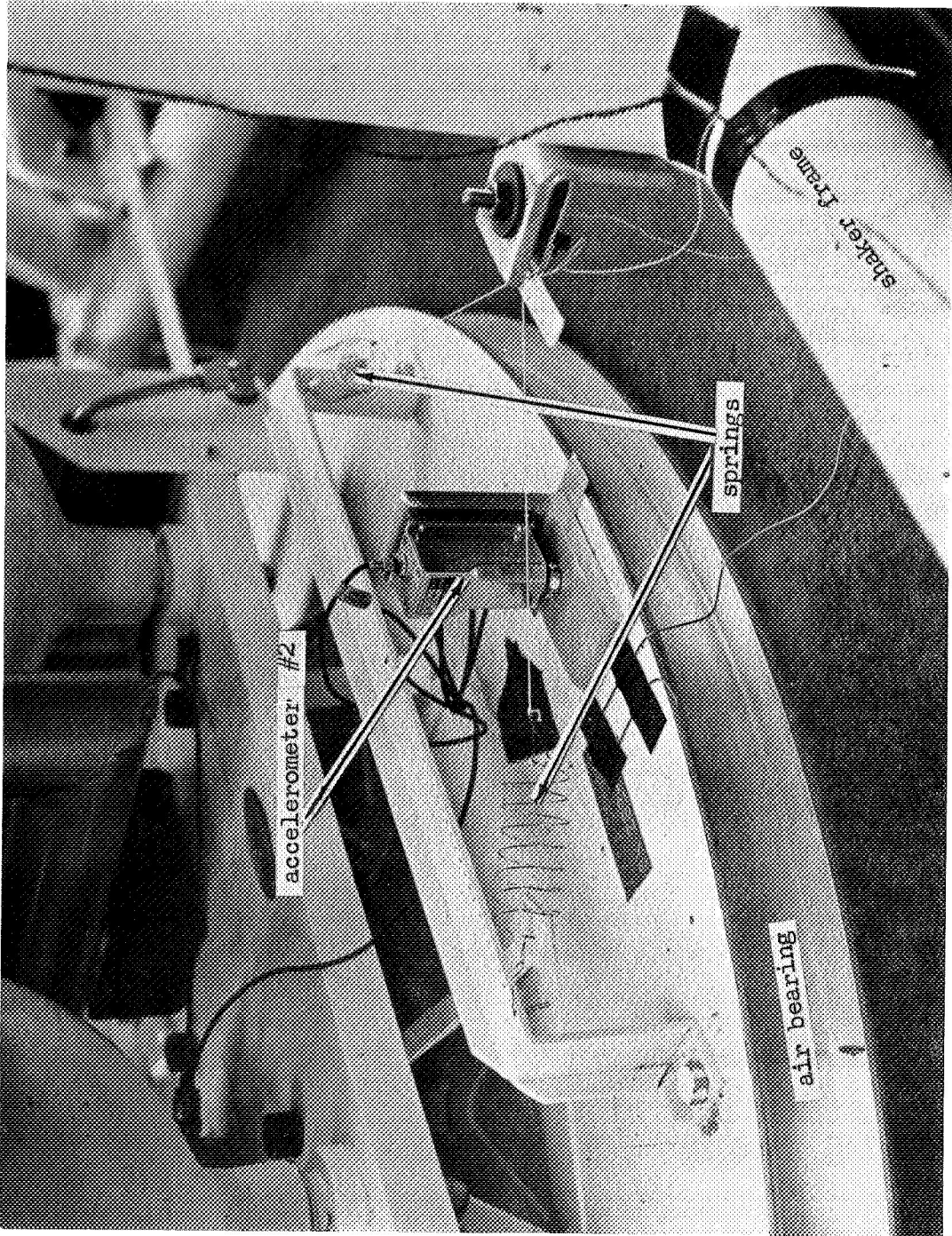
EAST

SHAKER FRAME

STRING

SPRINGS

AIR BEARING
PLATFORM

Figure 3.3-1 Spring suspension attachment

Figure 3.3-2 Spring Suspension

Labels in figure: shaker frame, springs, accelerometer #2, air bearing

17

AIR BEARING
PLATFORM

STRING

HYSTERESIS
SYSTEM

SHAKER
FRAME

DIRECTION OF
SHAKER MOTION

NORTH
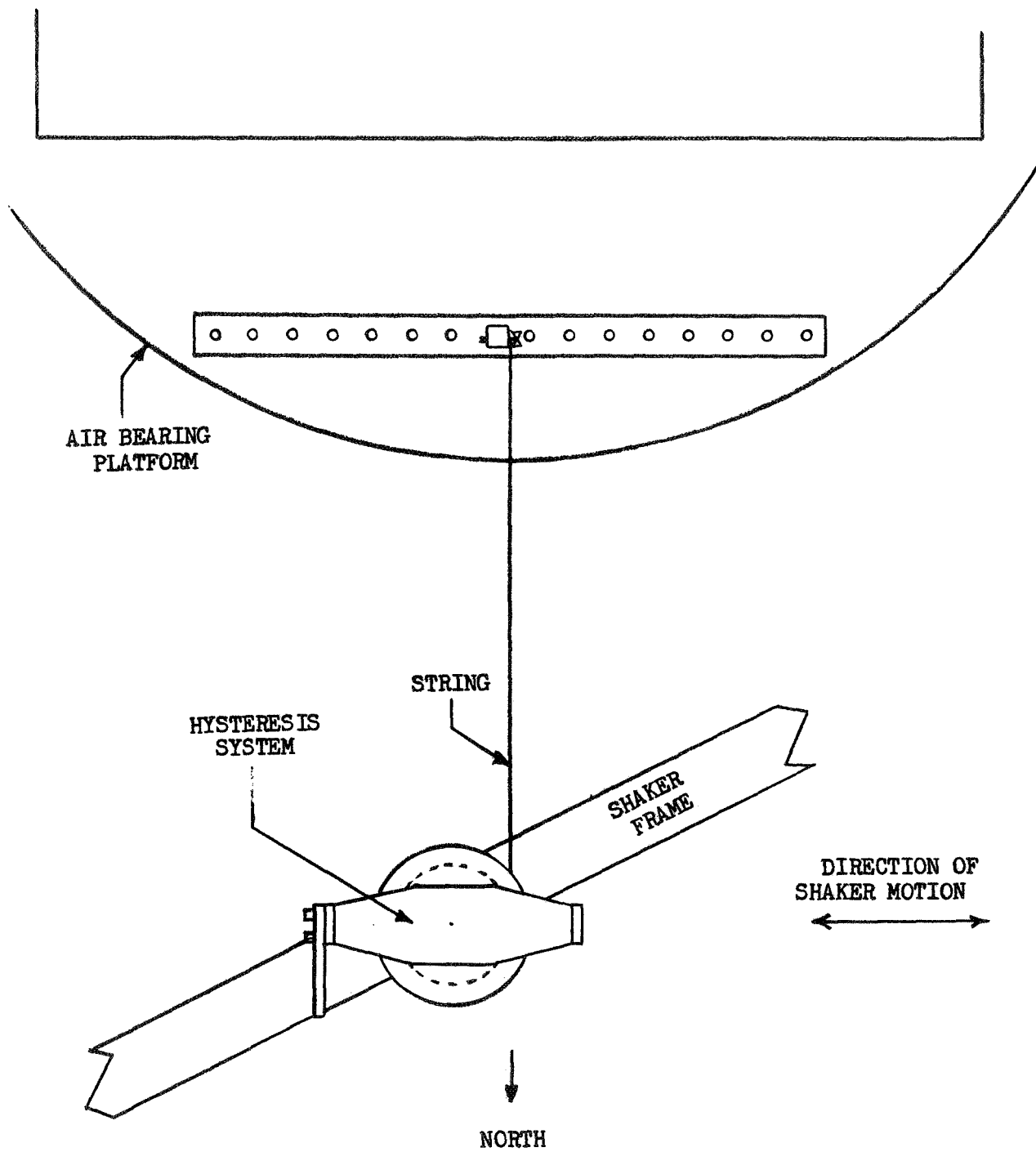
Figure 3.3-3   Hysteresis suspension attachment

hysteresis damper

attachment string

shaker frame

accelerometer #3
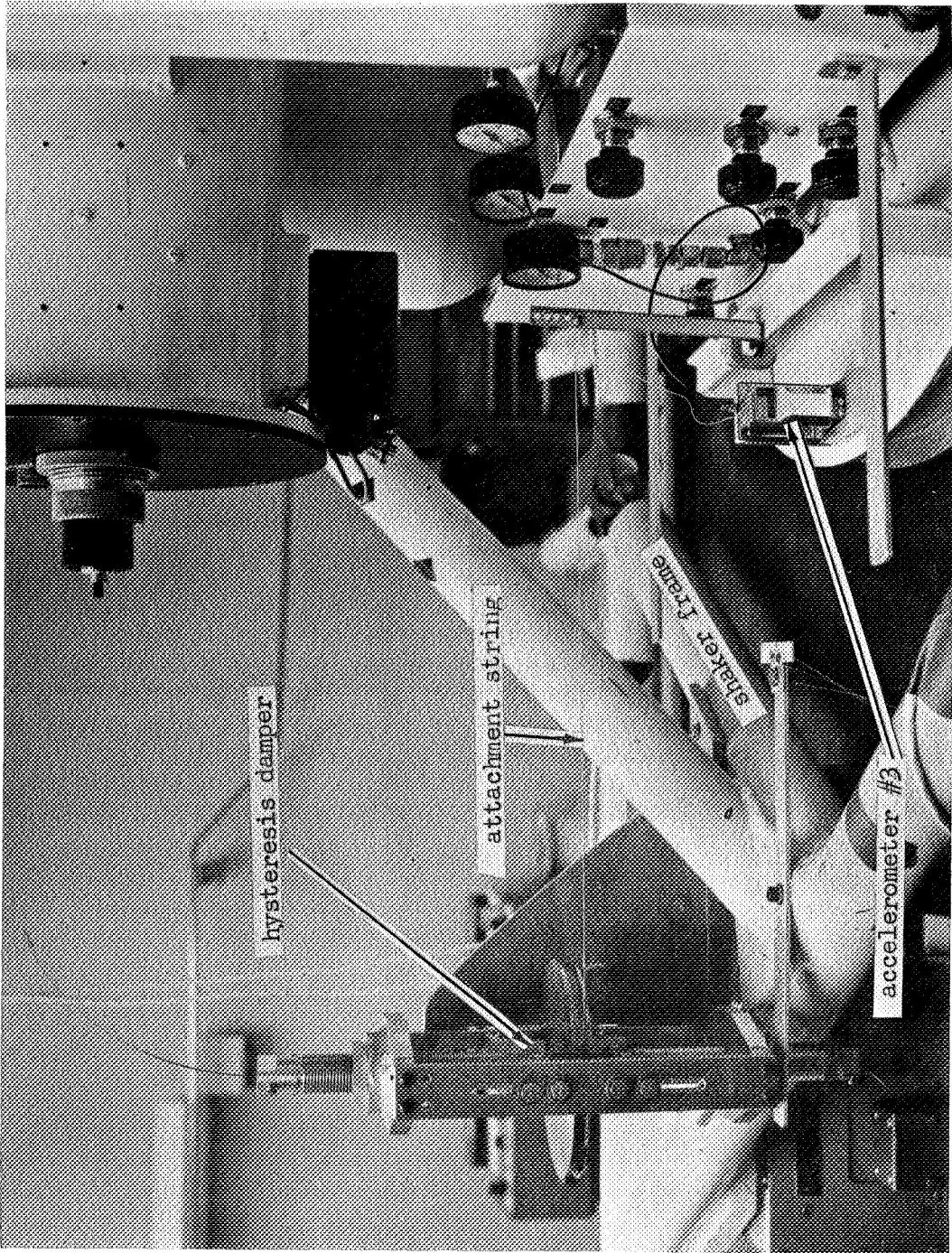
Figure 3.3-4 Hysteresis Damper

19

A separate test was made to test the effectiveness of the hysteresis system with the magnets removed, i.e., with no hysteresis damping.

3.3.3 Magnetic Suspension System.

The basic magnetic suspension system consisted of two coils, which were attached to the shaker, and two discs attached to the platform. This arrangement is shown in Figures 3.3-5 and 3.3-6.

The coils were mounted coaxially and spaced approximately one inch apart. The discs were positioned so as to lie symmetrically within the field when the bearing was centered with respect to the shaker. The disc array consisted of a small flat circular ceramic magnet of diameter 2.8 centimeters placed on a 5 centimeter ferromagnetic disc. The ceramic magnet was placed so that its field was in the same direction as those of the coils. A more complete description of the magnetic suspension system is presented in Appendix B of this report.

The two coils form a Helmholtz coil arrangement to provide a restoring force to the discs which is dependent on the radial distance of the discs from the coil axes. Since each system will tend to restrict both X and Y displacement of the discs, the coils and discs could have been set up at any two suspension points. (If a single suspension point were used, the platform would tend to rotate about that point.) For convenience, the selected points of attachment were chosen to be on the X axis.

The basic suspension system was also used with a feedback circuit to vary the current in the coils. The feedback system consisted of a separate sensor coil, isolated from the Helmholtz coils but coaxial with them and attached to the shaker, and a small magnet attached to the air bearing. The magnet is extended from the bearing so as to lie directly below this coil when the bearing is centered. If the platform is moving to take the sensing magnet away from the axis of the sensing coil, the resultant signal acts to increase the current through the suspension coils and thereby increase the pull of the suspension coils on the discs and the bearing to which they are attached.

Tests were run on the feedback suspension system for several values of amplification of the sensor signal.
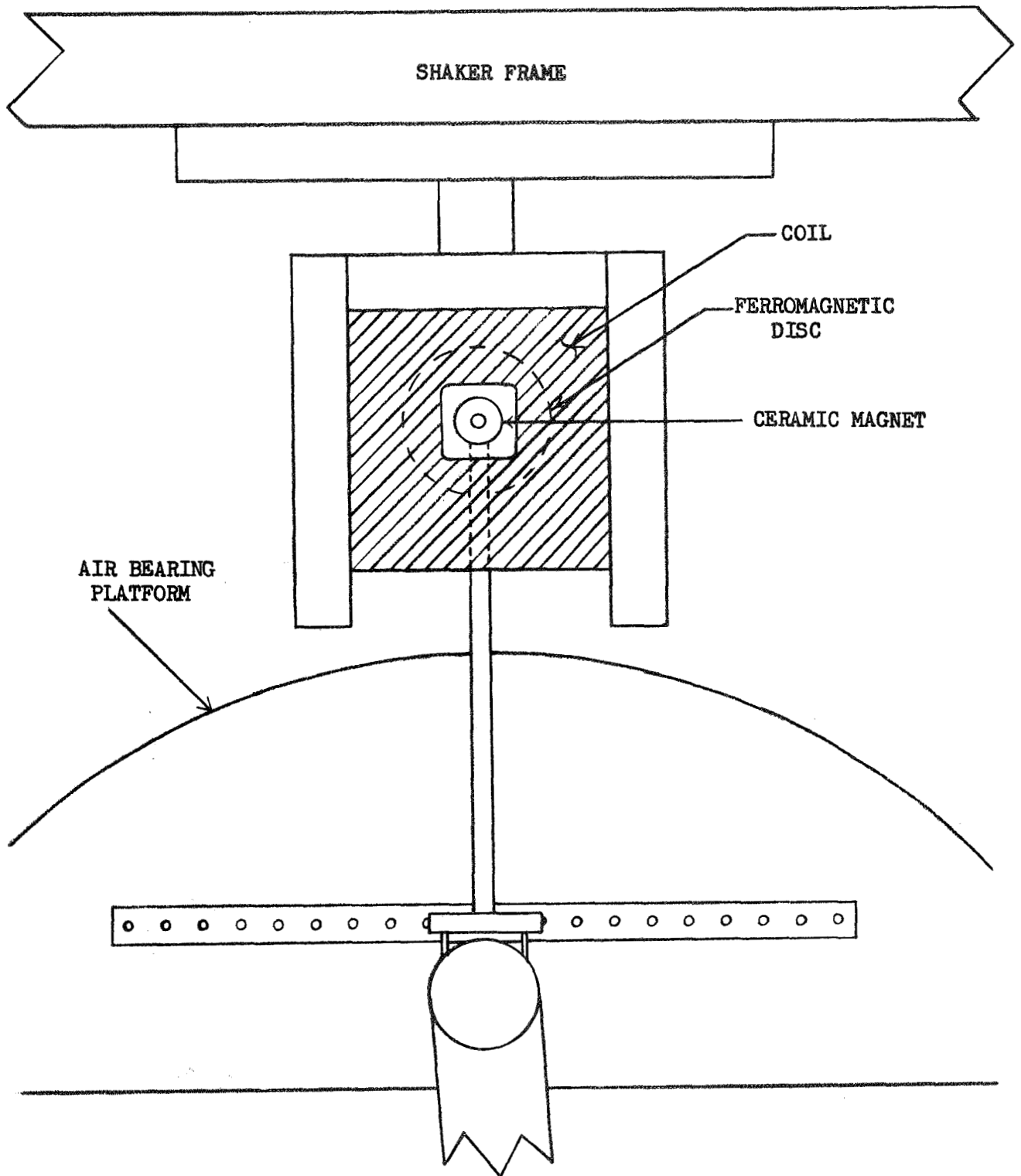
SHAKER FRAME

COIL

FERROMAGNETIC
DISC

CERAMIC MAGNET

AIR BEARING
PLATFORM

Figure 3.3-5 Magnetic suspension attachment

Figure 3.3-6 Magnetic Suspension

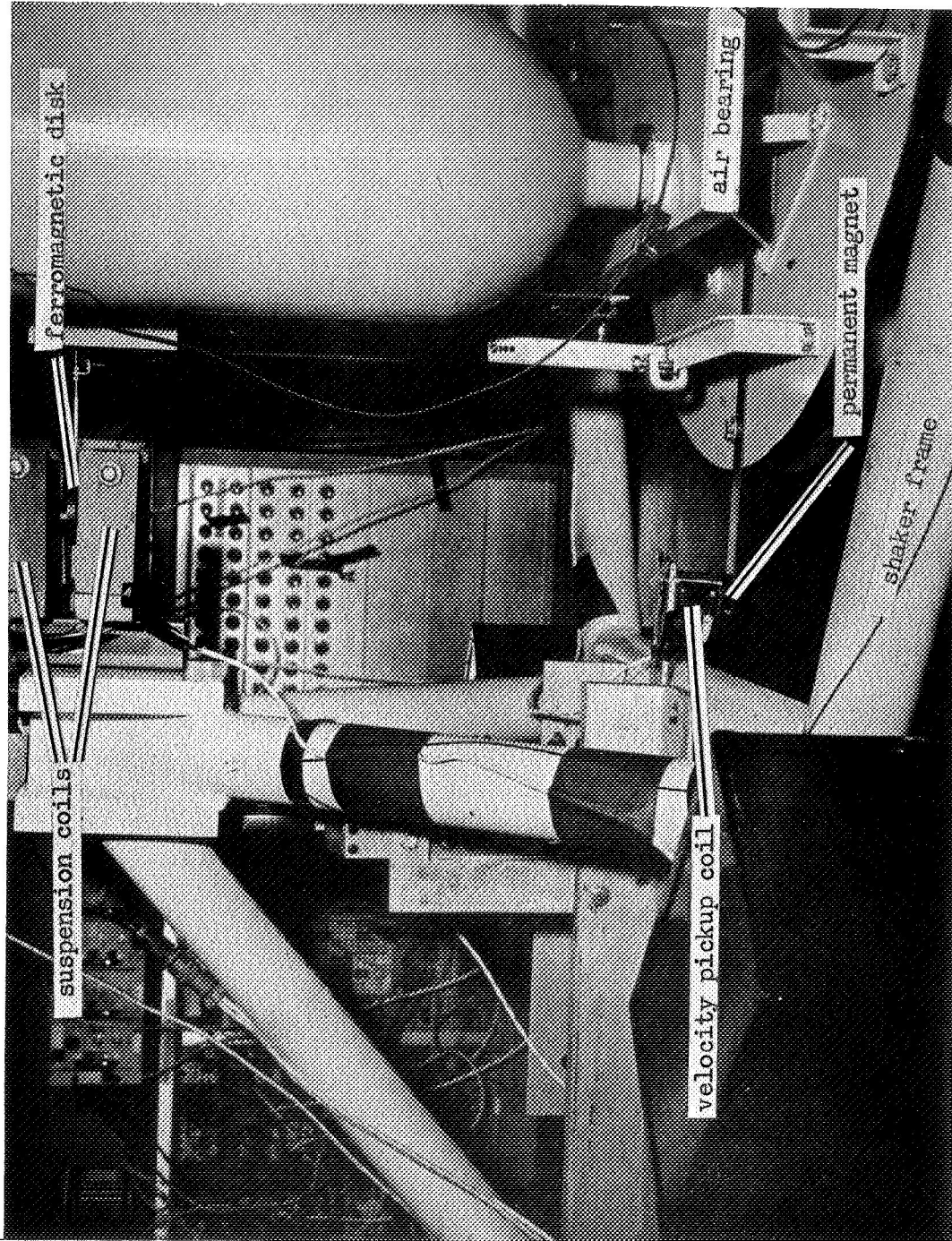Labels in figure: ferromagnetic disk, air bearing, permanent magnet, shaker frame, suspension coils, velocity pickup coil

3.4 SYSTEM GEOMETRY AND MASS CHARACTERISTICS

The weight and center of gravity of the air platform were determined by three load cells which were positioned so as to support the platform. This work was performed prior to installation of the weight support bar and associated weights described later in this section, so their effect was not included in this data.

The load cells were positioned at known points near the circumference of the platform and readings taken for several values of pressure (and hence weight) for the compressed air system used to float the platform. From this data the coordinates of the center of mass and the total weight of the platform were obtained. Variations due to changes in air pressure were found to be relatively small, and the values obtained for 1000 psi were used throughout the study.

The moment of inertia of the platform (again without the weights or support arm) was measured by supporting the floating bearing with a vertical torsion shaft which was attached to the ceiling, and applying torques to the bearing. The effective spring constant of the overall system was measured and the period of oscillation of the bearing was measured for several values of compressed air pressure. From this data, the moment of inertia, I, of the platform was determined. The moment of inertia was also relatively insensitive over the range of air pressures and a value of 19.1 kg-meter^2 was used for the moment of inertia for all tests.

In order to assess the effects of changes in moment of inertia and force moment arm on system characteristics, a slotted angle bar was attached to the air platform so as to lie along the Y'-axis. By positioning weights at different positions along this bar, the moment of inertia and the center of gravity along the Y'-axis could be changed. Since the disturbing forces are applied along the X'-axis, the applied moment arm is the distance Y', and therefore, only variations in $\bar{Y}'$ were effected.

Three weight configurations were selected:

o Both weights at the center of the bar. Because of the vertical center rod through the bar, the weights could not be placed at the exact center, but rather were positioned about each arm of the bar 5.1 cms. from the center. The arrangement is referred to as W_1.

o A weight on each arm of the bar, .92 meters from the center. This arrangement is W_2.

o Both weights on the same arm of the bar - one weight 1.14 meters from the center and the other .731 meters from the center. This arrangement is W_3.

These weight arrangements are diagrammed in Figure 3.4-1.

With weight arrangements W_1 and W_2 the platform has a common center of gravity, but different moments of inertia about the vertical axis. With arrangements W_2 and W_3 the platform moments of inertia about the vertical axis are equal but the centers of gravity are different. Since the line of

Weight Support Arm

W1

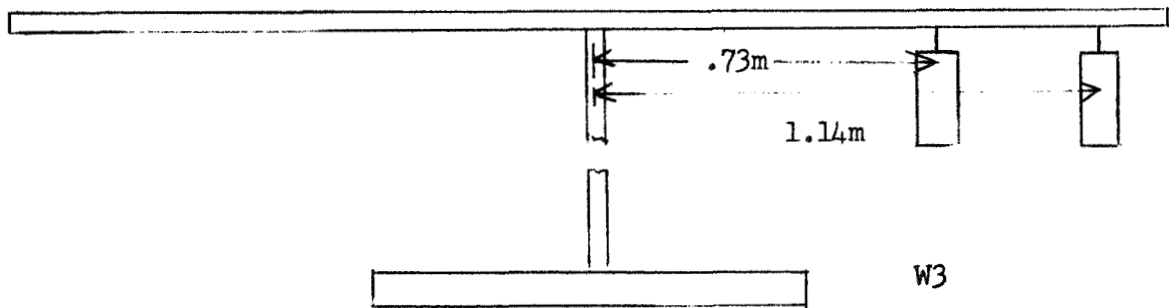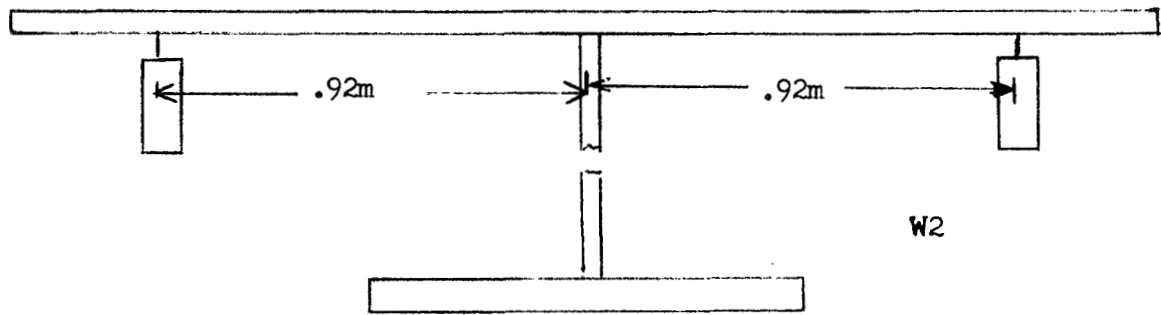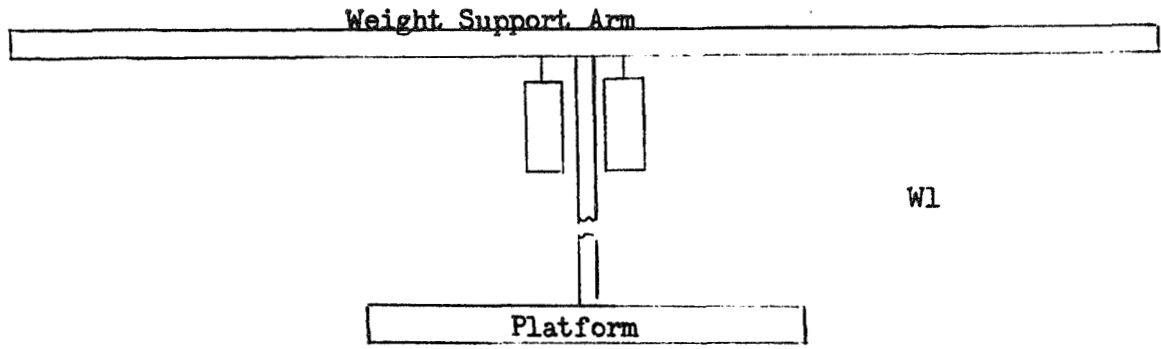Platform

.92m .92m

W2

.73m

1.14m

W3

Figure 3.4-1 Weight configurations

action of the applied disturbing force was constant for all tests on each type of suspension system, variations in the location of the center of gravity resulted in corresponding variations of the applied moment arm of an applied force. Thus, for a given suspension system (except for laboratory errors), variations in results between data obtained for arrangements W_1 and W_2 are attributable to the effects of change in the value of moment of inertia of the suspended system, variations for data obtained for arrangements W_2 and W_3 are attributable to the effect of changes in applied disturbing torque.

A greater change in applied moment arm could have been obtained by positioning the weights for arrangement W_3 on the north side of the support bar, so that the center of gravity for the system was on the same side of the X' axis as for W_1 and W_2, but displaced further from the center. This arrangement was examined, but produced an intolerable instability in the system, possibly due to a small tilt of the platform with respect to the table.

The significant geometry and mass characteristics of the total platform system are presented in Table 3.4-1 for the three weight configurations.

Table 3.4-1 Physical characteristics of the air platform

Weight Configuration	Mass (kg)	Moment of Inertia $(kg\text{-}m^2)$	Center of Gravity Offset (cm)
W1	250	22.5	1.78
W2	250	30.2	1.78
W3	250	30.2	1.46

3.5 DISTURBANCE PROGRAMS

The major disturbance programs applied as input to the suspension systems included the following:

1. **Sine Waves** These were generated over a frequency range from 0.01 Hz to 1.0 Hz at an amplitude of 1.11 cm peak-to-peak. Occasionally, additional data was taken for amplitudes of .635 cm peak-to-peak.

2. **Step Functions** Displacements of .635 cm were used for all systems, and an additional step of .32 cm displacement was used in some cases.

3. **Square Waves** Square pulses of .32 cm displacement and 10 seconds duration, 80 seconds apart, were applied. The pulses alternated in direction. Only one pair of pulses was applied for each test.

4. **Ramp Functions** Shaker displacement was linearly increased from zero to .635 cm in approximately 100 seconds.

The electrical input wave forms and the corresponding shaker displacements were both presented on the chart strip. The displacements faithfully followed the input wave forms except in the case of very slow displacement velocities, where the shaker occasionally hung up momentarily and then released. However, these were of very short time duration and did not significantly affect the platform motion.

3.6 TEST PROCEDURE

The technique for testing any suspension system was as follows:

1. If this was the first system to be tested that day, level the table. This was normally done manually, with the criteria for levelness being that point at which the floated bearing remained motionless.

2. Set the weights in the desired arrangement.

3. Attach (or energize) the suspension system.

4. Turn on shaker and team table pumps.

5. Adjust the suspension system to position the bearing at a location on the table such that the line of action of the suspension acts through a known point of the bearing. This point was nominally the center of geometry of the system.

6. Turn on all instrumentation and ancillary devices. This includes accelerometers, lights for displacement and rotation sensors, power supplies for shaker electronic input, recorders and power supply for suspension coils if that system was to be tested. Allow 15 minutes warm-up time. Adjust rotation detector and light source to be aligned coaxially.

7. Float the bearing and allow it to become as stationary as possible.

8. Apply disturbance waveform to shaker input. Normally the first waveforms were sine waves in the higher frequency decade, i.e., 0.1 Hz to 1.0 Hz. If, as in most cases, there was no discernible motion of the platform due to this disturbance, the frequency was changed to a new value without waiting for the platform to completely cease all natural modes of motion which may have begun, provided these motions were not excessive. It was felt that the smooth variation in the value of applied voltage accomplished by this technique was preferable to the initial step-type application caused in bringing the sine wave amplitude from zero to the final value.

    The platform was stopped prior to application of a given frequency disturbance if the platform was moving at, or near, that frequency.

    For the lower frequency sine waves, where resonance or near-resonance frequently occurred, a close watch was maintained to prevent any direct contact between the platform and the shaker which could cause damage to the accelerometers.

    After the sine wave tests were completed, the step, ramp and square wave functions were applied to the shaker. For these tests, the shaker motion was always minimized prior to application of the disturbance.

9. Turn off the accelerometers and move weights to next arrangement, or if this was the final weight arrangement for the system being tested, set up next suspension system. Accelerometers were turned off to prevent excessive

signal while the platform was being manually adjusted.

10. At the end of each day's testing, the position detector systems were cali-
brated. The translation detectors were calibrated by moving the detector
manually along each direction and marking the position of the detector
trace on the recorder for each centimeter of actual platform travel in that
direction.

The rotation detector was calibrated by moving the detector relative to the
platform rather than the platform relative to the detector. This was done
as a matter of convenience since the detector could easily and accurately
be rotated about a fixed axis, while rotating and restraining the platform
about small angles was difficult and time consuming. The detector housing
was rotated in steps of arc length of travel of 1 mm and the corresponding
position of the rotation detector trace on the recorder was noted. Since
the radius of rotation of the detector housing was known, the arc length of
travel could be converted to angular measurement in radians. The angle
through which the detector must be rotated to move the incident light from
a fixed source over a certain region of the detector is the same angle as
that through which the source would have to be rotated to move the light
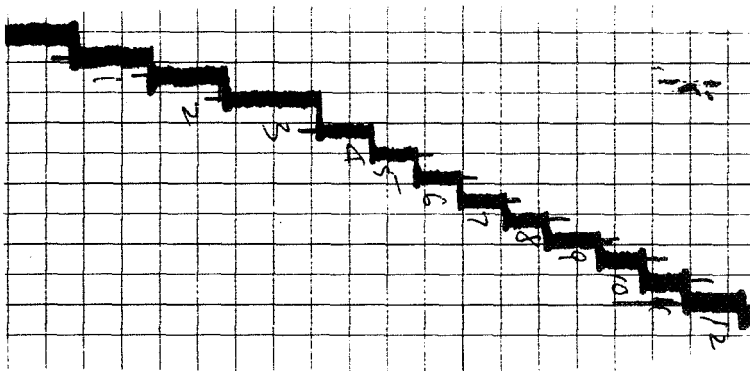over the same region of a fixed detector.

Typical calibration data for the position sensors are shown in Figure 3.6-1.
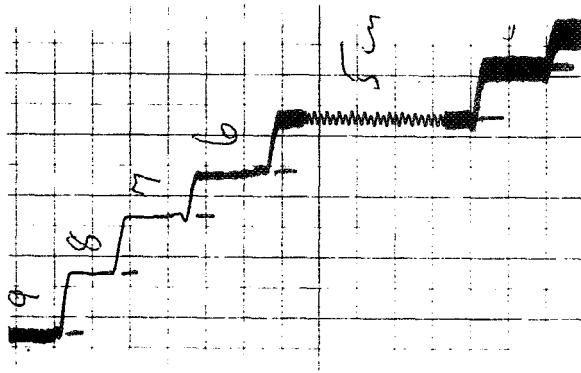
X-calibration----Each step
represents one cm. displacement
in the X-direction
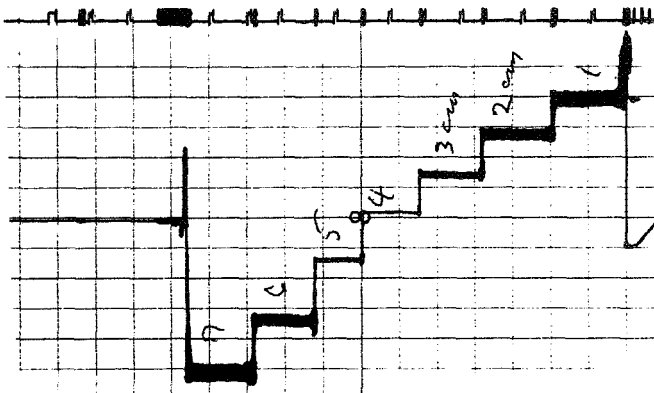
Y-calibration---- Each step
represents one cm. displacement
in the Y-direction

θ-calibration---- Each step
represents one mm. of displacement
of the gunsight along an arc, and
is equivalent to 11.6 minutes of
bearing rotation

Figure 3.6-1 Sensor Calibration Data

4.0 TEST RESULTS

4.1 GENERAL DISCUSSION

4.1.1 Measured Parameters

For all tests, six major parameters were measured to define the suspension/platform characteristics.

These parameters were:

(1) Acceleration in the line of shaker motion ($\ddot{X}$)
(2) Acceleration transverse to the line of shaker motion ($\ddot{Y}$)
(3) Rotational acceleration in the horizontal plane ($\ddot{\theta}$)
(4) Translation in the line of shaker motion (X)
(5) Translation transverse to the line of shaker motion (Y)
(6) Rotation in the horizontal plane (θ)

The parameters were recorded as a function of time for all disturbances and suspension systems specified in this report.

For sinusoidal disturbances, only the displacement or acceleration at, or near, the driving frequency was measured. That is, any motion at the natural frequency was not considered if that frequency was significantly ($\sim$20%) different from the driving frequency.

As discussed previously in Section 3.2, difficulties were encountered in the measurement of bearing rotation displacement, primarily due to the effect of translational position on the rotation detector system. This situation gradually worsened to the extent that for one suspension system - the 0.01 springs - the angular displacement data was not considered sufficiently accurate to be included in this section. This situation developed too late for the purchase and installation of the new equipment necessary to correct the problem.

Two items in regard to system response are worth mentioning at this point. None of the suspension systems tested showed any response in displacement or acceleration to the applied ramp functions, except for a gradual displacement in the x-direction to the final value. Also, the 0.001 spring suspension system showed no response to any of the disturbances, except at a driving frequency of 0.01 Hz for which isolated values of the six measured parameters were noted. This system can be thought of as at, or beyond, the limits of measurement for this facility.

4.1.2 Recorded Data

Selected measured data and data ratios have been identified as most clearly defining the effectiveness and limits of the tested suspension systems and are recorded in this section in either graphical or tabular form. Generally, data was plotted if three or more data points were known. In some cases, particularly those involving resonance conditions, very gross interpolation was performed. These curves should be considered only as indicating a trend, and not as a method to obtain non-plotted data points. Because of the difference in

30

the physical characteristics of the three types of suspension systems there is some variation in the parameters which have been selected to appear later in this section.

In several instances, particularly for large values of response, the observed data curves were non-sinusoidal, although the suspension systems were supposedly linear. It was difficult to determine to what extent this apparent non-linearity was due to the system, to interaction between the various modes of motion, to non-linear detector response, or to modulation between the driving frequency and the natural system frequency for the particular mode of motion. For those cases where the waveform was almost sinusoidal, an approximation was made to a true sine wave and the amplitude value recorded. For those cases where the waveform was highly non-sinusoidal, but at the frequency of the driving disturbance, the peak value of amplitude was recorded as a lower bound for the possible true value. For example, a non-sinusoidal peak-to-peak amplitude of 4 centimeters was recorded as "> 4 cms."

4.1.3 Test Philosophy

As work progressed on the three types of systems, more and more emphasis was placed on the magnetic suspension. This was due to a number of reasons, but principally because it was felt that this system had the greatest potential to perform the job of isolating a large space telescope to the desired specifications.

A spring suspension system, in the simple form used for these tests, does not appear able to provide the necessary isolation, and can be studied analytically to define its characteristics.

The hysteresis system did not work as well as expected, but this appears to be a design problem rather than a failure of theory of operation. However, modification and optimization of this system would have required time and man-power expenditures which were far beyond the scope of this study.

The magnetic suspension system, on the other hand, was relatively easy to modify within restricted limits by varying either the separation between elements, e.g. the suspension coils, the current through the coils or the amount of feedback. Thus, some amount of optimization was performed on this system, and a corresponding greater amount of data was obtained.

4.2 SPRING SUSPENSION SYSTEMS

4.2.1 General

There was not sufficient motion or acceleration of the platform to provide significant readable data for any of the measured parameters with the .001 spring suspension system.

4.2.2 Equations of Motion

In order to compare the data with analytical values, the equations of motion for platform motion have been determined and some parameters have been calculated for the case where K=.01 pounds/inch.

Equations of Motion of Air Bearing with Linear Suspension System
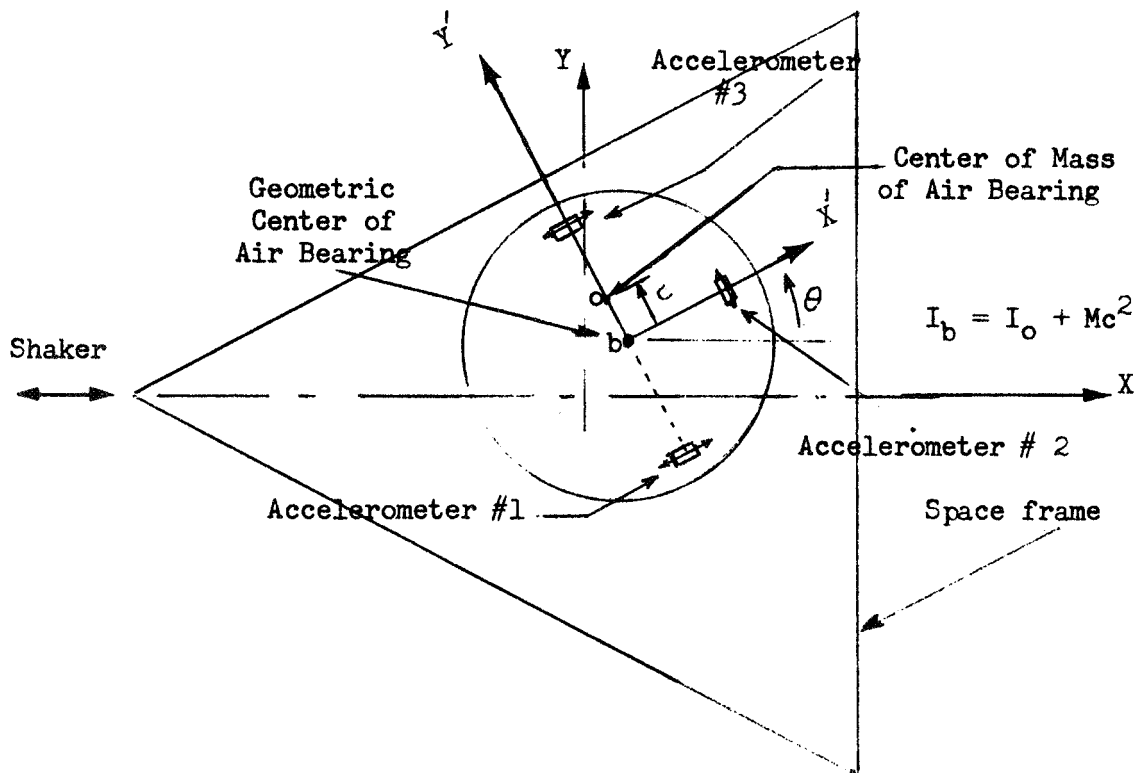
X,Y — Axes set fixed to space frame. The four isolation system attachment points on the space frame are assumed to be located on these axes.

X′,Y′ — Axes set fixed to air bearing. Aligned relative to accelerometers (1), (2) and (3) as shown in the sketch.

X_b, y_b — Coordinate of the geometric center of the bearing in the x,y system. X_b is not an inertial coordinate.

Let $\mu_b = X_b + X_I$, y_b represent the inertial coordinates of the bearing center.
X_I = shaker displacement

The equations of motion are:

Y — Direction

(1)　$M\ddot{y}_b + 2(K_R + K_T)y_b = 0$

K_R, K_T = radial and tangential spring constants at each suspension point

X — Direction

(2)　$M(\ddot{X}_b + \ddot{X}_I) + Mc\ddot{\theta} + 2(K_R + K_T)X_b = 0$

$K_T R^2$ = rotational spring constant at each suspension point

θ — Direction

(3)　$I_b\ddot{\theta} + M(\ddot{X}_b + \ddot{X}_I)c + 4K_T R^2\theta = 0$

Notes:

1. Equation (1) is uncoupled from equations (2) and (3) because acceleration in direction Y does not induce rotation in θ and vice versa. Actually, a very small coupling term, $Mc\cos\theta\,\ddot{\theta}$ has been dropped from equation (1) because it is of second order magnitude. Also, the term, $Mc\ddot{\theta}$, in equation (2) is actually $Mc\cos\theta\,\ddot{\theta}$

2. The external force application is contained in the term $2(K_R + K_T)X_b$ in equation (2). That is, motion of the space frame or of the bearing causes spring deflection, equal to relative motion X_b of the bearing with respect to the frame, and hence, a restoring force $-2(K_R + K_T)X_b$. In order to have all displacements measured relative to an inertial frame of reference, express equation (2) as

(4)　$M(\ddot{X}_b + \ddot{X}_I) + Mc\ddot{\theta} + 2(K_R + K_T)(X_b + X_I) = 2(K_R + K_T)X_I$

Now rewrite the equations in the following way:

(5)　$\ddot{y}_b + \omega_1^2\,y_b = 0$

(6)　$\ddot{\mu}_b + \omega_1^2\,\mu_b + c\ddot{\theta} = \omega_1^2 X_I$

(7)　$\beta\ddot{\mu}_b + c\ddot{\theta} + \omega_2^2\,(c\theta) = 0$

where　$\omega_1^2 = \dfrac{2(K_T + K_R)}{M}$　　$\beta = \dfrac{Mc^2}{I}$

$\omega_2^2 = \dfrac{4K_T R^2}{I_b}$　　$\mu_b = X_b + X_I$

33

The Laplace transformations for these equations are:

(8) $\quad (s^2 + \omega_1^2) \ddot{y}_b = \dot{y}_b(0) + sy_b(0)$

(9) $\quad (s^2 + \omega_1^2) \ddot{\mu}_b + s^2(c\bar{\theta}) = \omega_1^2 \ddot{X}_I + \dot{\mu}_b(0) + c\dot{\theta}(0) + s(\mu_b(0) + c\theta(0))$

(10) $\beta s^2 \ddot{\mu}_b + (s^2 + \omega_2)^2 c\bar{\theta} = \beta\dot{\mu}_b(0) + c\dot{\theta}(0) + s(\beta\mu_b(0) + c\theta(0))$

The solution of equations 8, 9, 10 is:

(11) $\quad y_b = \dfrac{\dot{y}_b(0) + sy_b(0)}{s^2 + \omega_1^2}$

(12)
$$\bar{\mu}_b = \dfrac{\begin{vmatrix} \omega_1^2 X_I + \dot{\mu}_b(0) + s(\mu_b(0) + c\theta(0)) + c\dot{\theta}(0) & s^2 \\ \beta\mu_b(0) + c\dot{\theta}(0) + s(\beta\mu_b(0) + c\theta(\theta)) & s^2 + \omega_2^2 \end{vmatrix}}{\Lambda}$$

(13)
$$c\bar{\theta} = \dfrac{\begin{vmatrix} s^2 + \omega_1^2 & \omega_1^2\bar{X}_I + \dot{\mu}_b(0) + s(\mu_b(0) + c\theta(0)) \\ \beta s^2 & \beta\mu_b(0) + c\dot{\theta}(0) + s(\beta\mu_b(0) + c\theta(0)) \end{vmatrix}}{\Delta}$$

where

(14) $\quad \Lambda = \begin{vmatrix} s^2 + \omega_1^2 & s^2 \\ \beta s^2 & s^2 + \omega_2^2 \end{vmatrix} = (1-\beta)s^4 + (\omega_1^2 + \omega_2^2)s^2 + \omega_1^2\omega_2^2$

Special Cases

1. **Initial conditions all zero, system free.**

a) $\mu_b(0) = c\theta(0) = \dot{\mu}_b(0) = c\dot{\theta}(0) = 0$

b) $x_I = 0$ i.e., shaker not moving

Then the solution for $c\theta$ and μ is given by:

(15) $\quad \Lambda = (1 - \beta)s^4 + (\omega_1^2 + \omega_2^2)s^2 + \omega_1^2\omega_2^2 = 0$

If the included angle between the springs is 90° (as is the approximate case for our system), then $K_R = K_T = 2(K_s)(\cos^2 45°) = K_s$, where K_s is the spring constant of the individual springs.

Then, $\quad \omega_1^2 = \dfrac{2(K_T + K_R)}{M} = \dfrac{4K_s}{M} \quad$ rad/sec^2

For the systems tested in this study, ω_1 is the natural frequency in the Y-direction. It would also be the natural frequency in the X-direction if the C.G. offset did not induce rotation.

34

The uncoupled natural frequency in rotation is ω_2.

The characteristic equation (Eq 15) is solved by setting $s^2 = -\Omega^2$ and $s^4 = \Omega^4$. Then Eq 15 becomes

$$(16) \quad \Omega^4 - \frac{(\omega_1^2 + \omega_2^2)\ \Omega^2}{(1-\beta)} + \frac{\omega_1^2\omega_2^2}{(1-\beta)} = 0$$

The values of Ω_1 and Ω_2 represent the angular frequencies for the system in translation and rotation.

The amplitude ratios for this system are obtained by using the Laplace transformation for Eq. 9 with

$$\bar{X}_I = \mu_b(0) = c\theta\ (0) = \dot{\mu}_b(0) = c\dot{\theta}(0) = 0.$$ Then Eq. 6 can be written

as $\quad (-\Omega^2 + \omega_1^2)\ \bar{\mu}_b - \Omega^2 (c\bar{\theta}) = 0,$ and

$$(17) \quad \frac{c\theta}{b} = \frac{\omega_1^2 - \Omega^2}{\Omega^2}$$

For cases where $\omega_1 \approx \Omega$, the expression for $\dfrac{c\bar{\theta}}{\bar{\mu}_b}$ can be more accurately determined by using the solution obtained in Eq. 7.

$$(18) \quad \frac{c\bar{\theta}}{\bar{\mu}_b} = \frac{\Omega^2\beta}{\Omega^2-\omega_2^2}$$

2. System Forced with Unit Step

a) Initial conditions are all zero.

b) $\bar{X}_I = \dfrac{1}{s}$

The solution for y will be the same as expressed in Equation 11; that is, for free motion.

$$(19) \quad \bar{\mu}_b = \frac{\begin{vmatrix} \dfrac{\omega_1^2}{s} & s^2 \\ 0 & s^2 + \omega^2 \end{vmatrix}}{\Lambda} = \frac{\left[\dfrac{\omega_1^2\ (s^2 + \omega_2^2)}{s} \right]}{(1-\beta)s^4 + (\omega_1^2 + \omega_2^2)s^2 + \omega_1^2\omega_2^2}$$

Using the solution of Eq. 16 for the denominator of Eq. 19, we obtain

$$(20) \quad \mu_b = \frac{\omega_1^2\ (s^2 + \omega_2^2)}{s(1-\beta)(s^2 + \Omega_2^2)(s^2 + \Omega_1^2)}$$

(21)
$$c\bar{\theta} = -\frac{\beta \omega_1^2 s}{(1-\beta)(s^2 + \Omega_2^2)(s^2 + \Omega_1^2)}$$

The solution for Eq. 20 is of the type:

(22) $\mu_b(t) = 1.0 - C_1\cos \Omega_1 t - C_2 \cos \Omega_2 t$

where C_1 and C_2 are constants.

The magnitude of the coupling between translational and rotational modes is indicated by the relative values of C_1 and C_2. If there were no rotational coupling, i.e., offset distance, $c=0$, then Eq. 22 would be of the form.

(23) $\mu_b(t) = 1.0 - 1.0 \cos \omega_1 t$

Solving Eq. 21 for the angular response, we obtain

(24) $\theta(t) = D (\cos \Omega_1 t - \cos \Omega_2 t)$

Where D is a constant.

3. Sinusoidal Forcing Function

a) Initial conditions are all zero.

b) $X_I(t) = \sin \omega t$

$X_I(s) = \dfrac{\omega_f}{s^2 + \omega_f^2}$, where f_f = forcing frequency

Then,

(25)
$$\bar{\mu}_b(s) = \frac{\begin{vmatrix} \dfrac{\omega_1^2 \omega_f}{s^2 + \omega^2} & s^2 \\ 0 & s^2 + \omega_f^2 \end{vmatrix}}{(1-\beta)s^4 + (\omega_1^2 + \omega_2^2)s^2 + \omega_1^2 \omega_2^2}$$

The complete transformation of $\bar{\mu}_b$ into a time domain is a complex and lengthy expression which is not presented here. If only the steady state response is considered, then terms involving $e^{j\omega_f t}$ will remain, and $\mu_b(t)$ can be written as

$$\mu_b(t) = \frac{\omega_1^2}{(1-\beta)} \left[\frac{(\omega_f^2 - \omega_2^2)(-1)(\sin \omega_f t)}{(\omega_f^2 - {}_2{}^2)(\omega_f^2 - {}_1{}^2)} \right]$$

The transmissibility ratio is defined here as $\left| \dfrac{\mu_b}{X_I} \right|$ and is given by

(26) $$TR_x = \frac{\omega_1^2 (\omega_f^2 - \omega_2^2)}{(1-\beta)(\omega_f^2 - \Omega_2^2)(\omega_f^2 - \Omega_1^2)}$$

For cases of weak coupling, where $\omega_2 \approx \Omega_2$ and $\beta \approx 0$, the expression for TR_x is approximated by

(27) $$TR_x \approx \omega_1^2 \times \left| \frac{1}{\omega_f^2 - \Omega_1^2} \right| , \text{ except near resonance.}$$

The expression for θ for a ,sinusoidal forcing function is

(28) $$c\theta = \frac{\begin{vmatrix} s^2 + \omega_1^2 & \frac{\omega_1^2 \omega_f}{s^2 + \omega_f^2} \\ \beta s^2 & 0 \end{vmatrix}}{(1-\beta)s^4 + (\omega_1^2 + \omega_2^2)s^2 + \omega_1^2 \omega_2^2}$$

In the time domain,

(29) $$\theta(t) = \left(\frac{\beta \omega_1^2}{c(1-\beta)} \right) \left(\frac{\omega_f^2 \sin \omega_f t}{(\omega_f^2 - \Omega_2^2)(\omega_f^2 - \Omega_1^2)} \right)$$

Then the transmissibility ratio for rotation is given by

(30) $$TR_\theta = \frac{\theta(t)}{X_I(t)} = \frac{\omega_1^2 \omega_f^2 .}{c(1-\beta)(\omega_f^2 - \Omega_2^2)(\omega_f^2 - \Omega_1^2)}$$

4.2.3 Sinusoidal Disturbances

The response of the spring suspension system is described by plotting or listing certain parameters as a function of applied disturbance frequency. The parameters are:

$$\frac{\dot{X}_{out}}{\dot{X}_{in}} , \quad \frac{X_{out}}{X_{in}} , \quad \frac{\ddot{Y}_{out}}{\ddot{X}_{in}} , \quad \frac{Y_{out}}{X_{in}} , \quad \frac{\ddot{\theta}_{out}}{\ddot{X}_{in}} , \quad \frac{\theta_{out}}{X_{in}}$$

In all cases, the shaker displacement was 1.11 centimeter p-p . The graphs and tables for these parameters are presented on the following pages.

The upper curves in Figures 4.2-4 through 4.2-6 represent the analytical values obtained for the .01 #/inch spring suspension system. No clear explanation is known for the discrepancy between the experimental and the actual transfer functions in these figures. An examination of the associated data shows that the values of resonant frequency for the two methods differ by less than three percent. Also, the experimental curve follows the expected rolloff
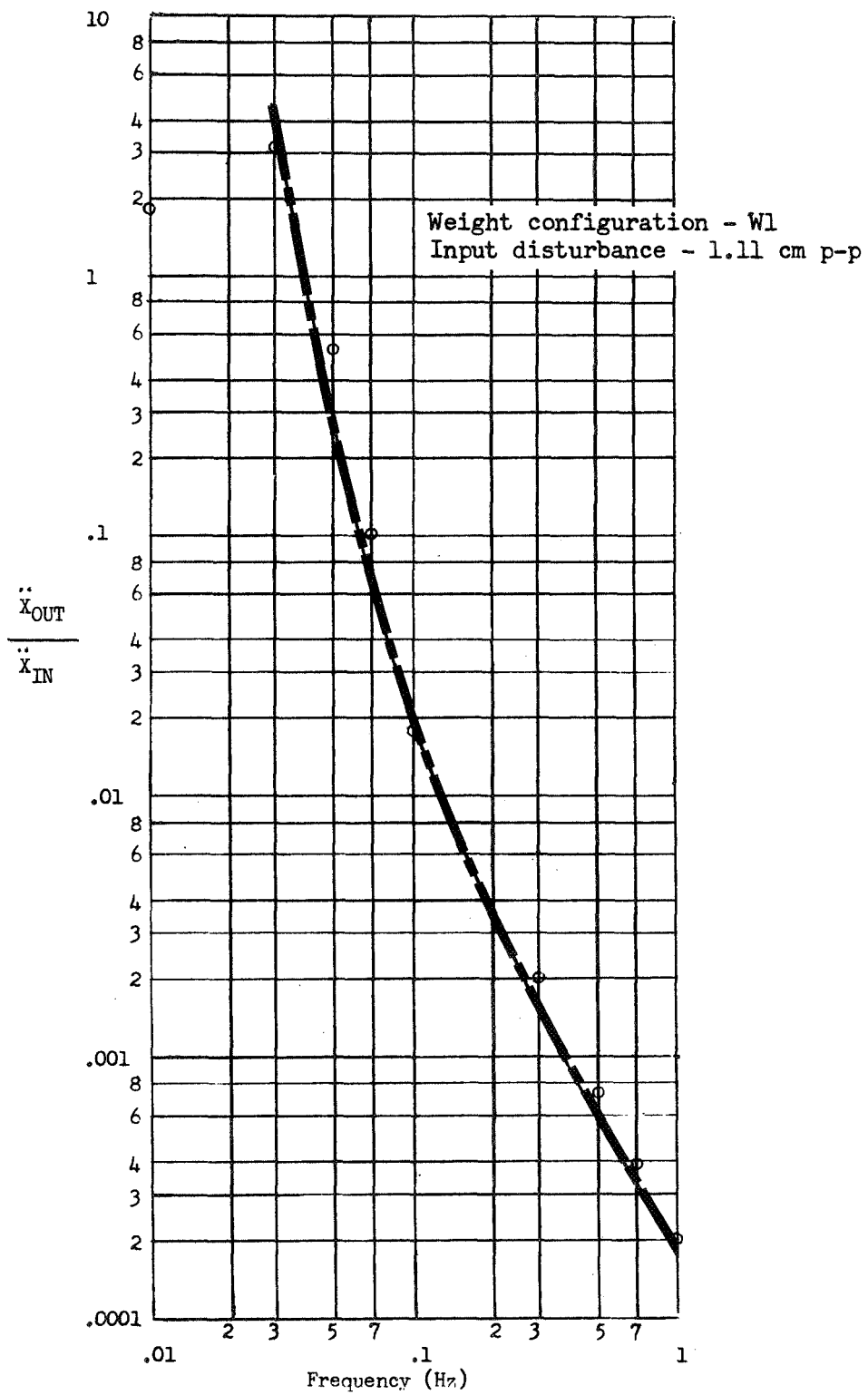
37

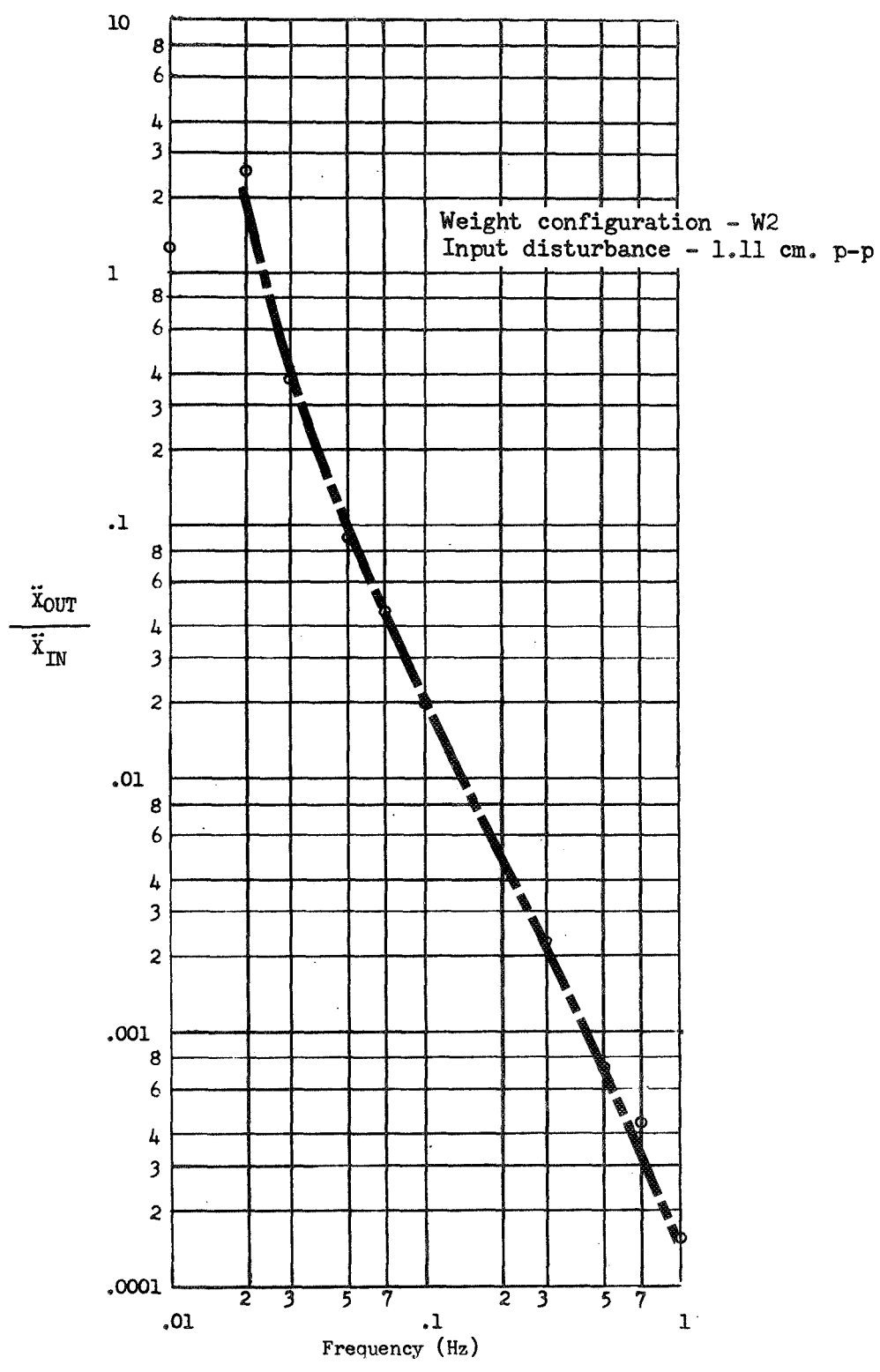Figure 4.2-1 Transfer function for spring suspension system (K=.005 #/inch)

Figure 4.2-2   Transfer function for spring suspension system (K=.005 #/inch)
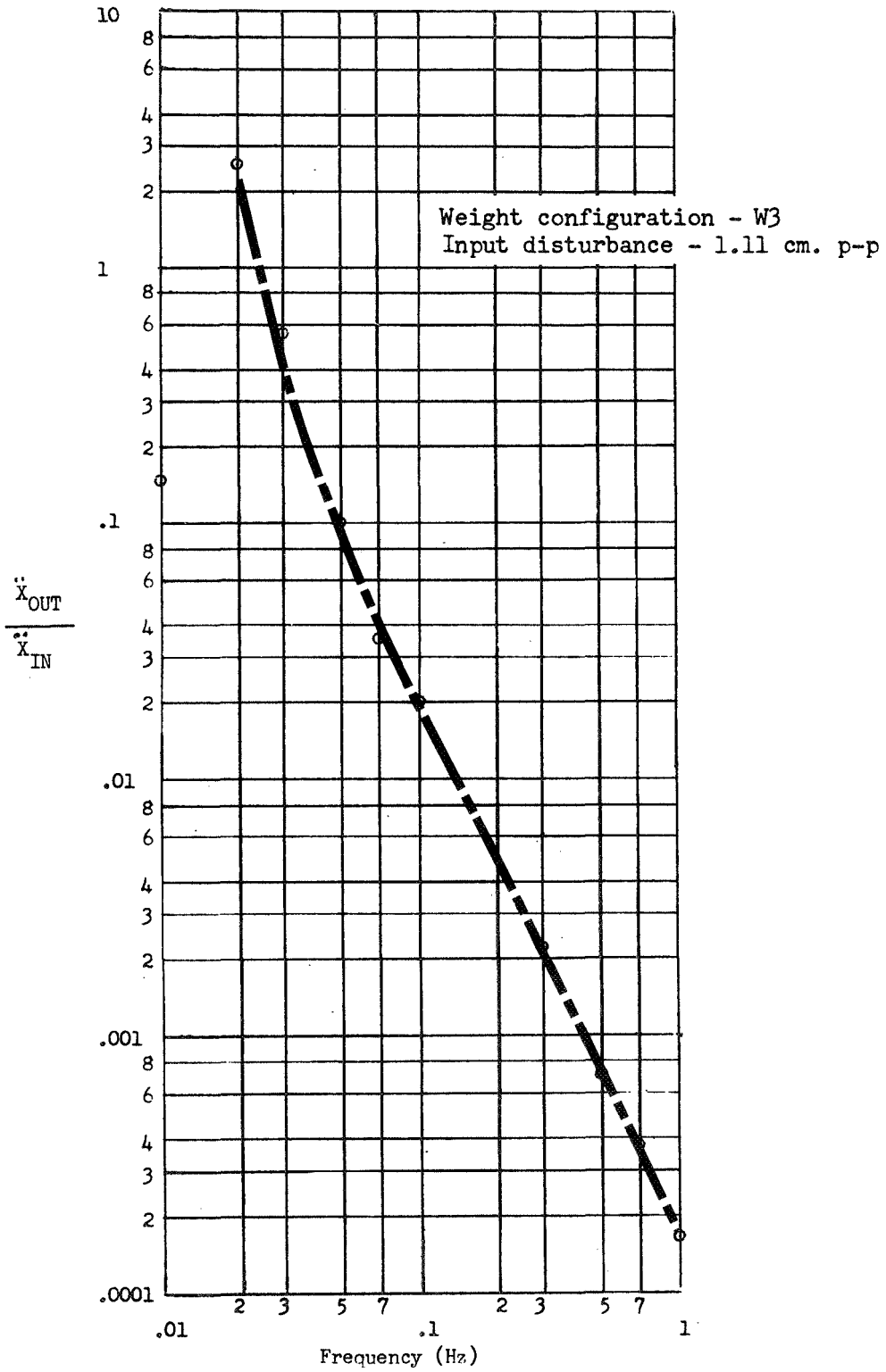
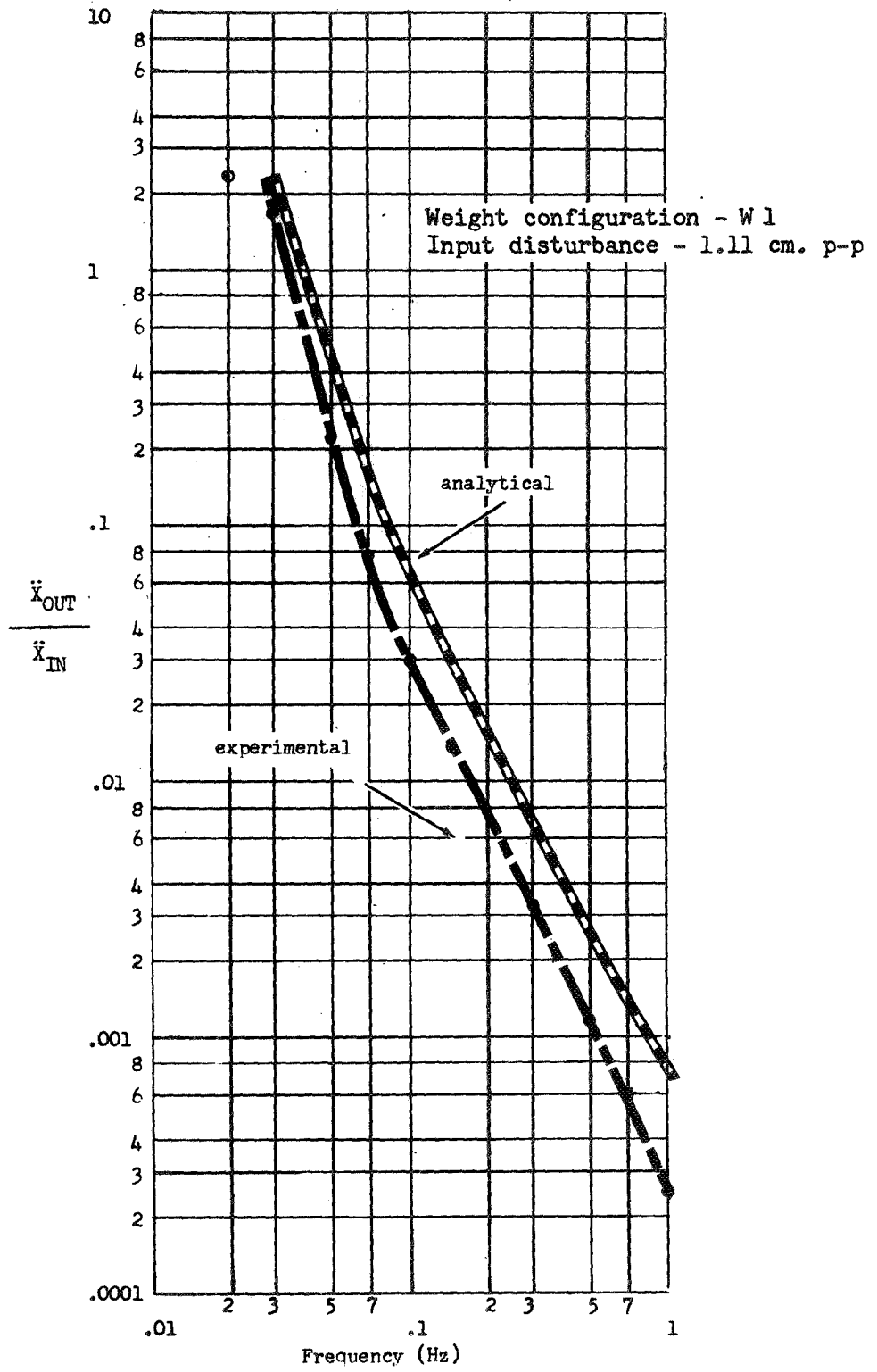Figure 4.2-3   Transfer function for spring suspension system (K=.005 #/inch)

40

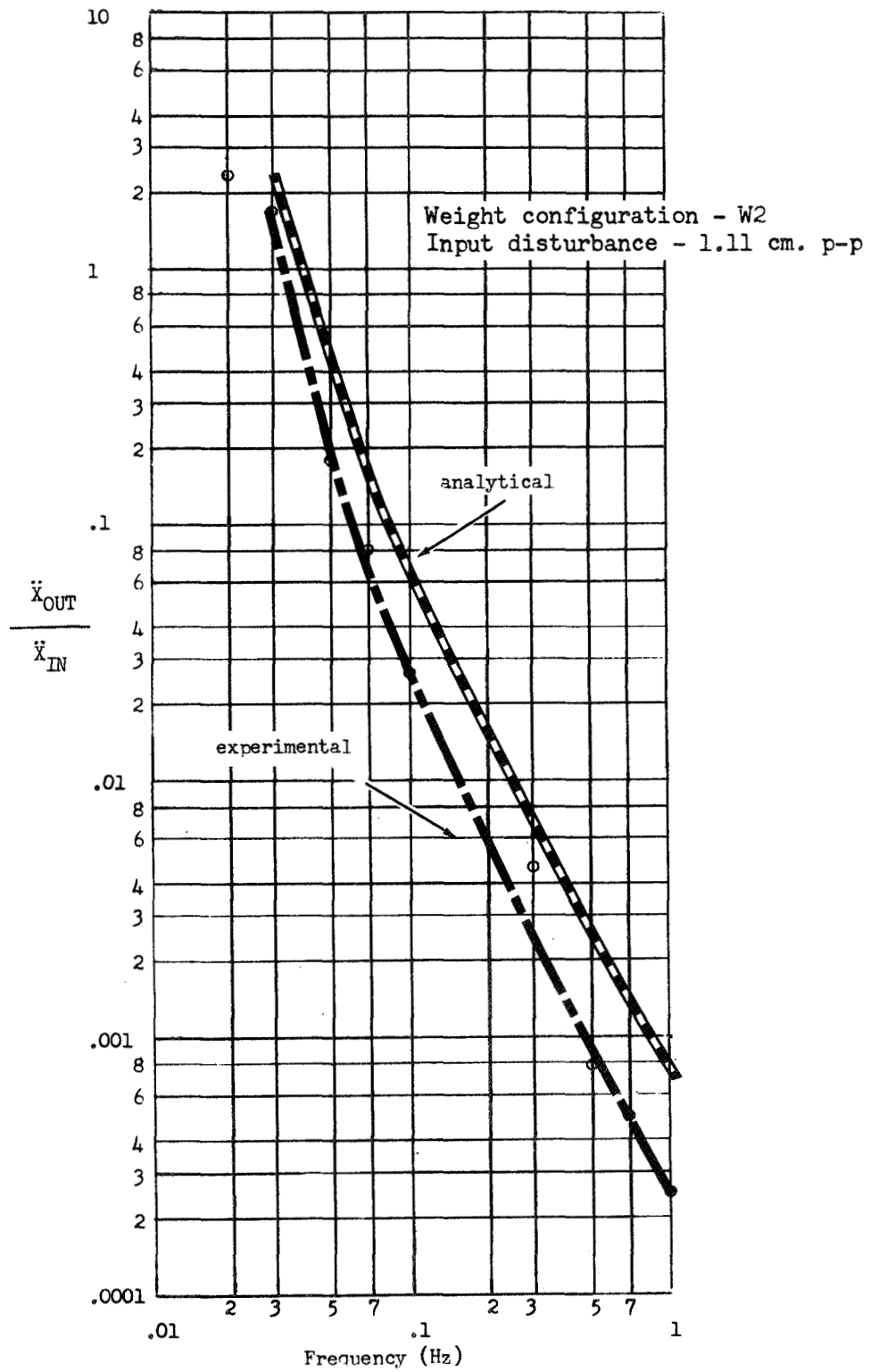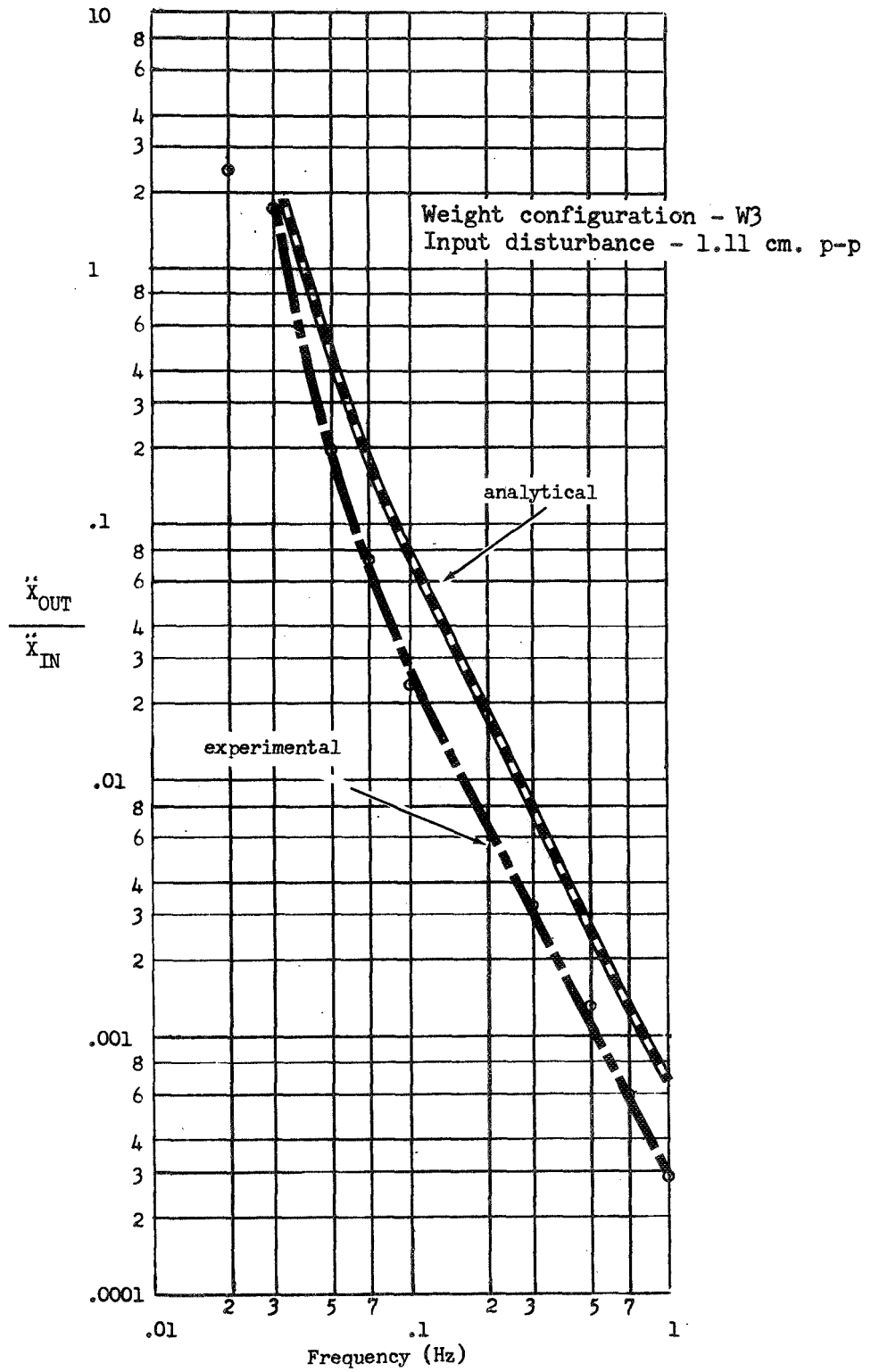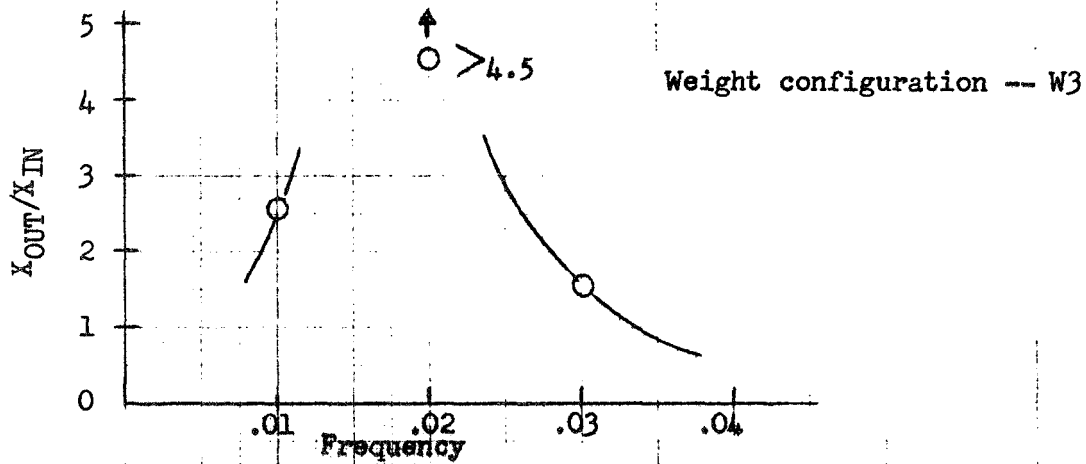Figure 4.2- 4 Transfer function for spring suspension system (K=.01 #/inch)
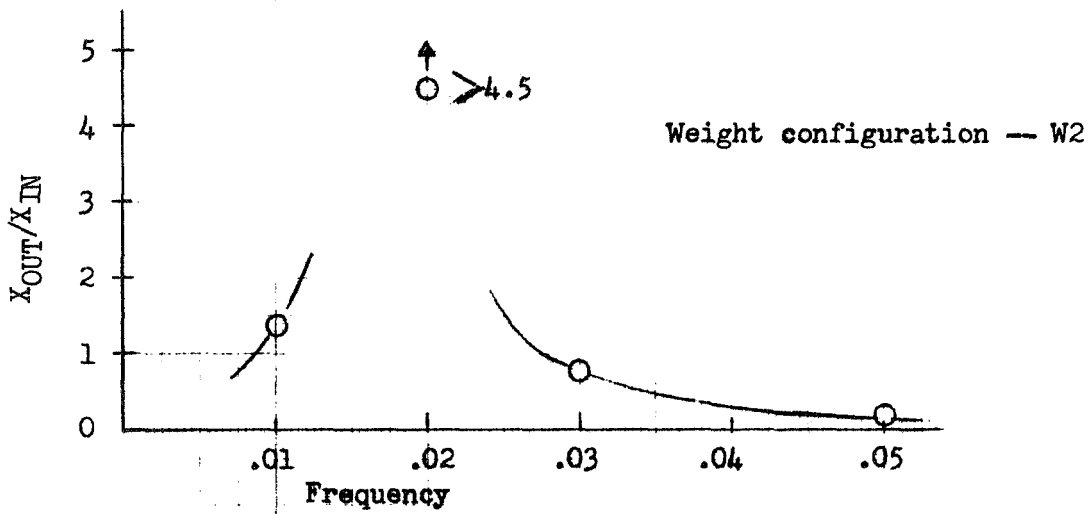
Weight configuration – W2
Input disturbance – 1.11 cm. p-p

analytical

experimental

$\dfrac{\ddot{X}_{OUT}}{\ddot{X}_{IN}}$

Frequency (Hz)

Figure 4.2-5 Transfer function for spring suspension system (K=.01 #/inch)

Figure 4.2-6 Transfer function for spring suspension system (K=.01 #/inch)
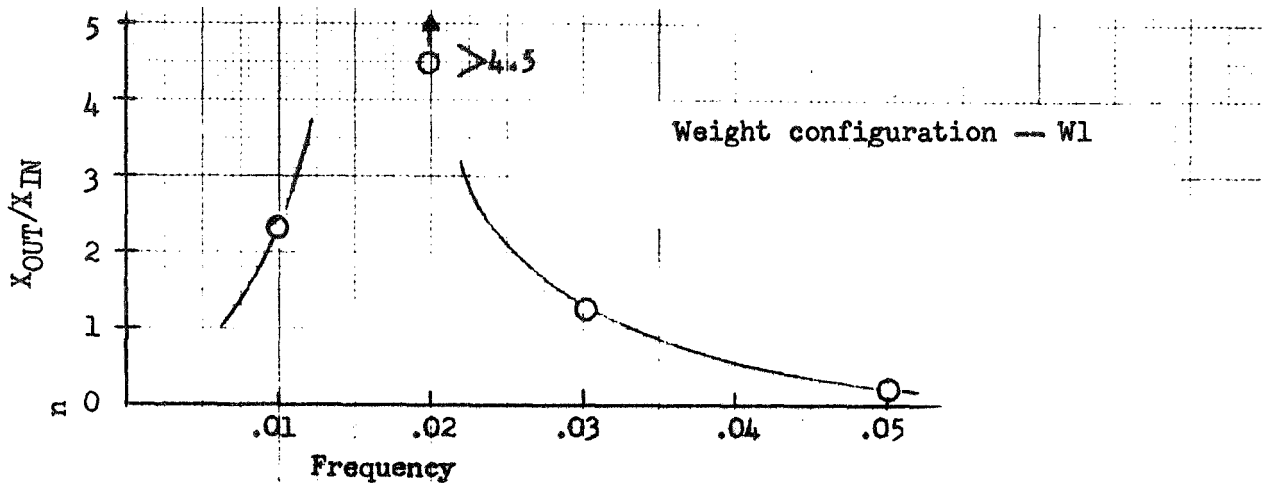
Figure 4.2-7 Displacement transmissibility of 0.005 #/inch spring suspension system for sinusoidal disturbance of 1.11 cm p-p
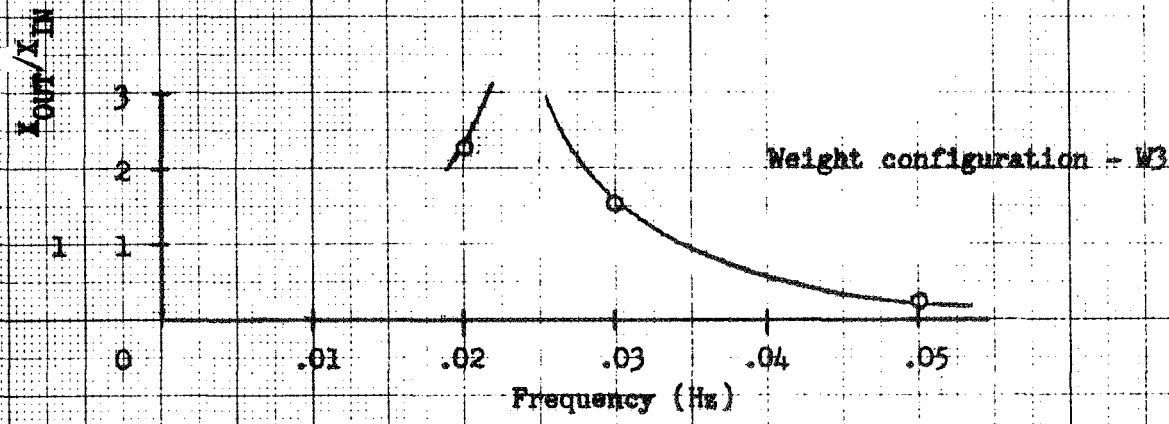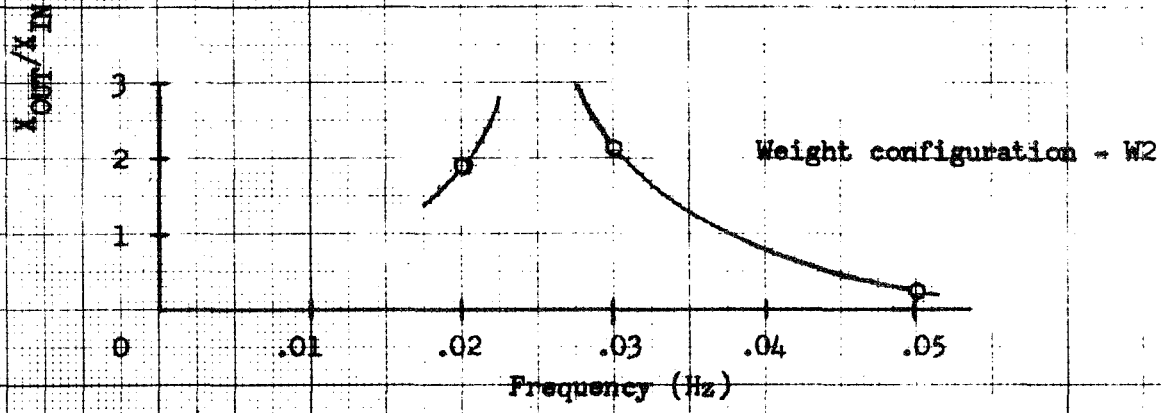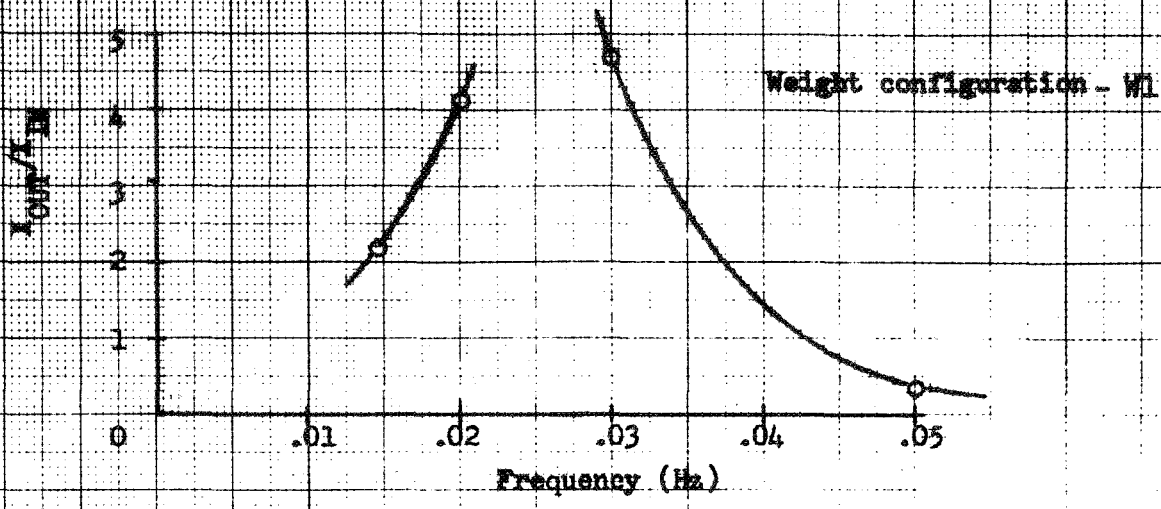
44

Figure 4.2-8 Displacement transmissibility of 0.01 #/inch spring suspension system for sinusoidal disturbance of 1.11 cm p-p

Table 4.2-1 Values of $\ddot{Y}_{OUT}/\ddot{X}_{IN}$ for spring suspension systems with sinusoidal driving force of 1.11 cm p-p

Spring Constant (#/inch)	Weight Configuration	Frequency (Hz)			
		.01	.02	.03	.05
K=.001		No discernible reading			
K=.005	W1	----	----	----	----
	W2	----	Trace	Trace	----
	W3	----	0.74	0.33	----
K=.01	W1	----	0.74	1.1	----
	W2	----	----	0.55	----
	W3	----	0.24	0.45	----

46

Table 4.2-2 Values of Y_{OUT}/X_{IN} for spring suspension systems with sinusoidal

driving force of 1.11 cm p-p

Spring Constant (#/inch)	Weight Configuration	Frequency(Hz)			
		.01	.02	.03	.05
K=.001		No discernible reading			
K=.005	W1	----	0.27	----	----
	W2	----	0.14	0.18	----
	W3	0.20	0.41	0.90	----
K=.01	W1	----	0.64	1.94	----
	W2	----	----	0.80	----
	W3	----	0.18	0.57	----

Table 4.2-3 Values of $\ddot{\Theta}_{OUT}/\ddot{X}_{IN}$ for spring suspension systems with sinusoidal driving force of 1.11 cm p-p

$$\left[\frac{\widehat{sec}/sec^2}{10^{-6}g}\right]$$

Spring Constant (#/inch)	Weight Configuration	Frequency (Hz)						
		.01	.02	.03	.05	.07	.1	.15
K=.001		No discernible reading						
K=.005	W1	4.84(6	1.8(6	1.6(4	----	----	----	----
	W2	----	1.21(6	4.3(6	----	----	----	----
	W3	----	3.64(6	1.27(7	----	----	----	----
K=.01	W1	----	----	----	8.8(5	4.9(4	1.2(4	5.4(3
	W2	----	----	----	1.93(5	Trace	----	----
	W3	----	----	----	0.97(5	----	----	----

48

Table 4.2-4 Values of θ_{OUT}/X_{IN} for spring suspension systems with sinusoidal driving force of 1.11 cm p-p

(sec/cm)

Spring Constant (#/inch)	Weight Configuration	Frequency (Hz)			
		.01	.02	.03	.05
K=.001		No discernible reading			
K=.005	W1	----	2300	1620	----
	W2	----	3100	5660	----
	W3	3800	1200	8100	----
K=.01		No valid data taken			

for driving frequencies much greater than the resonant frequency of the system.
It appears that the recorded value for platform acceleration is simply less
than the predicted value by a constant factor of approximately two. Among the
factors which have been considered as possible causes for low readings of out-
put acceleration are cable drag, drag between the platform and the table, and
faulty accelerometer calibration. Since an examination of the platform in the
free floating condition does not show any appreciable damping, the response of
the accelerometers for the test range and frequency is being investigated.

4.2.4 Non-sinusoidal Disturbances

As previously mentioned, the ramp disturbances provided no measurable
amount of platform motion, except for a steady variation in the X-direction to
the final displacement.

Data for the square wave pulses and the step function are presented in
Table 4.2-5 and Table 4.2-6. A comparison of the analytical and laboratory
values obtained for the 0.01 springs is presented in Table 4.2-7 for the step
function.

The recorded data for the square wave pulses is the maximum value during
and immediately after application of the pulses. The response of the system for
this disturbance was dependent on the phase of the response at the time the sec-
ond pulse was applied. No analytical study was made for this response.

4.2.5 Discussion

Generally, the spring suspension system showed no surprises, and behaved
as the equations of motion predicted.

Excluding those tests where a forcing function near the resonant frequency
was applied, the only parameters which could be consistently measured were the
X-acceleration and, to a lesser extent, the angular acceleration and X-displace-
ment. Cases where no data is recorded for a parameter means that the value of
that parameter was below the resolution capabilities of its overall detector
system. The resolutions of the various detector systems are given below. All
values are approximate since they depend on the ability of the laboratory
personnel to read small variations on the recorder strip.

X, Y	-	0.1 cms
$\ddot{X}$	-	$2 \times 10^{-6} g$
$\ddot{Y}$	-	$4.5 \times 10^{-6} g$
$\ddot{\theta}$	-	11 $\widehat{sec}/\overline{sec}^2$
θ	-	4 min., but dependent on X-displacement

Since, virtually no data was recorded for the .001 spring system, it cer-
tainly is a lower boundary for the force constant of a system to be operated
within constraints equal to the resolution values cited above for the instru-
mentation.

It is apparent that future quantitative tests of this nature will require
more sensitive instrumentation and/or some modification of the suspension

50

Table 4.2-5   Response of spring suspension system (K=.01 #/inch) to:
(a) 0.635 cm step function
(b) 1.27 cm p-p square wave

Weight Configuration	Type of Disturbance	$\ddot{x}_{OUT}$ $(10^{-5}g)$	$\ddot{\theta}_{OUT}$ $(\widehat{sec}/sec^2)$	x_{OUT} (cm)
W1	Step	1.5	13.5	1.2
	Square wave	2.2	37.8	1.9
W2	Step	1.4	17.4	1.2
	Square wave	2.1	46.5	2.0
W3	Step	1.2	-----	0.7
	Square wave	1.7	16.2	0.8

Table 4.2-6 Response of spring suspension system (K=.005 #/inch) to:
(a) 0.635 cm step function
(b) 1.27 cm p-p square wave

Weight Configuration	Type of Disturbance	$\ddot{X}_{OUT}$ $(10^{-5}g)$	$\ddot{\theta}_{OUT}$ $(\widehat{sec}/sec^2)$	X_{OUT} (cm)	θ_{OUT} $(\widehat{sec})$
W1	Step	0.9	---	0.8	4.4
W1	Square wave	1.1	---	1.3	11.6
W2	Step	0.9	---	0.7	---
W2	Square wave	0.67	---	0.5	---
W3	Step	0.67	21.7	0.48	1400
W3	Square wave	0.9	38	0.72	1900

Table 4.2-7 Values for measured and calculated responses of spring suspension
system (K=.01 #/inch) to 0.635 cm step function

Weight Configuration	Parameter	Measured Value	Calculated Value
W1	X Period (sec)	38	37.6
	θ Period (sec)	24	24.4
	X (cm)	0.24	0.25
	$\ddot{X}$ (10^{-5}g)	1.5	1.8
	$\ddot{\theta}$ (sec/sec^2)	13.5	12.8
W2	X Period (sec)	39	37.6
	θ Period (sec)	26	28.5
	X (cm)	0.24	0.25
	$\ddot{X}$ (10^{-5}g)	1.4	1.8
	$\ddot{\theta}$ (sec/sec^2)	17.4	12.6
W3	X Period (sec)	39	37.6
	θ Period (sec)	26	28.5
	X (cm)	0.17	0.25
	$\ddot{X}$ (10^{-5}g)	1.2	1.8
	$\ddot{\theta}$ (sec/sec^2)	10.8	10.5

systems, the platform mass characteristics or the shaker stroke.

One other point is worthy of mention that does not appear in the recorded data of this section. In several cases where a ramp function was applied to a free floating system which had some small translational and rotational motion prior to the application of the ramp, there was a noticeable dimunition of this motion while the ramp was being applied.

54

4.3 HYSTERESIS SYSTEM

4.3.1 General

Tests were made with the hysteresis system for the three weight arrangements and for weight arrangement W2 with the magnets removed from the suspension system. This last test, therefore, has no hysteresis damping and was made as a control case to better assess the effects of this type of damping.

4.3.2 Sinusoidal Disturbances

The response of the systems to sinusoidal disturbances is presented in Figures 4.3-1 through 4.3-10 and in Tables 4.3-1 and 4.3-2.

The transfer function curves for $\ddot{X}$ in Figures 4.3-1 through 4.3-4 behave as expected. Since the curves are relatively smooth with the chosen data points, no break has been drawn to indicate any resonance conditions except at the lower resonant frequency, where it is evident. The response as a function of weight arrangement varies less than the same function for the spring systems. A comparison of Figures 4.2-2 and 4.2-4 shown that the transmissibility is reduced when the magnets are removed, or, stated another way, that the damping increases the transmissibility. This is to be expected.

The reverse in slope at the higher frequencies in Figures 4.3-1 through 4.3-4 is due to a "slap" in the string which is used to attach the hysteresis system to the platform. At these frequencies the hysteresis disc cannot respond as fast as the shaker is moving, and some slack occurs. When this slack is taken up it causes an impulse motion to be applied to the platform.

Figures 4.3-8 through 4.3-10 show a marked increase in the ratios of $\ddot{\theta}/\ddot{X}$-in over those for the spring suspension system. To some extent this was due to the higher value of effective spring constant, but primarily it is due to the loss of tangential restoring force caused by the suspension arrangement, in which all restraining forces are initially aligned along the X and Y axes. Again, Figure 4.3-10 shows a reduction in transmissibility over that of the damped systems.

4.3.3 Non-sinusoidal disturbances

The ramp function did not produce any detectable motion except for a constant displacement to the final position along the X-axis.

Data for the square wave pulses was significantly affected by the string slap. By pre-tensioning the string it was possible to obtain reliable initial data in one direction of shaker motion, i.e., when the shaker acted to pull on the string. However, when the shaker returned suddenly to its original position, slack appeared in the string. An attempt was made to overcome this problem by reducing the height of the pulses, but the response was too small to be measured.

Data for the step function is shown in Figures 4.3-11 through 4.3-14 and Table 4.3-3. Apparently there is some frictional damping occurring, since the peak amplitudes for the system with no magnets show a decrease in peak amplitude as a function of the number of cycles, as represented in Figure 4.3-14.
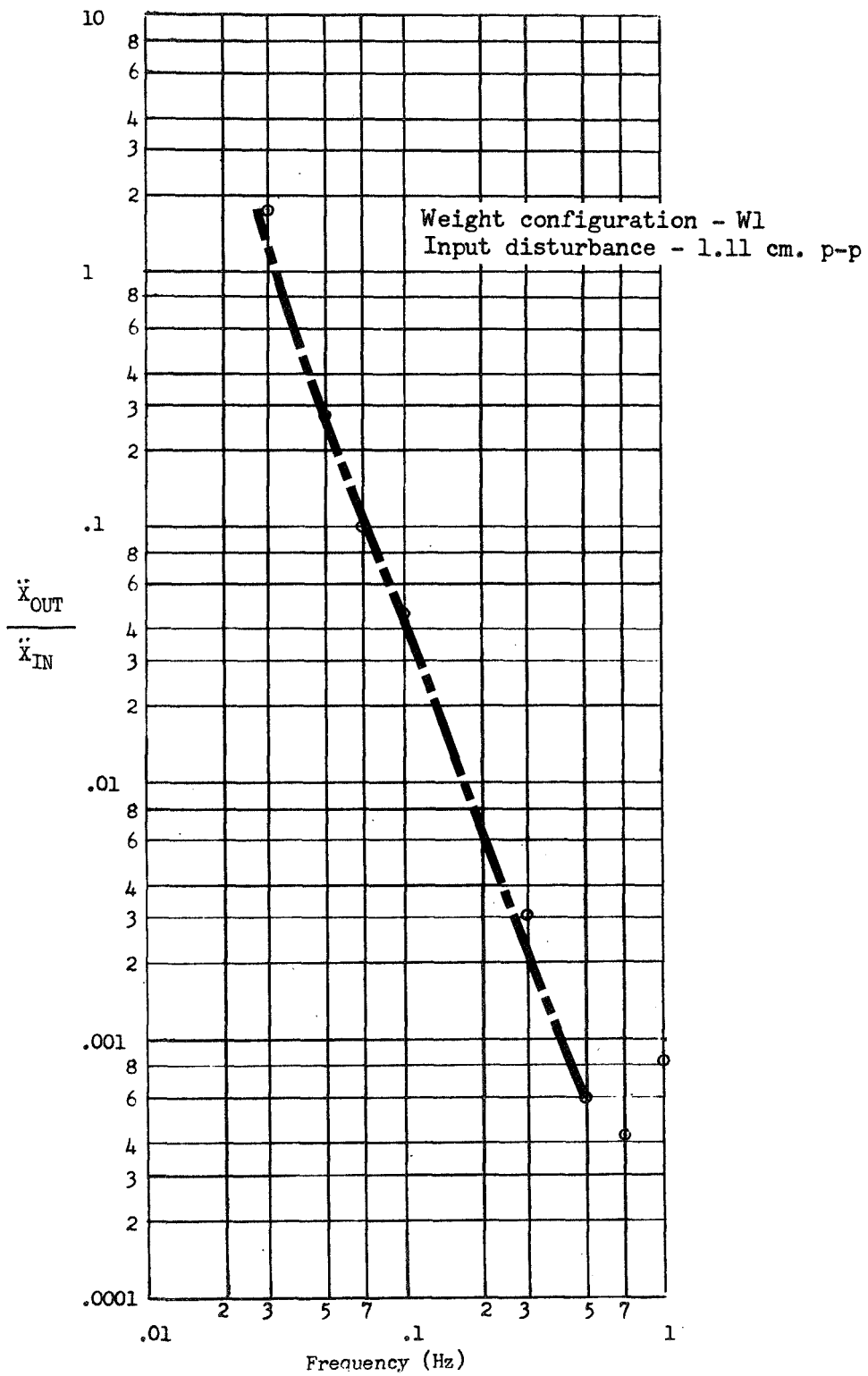
Weight configuration - W1
Input disturbance - 1.11 cm. p-p

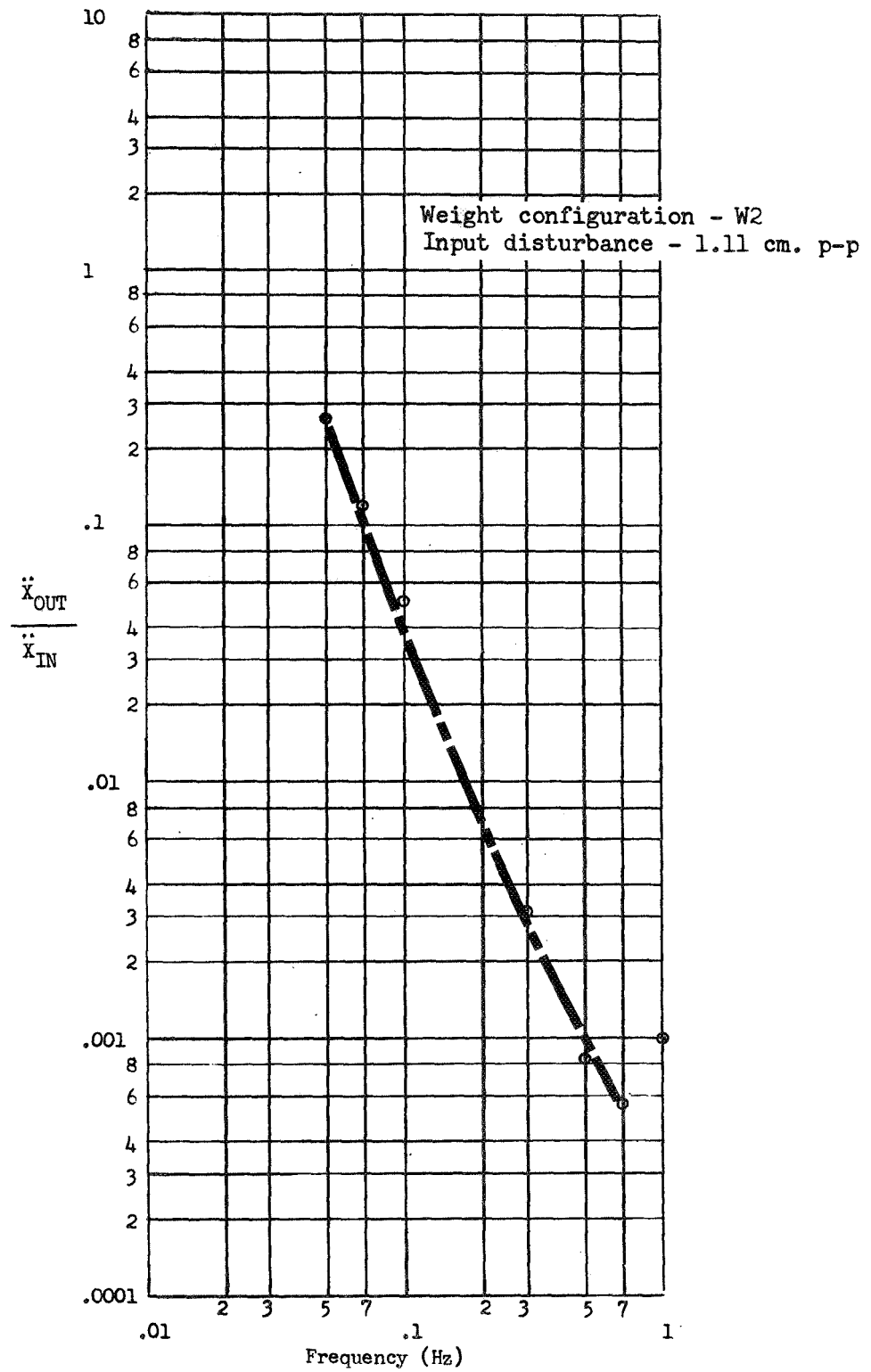Figure 4.3-1   Transfer function for hysteresis suspension system

56

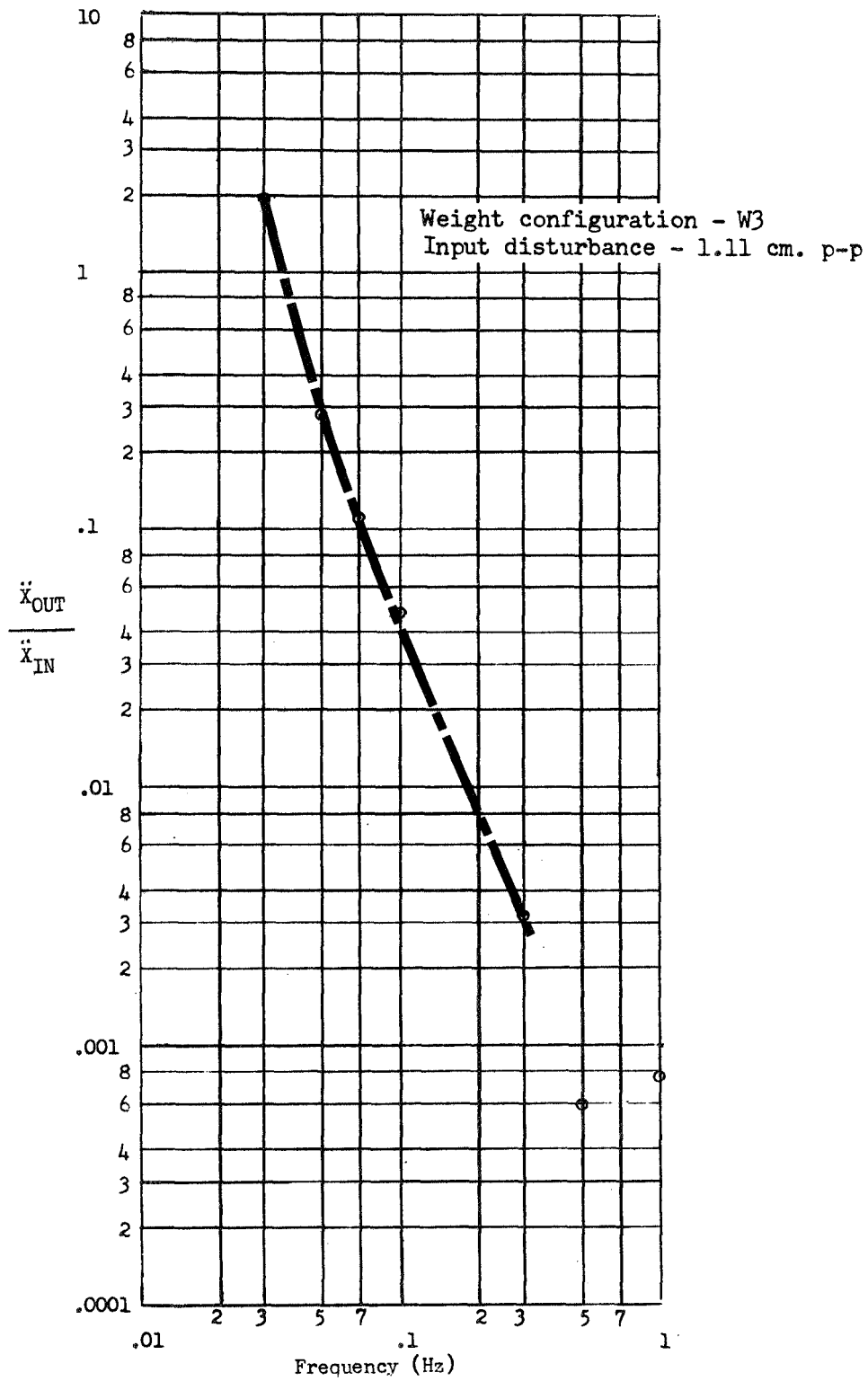Figure 4.3-2 Transfer function for hysteresis suspension system

Figure 4.3-3   Transfer function for hysteresis suspension system
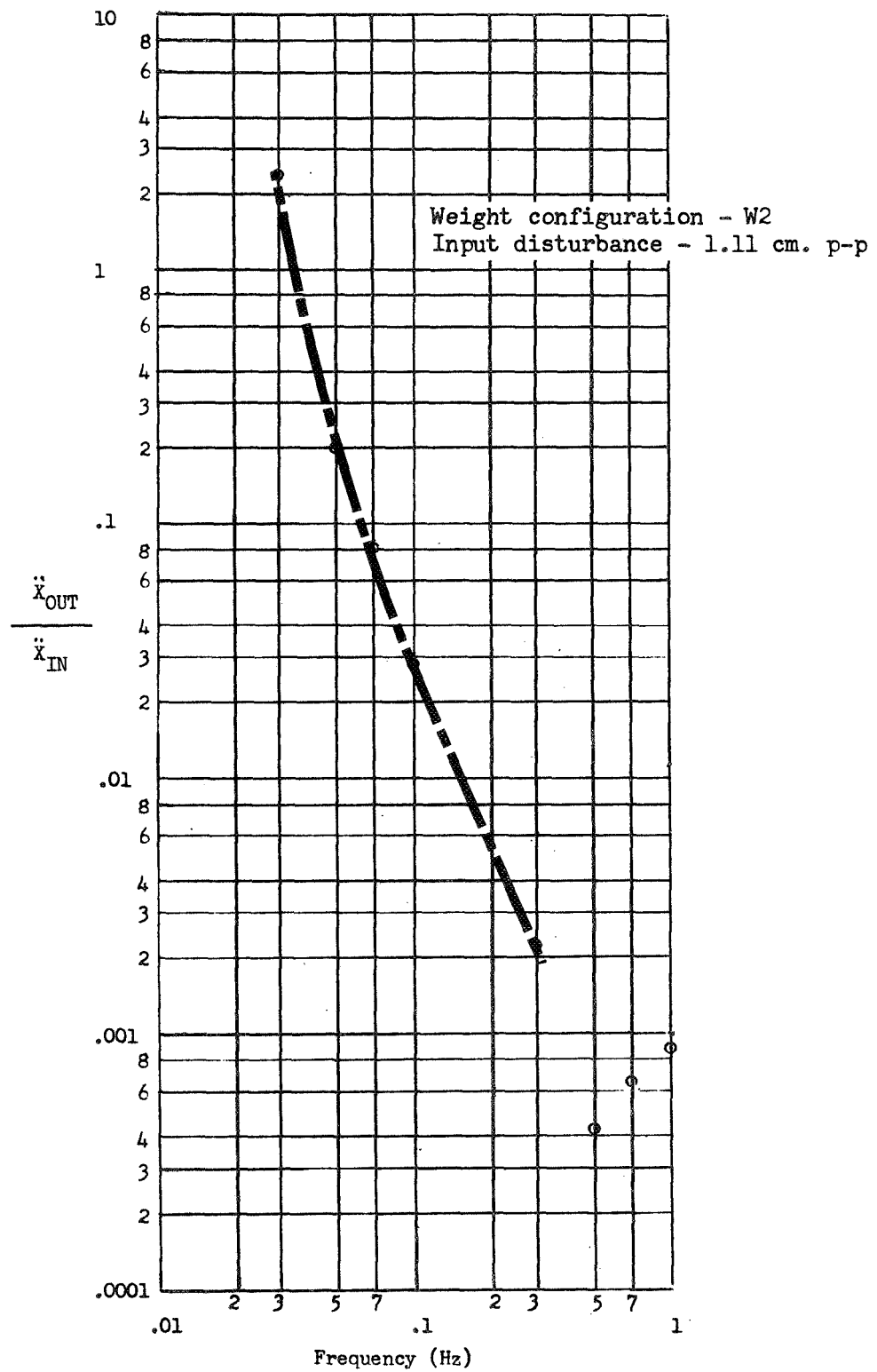
58

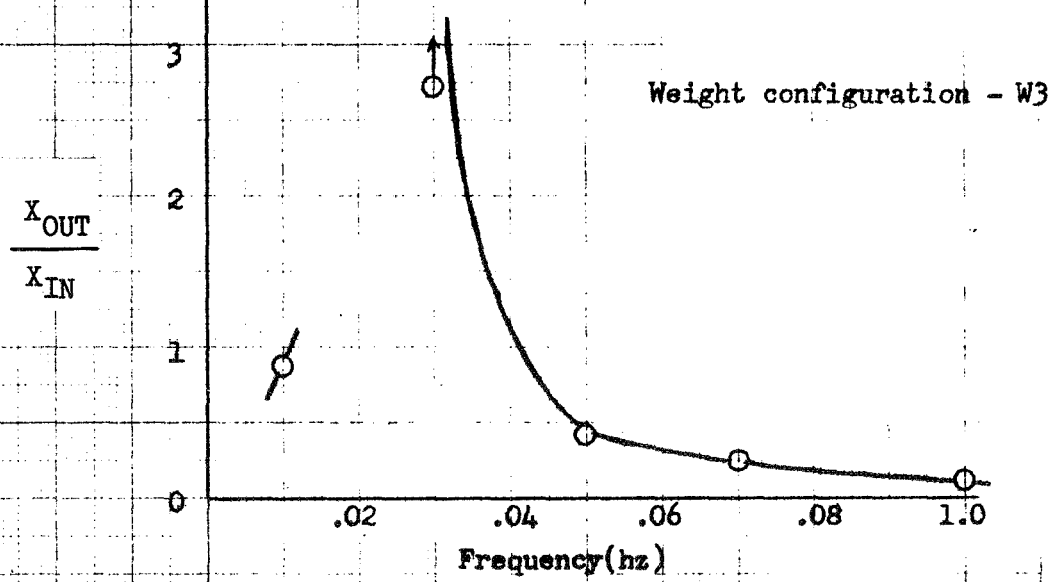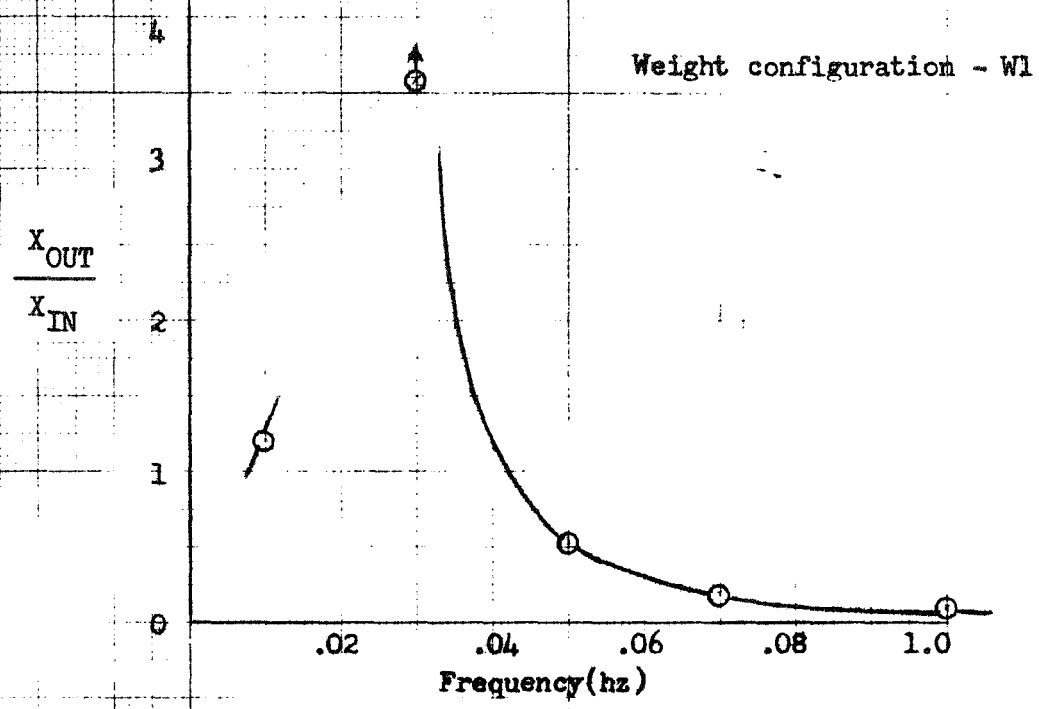Figure 4.3-4   Transfer function for hysteresis suspension system w/o magnets

59

Figure 4.3-5 Displacement transmissibility of hysteresis suspension system
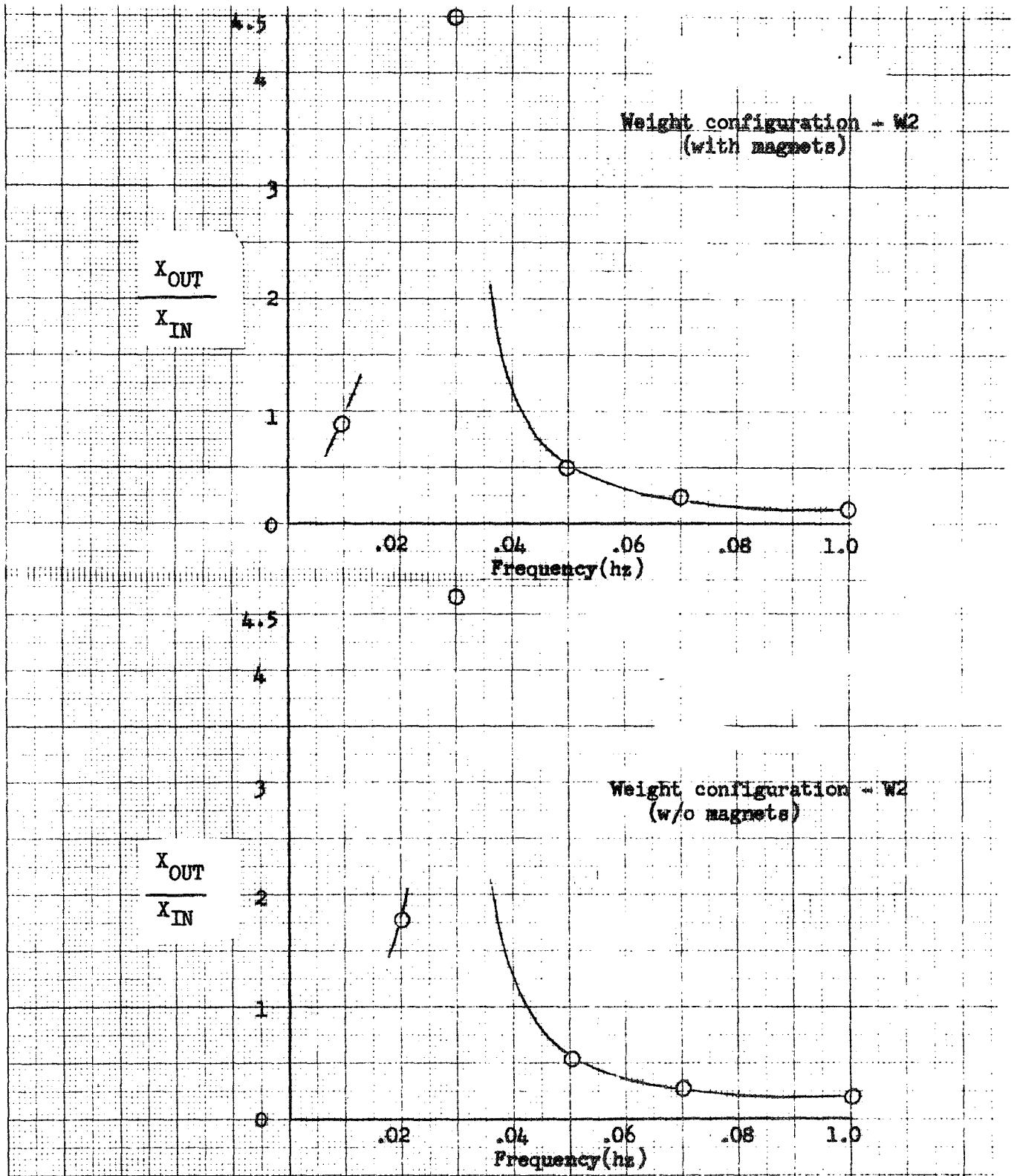for sinusoidal disturbance of 1.11 cm p-p

60

Figure 4.3-6 Displacement transmissibility of hysteresis suspension system (with and w/o magnets) for sinusoidal disturbance of 1.11 cm p-p
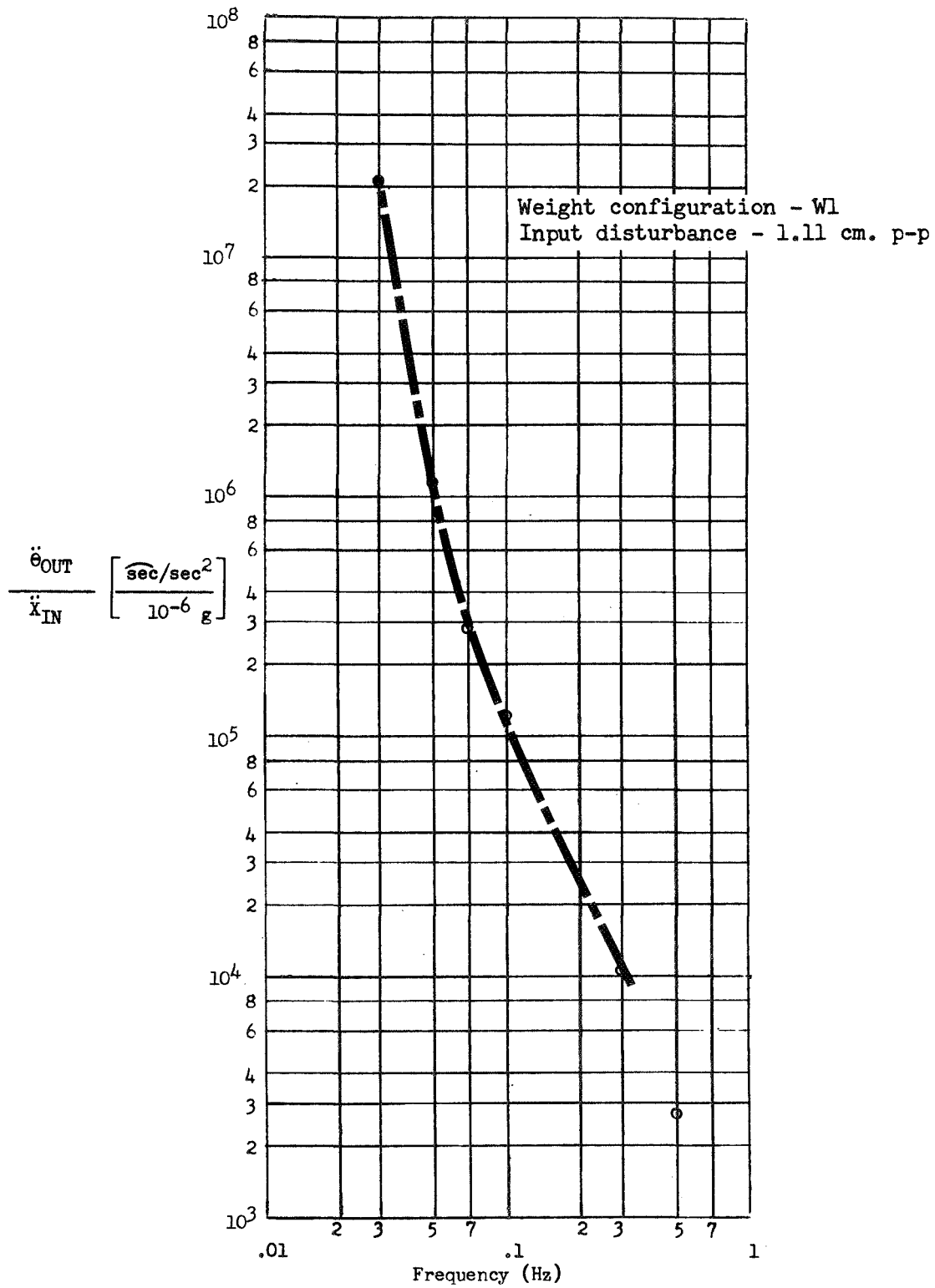
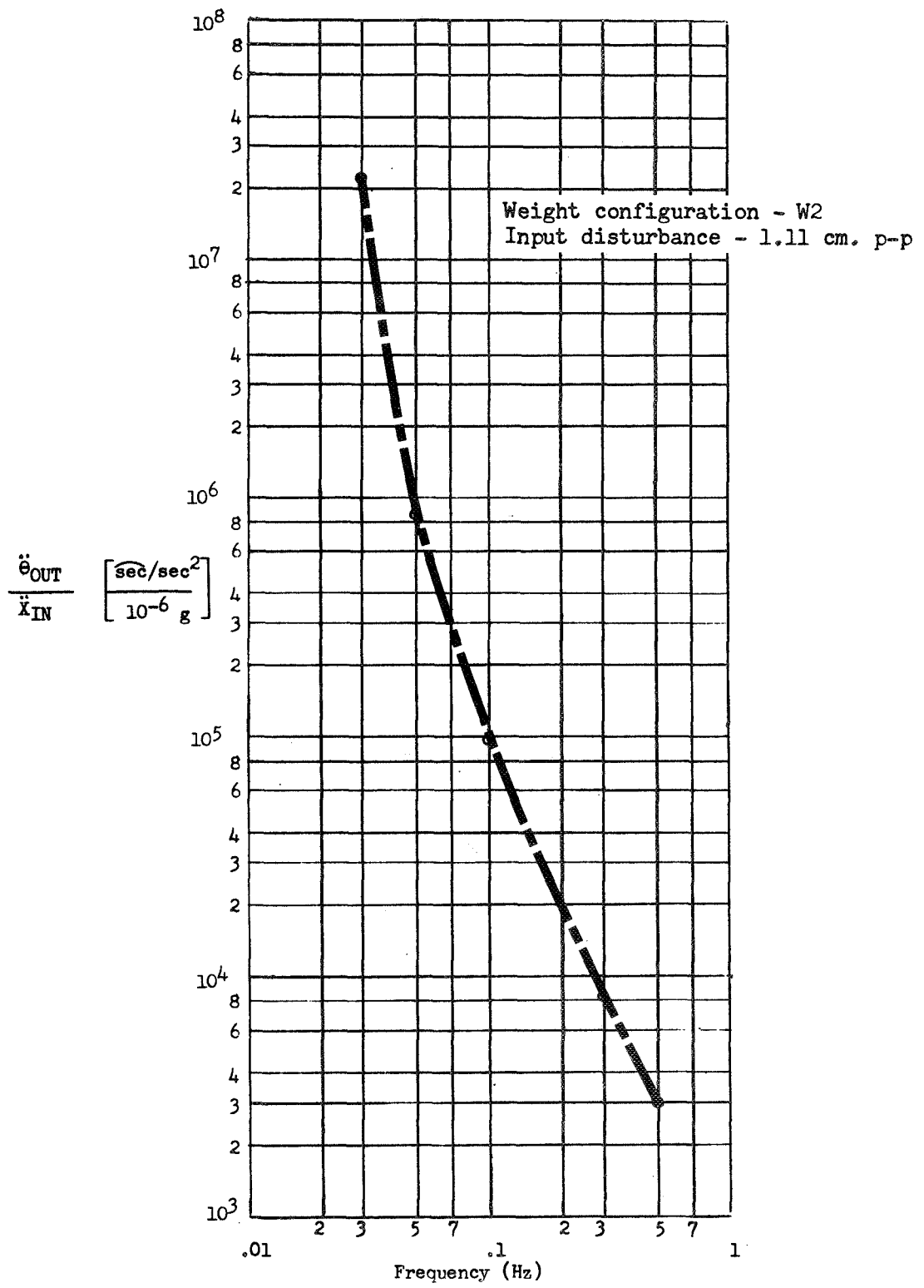Figure 4.3-7   Transfer function for hysteresis suspension system

62

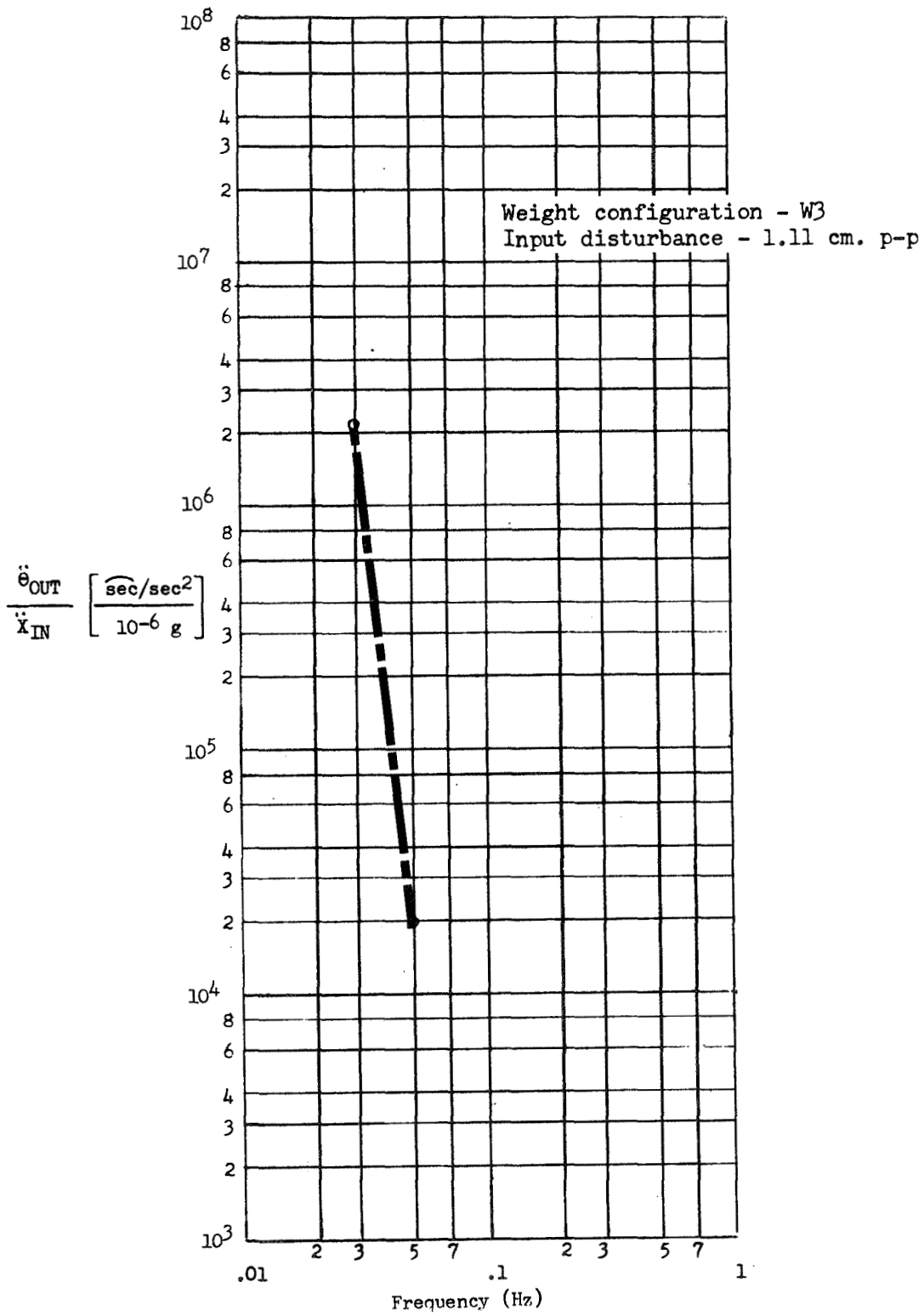Figure 4.3-8   Transfer function for hysteresis suspension system

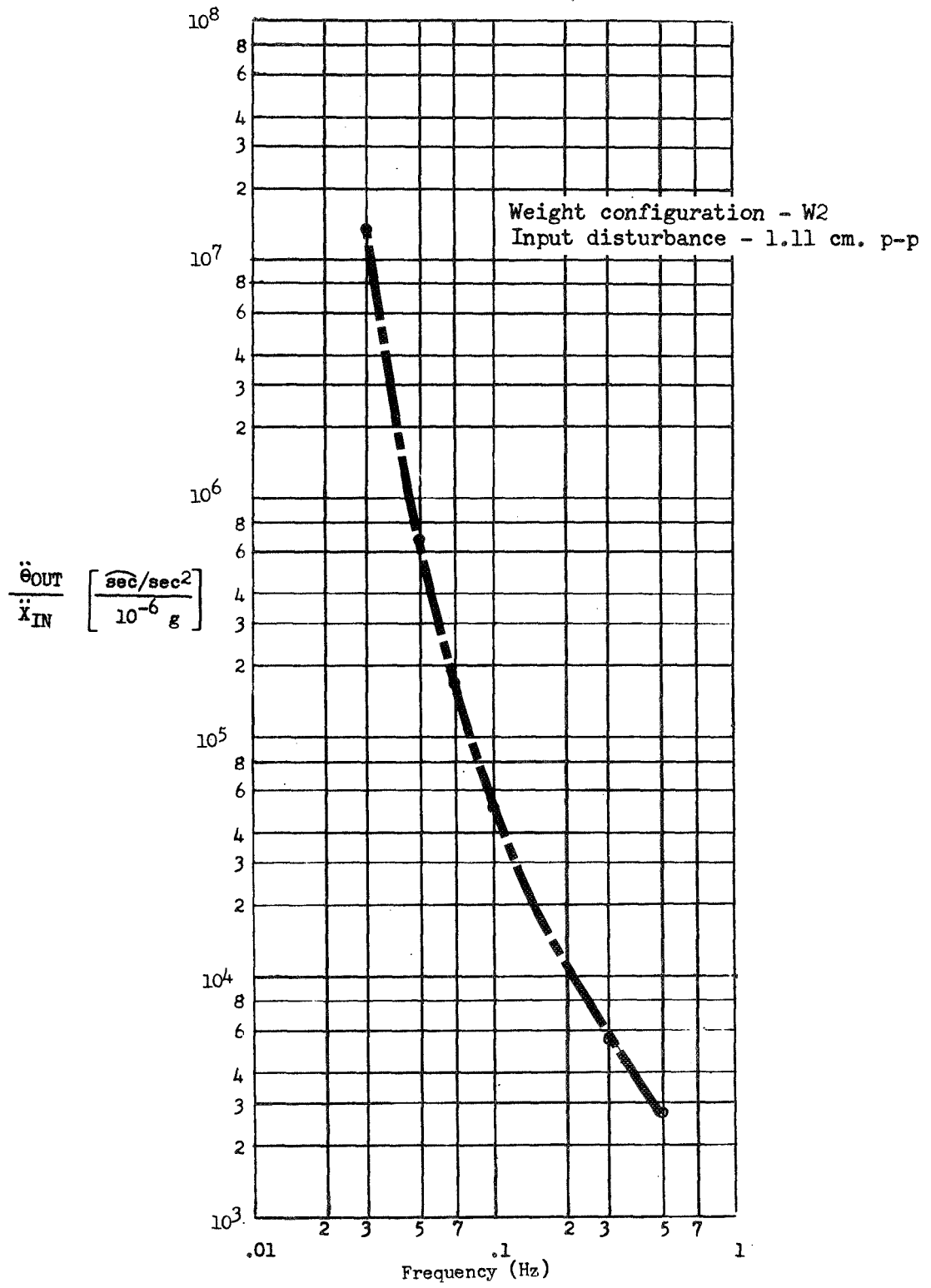Figure 4.3-9 Transfer function for hysteresis suspension system

Figure 4.3-10 Transfer function for hysteresis suspension system w/o magnets

Table 4.3-1 Values of $\ddot{Y}_{OUT}/\ddot{X}_{IN}$ for hysteresis suspension system
with sinusoidal disturbance of 1.11 cm p-p

	Weight Configuration	Frequency (Hz)			
		.02	.03	.05	.07
With magnets	W1	---	.22	---	---
	W2	---	.17	.04	---
	W3	---	.11	.04	---
w/o magnets	W2	---	---	.14	---

Table 4.3-2 Values of Y_{OUT}/X_{IN} and θ_{OUT}/X_{IN} for hysteresis suspension system with sinusoidal disturbance of 1.11 cm p-p

Y_{OUT}/X_{IN}

	Weight Configuration	Frequency (Hz)				
		.02	.03	.05	.07	.10
With magnets	W1	---	0.9	---	---	---
	W2	---	0.63	0.18	---	---
	W3	---	0.59	0.14	---	---
w/o magnets	W2	---	0.63	0.10	---	---

θ_{OUT}/X_{IN} (sec/cm)

	Weight Configuration	Frequency (Hz)				
		.02	.03	.05	.07	.10
With magnets	W1	---	700[†]	---	---	---
	W2	---	650	220	135	---
	W3	---	254[†]	---	---	---
w/o magnets	W2	---	650	---	---	---

† Cut off by sensor

67

A_1 = Height of first response peak after application of disturbance

A_N = Height of N'th response peak after application of disturbance
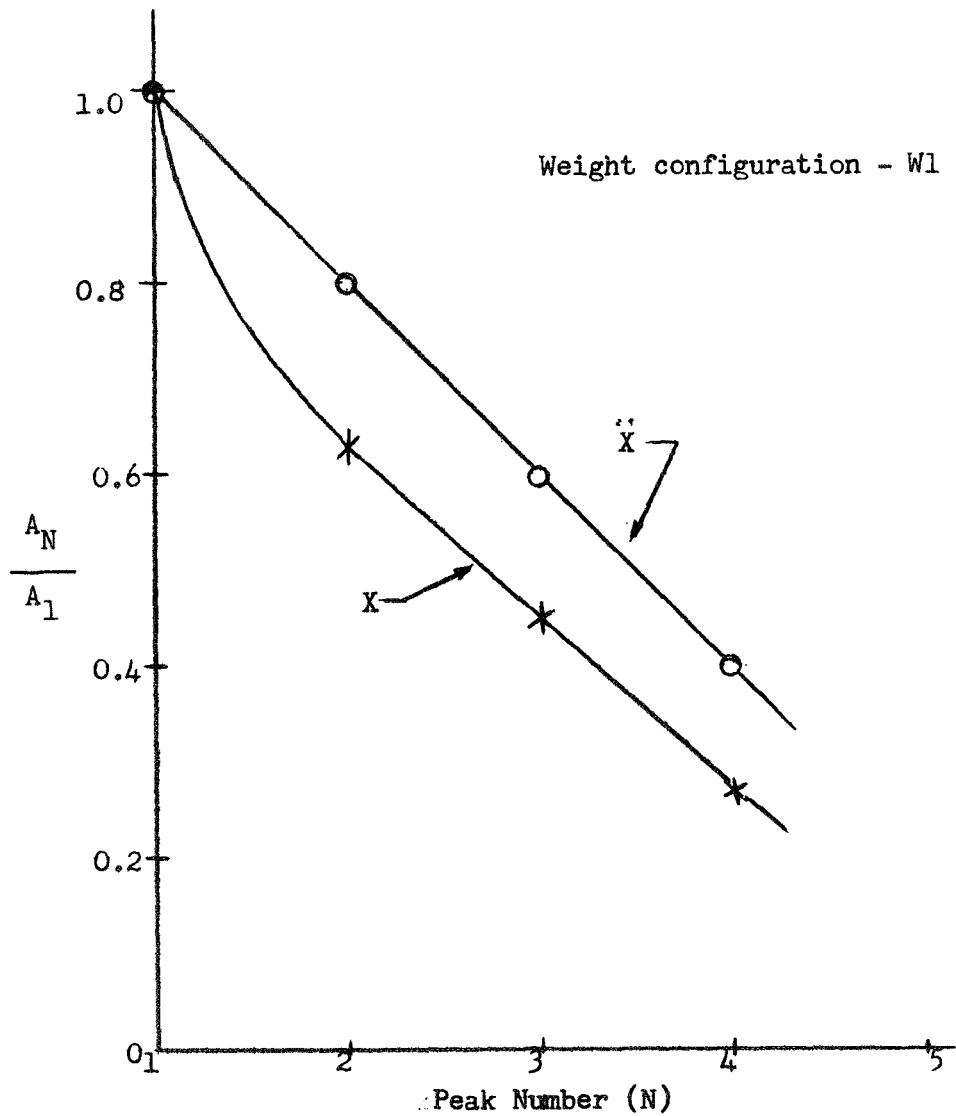

Figure 4.3-11   Peak height ratios for response of hysteresis system
to .635 cm step function

A_1 = Height of first response peak after application of disturbance

A_N = Height of N'th response peak after application of disturbance
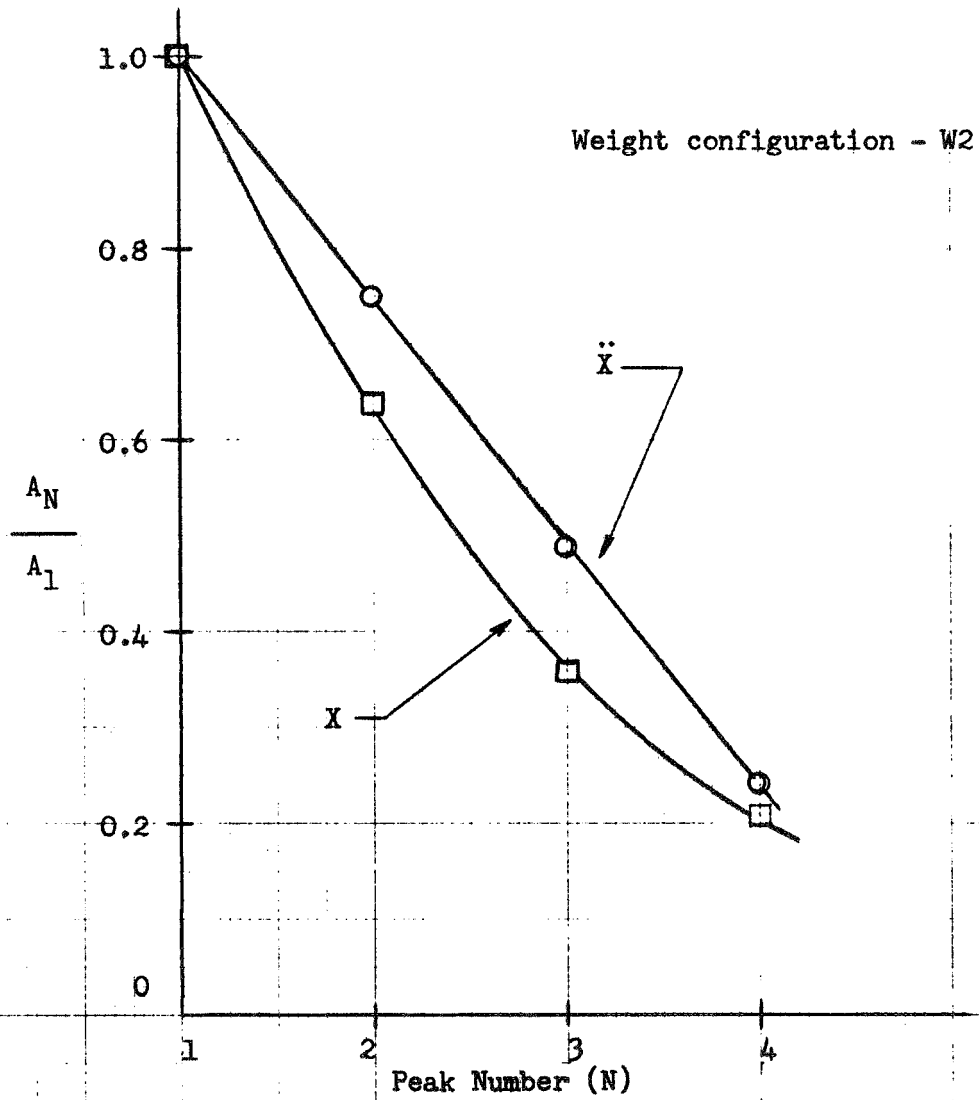

Figure 4.3-12 Peak height ratios for response of hysteresis system to .635 cm step function

A_1 = Height of first response peak after application of disturbance

A_N = Height of N'th response peak after application of disturbance
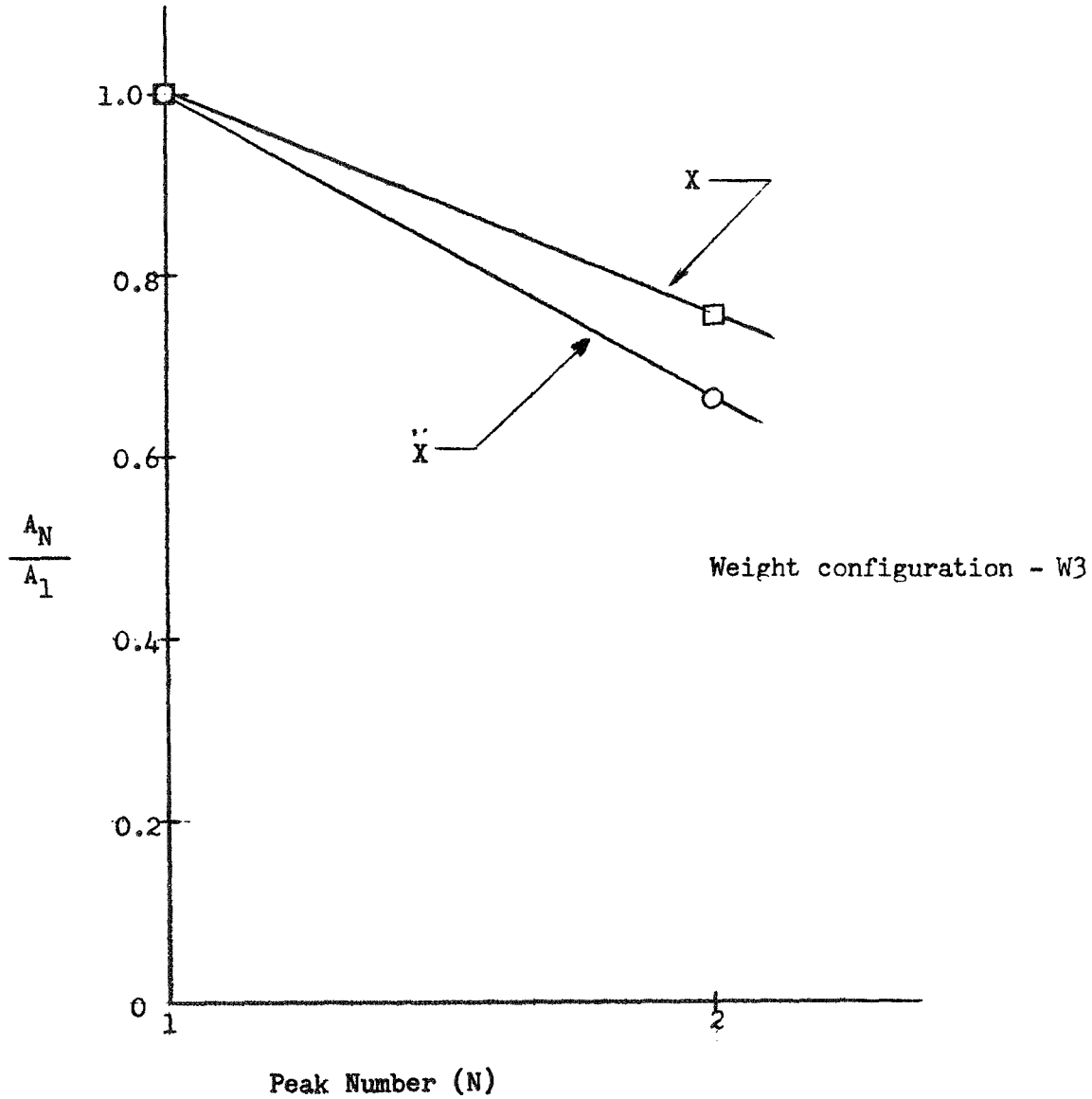

Figure 4.3-13   Peak height ratios for response of hysteresis system
to .635 cm step function

A_1 = Height of first response peak after application of disturbance

A_N = Height of N'th response peak after application of disturbance

Weight configuration - W2
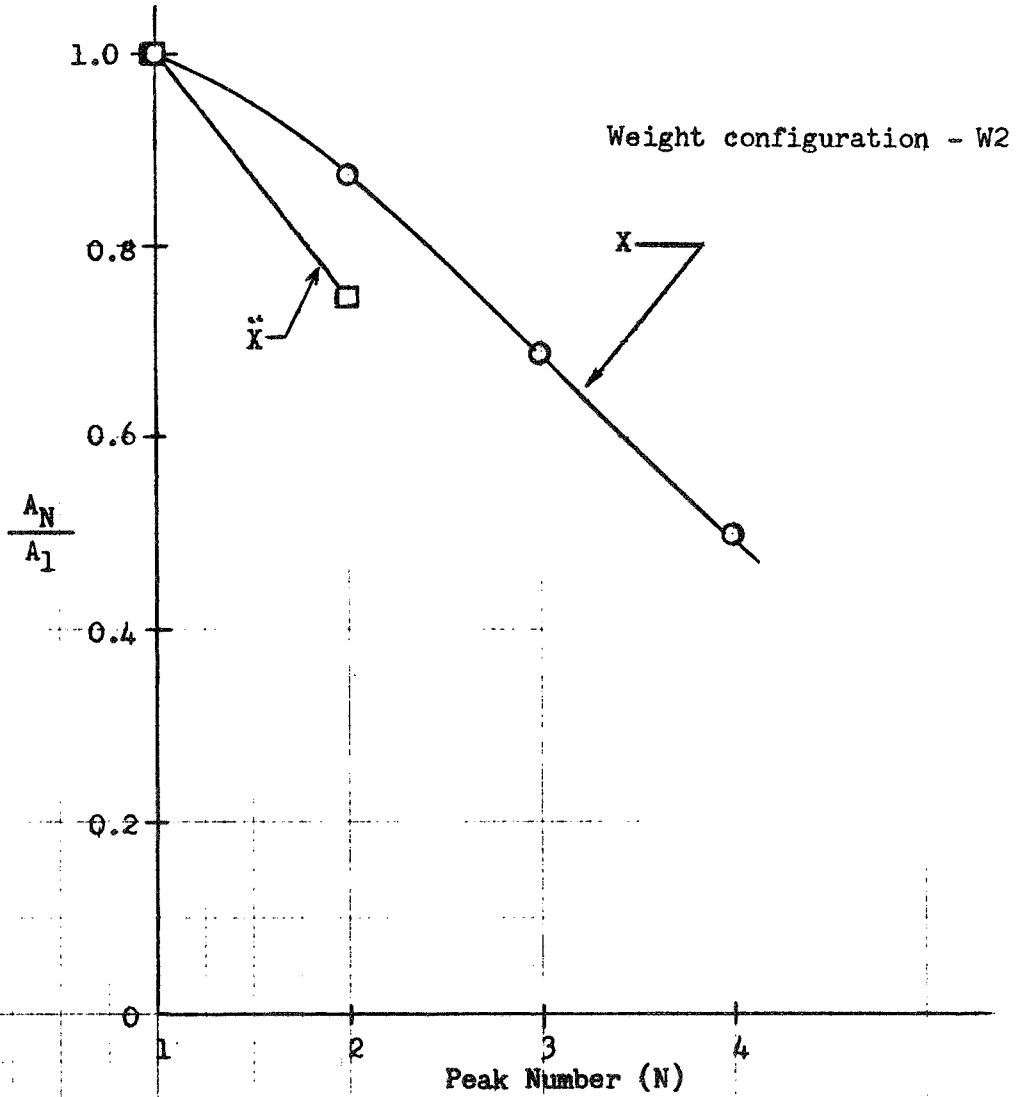
X

Ẍ

$\dfrac{A_N}{A_1}$

Peak Number (N)

Figure 4.3-14   Peak height ratios for response of hysteresis system without magnets to .635 cm step function

Table 4.3-3 Percent overshoot of hysteresis system
for 0.635 cm step function input

| Weight Configuration | Percent Overshoot | |
	1st Peak	2nd Peak
With magnets		
W1	100	33
W2	100	44
W3	50	17
w/o magnets		
W2	90	70

4.3.4 Discussion

This system did not behave as well as had been expected, but to a large extent, this appears to be a problem of design rather than theory. The string slap effect, for example, could be greatly reduced or eliminated by having a hysteresis system on each side of the bearing along an axis. Also, a system needs to be devised, possibly with an ancillary system, such as springs, to provide increased tangential restraint.

There also appears to be a significant amount of friction between the wire supporting the disc and the teflon inserts through which this wire passes. These inserts are necessary to prevent the disc from cocking up or down toward one of the magnets positioned above or below it. Initial alignment of these magnets with respect to the disc is a tedious job, since they must be positioned as close to the disc as possible to maximize the magnetic field. If this friction can be maintained within a minimum level, it could be used to provide additional damping without deleterious effects.

Even in its present setup, the system proved its ability to provide desirable damping for impulse types of disturbances.

4.4 MAGNETIC SUSPENSION

4.4.1 Sinusoidal response

The response of the magnetic suspension system was measured for sinusoidal input disturbances of frequencies from 0.01 Hz to 1.0 Hz. Some typical output data is shown in Figures 4.4.1 to 4.4.1-3. Also shown in the figures is the instantaneous voltage across the two suspension coils. It will be noticed that for the higher values of damping (high amplifier gain) the control signal becomes large enough to saturate the voltage controlled power supply, i.e. the signal tried to increase the suspension current beyond the capability of the power supply. This introduced further nonlinearities in the system, but damping was still obtained, and the response of the system was recorded for this additional case. The suspension characteristics were not drastically altered and damping was still obtained when the amplifiers in the feedback loop saturated as the air bearing passed through equilibrium with a high velocity. This occurs at high disturbance amplitudes or high disturbance frequencies at smaller amplitudes. This is considered an advantage for this type of system. In other words the control signal circuits affect only the damping and not the suspension characteristics. The suspension can be considered "passive" in that it does not require a control signal or feedback loop for stability, and a malfunction in the amplifier systems will not affect the suspension, only the damping.

Figure 4.4.1-1 shows the response of the system (W1) to a sinusoidal input of 0.635 centimeter peak to peak amplitude at a frequency of 0.1 Hz. In this setup there is no damping and the accelerometer output is sinusoidal. The angular acceleration is below the noise level of the accelerometers. The angular rotation record is essentially unchanged after the application of the driving functions, but some rotation at the natural frequency is present.

The second figure, Figure 4.4.1-2 is the same system with damping applied. Three different values of damping are shown in the figure. The first third of the chart represents a damping ration of $Z=.0275$. (Damping ratio is the ratio of the actual damping coefficient to the coefficient for critical damping, see section 4.4.2). This is reduced to $Z=.0168$ and finally to $Z=.0095$. For the larger damping ratios some angular acceleration does appear. However, this becomes smaller as the damping is decreased. A classical damped system behaves in the same way. The transmissibility is inversely proportional to the amount of damping. However, an increase in damping does tend to reduce the amplitude of the motion at the natural frequency. This can be seen from the X-displacement recording. A decrease in damping also decreased the transmissibility in the X-direction, but the decrease allowed a larger oscillatory motion at the natural frequency. In time this natural frequency component will damp out, but the damping is much more rapid for higher damping ratios, even though the transmissibility is greater for high Z.

In this system the damping ratio is easily controlled, and in an actual application a very high damping could be switched into the control system to reduce the initial disturbance at the low natural frequency. The damping would then be reduced as the transients died down. An interesting modification of this system would be the insertion of a band pass filter in the control system
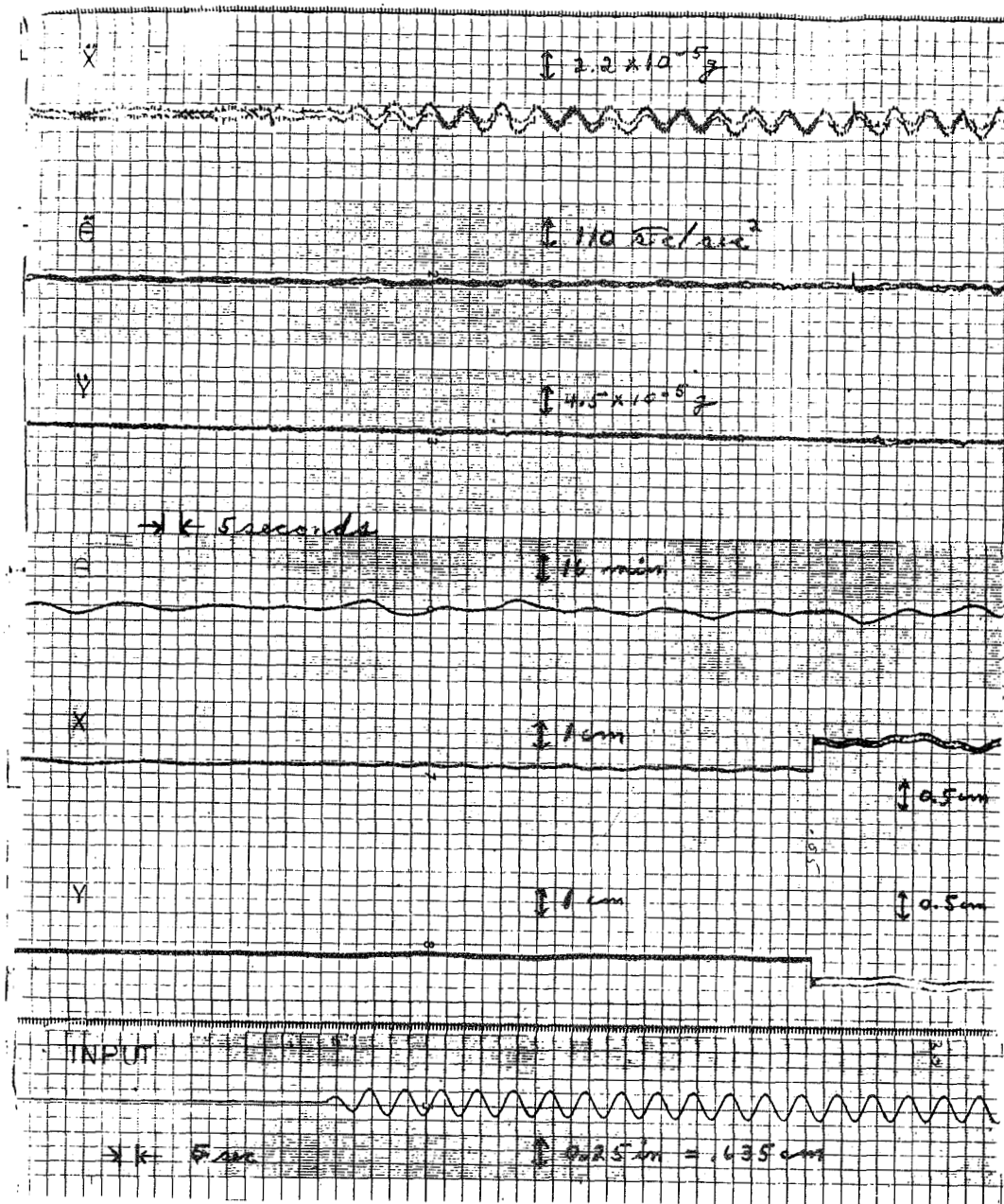
Figure 4.4.1-1, Sinusoidal Response, Zero Damping
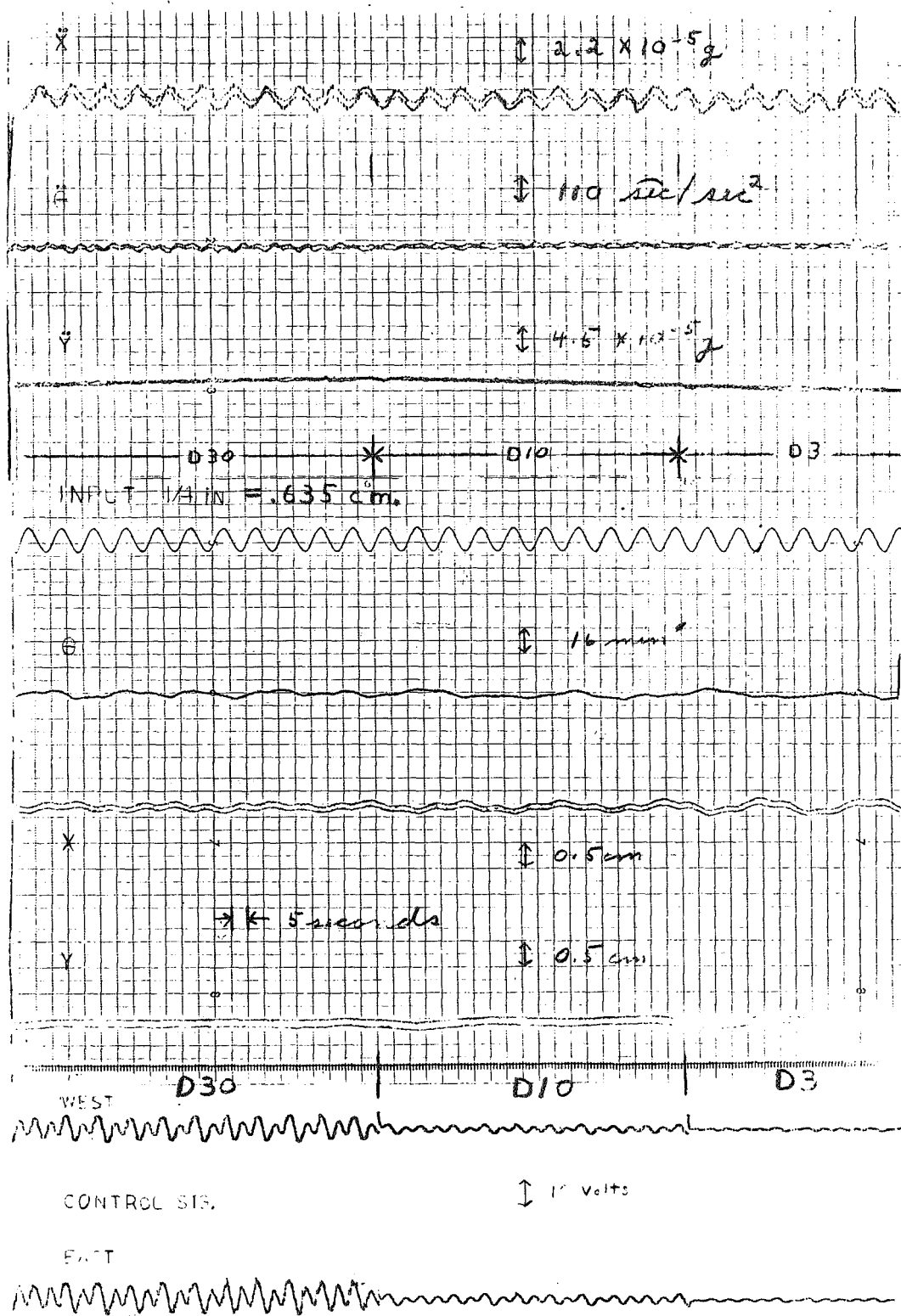
74

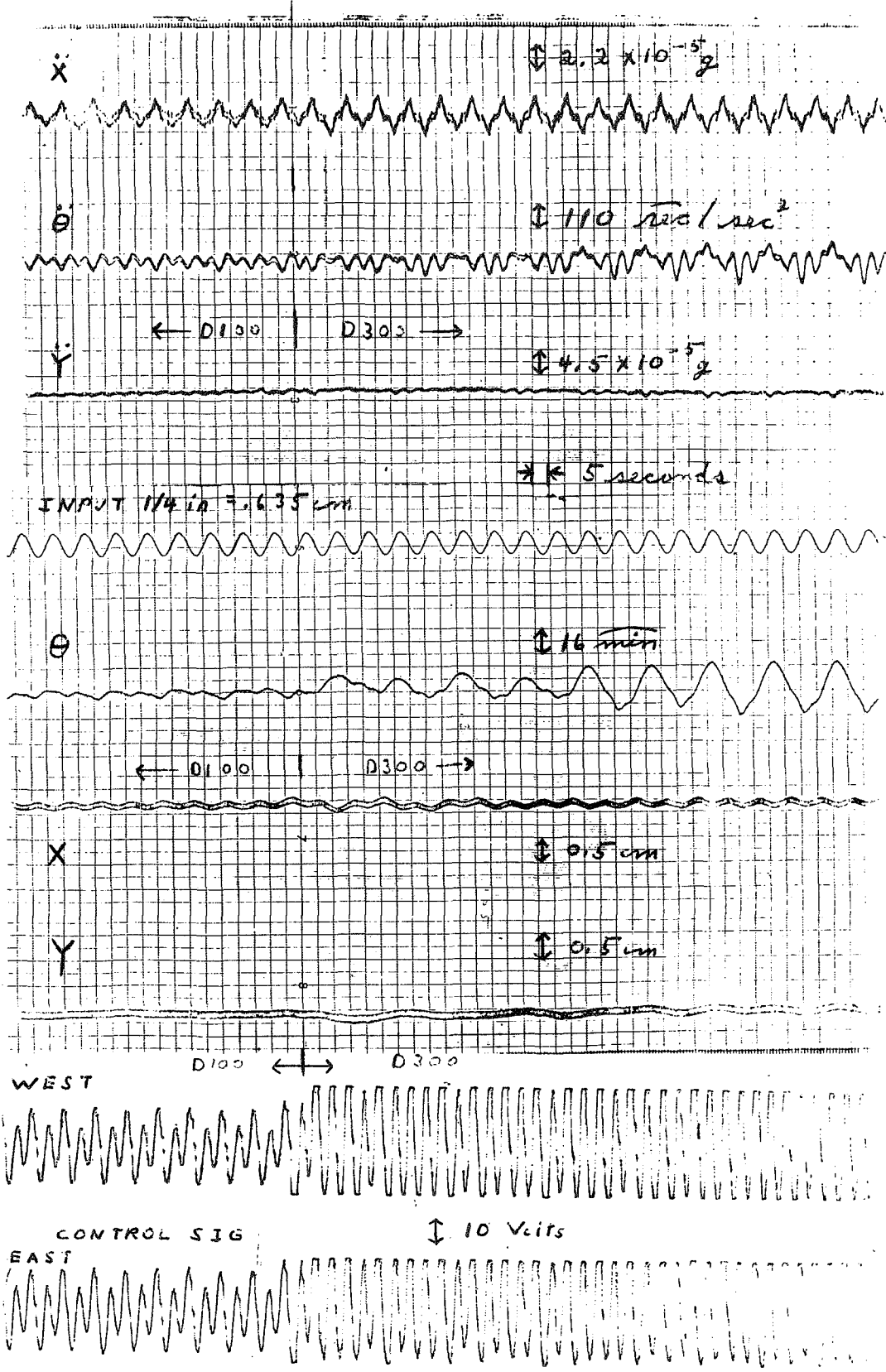Figure 4.4.1-2, Sinusoidal Response, D30, D10, D3

Figure 4.4.1-3, Sinusoidal Response, D100, D300

electronics to provide large damping only at the natural frequency and relatively small amounts at the disburbance frequencies.

Figure 4.4.1-3 shows the effect of further increases in damping ratio. The first half of the recording corresponds to a damping ratio of Z=.0333 and the second half corresponds to Z=.0674 It is again seen that an increase in damping creates a decrease in the transmissibility. A small amount of motion is also seen in the Y-direction although it is believed that this can be eliminated by a more careful design of the suspension coils. The waveforms are highly non-sinusoidal, but some of this is due to the saturation of the control signal electronics for the highest value of Z. This is the cause of the clipped waveform of the control signal.

Transfer functions

Since the magnetic suspension is definitely nonlinear when damping is introduced, it is not possible to obtain transfer function curves for sinusoidal inputs as was the case in the linear spring system. However, for comparison purposes, it seemed instructive to define a transfer ratio as the <u>peak to peak</u> output disturbance to the peak to peak amplitude of the sinusoidal input, even though the output in most cases is extremely nonsinusoidal and not at the same frequency as the driving force. Only in the case of zero damping is the transfer function a true transfer function as normally defined.

However, the present definition does represent the peak accelerations introduced to the system, and shows that aside from the detailed waveshape of the output function the system has many similarities to a linear spring system. It is seen that for driving frequencies above resonance an increase in the value of damping reduces the isolation. This is identical to the behavior of a spring system.

The curves on the following pages show the transmissibility of the magnetic suspension as a function of driving frequency and damping ratio. The driving frequencies were sinusoidal disturbances of 0.635 centimeter amplitude applied along the X-axis. During the course of the investigation amplitudes of 1.11 cm. were also tried but were found to be too large a disturbance at the higher frequencies. However, some of the data taken at the larger amplitude is shown in the following pages.

TRANSFER FUNCTIONS for MAGNETIC SUSPENSION
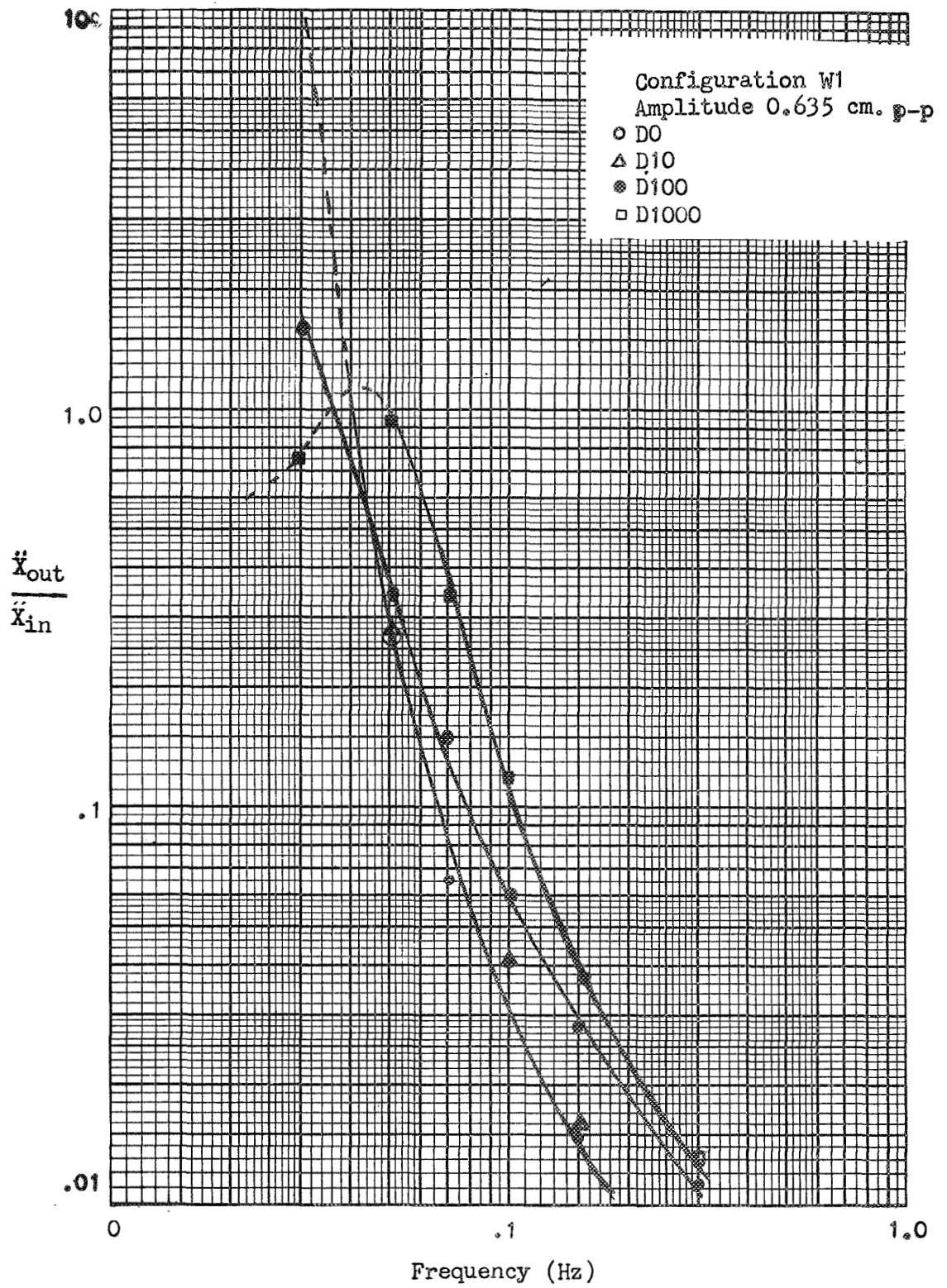
Weight Configuration W1

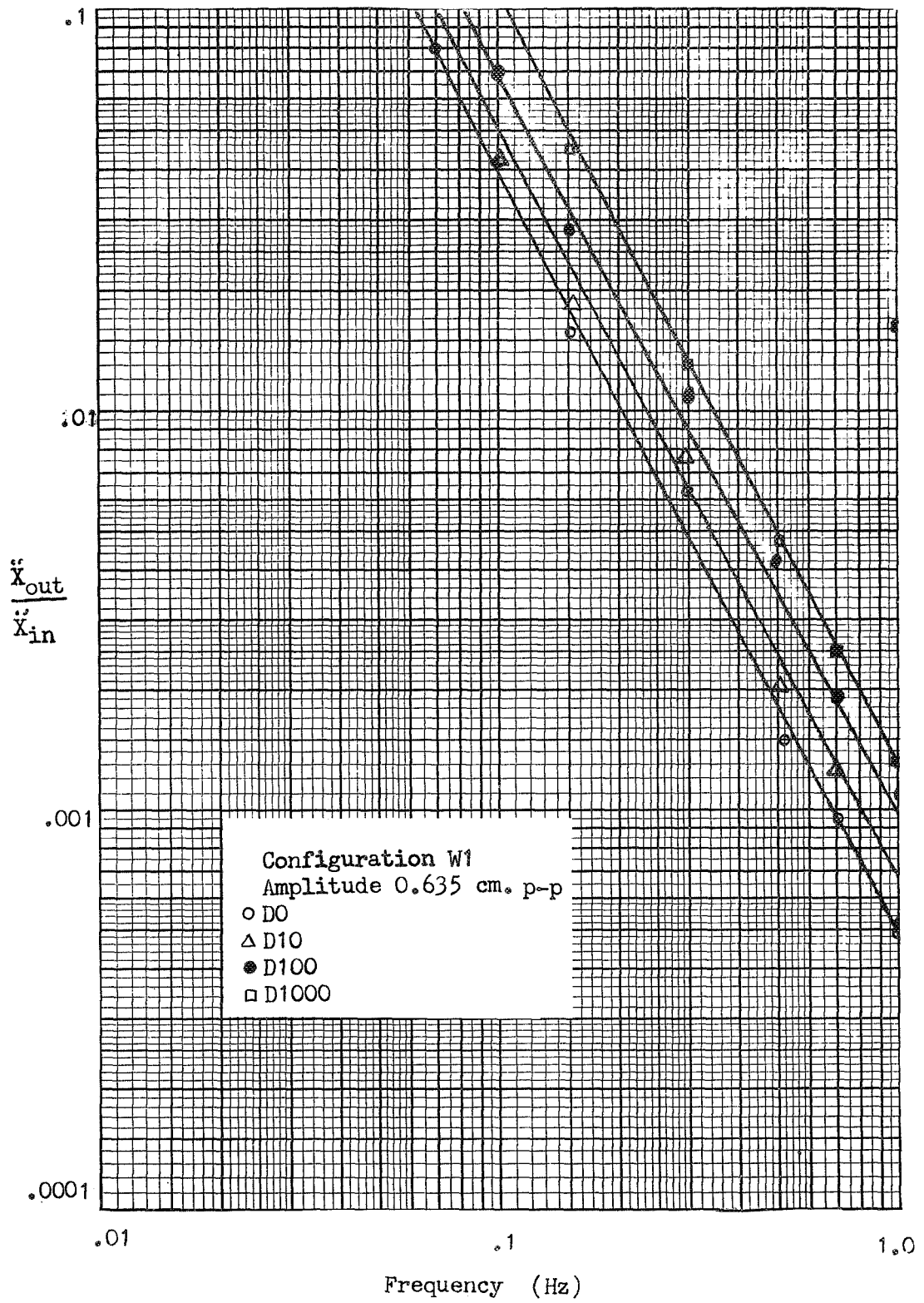Figure 4.4.1-4, Transfer Function for Magnetic Suspension

Figure 4.4.1-4, Continued

Figure 4.4.1-5, Transfer Function for Magnetic Suspension

Figure 4.4.1-5, Continued

Figure 4.4.1-6, Transfer Function for Magnetic Suspension

Figure 4.4.1-6, Continued
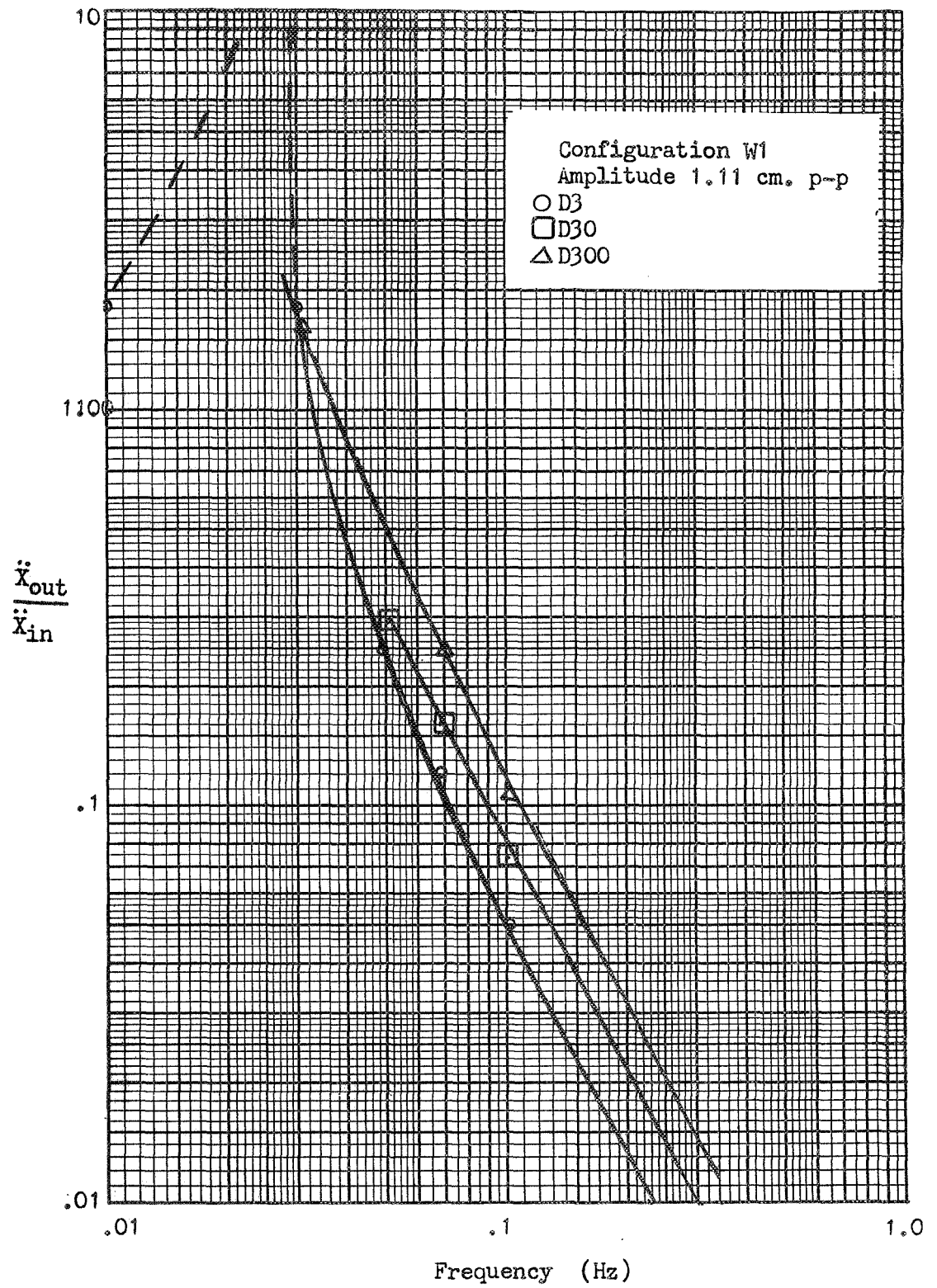
Figure 4.4.1-7, Transfer Function for Magnetic Suspension

85

Configuration W1
Amplitude 1.11 cm. p-p
D3
D30
D300

Frequency (Hz)

Figure 4.4.1-7, Continued

86

TRANSFER FUNCTIONS for MAGNETIC SUSPENSION

Weight Configuration W2

Figure 4.4.1-8, Transfer Function for Magnetic Suspension
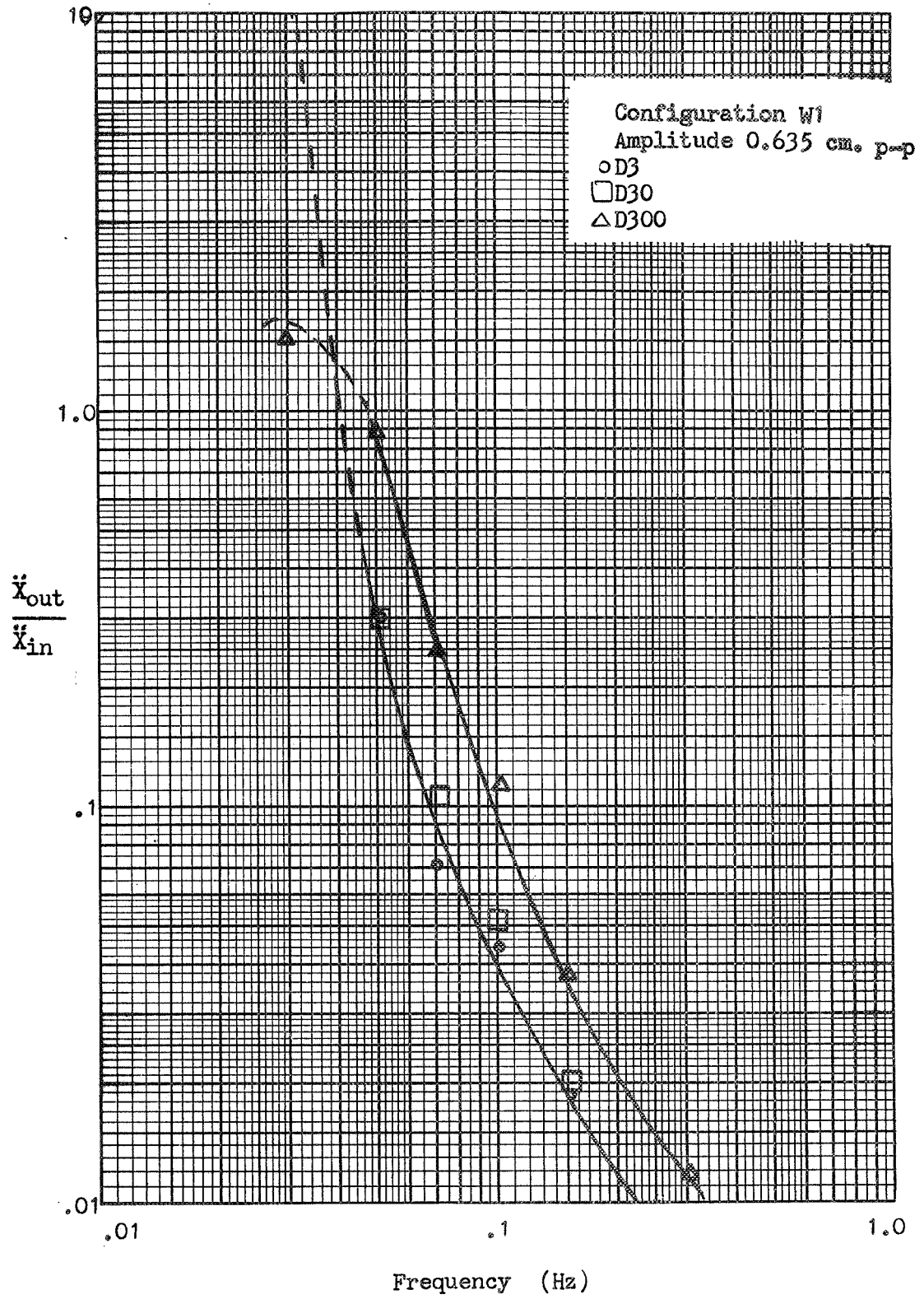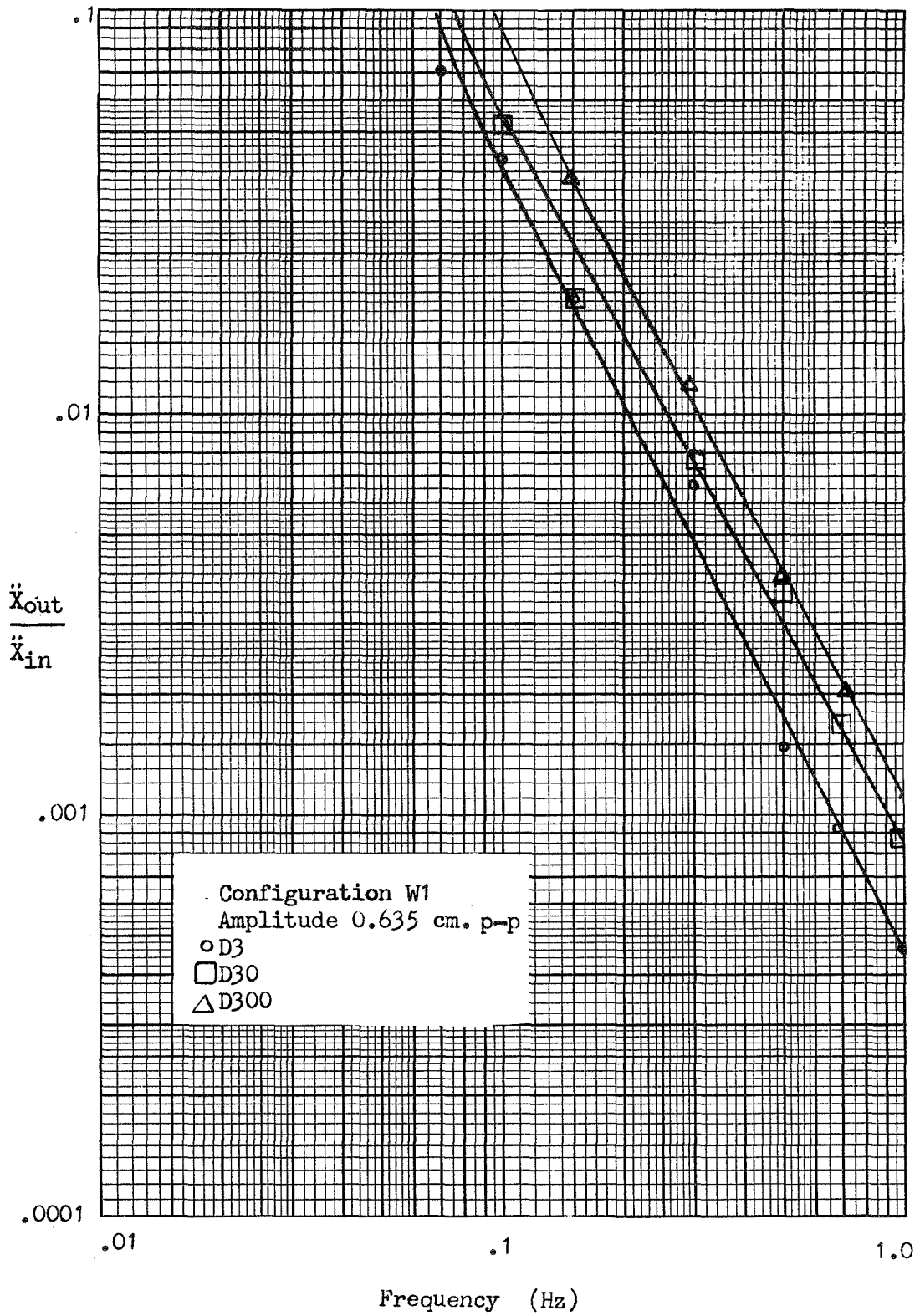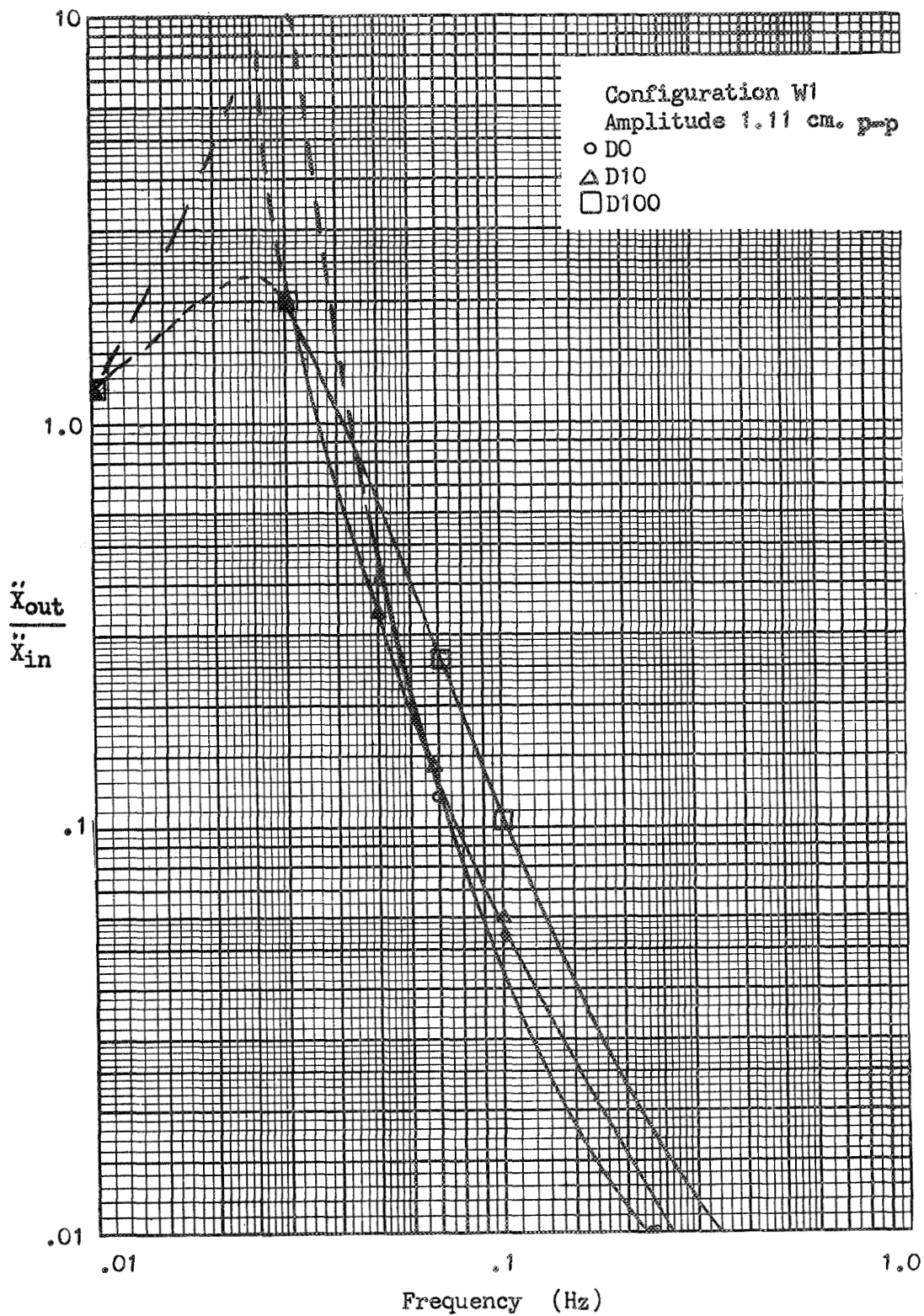
Figure 4.4.1-8, Continued

Figure 4.4.1-9, Transfer function for Magnetic Suspension

Figure 4.4.1-9, Continued

Figure 4.4.1-10, Transfer function for Magnetic Suspension

Figure 4.4.1-10, Continued

Figure 4.4.1-11, Transfer Function for Magnetic Suspension

94

The plot shows $\frac{X_{out}}{X_{in}}$ (vertical axis, logarithmic from .0001 to .1) versus Frequency (Hz) (horizontal axis, logarithmic from .01 to 1.0).

Configuration W2
Amplitude 1.11 cm. p-p
○ D3
▢ D30

Figure 4.4.1-11, Continued

TRANSFER FUNCTIONS for MAGNETIC SUSPENSION

Weight Configuration W3

Figure 4.4.1-12, Transfer Function for Magnetic Suspension

Figure 4.4.1-12, Continued

98
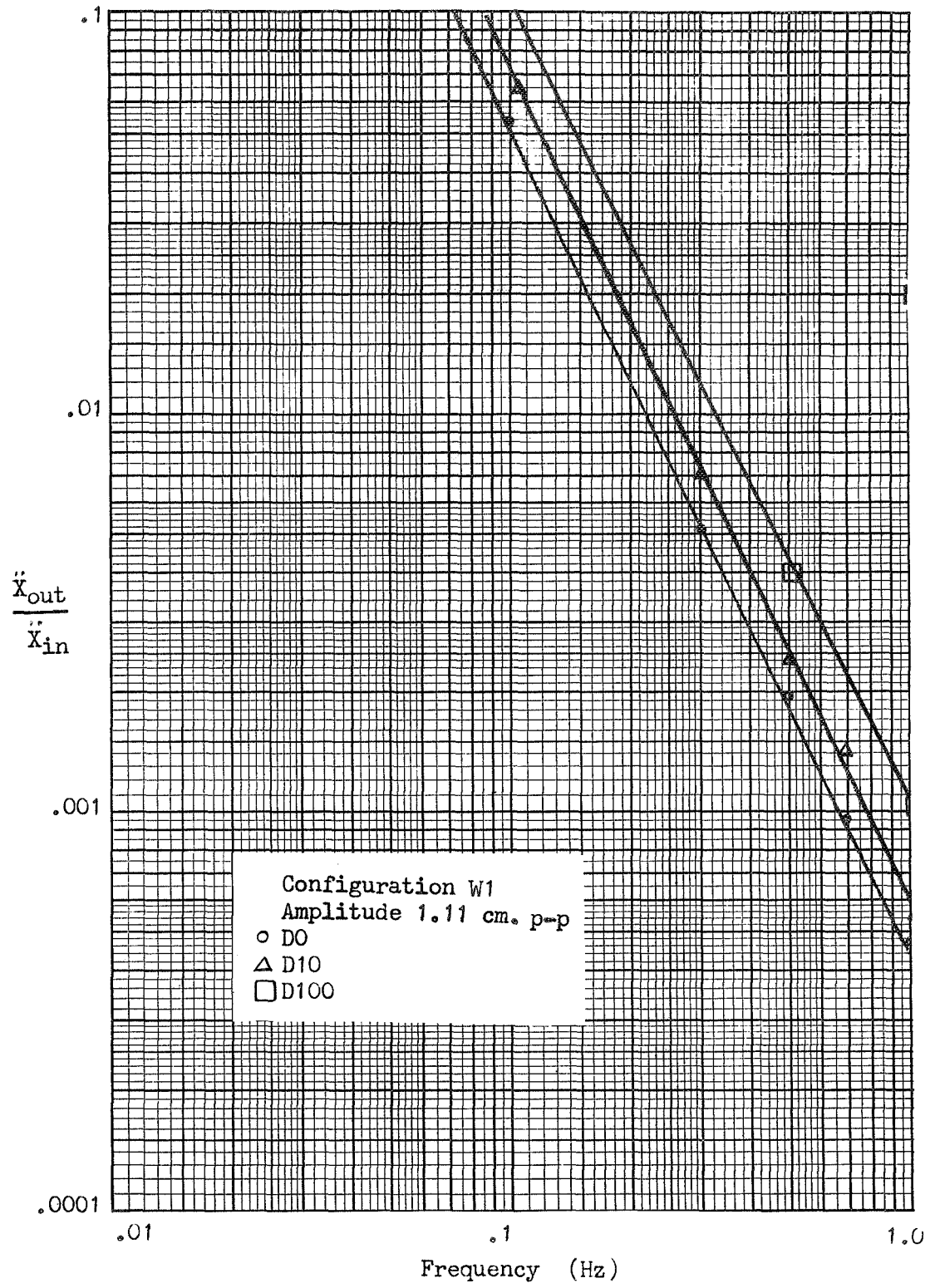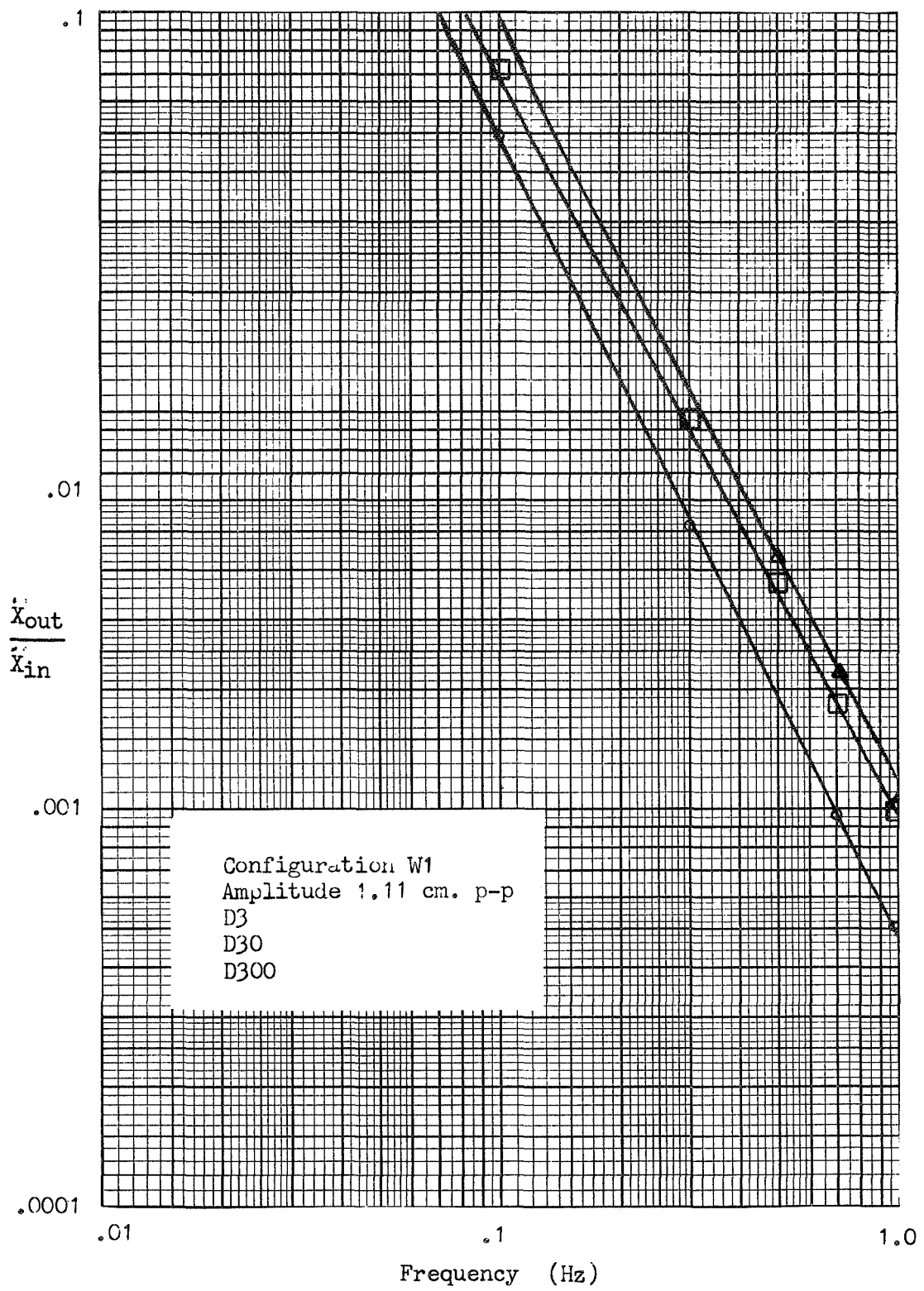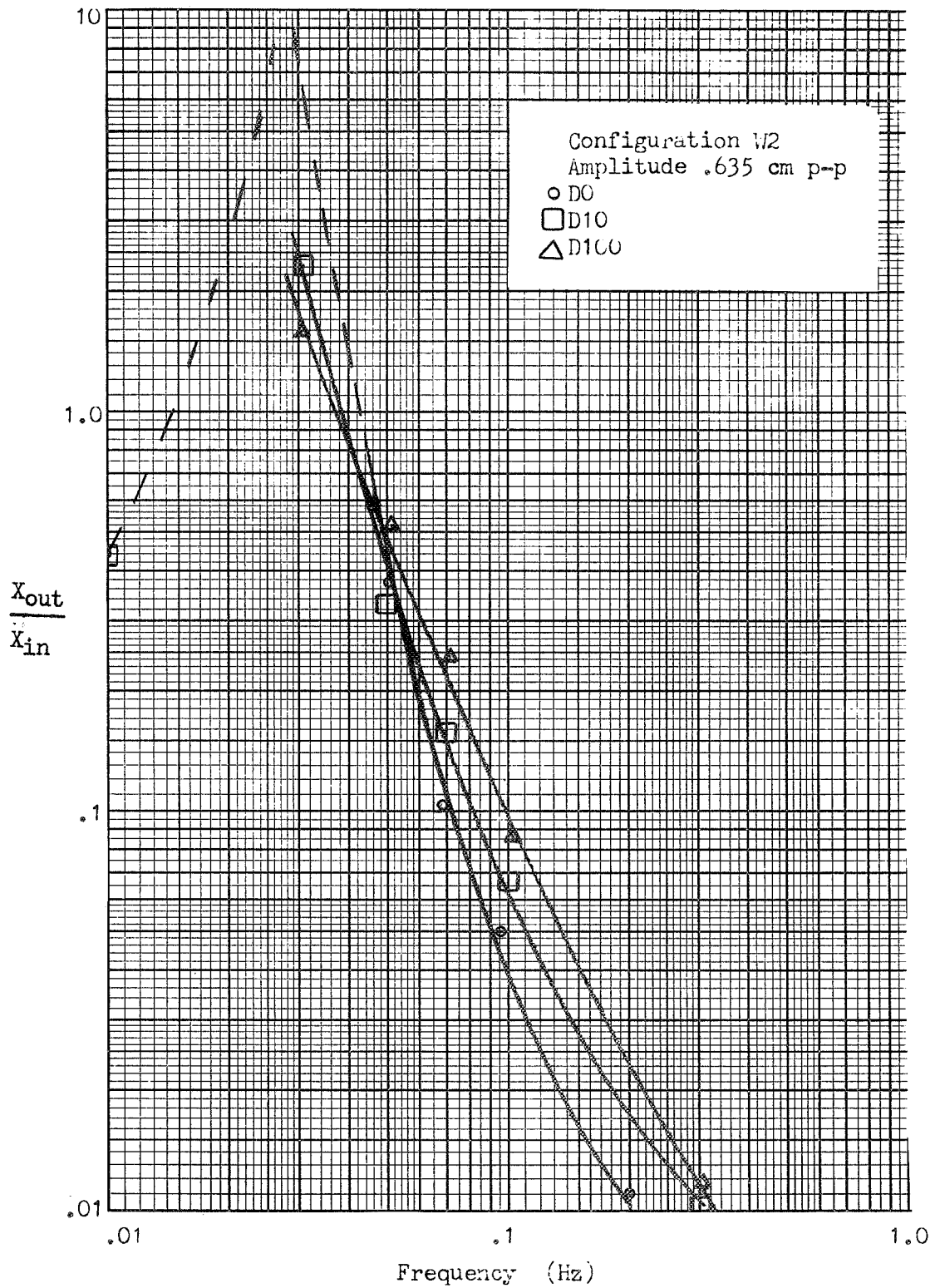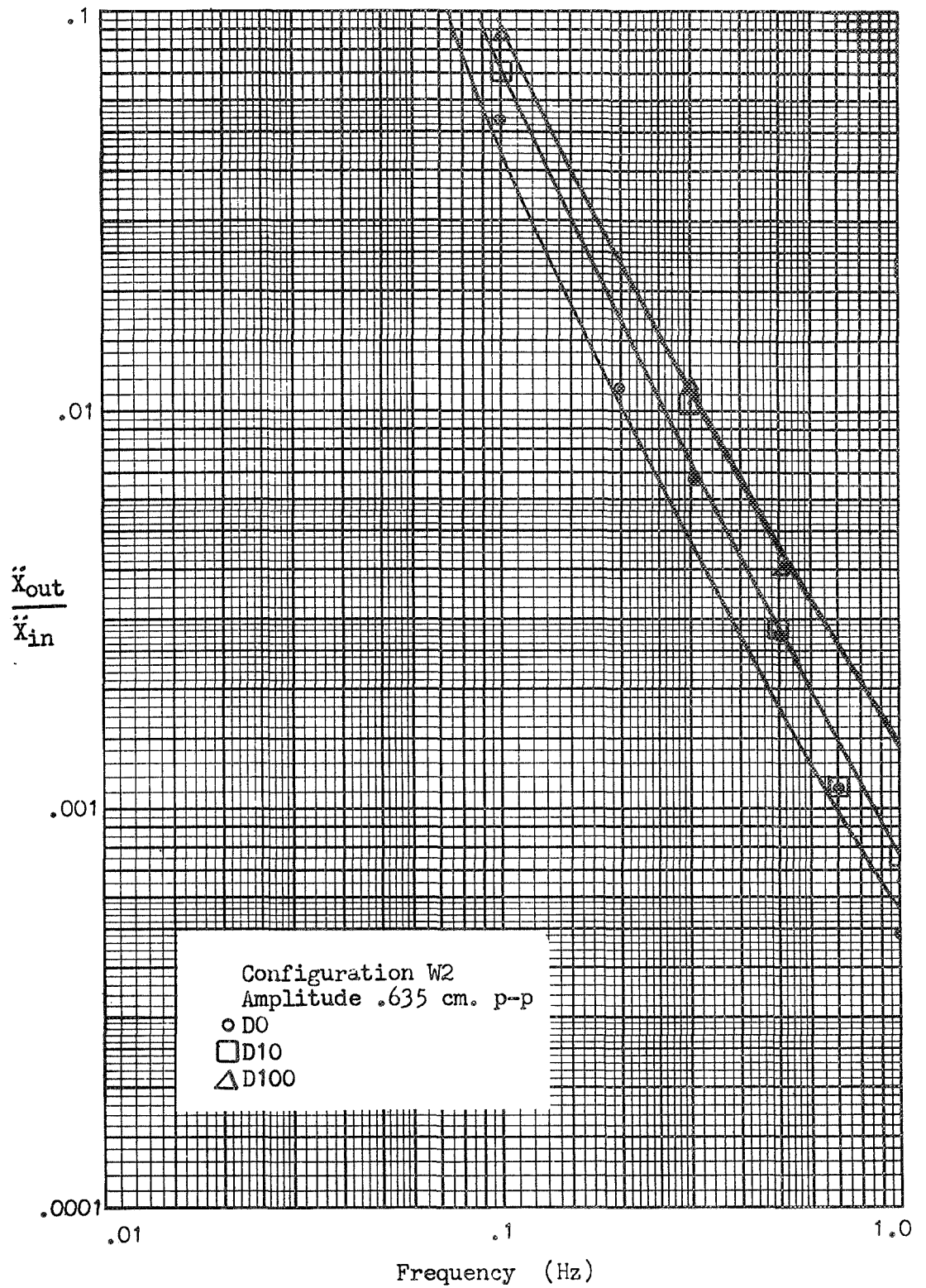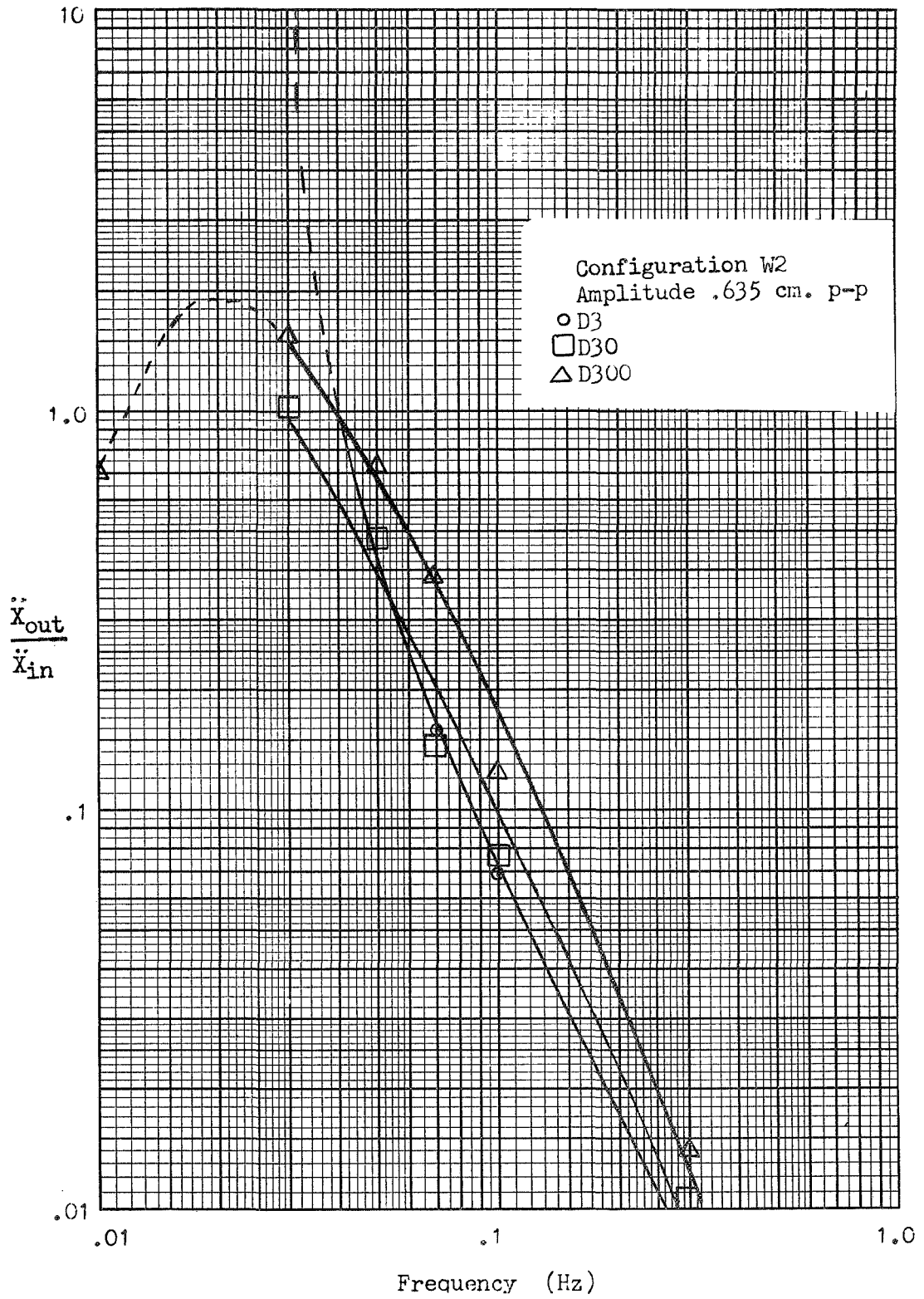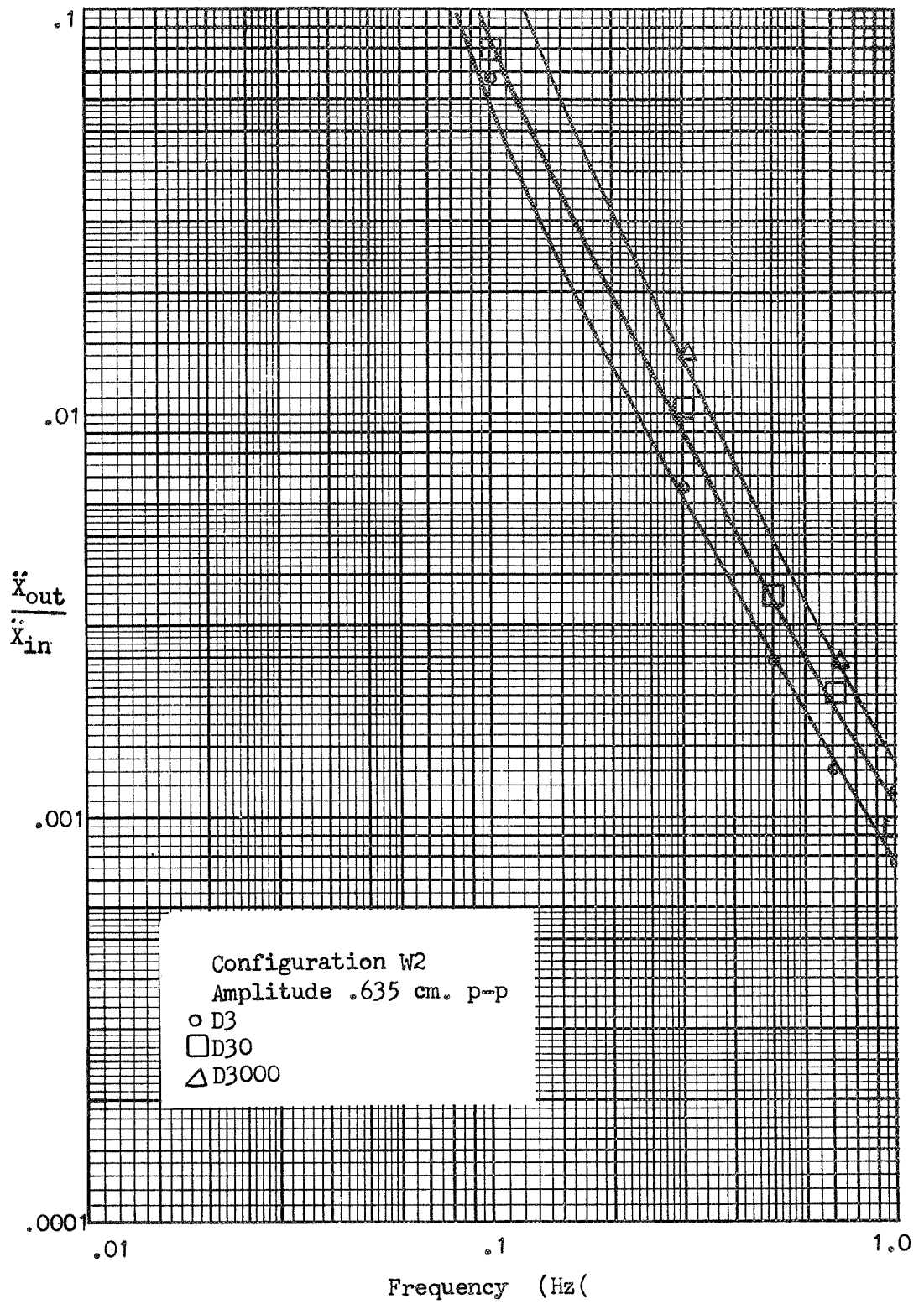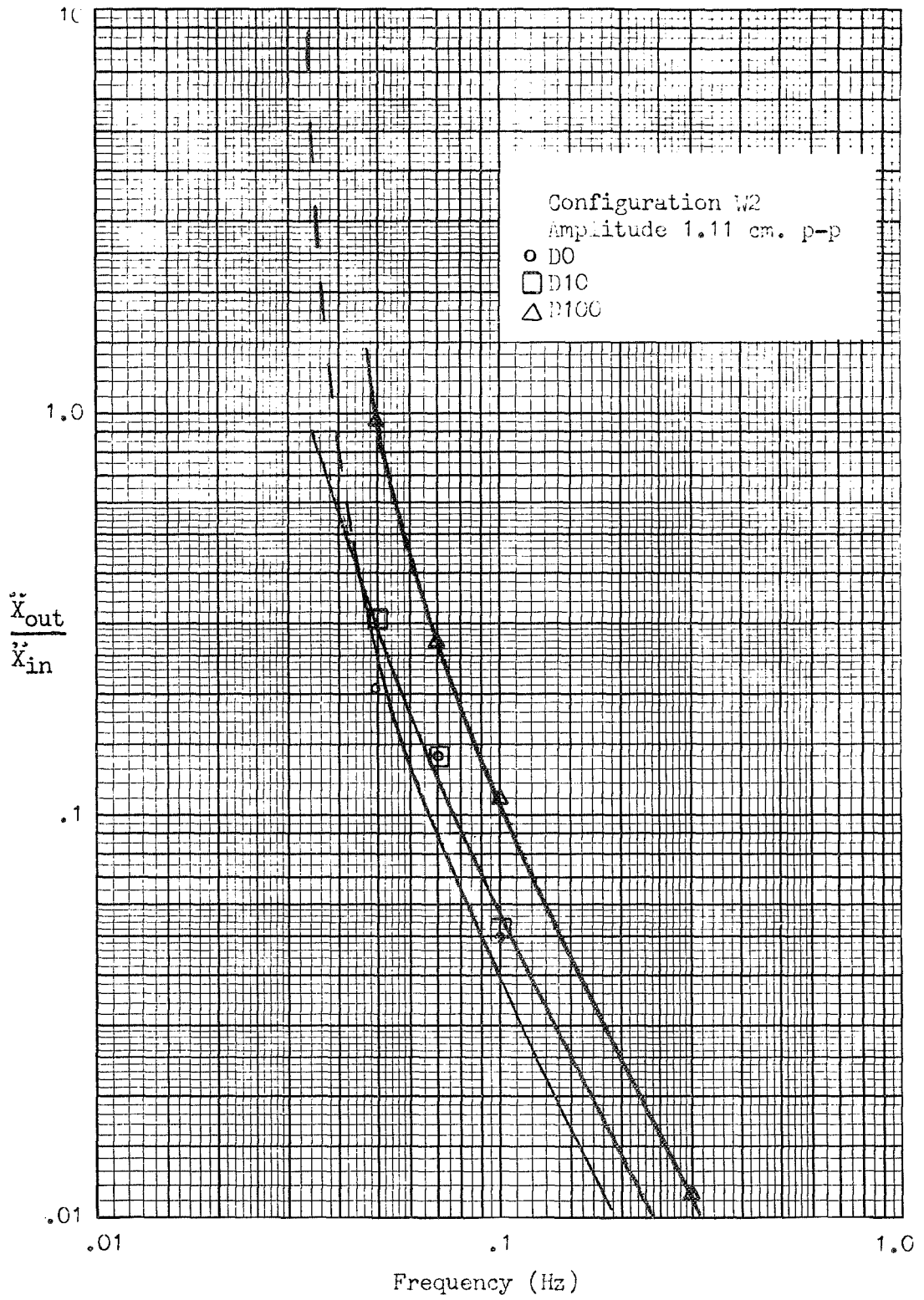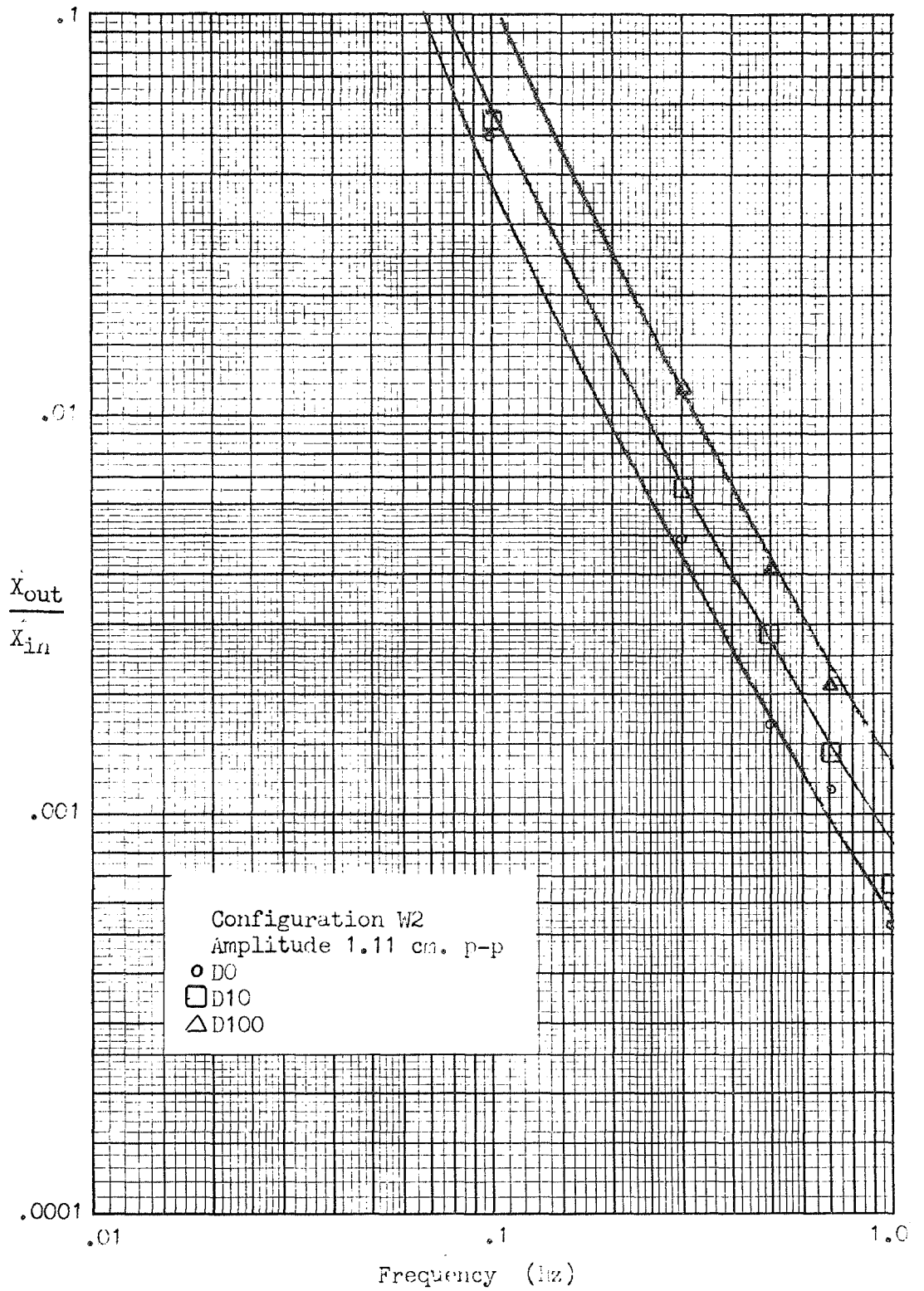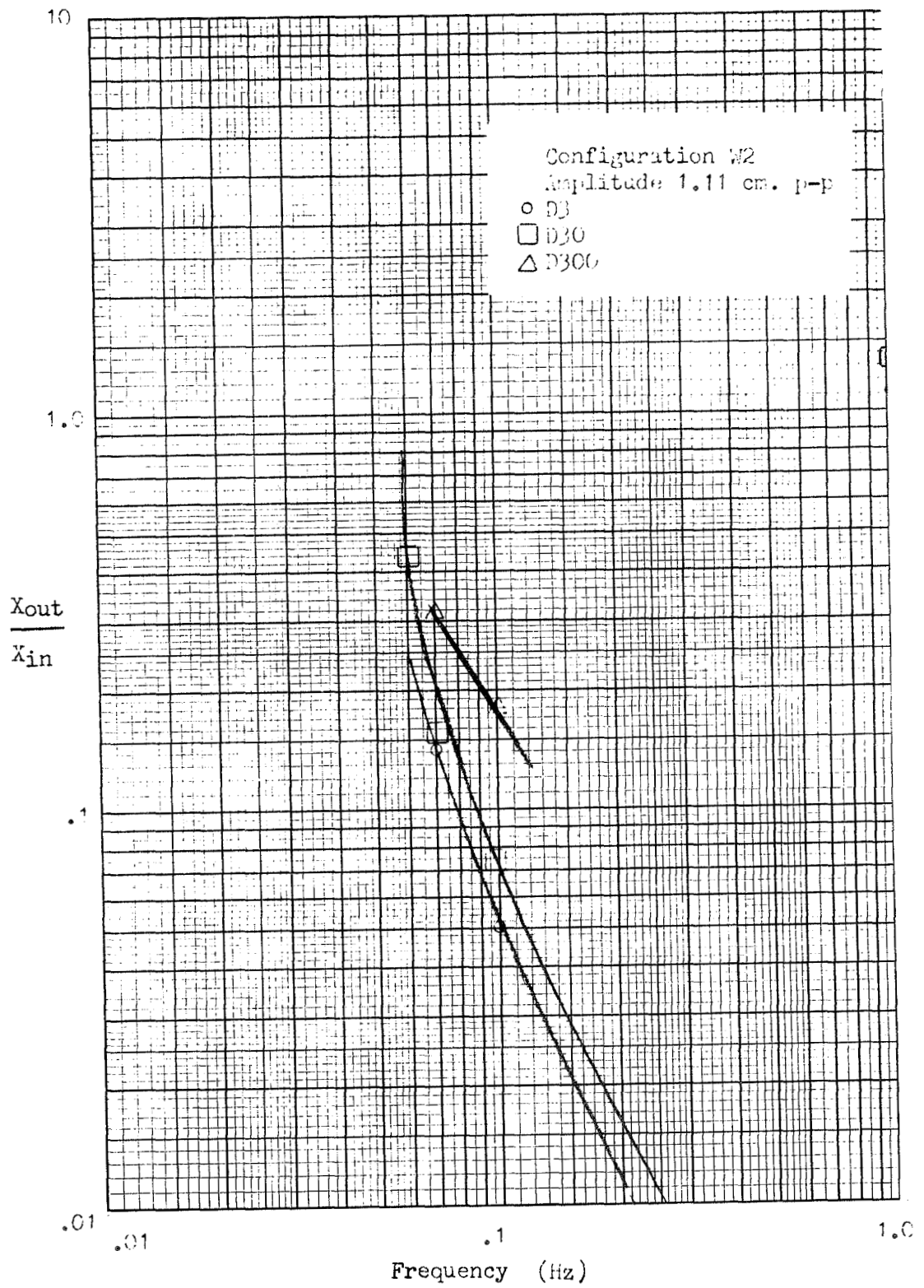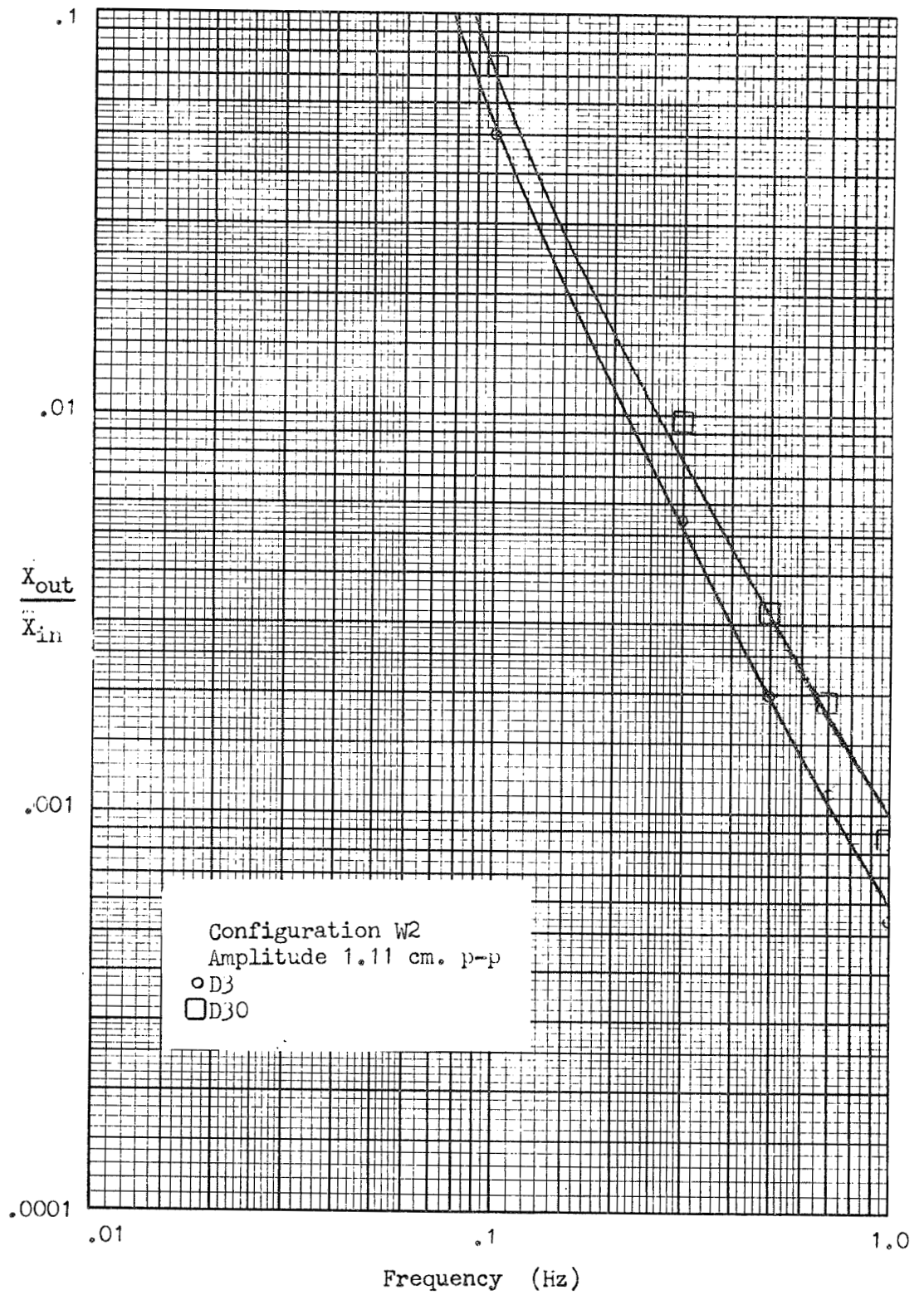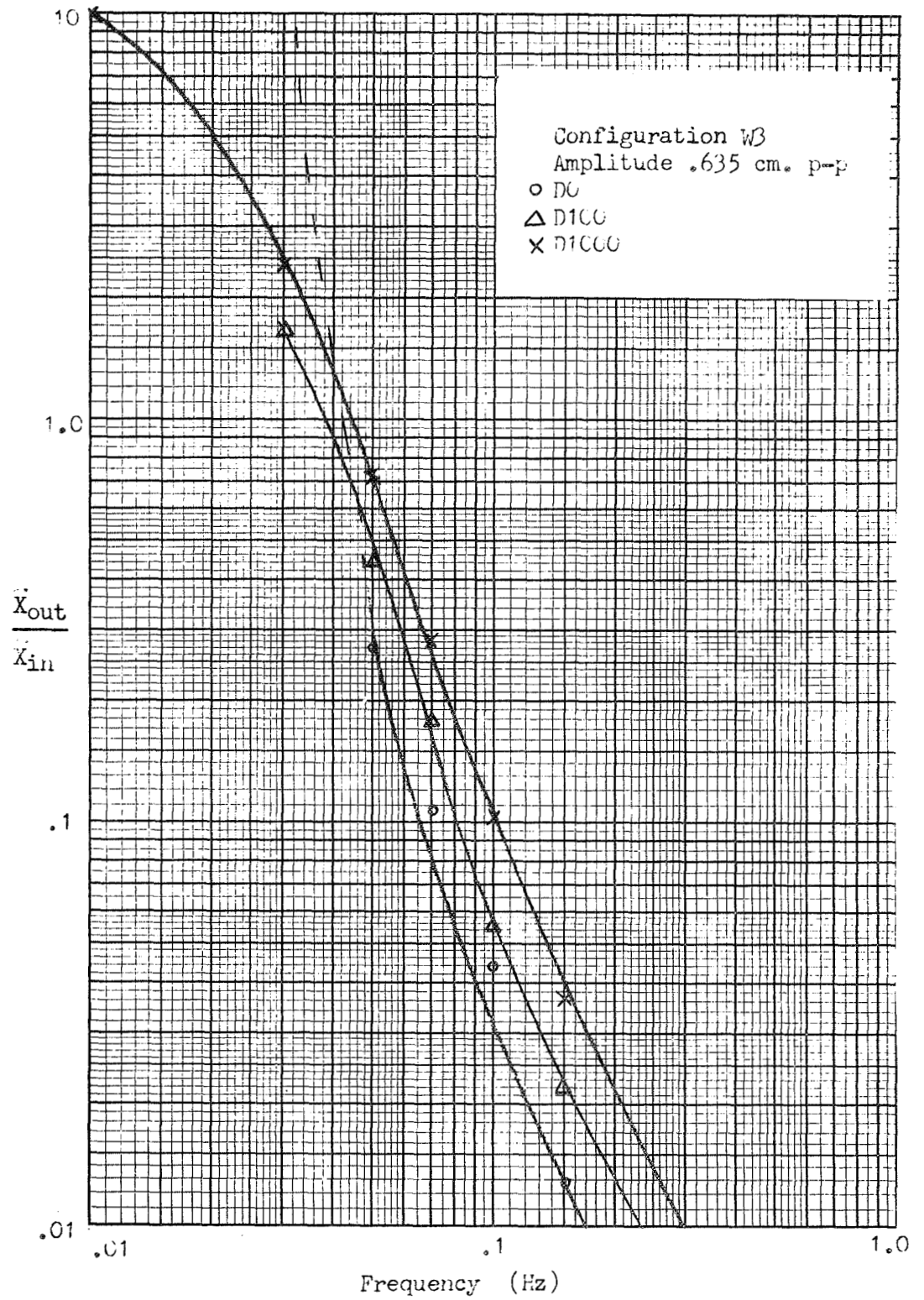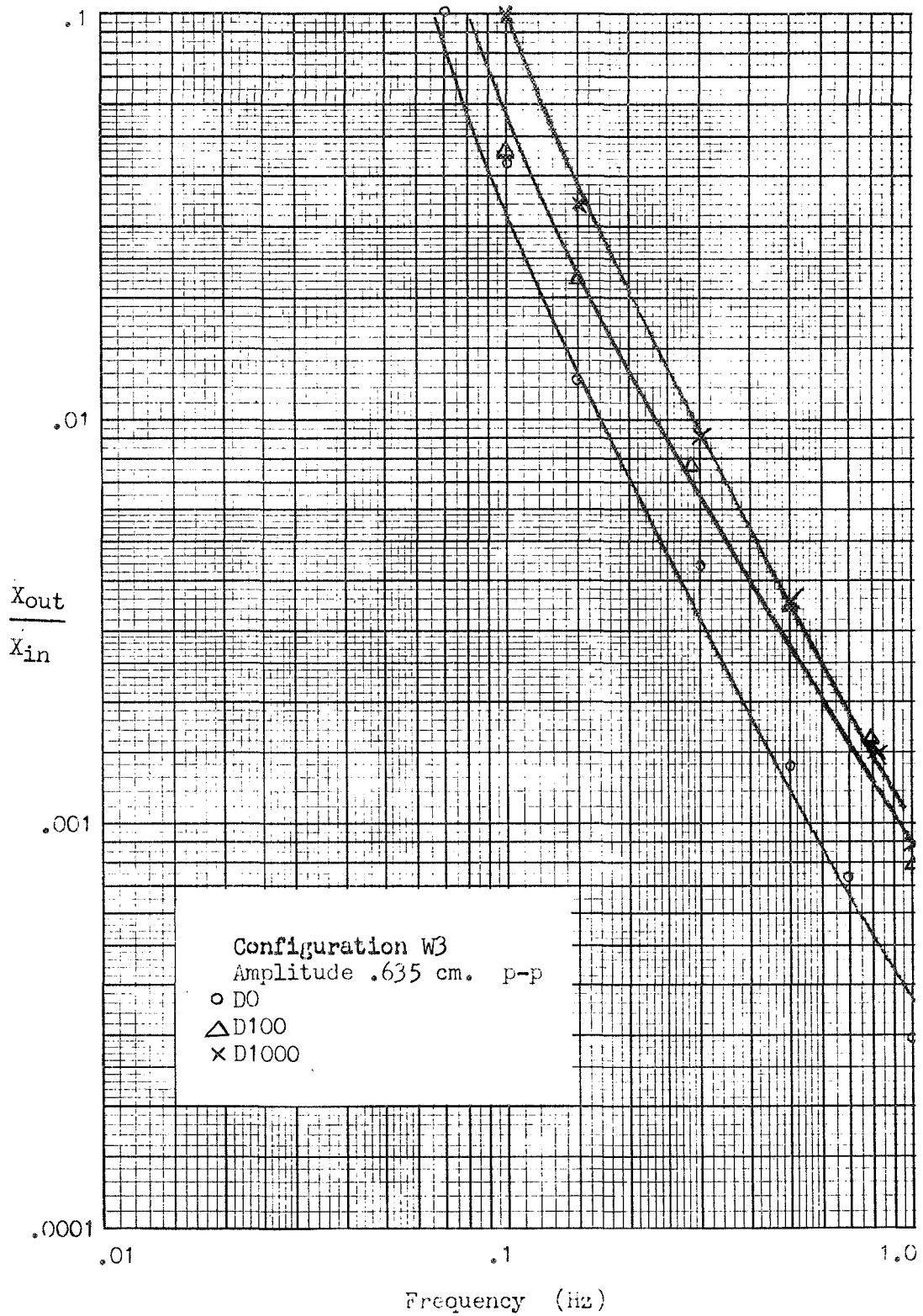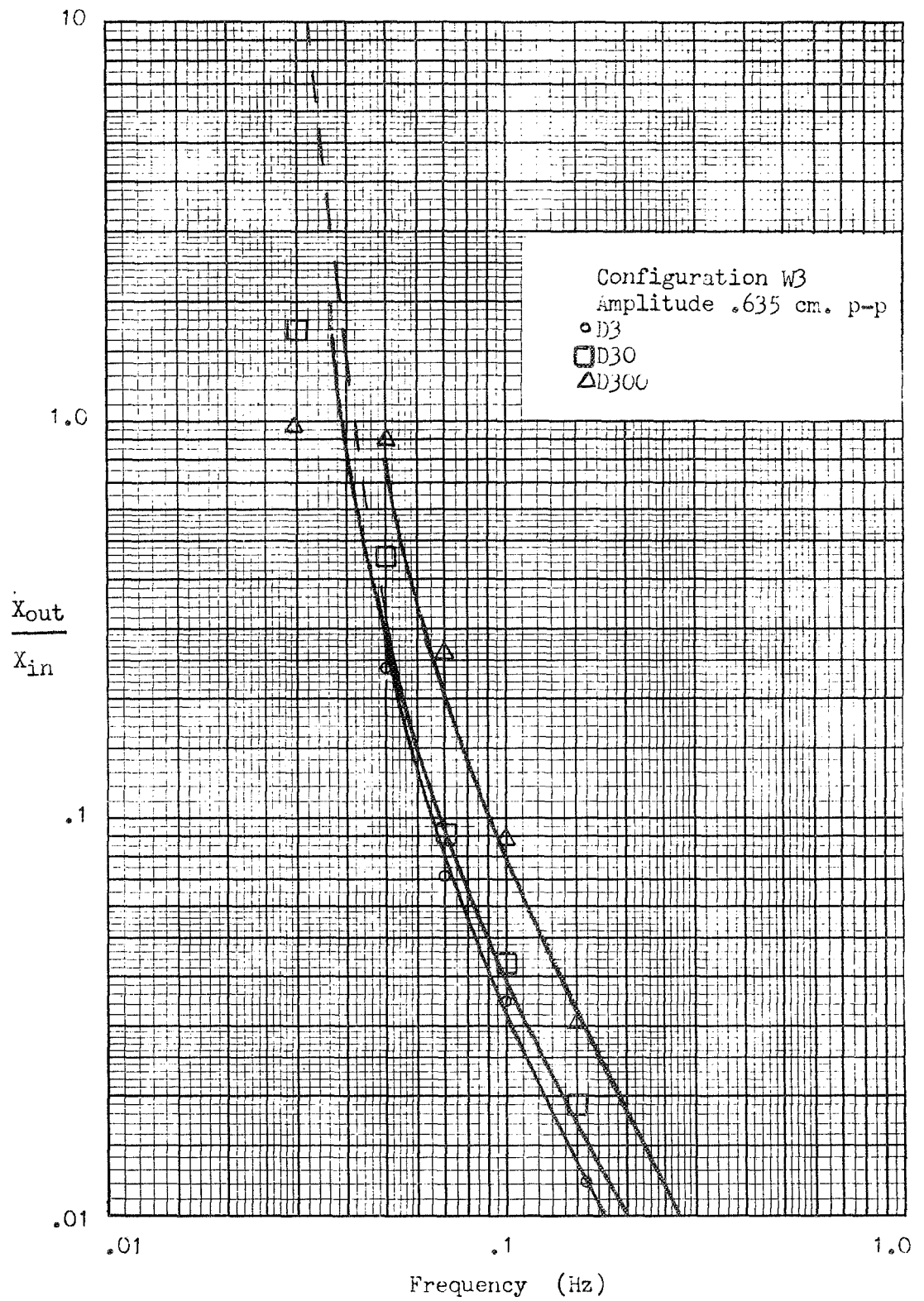
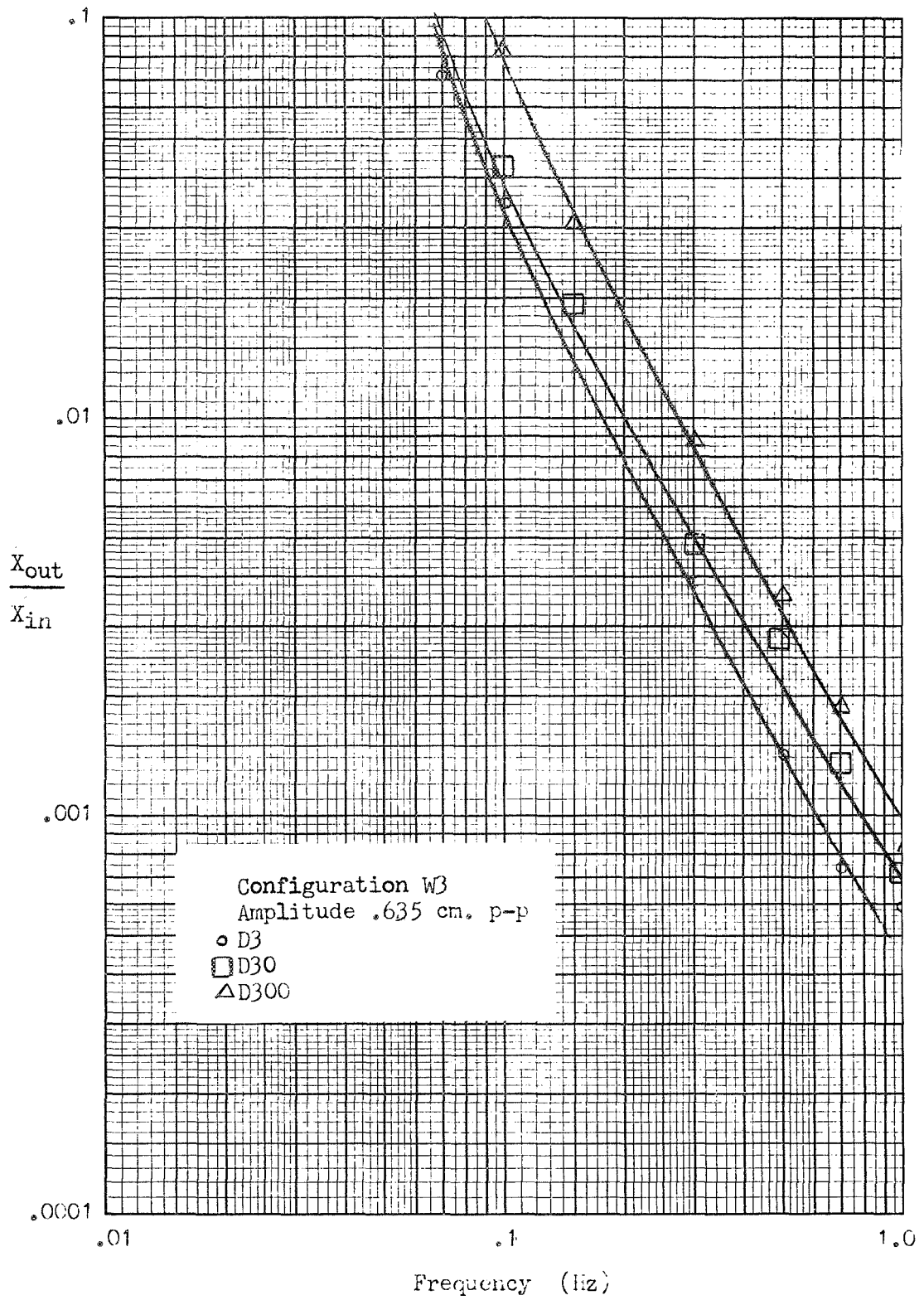Figure 4.4.1-13, Transfer Function for Magnetic Suspension

Figure 4.4.1-13, Continued

Natural frequency variations

Some unusual behavior was noted when damping was applied to the system. At the higher frequencies (0.5 to 1.0 Hz) the acceleration transmitted through the suspension to the air bearing could be seen superimposed on top of any residual motion which existed at the natural period of the system. This was to be expected. However, it could be seen that as the damping increased the frequency of this natural motion also increased. The change is shown on the graph on the following page. This increase in natural frequency appears only when a significant control or velocity signal is present. No significant change in natural periods is seen when the air bearing is moving very slowly. This effect is unexplained at present but can probably be accounted for in a detailed analysis of the equation of motion. A possible cause of this decrease in period could be due to amplifier saturation or nonlinearities in the suspension and pickup coils. The average current in the suspension coils would then be greater than I_o, which would increase the natural frequency of the system.

Configuration comparison

In tables 4.4.1-1, 4.4.1-2 and 4.4.1-3 are shown the transmissibilities in the X and Y directions and the angular acceleration of the air bearing for different driving frequencies and different values of damping. Driving amplitudes are 0.635 centimeter peak to peak. The transmissibilities and rotational acceleration are shown for each weight configuration.

It can immediately be seen that for W3 the transmissibility in the X-direction, $\ddot{X}$ out/$\ddot{X}$ in is smaller than the transmissibilities of configurations W2 and W1. This was to be expected since W3 has the greatest offset of center of gravity from the line of action of the applied disturbance. This offset allows the disturbance force to exert a torque on the air bearing. This means that some of the energy which would ordinarily be transmitted into X-acceleration of the bearing is now converted into angular rotation. The result is the reduction of the transmissibility and at the same time an increase in the angular acceleration. This is shown in the tables. The angular accelerations which were recorded were small and highly non-sinusoidal. The values indicated in the table represent an estimate of the peak to peak value of the angular acceleration. The resolution is only about 10 $\widehat{sec}/sec^2$. One trend that can be seen, however, is that the rotational acceleration of configuration W3 is greater than the others, which is to be expected.

Since W2 has a larger moment of inertia than W1 it is expected that W2 would be less susceptible to rotation. This also implies that for W2 the transmissibility in the X direction would be somewhat greater than W1. Such a trend can possibly be seen in the data but actually the difference in moments of inertia between W1 and W2 is not large enough to significantly affect the data.

It was also noticed that for some of the higher damping values, a small amount of energy was transmitted to other modes of vibration. That is a disturbance was recorded in the Y-direction. It appears that this is not a fundamental characteristic of the system, but could be eliminated with an optimum coil design for the suspension. This interaction was not seen often enough to

Weight Configuration W1
Sinusoidal disturbance,
p-p amplitude 0.635 cm.,
frequency .1 to 1.0 Hz.
$T_o = 31.5$ sec.

Z (Damping Ratio)

T/T_o
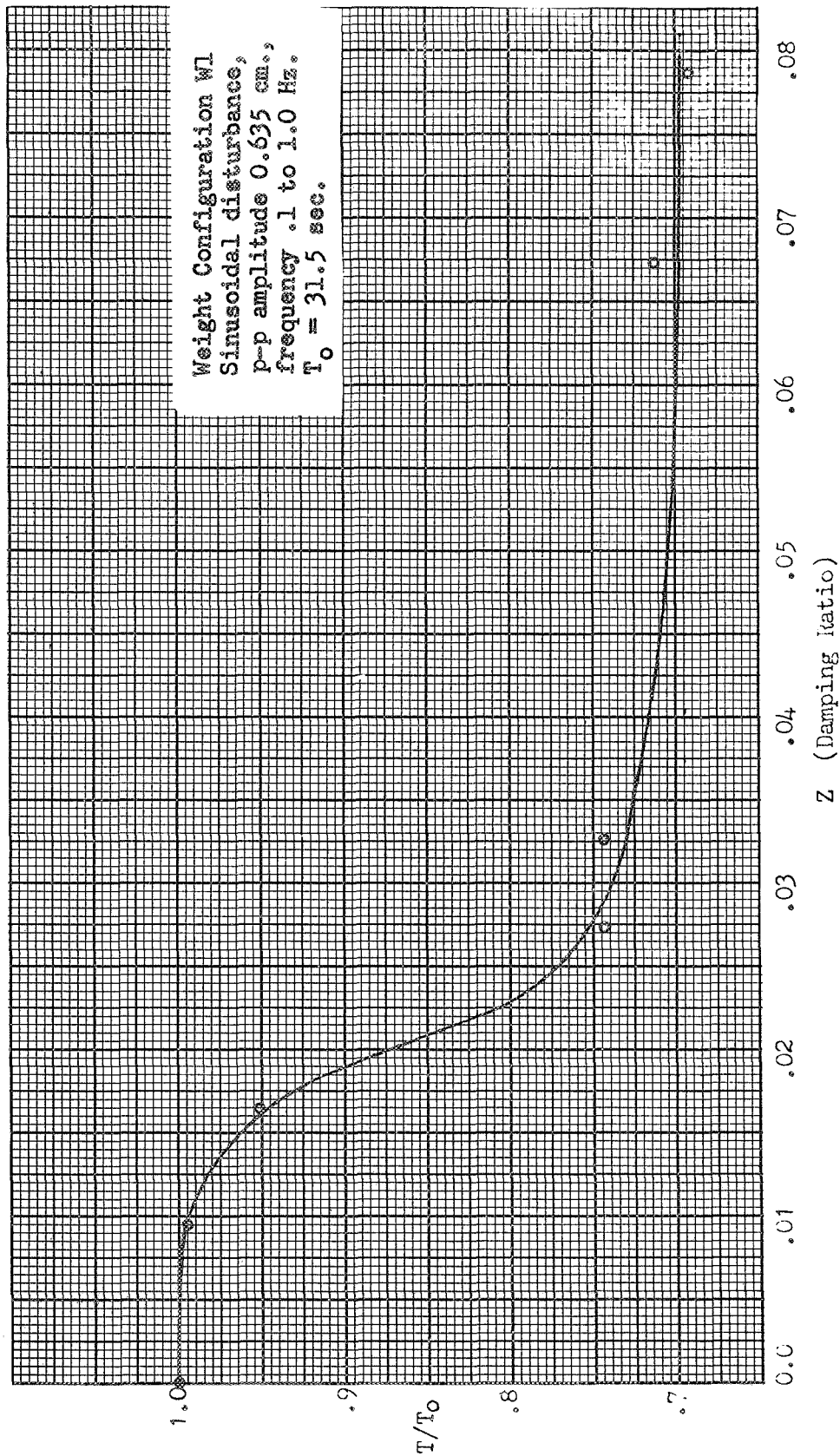
Figure 4.4.1-14, Variation of Natural Frequency with Damping

102

obtain enough points for a curve. The isolation in the Y-direction, $\ddot{Y}$ out/$\ddot{X}$ in
is shown in Table 4.4.1-2 whenever it appeared.

Table 4.4.1-1, Transfer Ratios for Magnetic Suspension (X-axis)
(disturbance amplitude = .635 cm. peak to peak)

Frequency	Damping	$\ddot{X}_{out}/\ddot{X}_{in}$ W1	W2	W3
1.0 Hz	D = 0	4.85×10^{-4}	4.82×10^{-4}	2.90×10^{-4}
	3	4.85	7.73	3.87
	10	5.33	7.73	5.80
	30	8.68	9.64	5.80
	100	1.06×10^{-3}	6.76	7.73
	300	1.11		8.23
	1000	1.26		8.70
0.7	0	9.37×10^{-4}	1.12×10^{-3}	7.48×10^{-4}
	3	9.37	1.31	7.48
	10	1.31×10^{-3}	1.12	9.35
	30	1.68	2.06	1.31×10^{-3}
	100	1.97	2.25	1.68
	300	2.06	2.43	1.87
	1000	2.43		1.50
0.5	0	1.42	2.84	1.39
	3	1.42	2.48	1.39
	10	1.96	2.84	1.74
	30	3.57	3.55	2.78
	100	4.28	4.26	3.48
	300	3.93		3.48
	1000	4.48		3.48
0.3	0	6.75	6.76	4.35
	3	6.75	6.76	3.87
	10	7.73	1.05×10^{-2}	3.87
	30	7.73	1.05	4.83
	100	1.16×10^{-2}	1.16	7.74
	300	1.21	1.45	8.70
	1000	1.35		8.70
0.15	0	1.58	1.42	1.26
	3	1.90	1.58	1.26
	10	1.58	1.58	1.58
	30	1.90	1.58	1.90
	100	2.85	2.52	2.20
	300	3.79	3.31	3.15
	1000	3.79		3.47
0.1	0	4.34	5.23	4.35
	3	4.34	6.96	3.48
	10	4.34	6.96	3.48
	30	5.22	7.84	4.35
	100	6.08	8.67	5.65
	300	1.13×10^{-1}	1.22×10^{-1}	8.70

Table 4.4.1-1   Continued

Frequency	Damping	$\dot{X}_{out}/\dot{X}_{in}$		
		W1	W2	W3
0.1	1000	1.22×10^{-1}	1.35×10^{-1}	1.00×10^{-1}
0.07	0	7.03×10^{-2}	1.07	1.07
	3	7.03	1.60	7.10×10^{-2}
	10	1.07×10^{-1}	1.60	8.90
	30	1.07	1.42	8.90
	100	1.51	2.49	1.78×10^{-1}
	300	2.48	3.90	2.67
	1000	3.15		2.84
0.05	0	2.79	3.79	2.78
	3	2.79		2.44
	10	2.79	3.48	1.74
	30	2.79	5.22	4.46
	100	3.49	5.22	4.46
	300	8.72	7.66	9.05
	1000	9.75		7.65
0.03	0	off scale	off scale	off scale
	3	"	"	"
	10	"	2.42	"
	30	"	1.00	1.74
	100	1.64	1.64	1.64
	300	1.55	1.55	1.00
	1000	0.77		2.42
0.01	0 to 300	too small to measure	too small to measure	too small to measure
	1000	"	"	10.4

105

Table 4.4.1-2, Transfer Ratios for Magnetic Suspension (Y-axis) (disturbance amplitude = .635 cm. peak to peak)

Frequency	Damping	$\ddot{Y}out/\ddot{X}in$ W1	W2	W3
1.0 Hz	D = 0-1000	0.0	0.0	0.0
0.7	0-3	0.0	0.0	0.0
	10	0.0	0.0	1.87×10^{-4}
	30	0.0	0.0	1.87
	100-1000	0.0	0.0	0.0
0.5	0-10	0.0	0.0	0.0
	30	0.0	0.0	3.48×10^{-4}
	100	0.0	0.0	3.48
	100-1000	0.0	0.0	0.0
0.3	0-10	0.0	0.0	0.0
	30	0.0	0.0	9.66×10^{-4}
	100	0.0	0.0	1.93×10^{-3}
	300	0.0	0.0	1.93
	1000	0.0	0.0	0.0
0.15	0-30	0.0	0.0	0.0
	100	0.0	0.0	7.3×10^{-3}
	300	0.0	0.0	7.3
	1000	0.0	0.0	0.0
0.1	0-30	0.0	0.0	0.0
	100	0.0	1.73×10^{-2}	8.70×10^{-3}
	300	0.0	3.46	1.74×10^{-2}
	1000	0.0	4.34	0.0
0.07	0-100	0.0	0.0	0.0
	300	0.0	7.4×10^{-2}	3.56×10^{-2}
	1000	1.4×10^{-1}	0.0	0.0
0.05	0-10	0.0	0.0	0.0
	30	0.0	0.0	1.4×10^{-1}
	100	7.98×10^{-2}	0.0	2.8
	300	0.0	4.2×10^{-1}	3.4
	1000	7.98	0.0	3.4
0.03	0-3	0.0	0.0	0.0
	10	0.0	4.8×10^{-1}	0.0
	30	0.0	1.3	5.8×10^{-1}
	100	0.0	4.8	5.8
	300	0.0	3.9	3.8
	1000	0.0		7.8

Table 4.4.1-3, Angular Accelerations for Magnetic Suspension

Frequency	Damping	$\ddot{\theta}$ (arcsec/sec^2)		
		W1	W2	W3
1.0 Hz	D = 0	0	0	10
	3	20	0	10
	10	20	0	20
	30	20	20	30-40
	100	10	20	30-40
	300	10	30	30-40
	1000	10	30	5
0.7	0	0	0	10
	3	0	10	20
	10	20	20	30
	30	40	30	30
	100	20		10
	300	0	60	10
	1000	0		5
0.5	0	0	0	10
	3	0	5	10
	10	20	10	10
	30	50	40	30
	100	30	50	30
	300	10		20
	1000			0
0.3	0	0	0	0
	3	0	5	5
	10	10	10	5
	30	40	60	10
	100	20	70	40
	300	0	60	40
	1000	10		5
0.1	0	0	0	0
	3	0	0	0
	10	0	5	0
	30	15	10	20
	100	50	60	40
	300	170	50	50
	1000	30	160	20

Table 4.4.1-3 Continued

Frequency	Damping	$\ddot{\theta}$ (arcsec/sec^2)		
		W1	W2	W3
0.07 Hz	D = 0	0	0	0
	3	0	0	0
	10	5	0	0
	30	17	10	20
	100	40	40	20-30
	300	110	100	50
	1000			50
0.05	0	30	20	15
	3	20	20	10
	10	30	15	10
	30	60	30	100
	100	200	180	200
	300	30	440	300
	1000	50	off-scale	off-scale
0.03	0	off-scale	off-scale	off-scale
	3	"	"	"
	10	"	"	"
	30	"	"	50
	100	"	"	50
	300	50-100	90	75
	1000	50-60		200

108

4.4.2 Step response

Figures 4.4.2-1 through 4.4.2-4 are typical system responses for input step disturbances of 0.635 centimeter. The first figure shows the response of the undamped magnetic suspension system, D=0 . The X-position displacements and accelerations are approximately sinusoidal, indicating a linear system. No significant decrease in amplitude with time (damping) is seen. A very slight angular acceleration can be seen, although it is close to the noise level of the accelerometer and amplifiers.

The second figure, Figure 4.4.2-2 corresponds to D=100, or in this case a damping ratio (as shown in a later discussion) of .0333. The X-acceleration is less than in the case with no damping and is slightly non-sinusoidal. A slightly larger angular acceleration can be seen but no Y-acceleration. The two curves at the bottom of the figure are the instantaneous voltages across each set of suspension coils. These curves are proportional to the velocities of the magnet arms attached to the air bearing and hence they are proportional to the air bearing velocity (with respect to the shaker) for small rotations. A sharp initial impulse is seen as the step is applied. After this initial impulse the velocity (or control signal) is seen to decrease with decreasing X-displacement and acceleration. The frequency of the control signal is approximately twice that of the X-displacements. This is characteristic of the system since the velocity being measured is velocity toward or away from equilibrium, and motion toward (or away) from equilibrium occurs twice each cycle. (If there is a small amount of rotation in the system, the frequency will tend to be somewhat different).

Figure 4.4.2-3 is for the same system but with a damping ratio of .0674 . Greater non-linearities are seen in all of the outputs except that of position, since at the scale shown the position resolution is not great enough to record the finer movements. Larger angular accelerations and rotations are seen at this higher damping but some of this is believed to be due to the fact that the amplifier in the control signal loop saturated with the large initial velocity signals. It can be seen that the first two peaks of the control signals are clipped due to the saturation.

In the next figure, Figure 4.4.2-4, the damping constant is .0784. Larger deviations from sinusoidal response are seen, although even in this case very little acceleration was transferred to the Y-axis. The control system saturated a number of times in the first few cycles after the occurrence of the step. The gain in the control system amplifier (K=1000) was actually too gɪ ɪat for the components in this system. A great deal of noise as well as amplifier saturation can be seen in one of the control signals. This data was taken to show the versatility of the magnetic damping system and the independence of the suspension characteristics on the detailed properties of the control signal electronics. Since system stability is not dependent on a control signal (as it is in some types of magnetic suspension systems) the system remained operational even though the amplifiers occasionally saturated and the noise in one circuit was greater than the signal for most of the observation time. Even under such conditions, suspension and isolation were maintained and a damping ratio of .0784 was obtained.
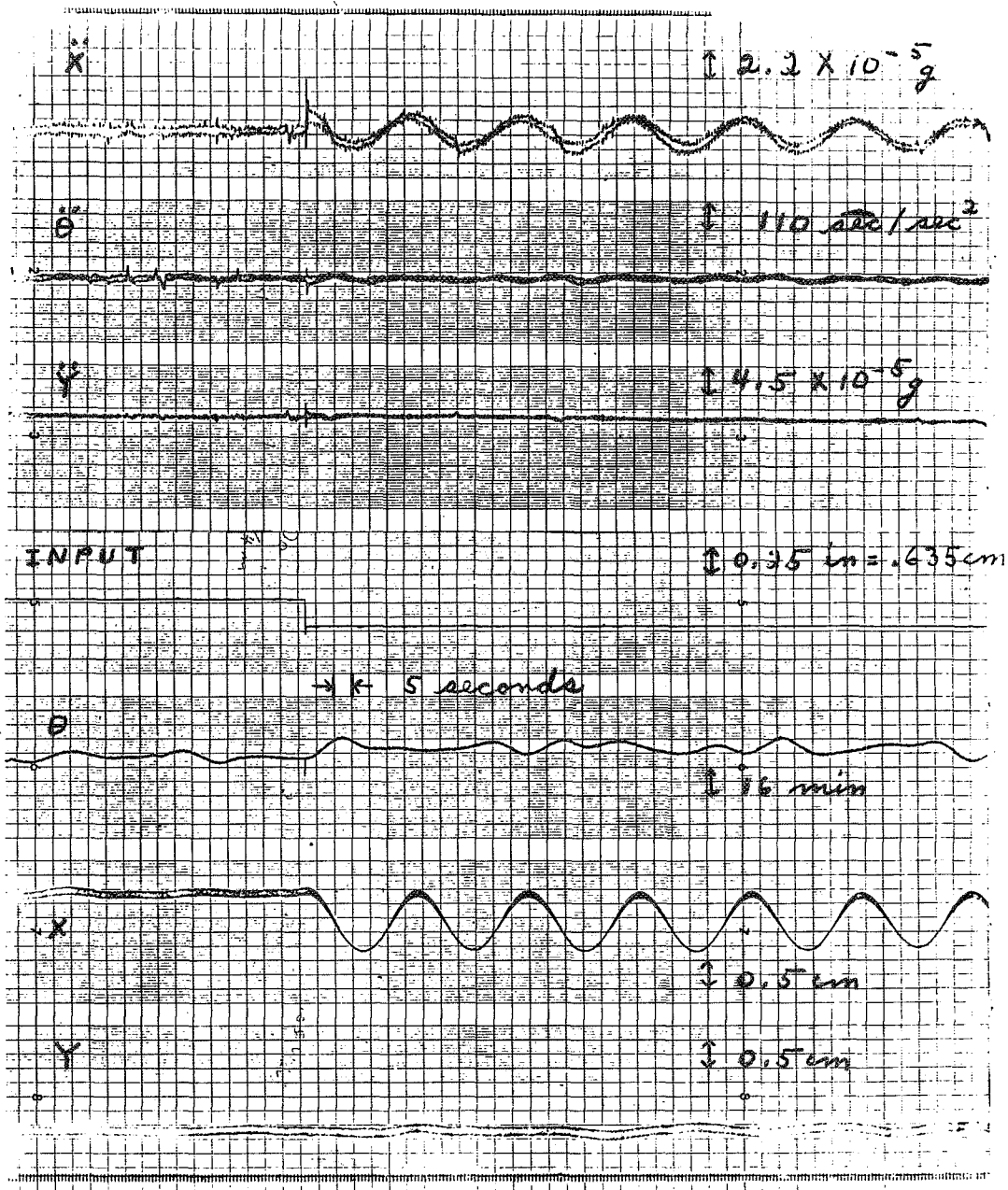
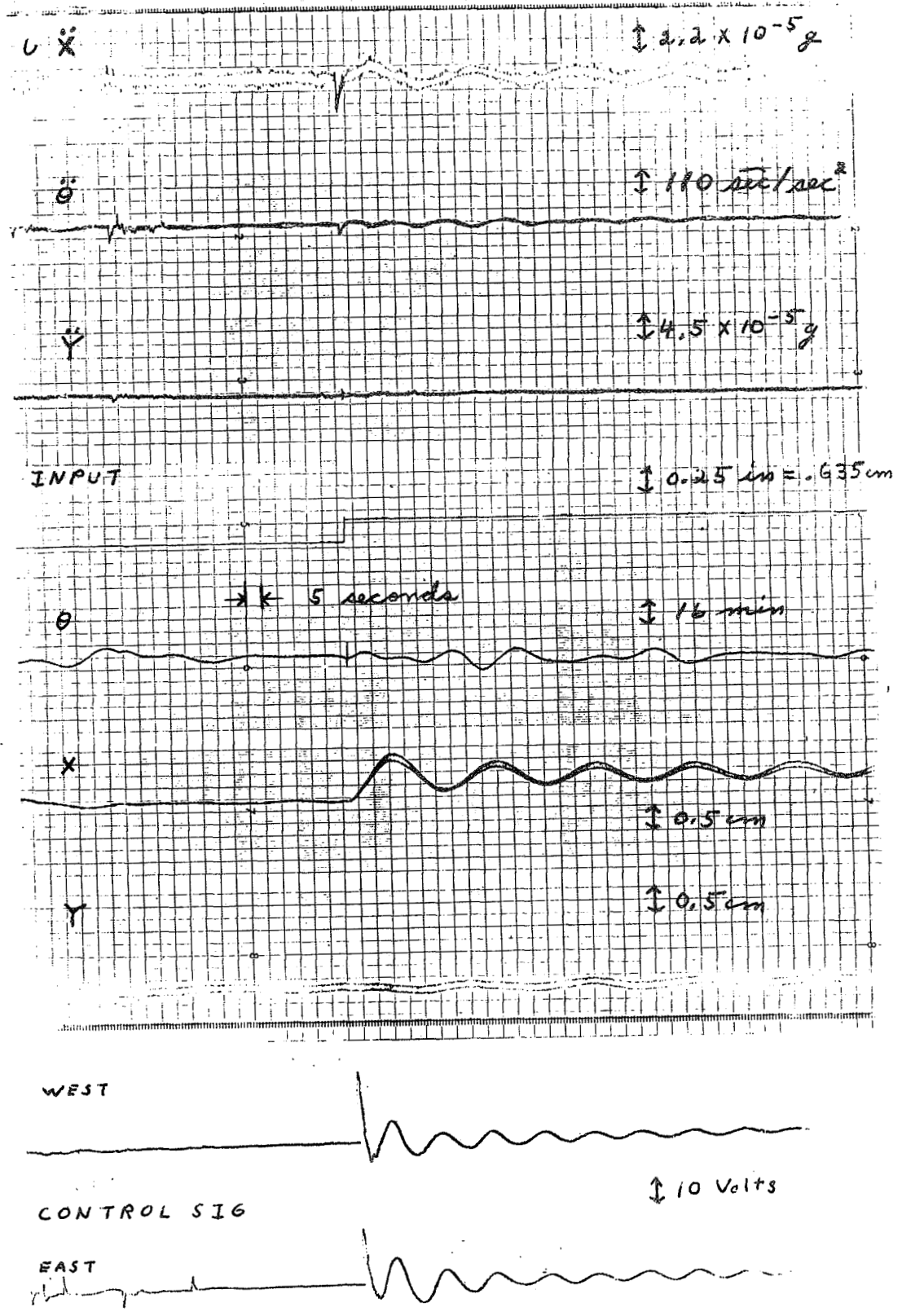Figure 4.4.2-1, Step Response, No Damping

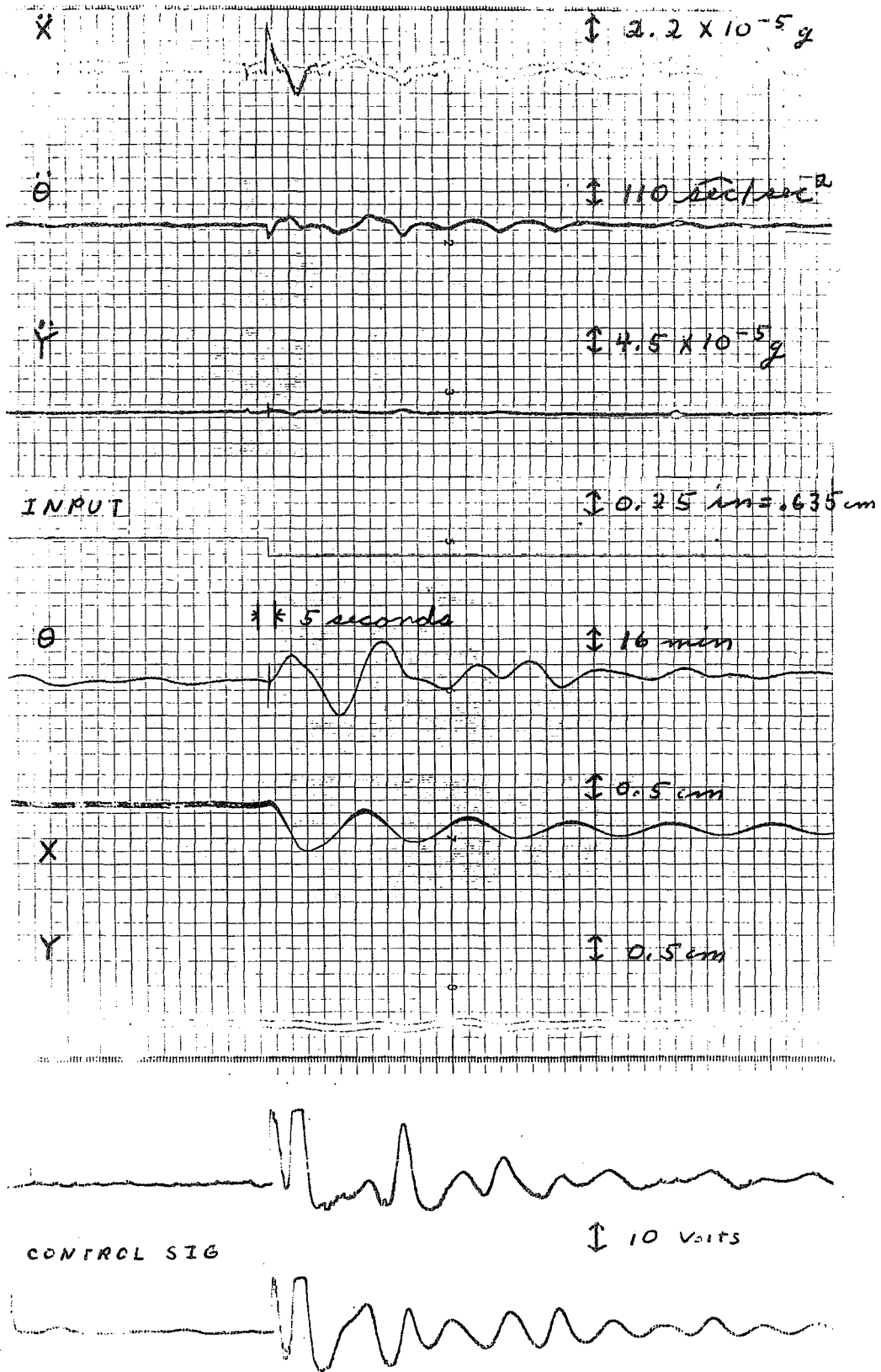Figure 4.4.2-2, Step Response, D100

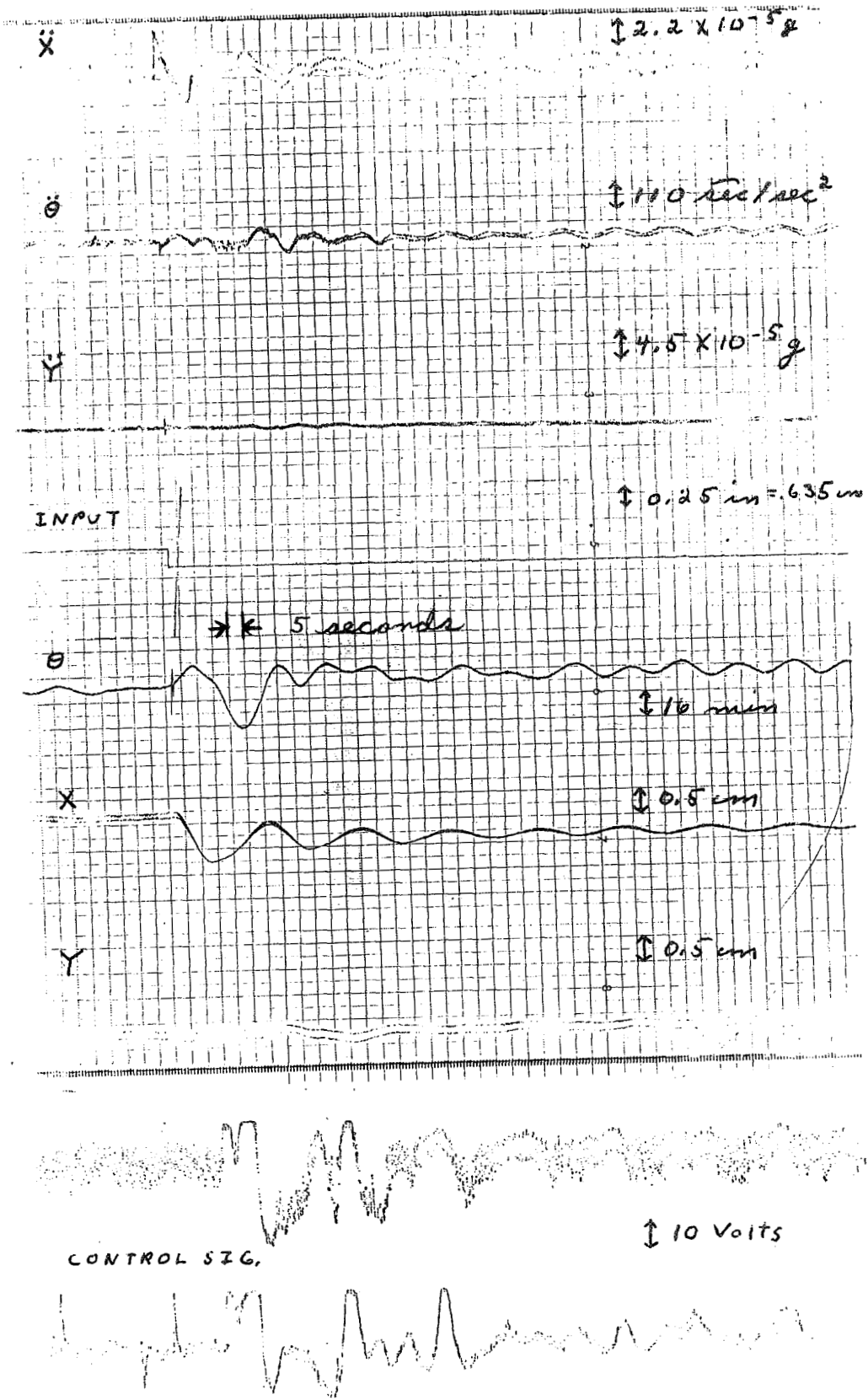Figure 4.4.2-3, Step Response, D300

Figure 4.4.2-4, Step Response, D1000

It should be possible to eliminate this noise by means of low pass filters, since the frequency of the noise is much higher than that of the system. Most of the noise is believed to be picked up from the overhead lights and other electrical circuits adjacent to the velocity sensing coils. It was also found that at the higher gains for the control signal loop, the output voltages were a more sensitive indication of air bearing movement than the accelerometers.

Calculation of damping ratio

The response of the magnetic system to the application of approximately sinusoidal, and by comparing this response in the X direction to a one dimensional classical oscillator, one can obtain a rough approximation to a damping ratio.

The differential equation for a one dimensional classical oscillator is

$$\frac{d^2x}{dt^2} + \frac{\beta}{m}\frac{dx}{dt} + \frac{k}{m}x = 0$$

or

$$\frac{d^2x}{dt^2} + \gamma\frac{dx}{dt} + \omega_0^2 x = 0$$

where

$$\omega_0 = \sqrt{k/m}$$

and

$$\gamma = \beta/m$$

The damped vibration is at a lower frequency than the undamped vibration, as noted in the equation below.

$$\omega_0' = \sqrt{\frac{k}{m} - \frac{\beta^2}{4m}} = \sqrt{\frac{k}{m} - \frac{\gamma^2}{4}}$$

Critical damping occurs when

$$\beta_c^2 = 4km$$

or

$$\gamma_c^2 = 4k/m = 4\omega_0^2$$

i.e.

$$\gamma_c = 2\omega_0$$

114

The differential equation can then be written

$$\frac{d^2x}{dt^2} + z\gamma_c \frac{dx}{dt} + \omega_o^2 x = 0$$

where

$$z = \gamma/\gamma_c = \text{damping ratio}$$

$$z = 0 \qquad \text{no damping}$$

$$z < 1 \qquad \text{damping}$$

$$z = 1 \qquad \text{critical damping}$$

$$z > 1 \qquad \text{over damping}$$

The ratio, p, of two maximum deflections separated in time by n cycles is given by

$$p = \frac{x(t)}{x(t + nT)} = \exp(\tfrac{1}{2}n\gamma T)$$

$$= \exp(\tfrac{1}{2}nz\gamma_c T)$$

The logarithmic decrement, δ, is defined as

$$\delta_n = \ln p = \tfrac{1}{2}n\gamma T$$

or

$$\frac{d(\log p)}{dn} = \tfrac{1}{2}\gamma T \log e = m = \text{slope}$$

where $\log p$ signifies base ten logarithm.

Therefore, if the successive amplitudes on a ligarithmic scale are plotted as a function of time (or the number of cycles), the result is a straight line whose slope, m, is related to the damping ratio, z, by:

$$z = \frac{1}{2\pi \log e} \frac{T_o}{T} m = .3665 \frac{T_o}{T} m$$

115

where To is the natural period of the undamped system and T is the period of the damped system.

The graphs on the following pages show the decreasing successive amplitudes as a function of time (n cycles). From the slopes of these curves, the damping ratios are obtained according to the preceding equation.

The graphs are titled according to the gain of the 1st amplifier in the velocity feedback loop, i.e. referring to figure B5 in appendix B, D_3 signifies that K = 3. It will be noticed that especially for the larger values of damping, the lines in these graphs do not always fall midway between the data points. Where a straight line could not be drawn through all of the data points, only the first 3 or 4 points were used (for example D 300) as these were considered the most accurate. For large damping the amplitude became very small after 3 or 4 cycles and hence the accuracy of the measurements suffered. Also, at the small amplitudes external disturbances have a greater effect on the accuracy of the successive ratios than at larger amplitudes.

Because the system is non-linear, the damping ratios obtained by the above procedure are only approximate. The ratios are used only as a comparison to a classical one dimensional oscillation. The one dimensional assumption is partially justified by the fact that the disturbance transmitted in the Y direction is relatively small (approximately 1:10).

AMPLITUDE ATTENUATION

$$\frac{X(t + NT_o)}{X(t)} \quad \text{vs. } N$$

Configuration W1

Figure 4.4.2-5, Amplitude Attenuation, D3

Figure 4.4.2-6, Amplitude Attenuation, D10

The graph shows a plot with the y-axis labeled $\frac{X(nT_0)}{X(0)}$ ranging from .1 to 1.0 (logarithmic scale) and the x-axis labeled n (cycles) ranging from 0 to 8.

Weight Configuration W1
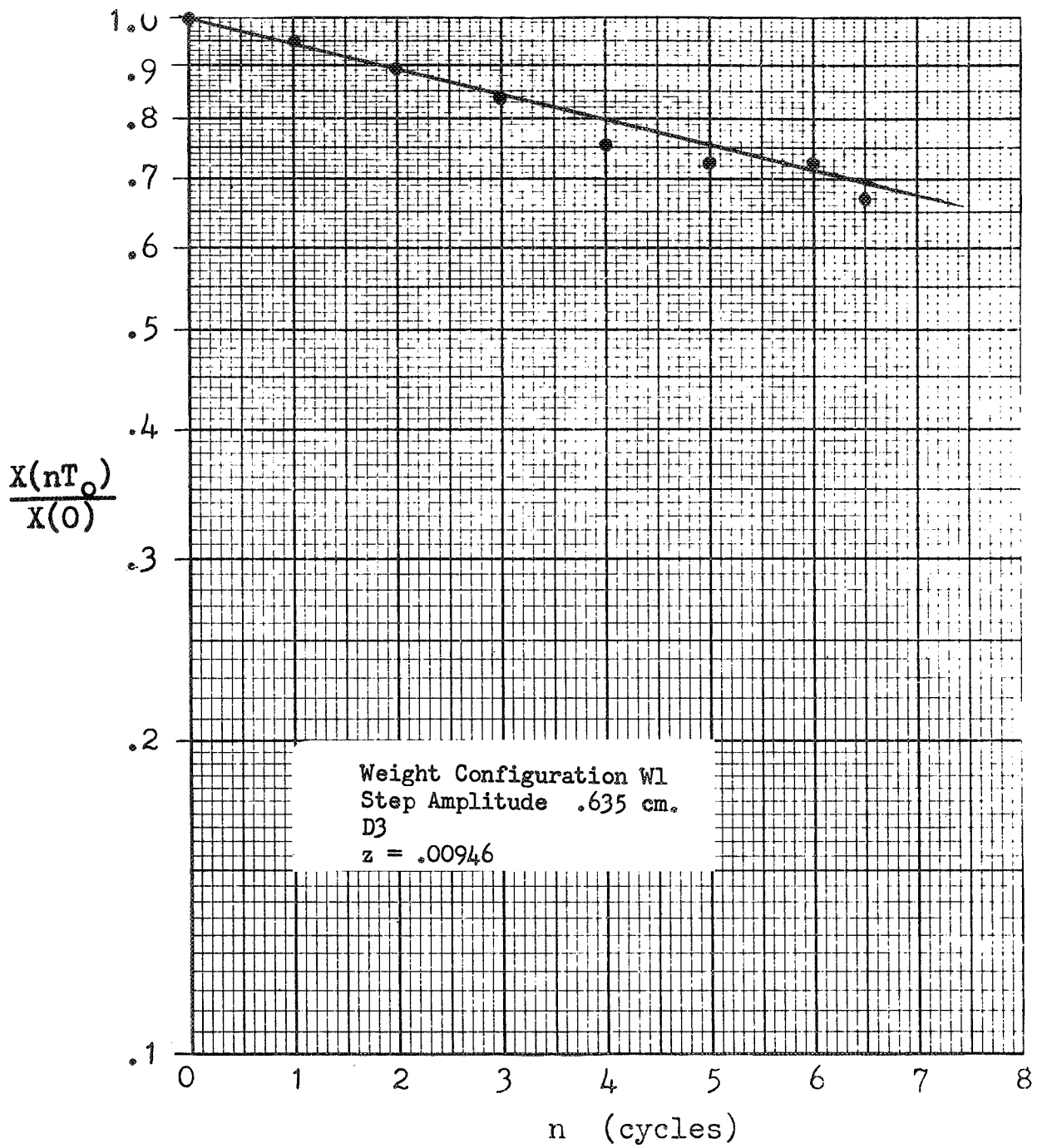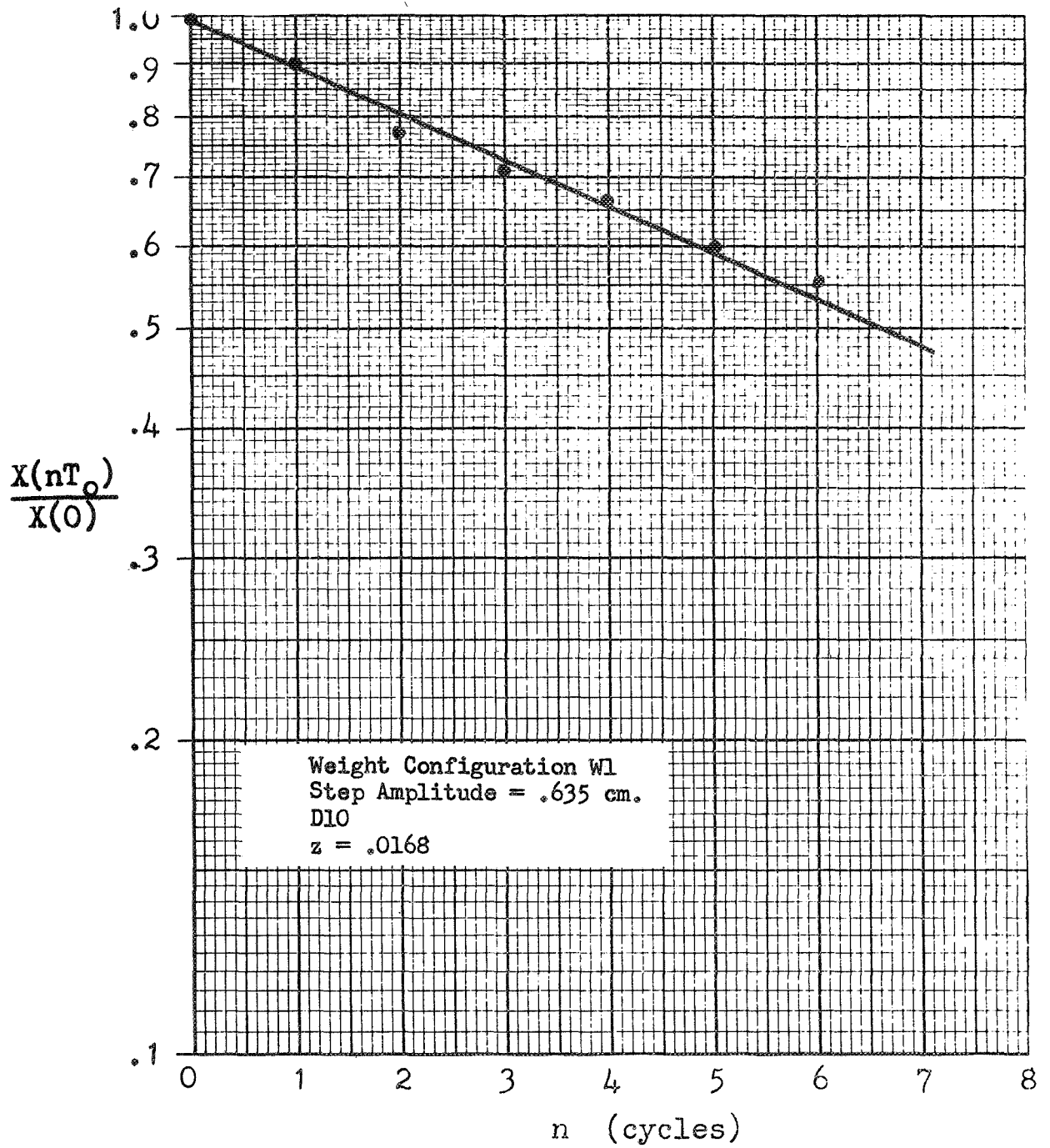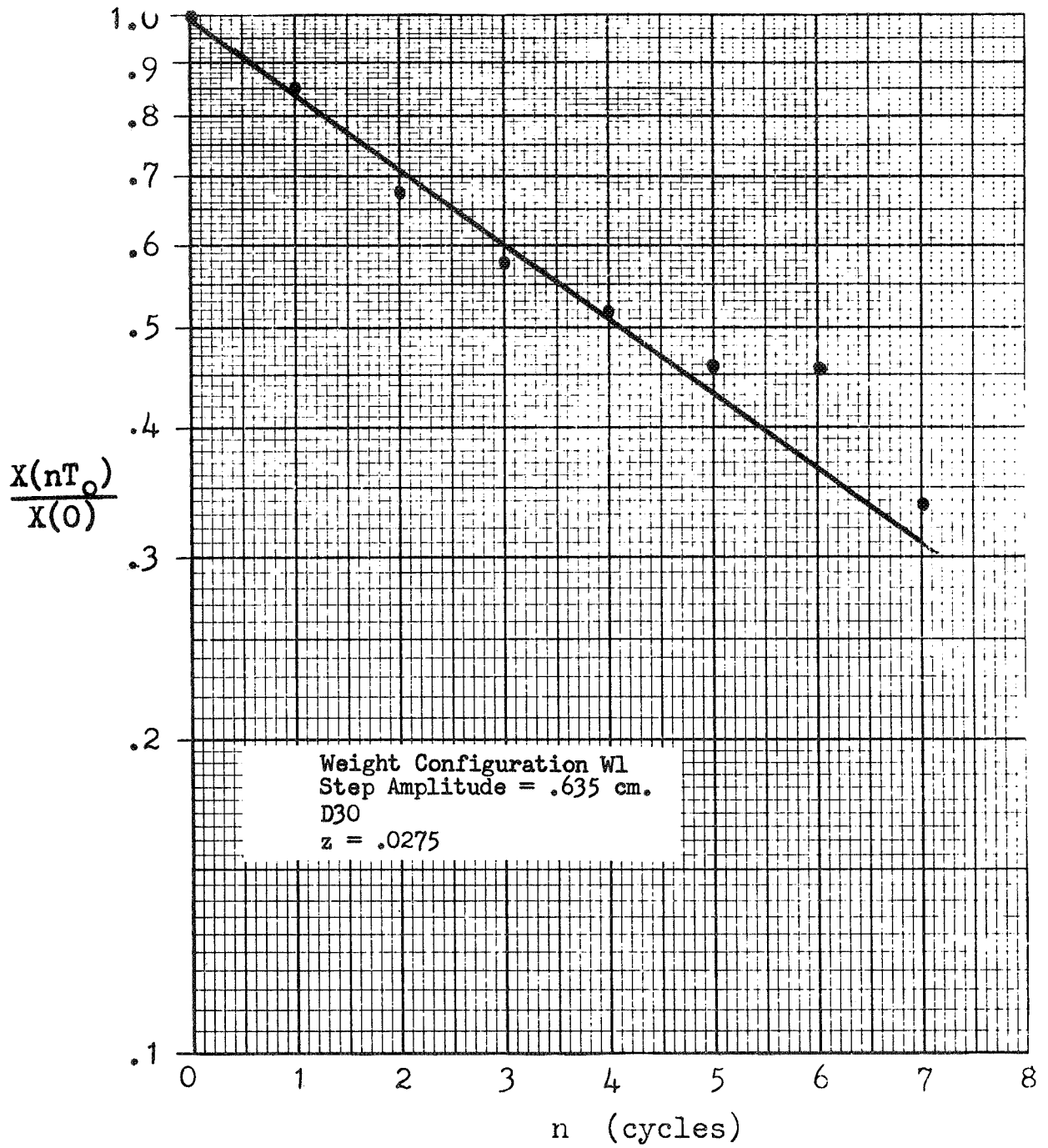Step Amplitude = .635 cm.
D10
z = .0168

Figure 4.4.2-7, Amplitude Attenuation, D30

Figure 4.4.2-8, Amplitude Attenuation, D100
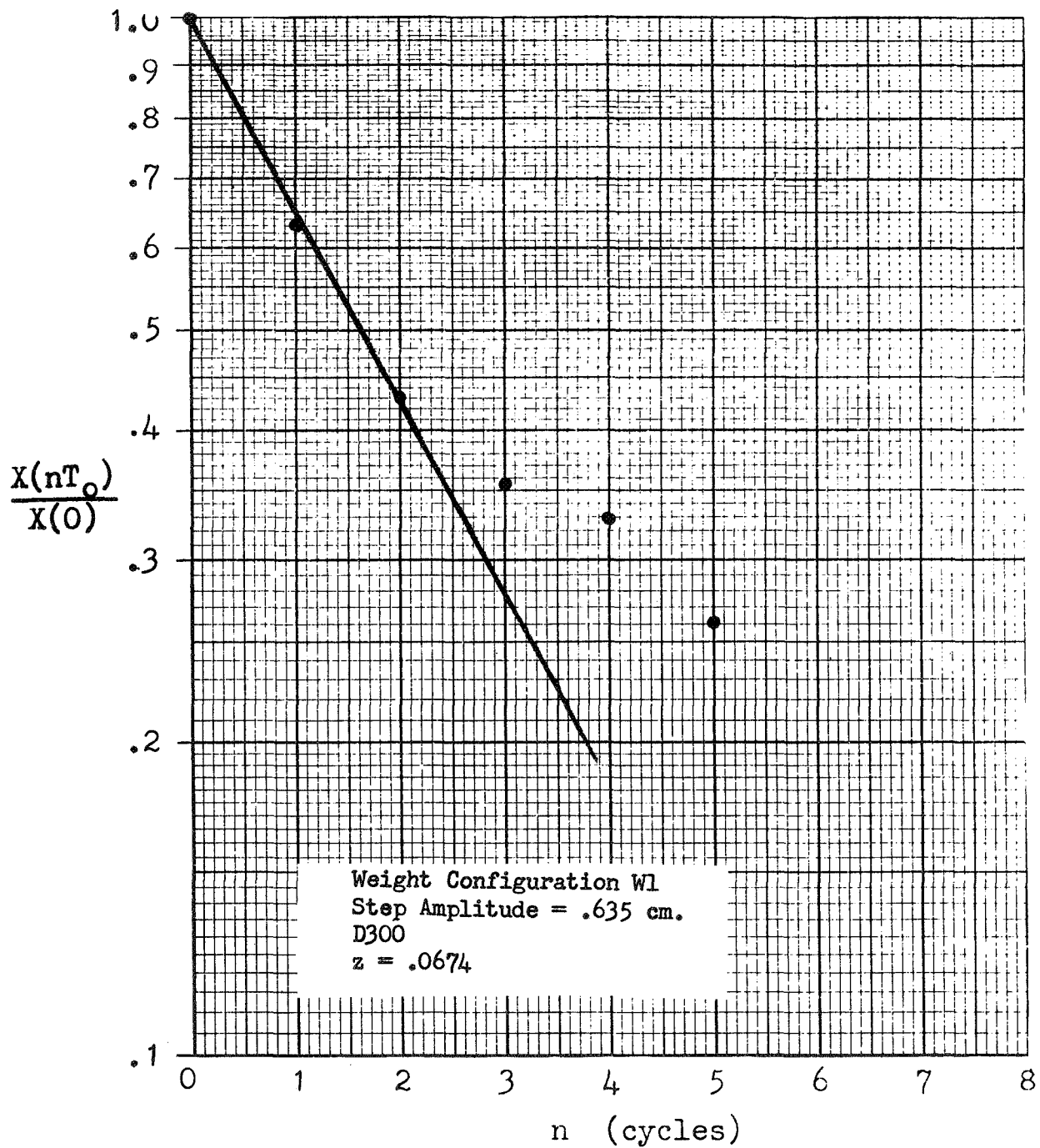
Figure 4.4.2-9, Amplitude Attenuation, D300

122

Figure 4.4.2-10, Amplitude Attenuation, D1000

123

AMPLITUDE ATTENUATION

$$\frac{X(t + NT_o)}{X(t)} \text{ vs. } N$$

Configuration W2

Figure 4.4.2-11, Amplitude Attenuation, D3

Figure 4.4.2-12, Amplitude Attenuation, D10
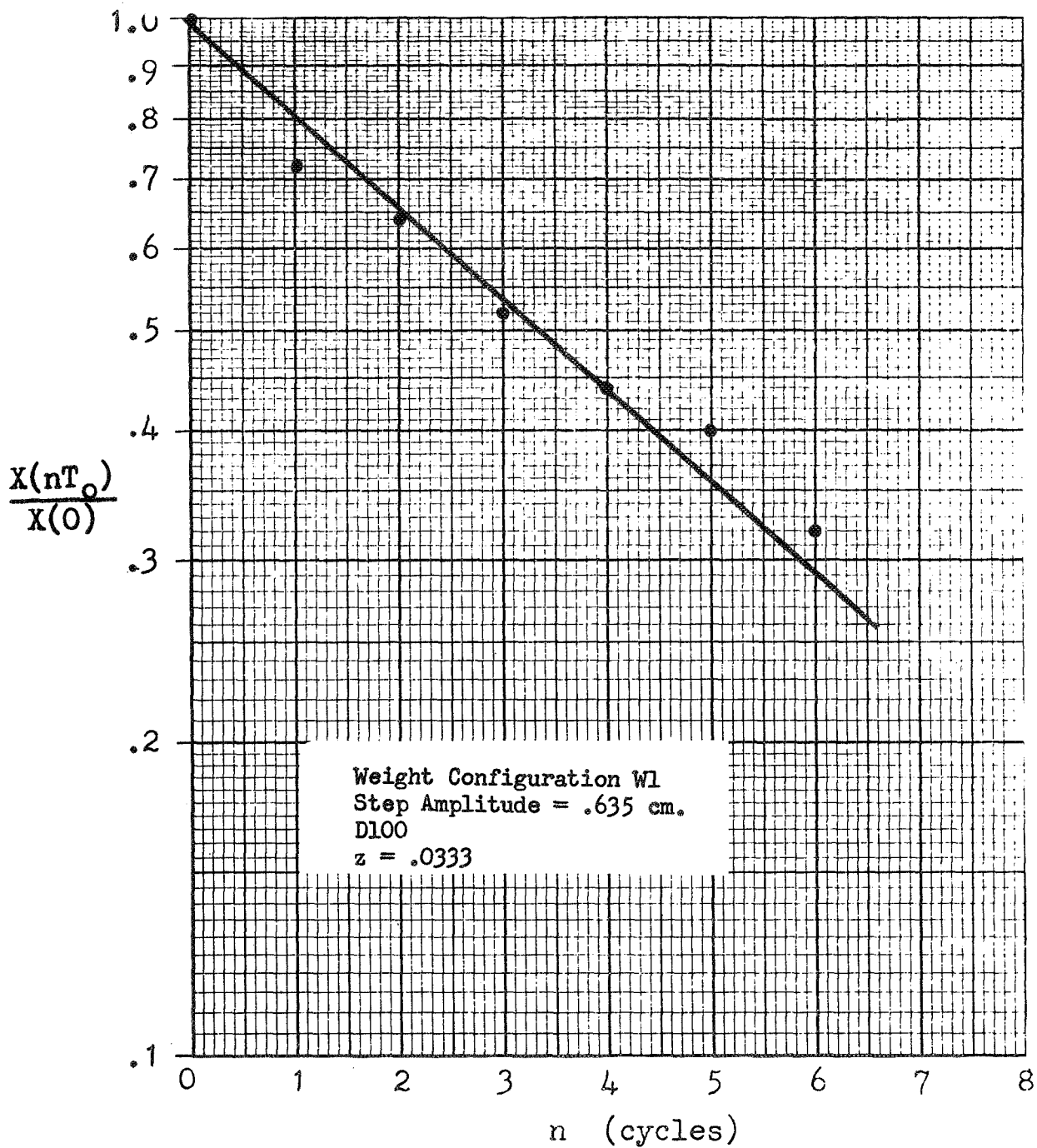
Figure 4.4.2-13, Amplitude Attenuation, D30

127

Figure 4.4.2-14, Amplitude Attenuation, D100

Figure 4.4.2-15, Amplitude Attenuation, D300

129

Figure 4.4.2-16, Amplitude Attenuation, D1000

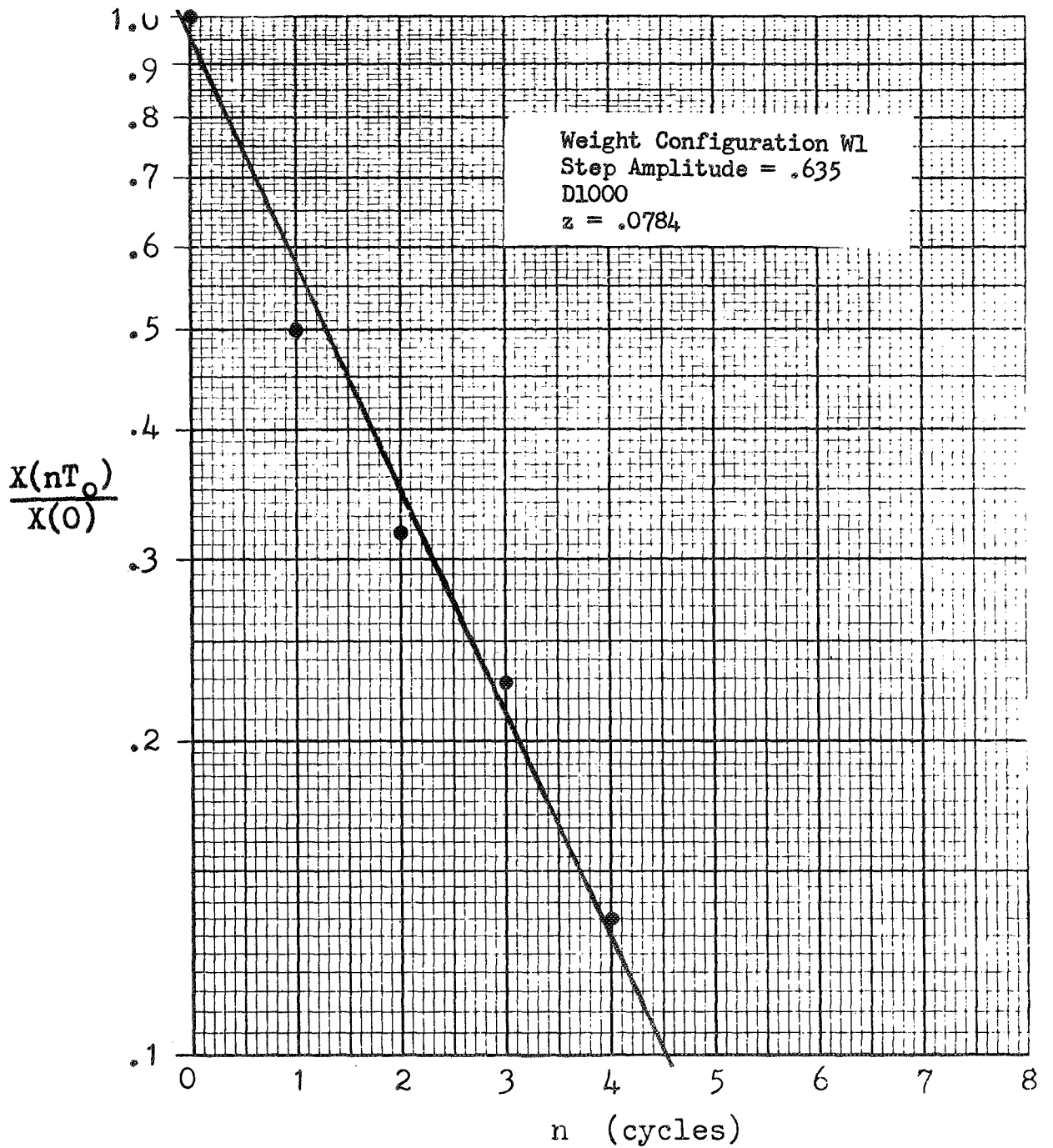The figure shows a semi-log plot with y-axis labeled $\frac{X(nT_0)}{X(0)}$ ranging from .1 to 1.0, and x-axis labeled n (cycles) from 0 to 8.

Text box on graph:
Weight Configuration W2
Step Amplitude = .635 cm.
D1000
z = .101

AMPLITUDE ATTENUATION

$$\frac{X(t + NT_o)}{X(t)} \text{ vs. } N$$

Configuration W3

Figure 4.4.2-17, Amplitude Attenuation, D3

The graph contains the following annotations:

$$\frac{X(nT_o)}{X(0)}$$

n (cycles)

Weight Configuration W3
Step Amplitude = .635 cm.
D3
z = .0150
△ $\ddot{X}(nT_o)/\ddot{X}(0)$

132
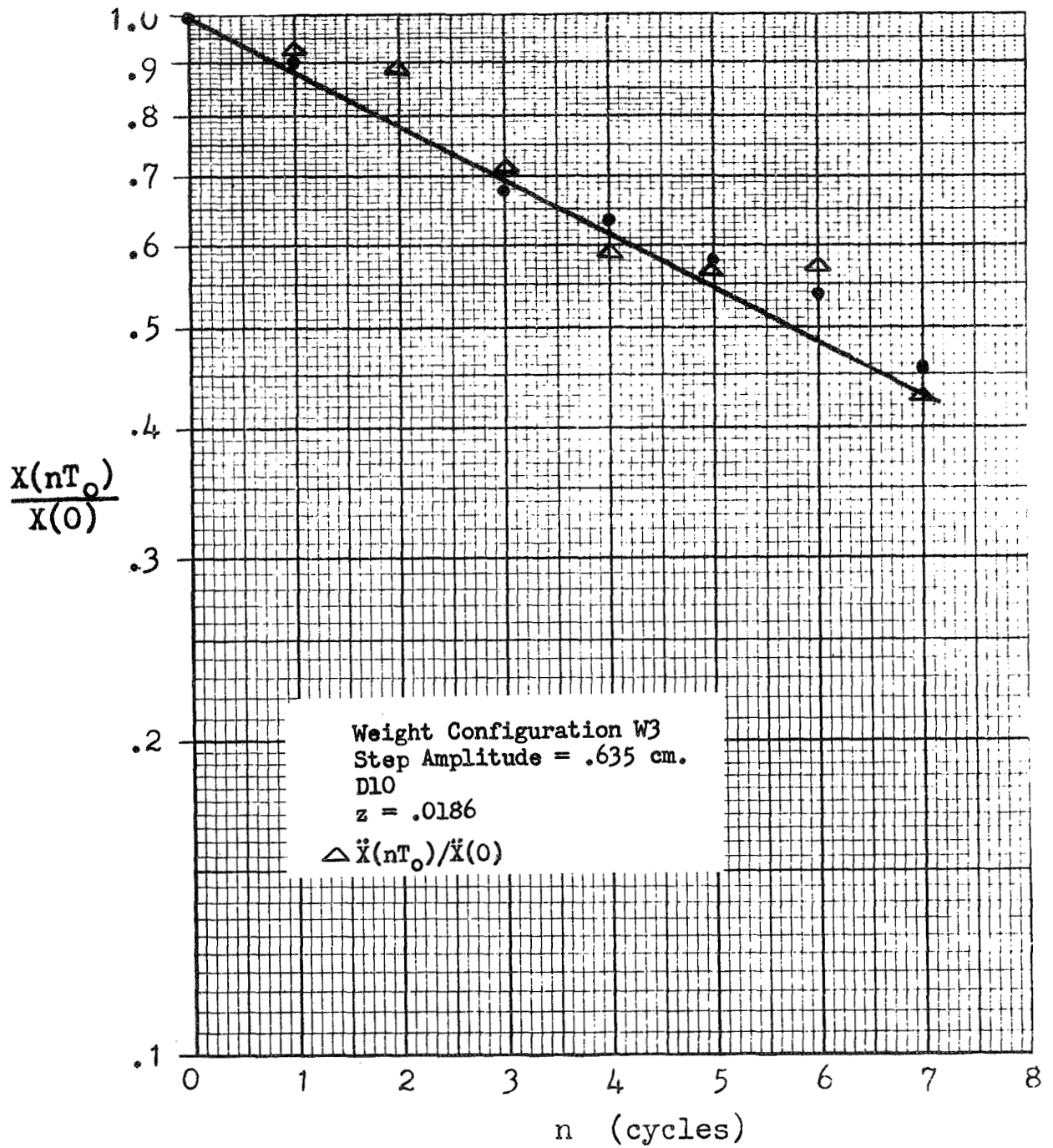
Figure 4.4.2-18, Amplitude Attenuation, D10

133
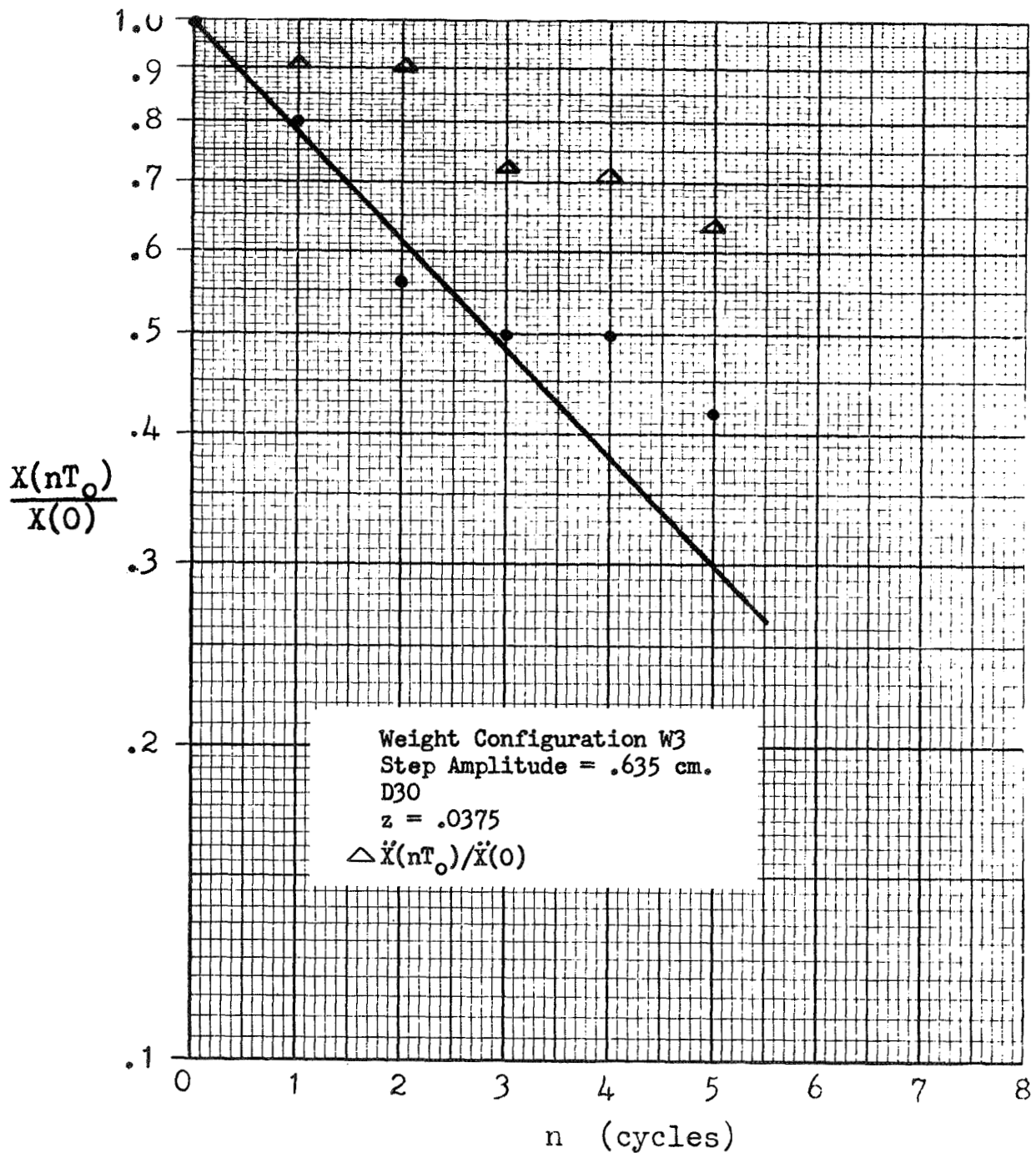
Figure 4.4.2-19, Amplitude Attenuation, D30

The figure contains the following annotations:

Weight Configuration W3
Step Amplitude = .635 cm.
D30
$z = .0375$
$\triangle \ddot{X}(nT_o)/\ddot{X}(0)$

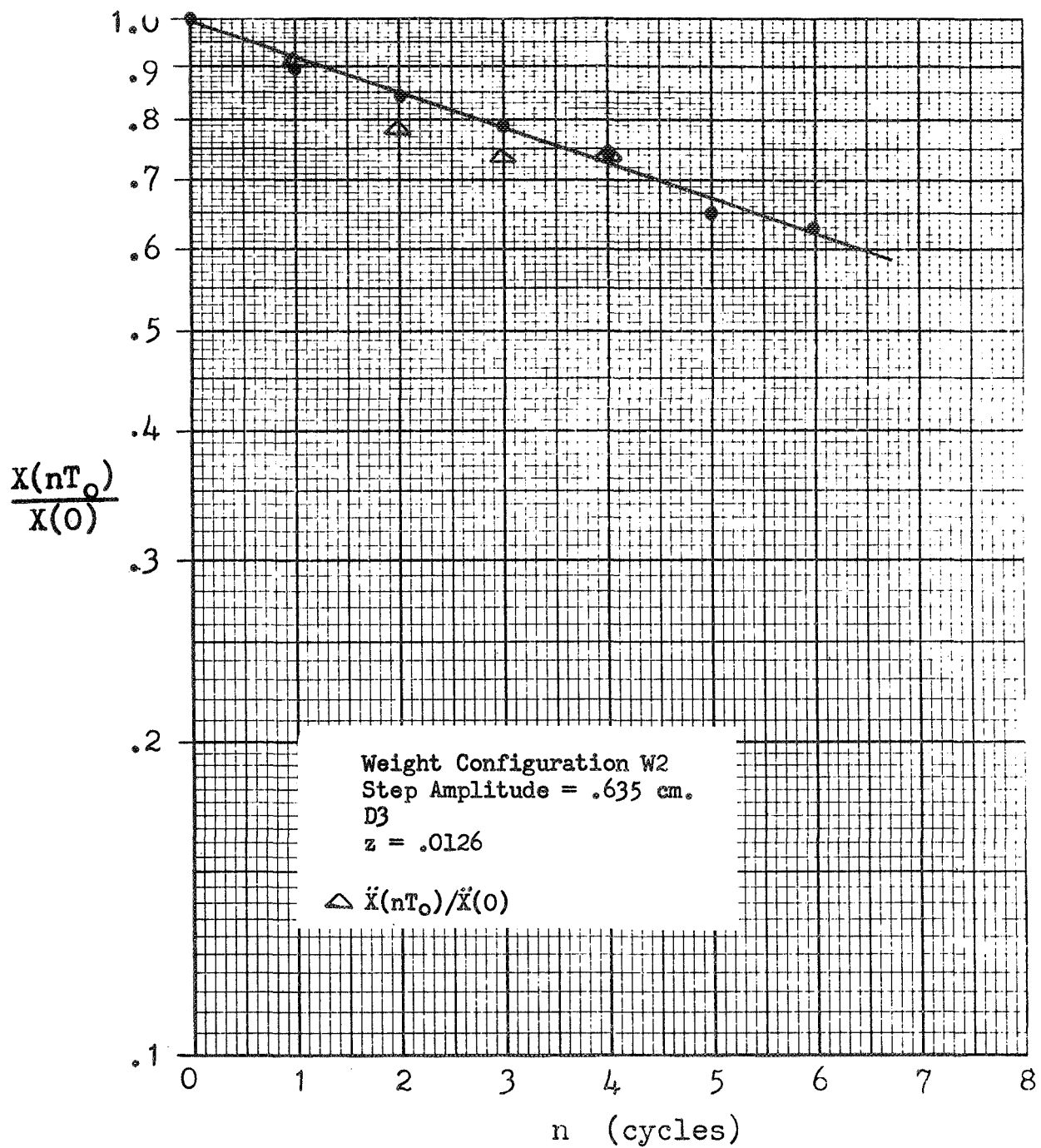Vertical axis: $\dfrac{X(nT_o)}{X(0)}$
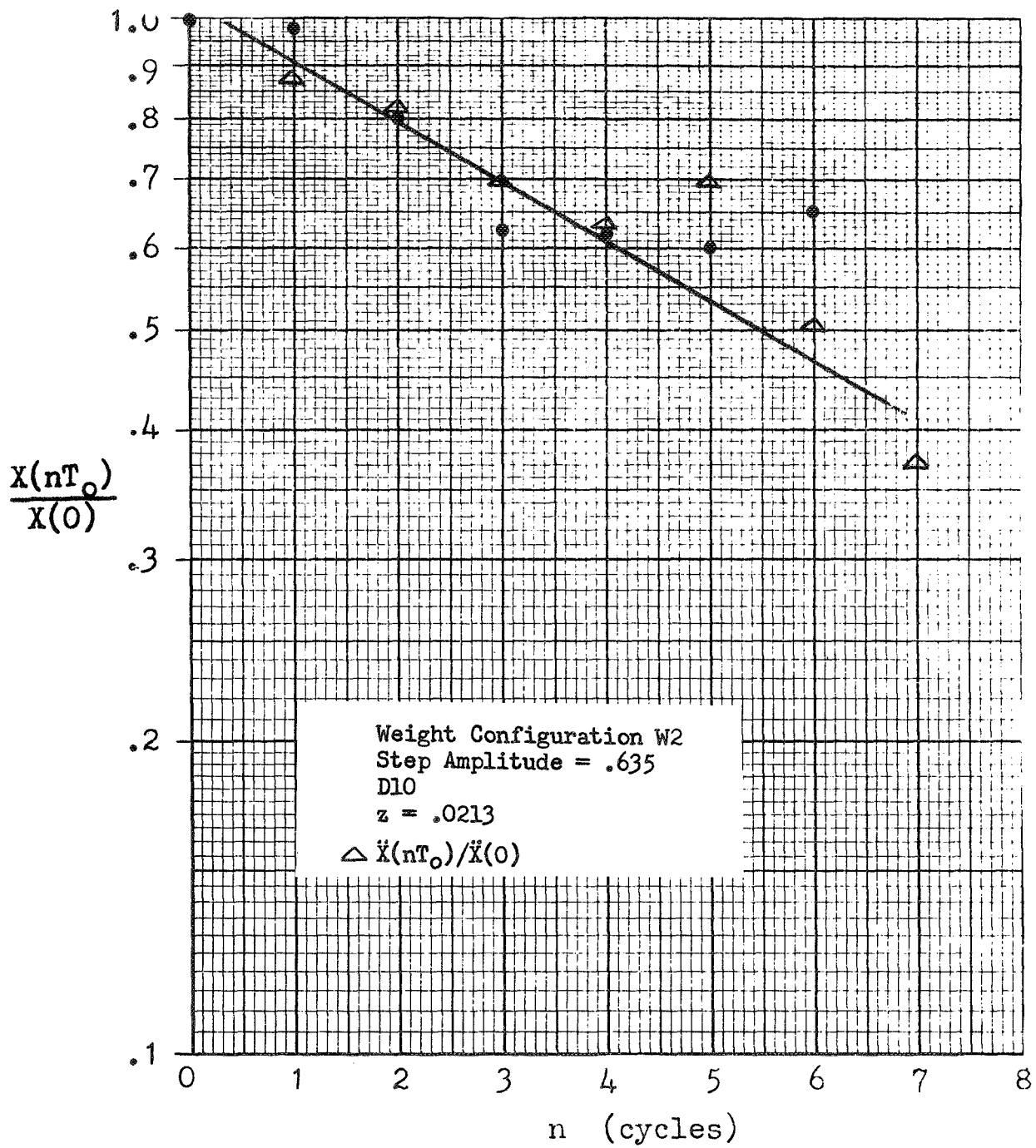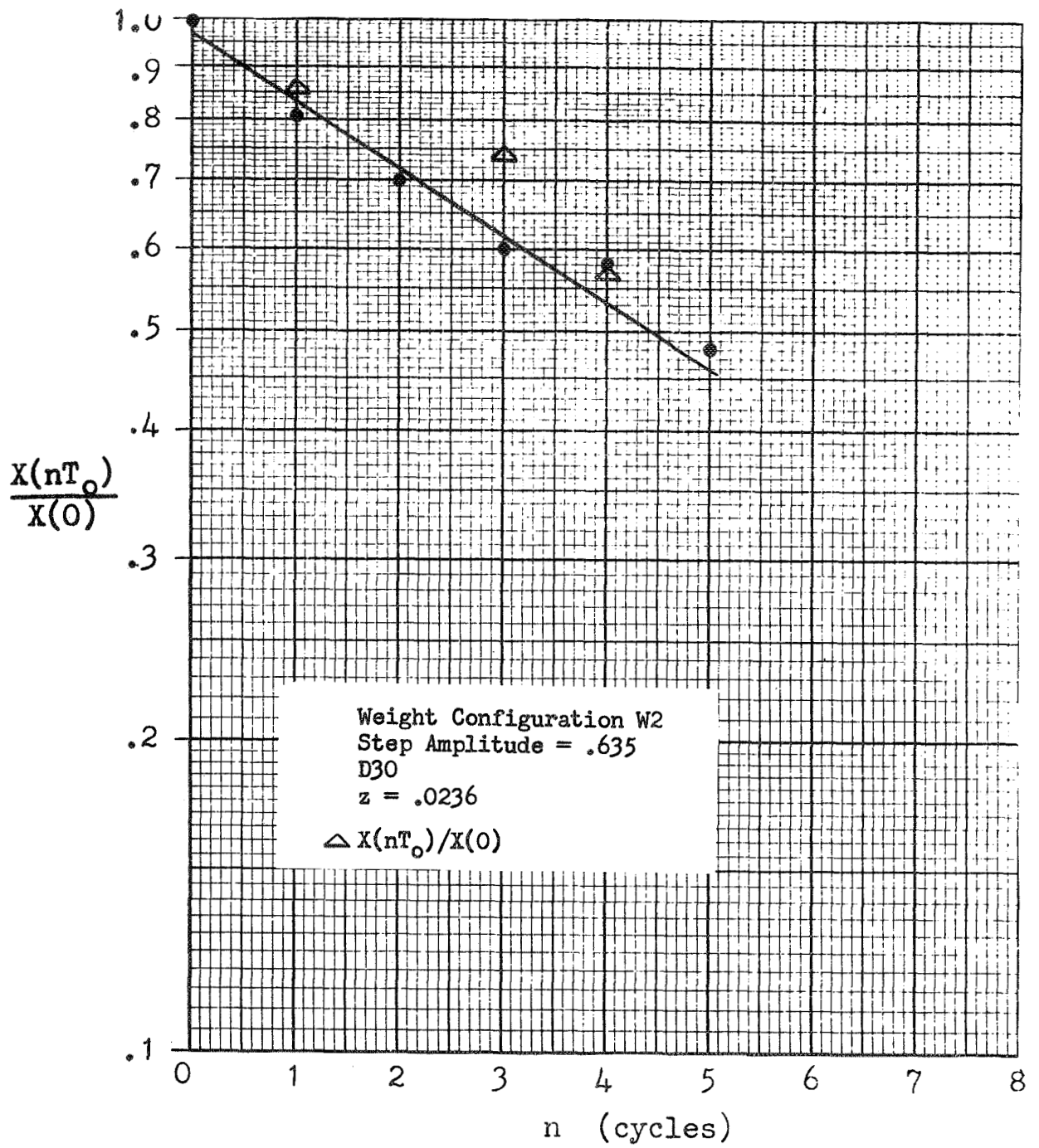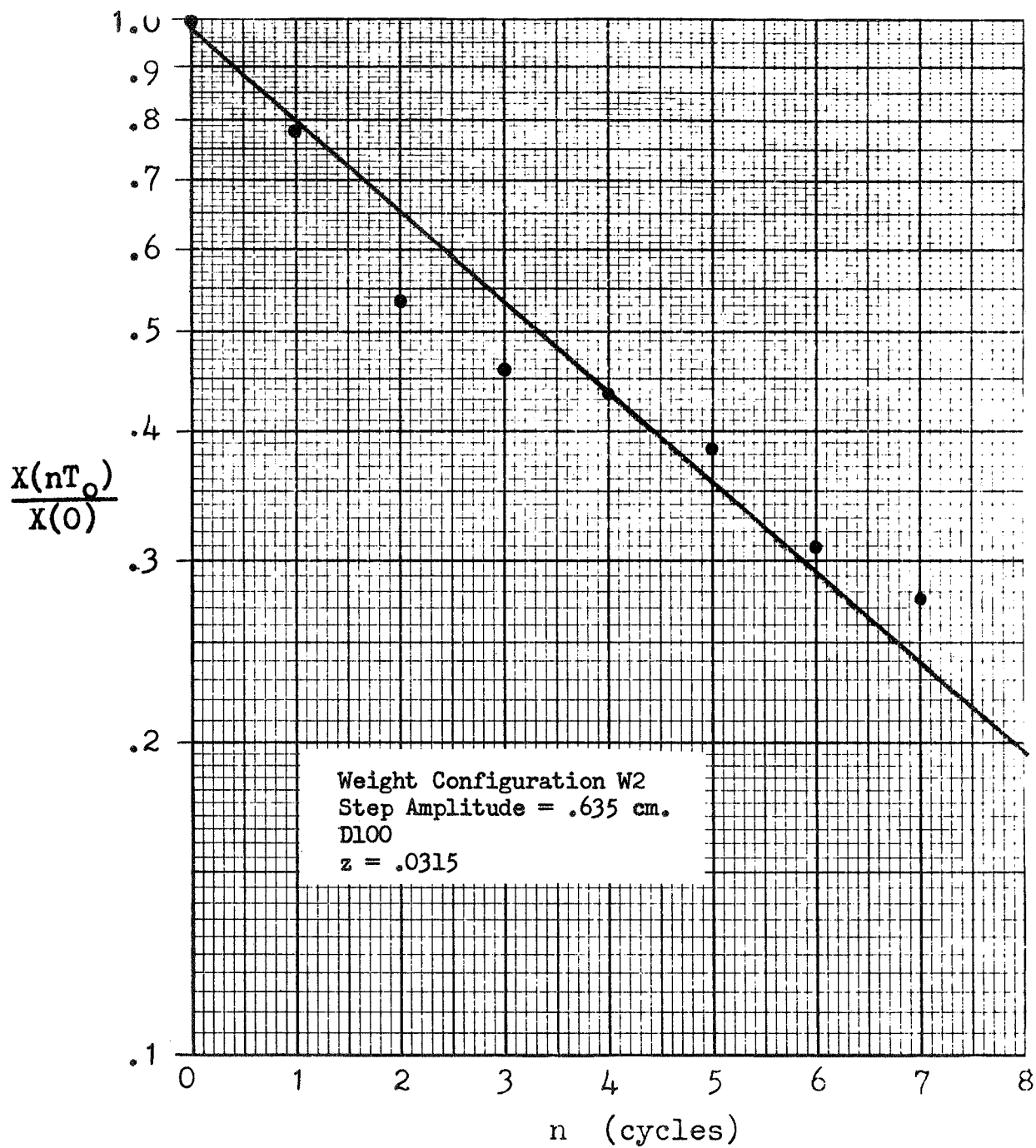
Horizontal axis: n (cycles)
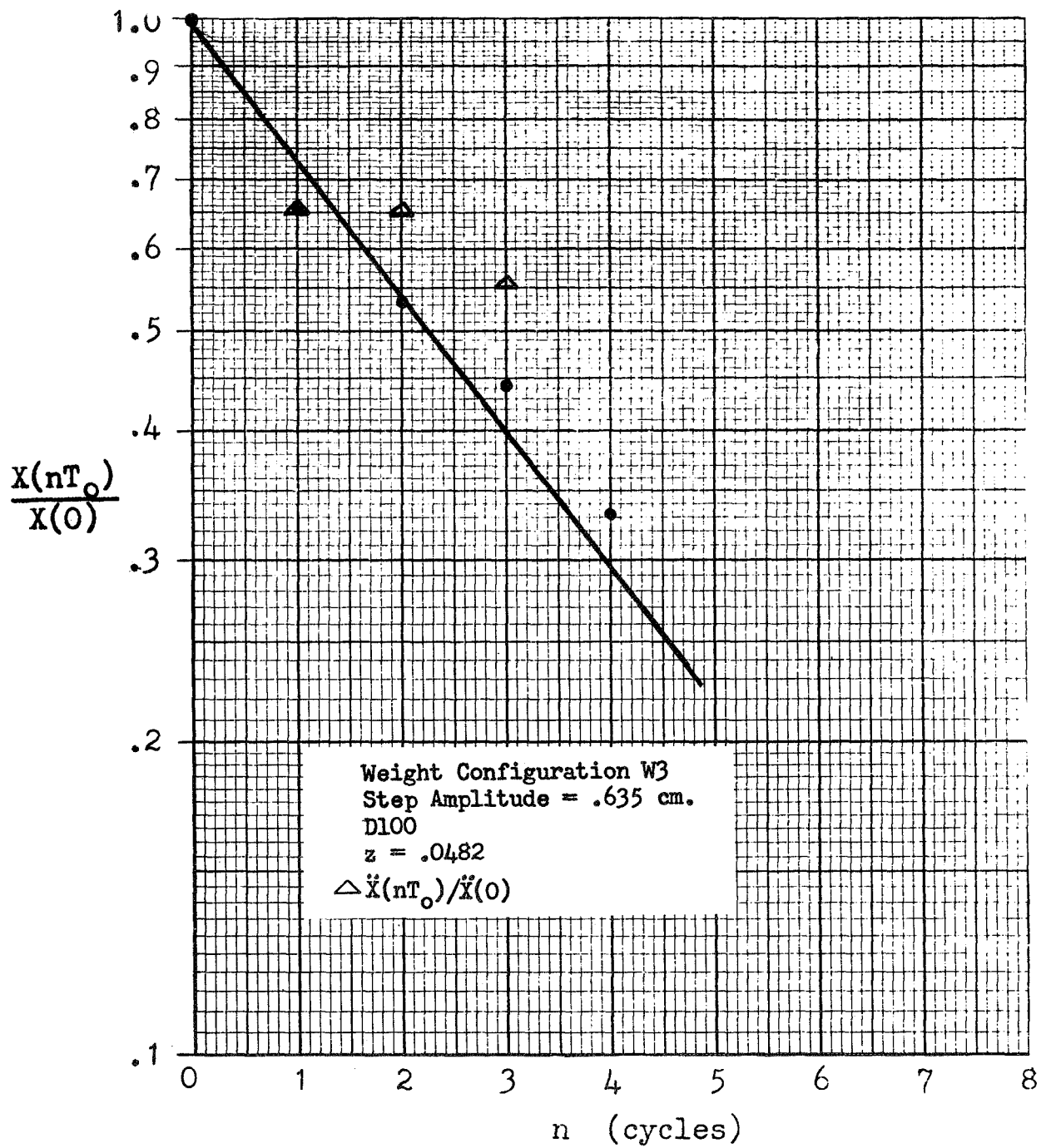
Figure 4.4.2-20, Amplitude Attenuation, D100
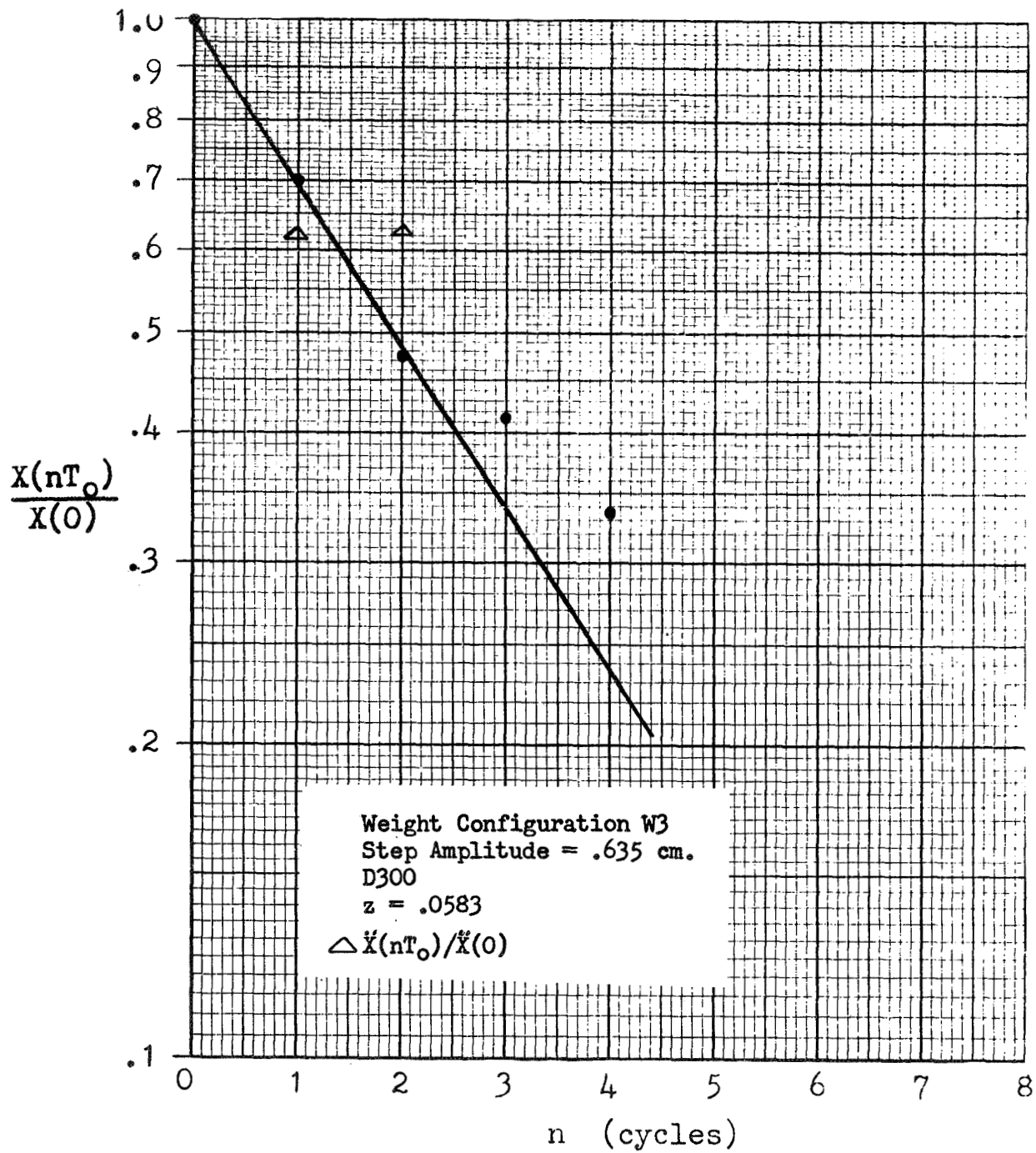
Figure 4.4.2-21, Amplitude Attenuation, D300
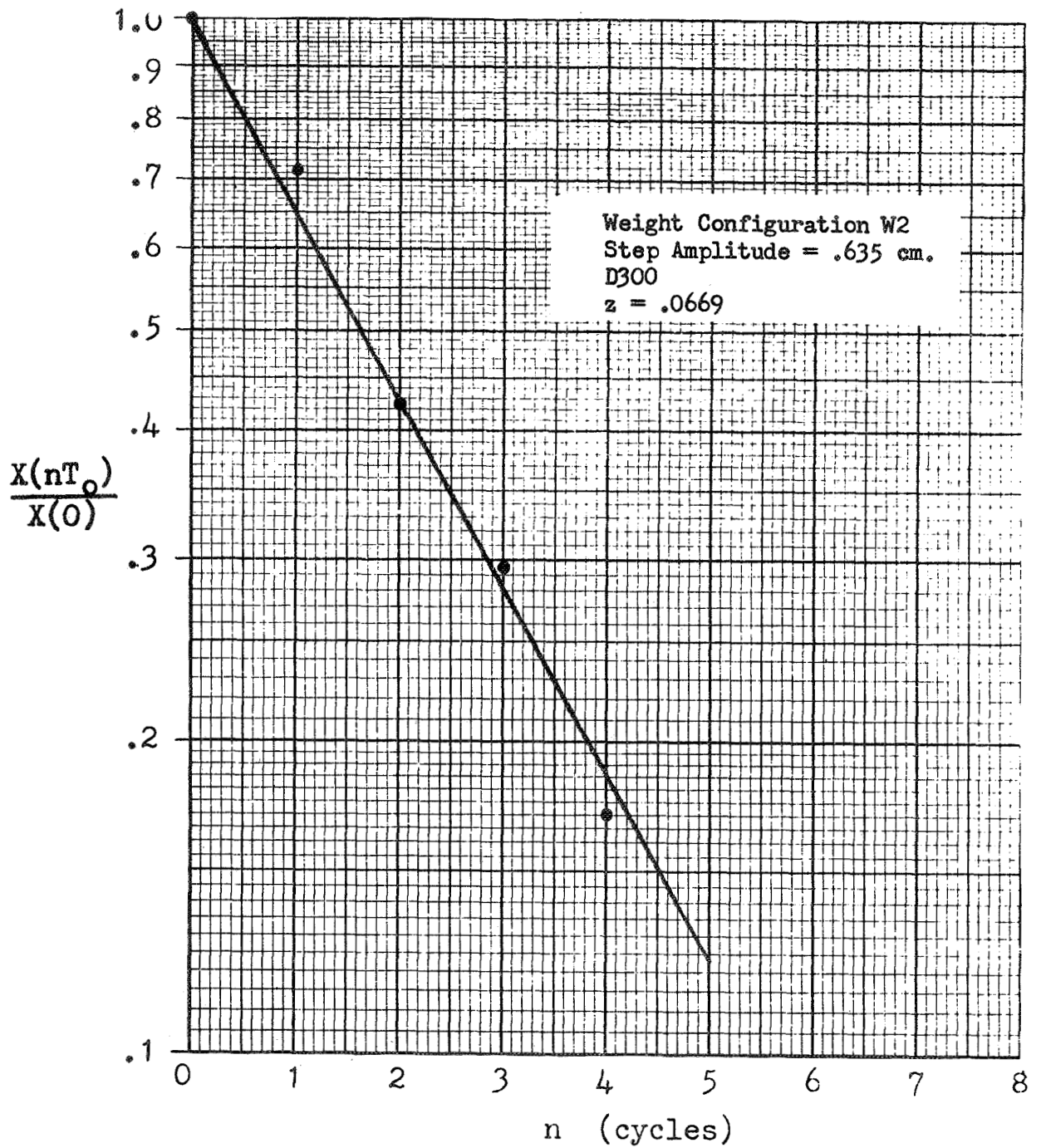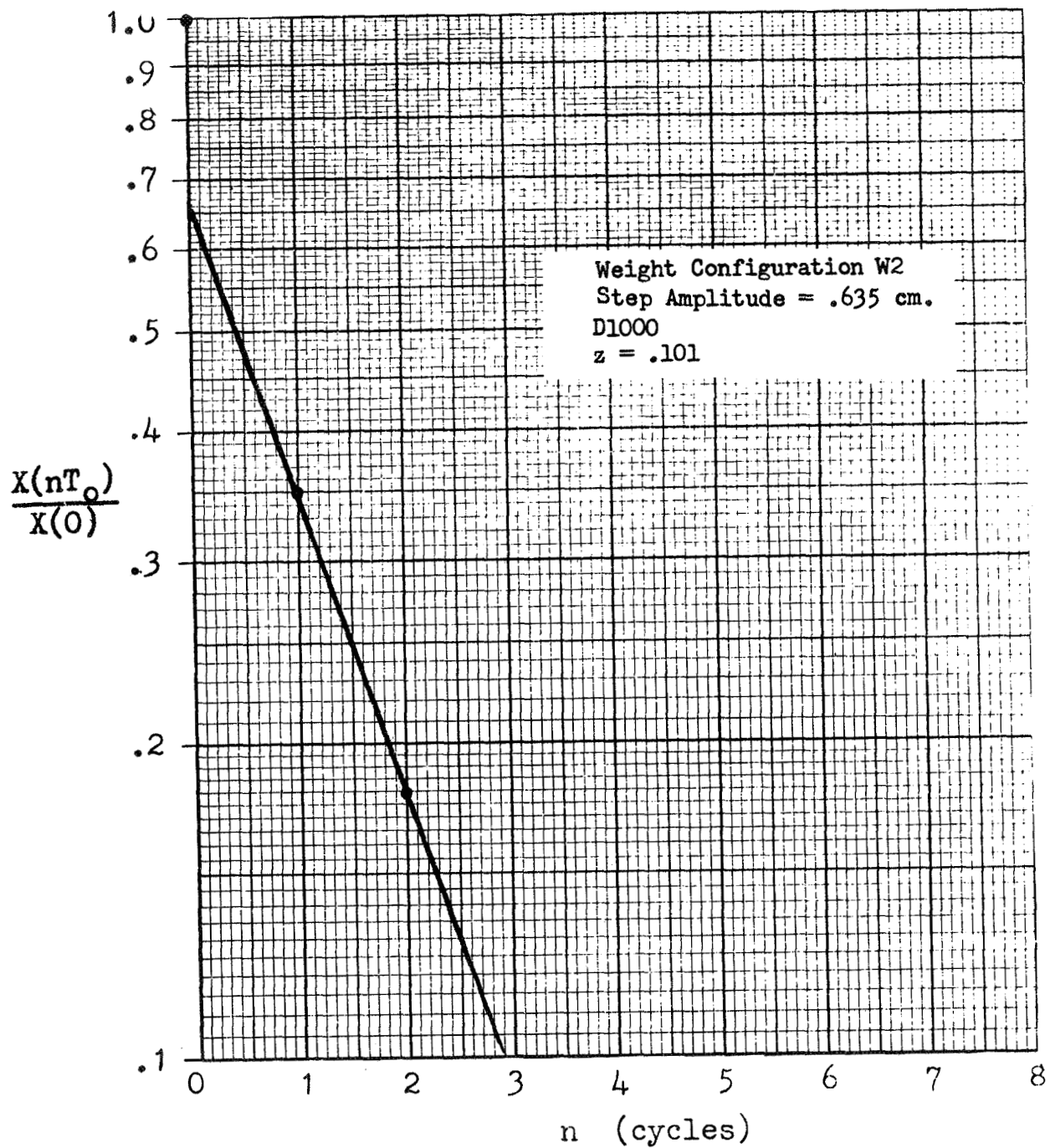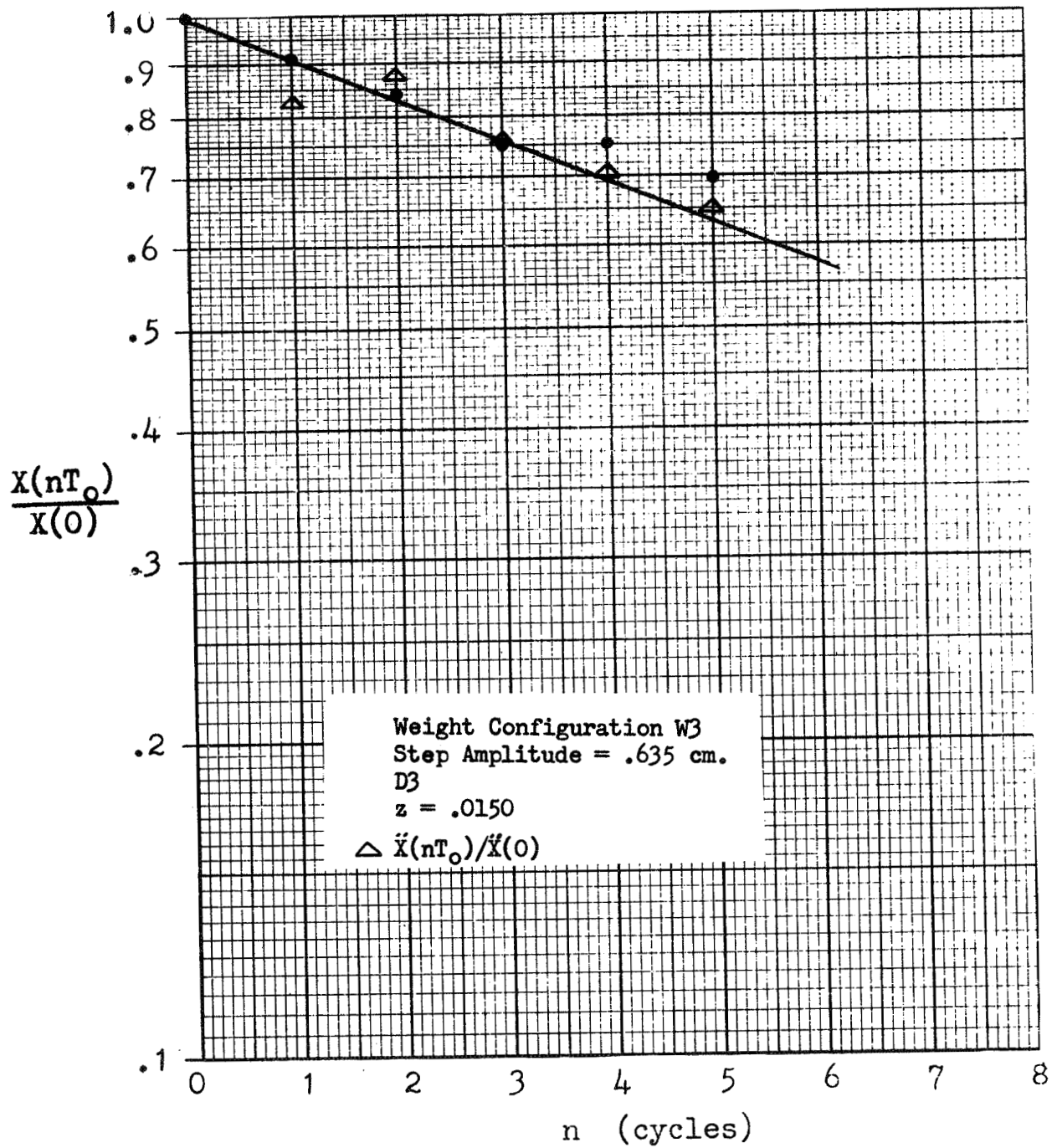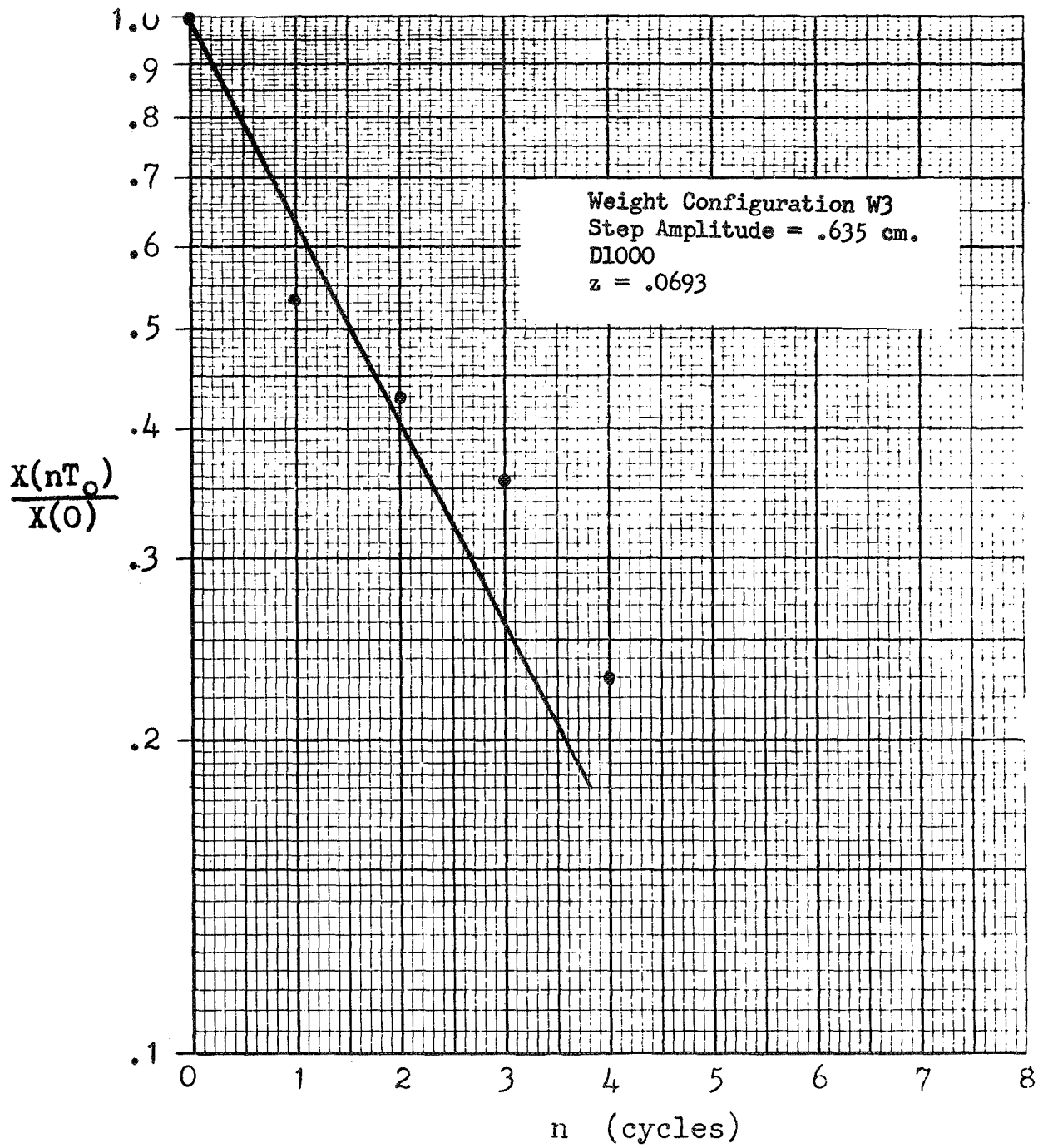
Figure 4.4.2-22, Amplitude Attenuation, D1000

Overshoot

A major difference between the behavior of the magnetic damping system and a classical linear damper appears in the graph of per cent overshoot as a function of damping. The overshoot is a measure of the output rise above the final steady state value for a step function. It is defined by (see figure 4.4.2-23)
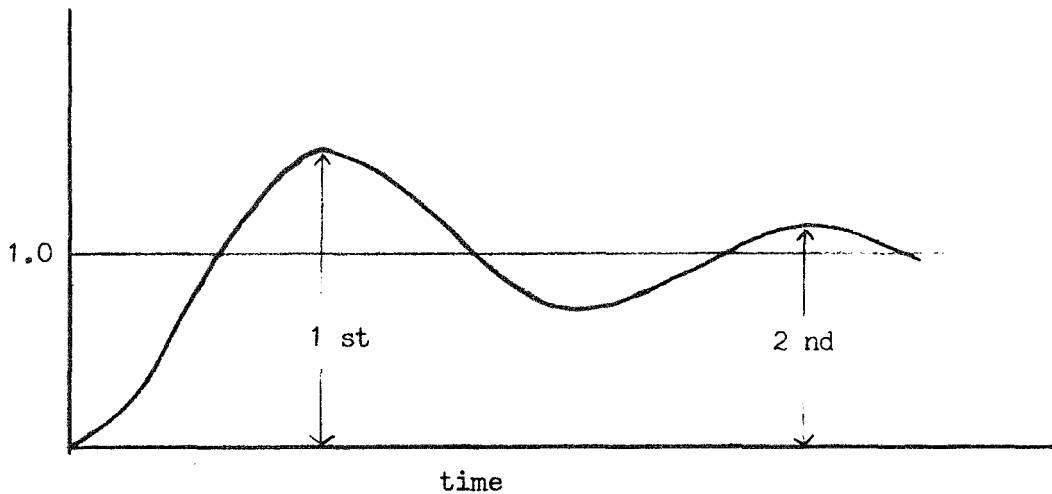
Figure 4.4.2-23 Overshoot

$$\frac{\text{max value reached in first overshoot - steady state value}}{\text{steady state value}} \quad X100$$

Also of interest is the second overshoot, defined by

$$\frac{\text{max value reached in second overshoot - steady state value}}{\text{steady state value}} \quad X100$$

In the classical damper the per cent overshoot decreases with increasing damping, until finally at critical damping, $Z = 1$, both first and second overshoots are zero.

For a simple classical spring-damper combination the percent first overshoot is given by

138
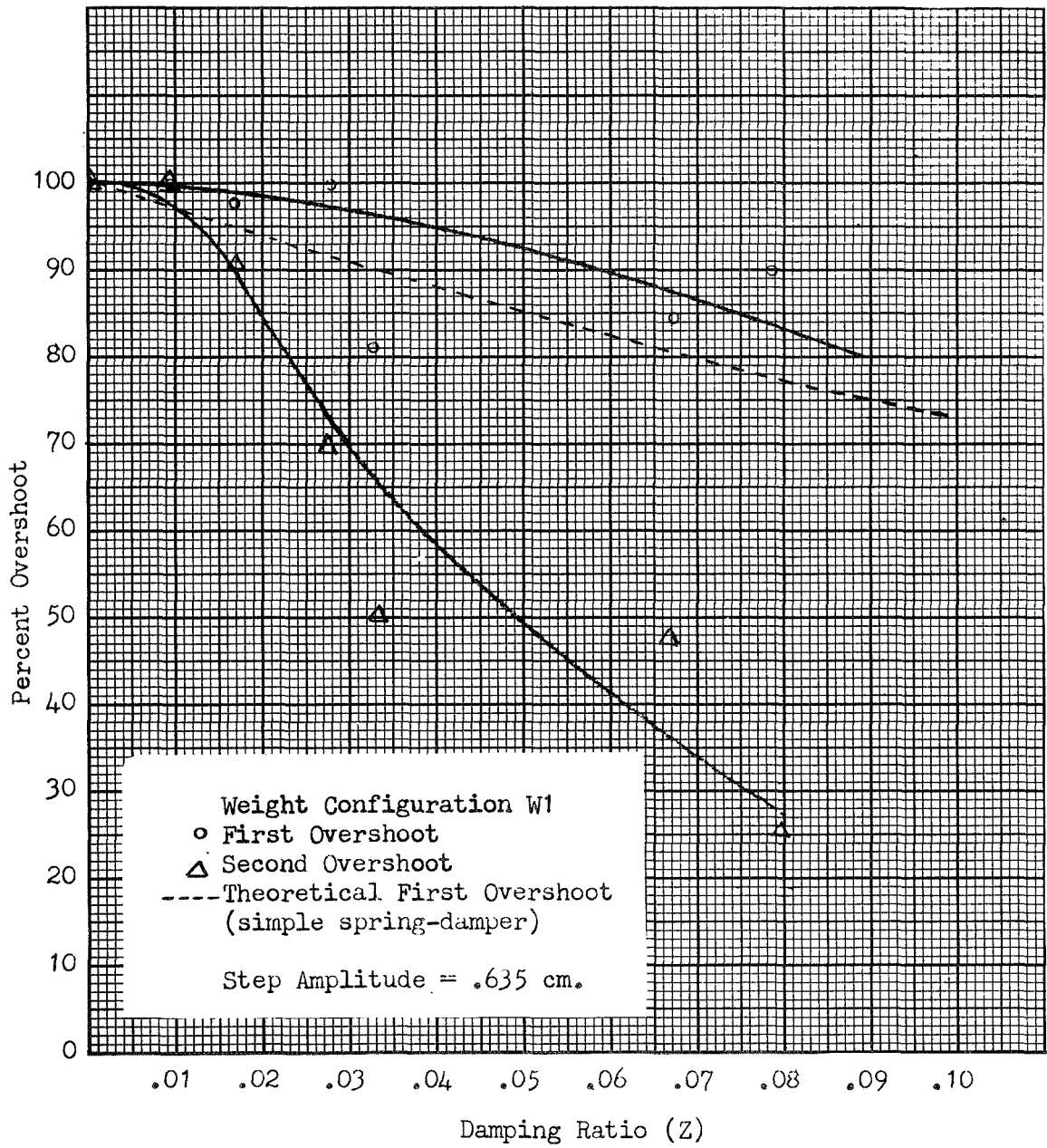
Figure 4.4.2-24, Percent Overshoot versus Damping Ratio
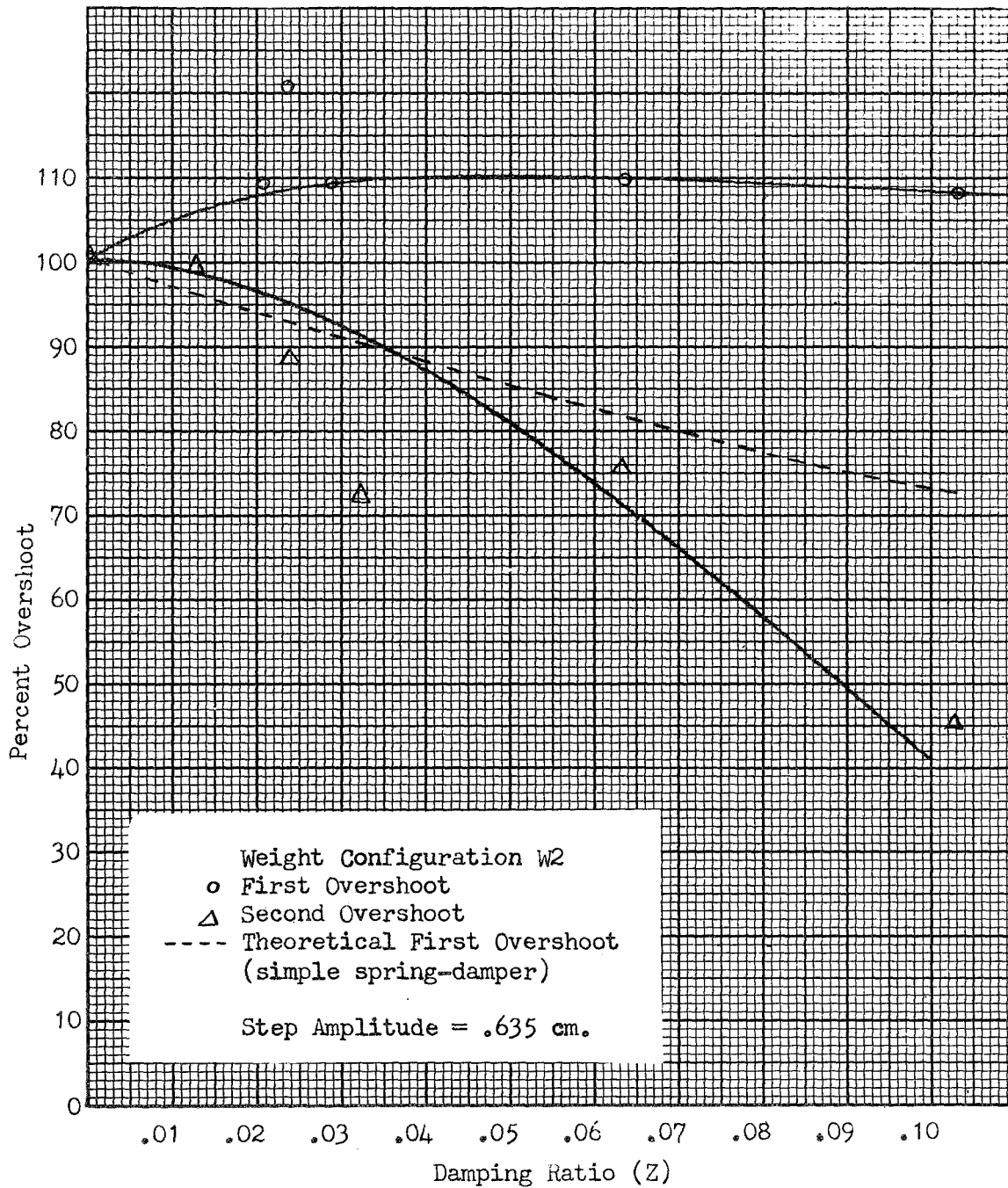
Figure 4.4.2-25, Percent Overshoot versus Damping Ratio
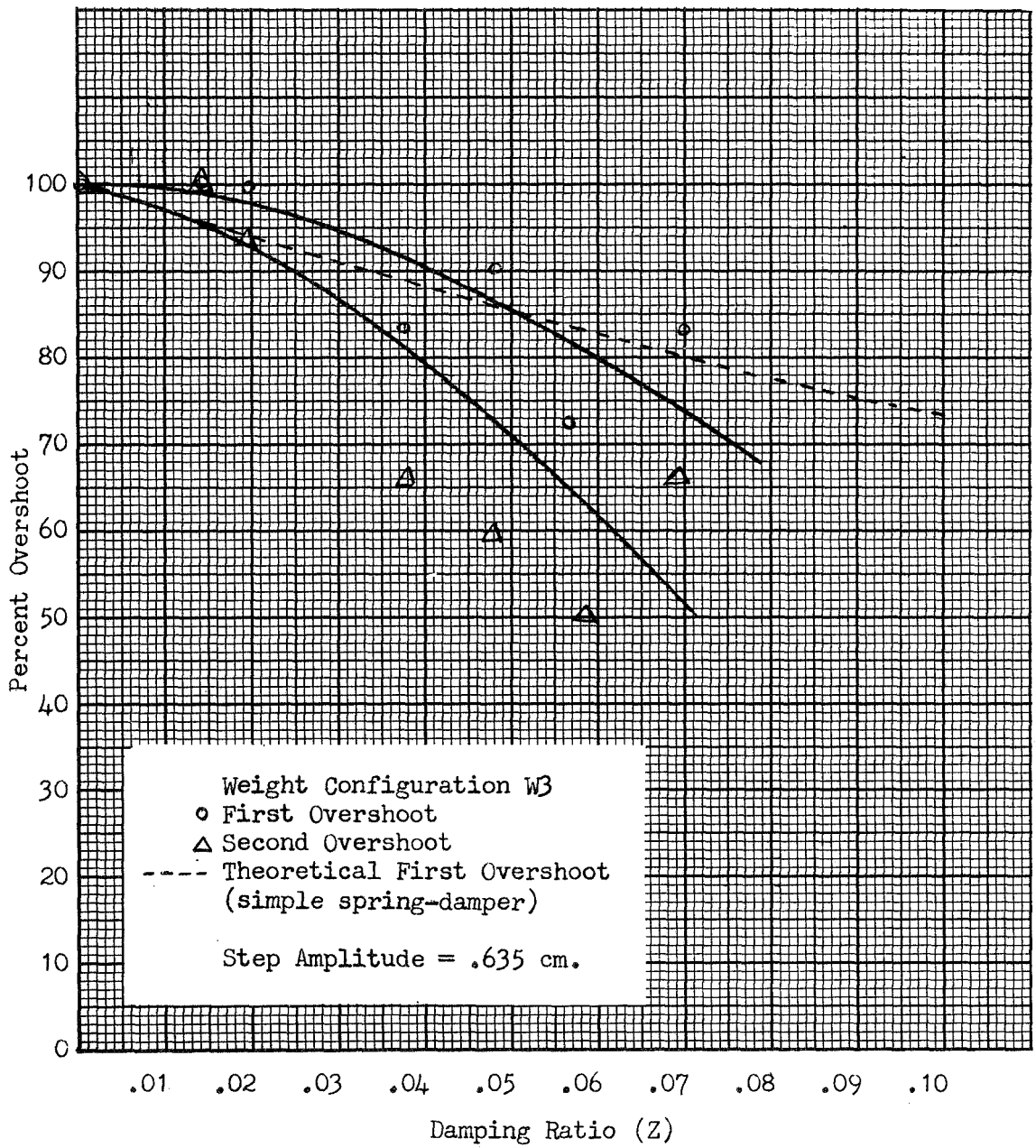
Figure 4.4.2-26, Percent Overshoot versus Damping Ratio

$$\exp\left(\frac{-\pi z}{\sqrt{1 - z^2}}\right)$$

where z is the damping ratio. This expression as well as the experimentally determined values of overshoot are shown in the following figures (Figures 4.4.2-24 to 4.4.2-26).

For the magnetic damper the first overshoot remains high and is relatively independent of the damping ratio for small z. This is probably due to the physical nature of the damper. Before the step is applied the bearing is essentially motionless with the magnet coil current at some steady state value, Io. With the application of a step the velocity sensor applies a sharp impulse to the magnet suspension coils and hence an impulse force to the bearing. This impulse force acts in the direction of the new equilibrium position of the shaker. Immediately after the impulse, the velocity of the bearing is relatively small and the current in the coils returns to the steady state value or slightly lower if the gain of the feedback amplifier is large (high z). The result is that as the bearing returns to the new equilibrium position, the effective spring constant is equal to or less than the steady state value (   ) and there is no force opposing the motion of the bearing, i.e. no damping. The bearing does not experience a true damping force (acting in a direction opposite to the direction of the velocity) until it crosses the new equilibrium position. As the bearing crosses the equilibrium position, it experiences a restoring force, corresponding to Io, plus an additional force proportional to its velocity away from equilibrium. For this reason the forces acting on the bearing immediately after the application of the step (for ¼ cycle) are nearly the same for all values of z. Unlike the classical damped oscillator, the per cent overshoot (analogus to "ringing" in an electrical circuit) of the magnet suspension is relatively independent of the total damping constant when the damping is small However, the second overshoot does depend significantly on the overall damping ratio, as shown in the graphs in Figures 4.4.2-24, 4.4.2-25 and 4.4.2-26.

Configuration comparison

Table 4.4.2-1 is a tabulation of the maximum peak to peak values of the linear and angular displacements and accelerations of the air bearing immediately after the application of a 0.635 centimeter step. The usual sharp acceleration peak occurring simultaneously with the step is not considered in this listing since it is of very short duration having little overall effect on the system. The maximum values of the parameters are listed for each center of gravity and moment of inertia configuration, W1, W2 and W3. Also shown are the damping ratios as obtained by the method previously described. Due to the interaction of the linear and angular position in the rotation sensor, the maximum values of angular position, θ, are not indicative of true angular swing, but are shown in the table for the sake of relative comparisons only, i.e., part of the large angular rotation signal shown in the table is due to an additional signal caused by the large x-displacement.

142

Table 4.4.2-1, Step Responses of Magnetic Suspension
(step amplitude = .035 cm.)

Damping	$\ddot{X}$ x 10^{-5}g			$\ddot{Y}$ x 10^{-6}g		
	W1	W2	W3	W1	W2	W3
D = 0	2.23	2.23	1.90	0.00	0.00	0.00
3	2.01	2.23	1.78	0.00	0.00	0.00
10	1.90	1.56	1.78	0.00	0.00	0.00
30	1.78	2.01	1.67	0.00	0.00	2.23
100	1.56	1.90	1.78	4.45	2.23	4.45
300	2.90sp	2.68sp	1.78sp	4.45	4.45	8.90
1000	3.12sp	2.90sp	3.12sp	4.45	8.90	11.1

$\ddot{\theta}$ arcsec/sec^2

Damping	W1	W2	W3
D = 0	10.9	00.0	21.8
3	00.0	00.0	16.3
10	16.3	5.5	16.3
30	21.8	21.8	21.8
100	21.8	21.8	21.8
300	76.2	65.3	43.6
1000	87.1	87.1	109.0

sp - sharp transient
 peak, remainder
 of response much
 smaller
nc - no change,

Damping	X cm			Y cm		
	W1	W2	W3	W1	W2	W3
D = 0	1.41	1.50	1.37	0.2	0.0	0.2
3	1.27	1.38	1.27	0.6	0.6	0.8
10	1.34	1.38	1.27	0.4	0.8	0.3
30	1.27	1.15	1.22	0.2	0.6	0.5
100	1.27	1.15	1.22	0.7	0.4	0.3
300	1.27	1.27	1.05	0.4	0.9	0.4
1000	1.27	1.38	1.16	0.4	0.6	0.6

Damping	θ arcmin			Z (damping)		
	W1	W2	W3	W1	W2	W3
D = 0	8	3 nc	35	.0000	.0000	.0000
3	13	3 nc	40	.0095	.0126	.0150
10	12	3 nc	33	.0168	.0213	.0186
30	8	7	25	.0275	.0236	.0375
100	18	5	25	.0333	.0315	.0482
300	48	18	30	.0674	.0669	.0583
1000	23	22	offscale	.0784	.1008	.0693

The amount of acceleration and displacement transmitted in the x-direction is significantly less than for the other two cases. At the same time, the amount of rotation and angular acceleration is greatest for this configuration.

This large center of mass offset allowed some of the energy imparted by the step to be translated into a rotational mode. This is to be expected since the offset allows a torque to be applied to the air bearing on the application of an input disturbance in the x-direction. The damping constants are also higher for this case since some of the energy is being transmitted to rotational modes and vibrations in the Y-direction. The damping ratios are actually one dimensional (x-direction) approximations. Any energy transferred to any other mode except the one along the x-direction will have the same effect as an increased damping ratio in the x-direction. Hence, higher values of Z (for the same value of D) represent greater amounts of energy being transferred to other vibrational modes.

Only a very small difference is seen between configurations W1 and W2. (W2 has the same center of gravity, but a larger moment of inertia). The configuration with the higher moment of inertia experiences less rotation and rotational acceleration which is to be expected. One would also expect the X displacements and accelerations to be less for W1. Such a trend can possibly be seen, but the difference in moment of inertia is actually too small to make a significant effect on the system response.

One significant difference in the behavior of W3 was noted for the two highest values of damping D=300 and D=1000. With these values for the damping and with zero input disturbance, it was not possible to reduce the rotational motion to the same low value as was done with the other configurations, W1 and W2. The system became extremely sensitive to random and accidental disturbances.

4.4.3 Ramp responses

Very little response was obtained when the system was subjected to ramp disturbances of 0.635 centimeter amplitude and ramp durations of from 30 to 120 seconds. In all cases the angular rotation was equal to or less than the residual value before the ramp was applied. No significant output was obtained from the accelerometers.

Figure 4.4.3-1 is the response of the system with zero damping to a one-quarter inch ramp of approximately 250 seconds duration. Figure 4.4.3-2 is the response of the system to the same disturbance function, but for a damping ratio of Z=0.324. In both cases, aside from the expected motion in the X-direction, there were no recordable accelerations. However, it was consistently noticed that when the damping electronics were in operation, the introduction of a ramp disturbance tended to reduce the oscillatory angular movement and sometimes the X-motion that the air bearing had before the application of the ramp. No significant output was obtained for the control signal and hence these two curves are not shown.

$\ddot{X}$ $\updownarrow$ 2.2 x 10^{-5} g

$\ddot{\theta}$ $\updownarrow$ 110 sec/sec^2

$\ddot{Y}$ $\updownarrow$ 4.5 x 10^{-5} g

INPUT ($\frac{1}{4}$ in. ramp)

END OF RAMP   .035 cm

$\rightarrow\!\Vert\!\leftarrow$ 5 seconds

BRUSH INSTRUMENTS

ELECTRICAL SIG.

X $\updownarrow$ 16 arcmin

X $\updownarrow$ 0.5 cm
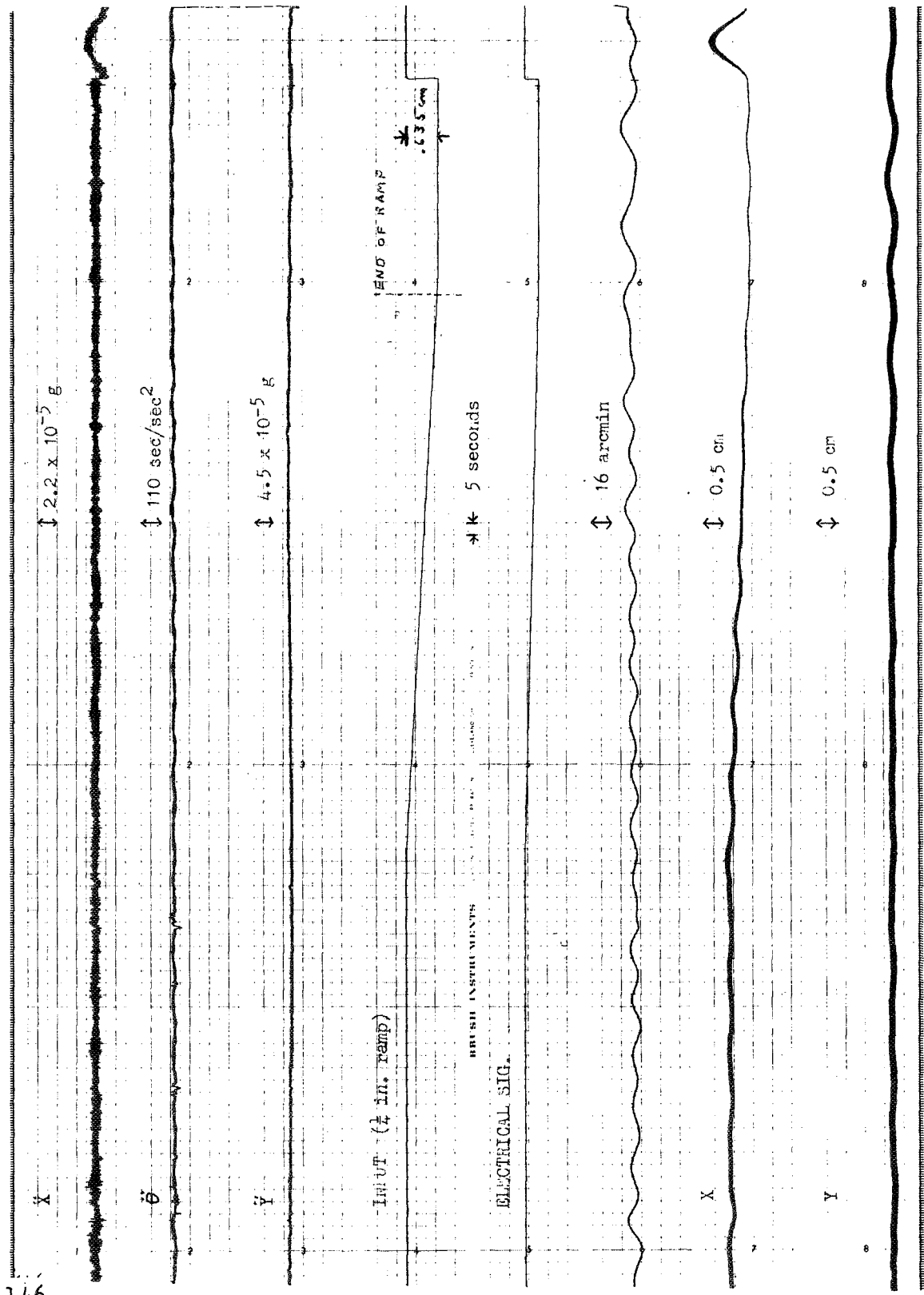
Y $\updownarrow$ 0.5 cm

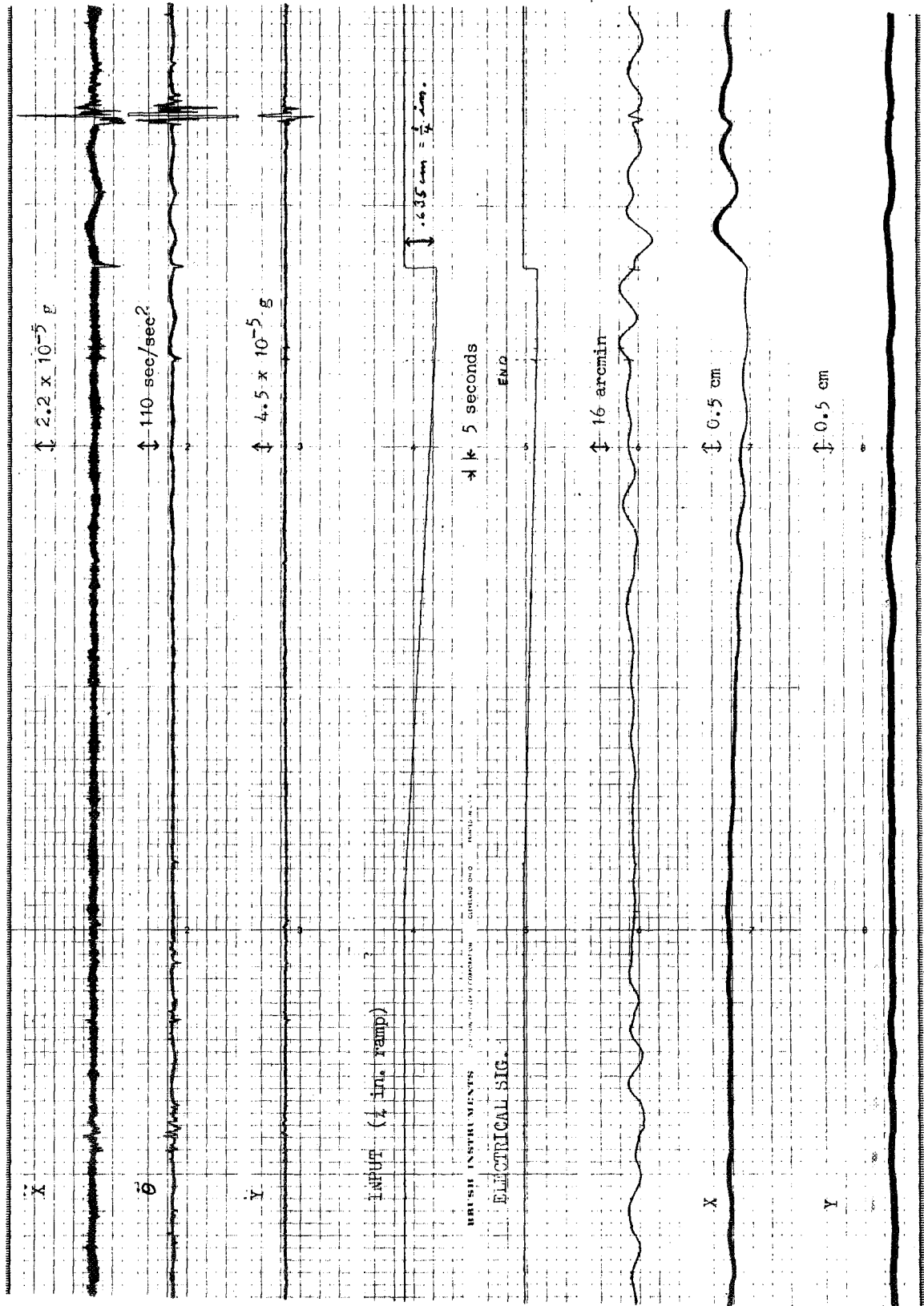Figure 4.4.3-1, Ramp Response, No Damping, #1

Figure 4.4.3-2, Ramp response, D100, W1

4.4.4 Impulse response

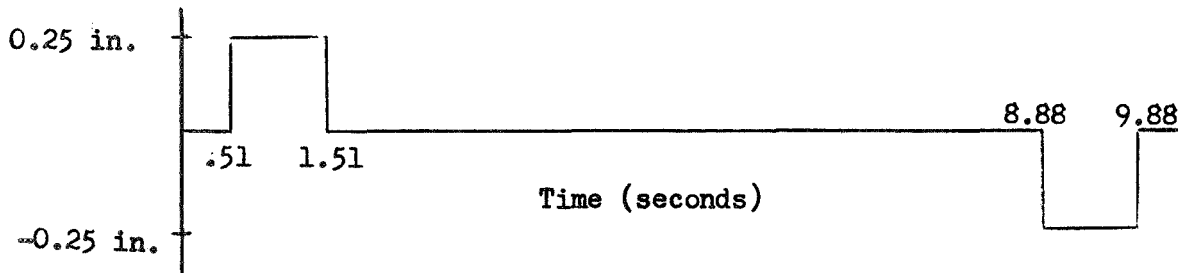The system was subjected to the following impulse disturbance:

Figure 4.4.4-1, Pulse Disturbance

Each pulse had an amplitude of 0.635 centimeter as measured from the equilibrium position.

Figures 4.4.4-2 and 4.4.4-3 are typical responses of the system with damping ratios of 0.0 and 0.324 (D = 0 and D = 100) respectively. The system response in both cases is considerable. For zero damping the amplitude of the bearing acceleration and displacement is sinusoidal and remains high after the last pulse. With damping the response is not sinusoidal and the system experiences a sharp peak of acceleration about one cycle after the last pulse. Then the motion resembles a damped sinusoidal response. An increase in damping from D = 0 to D = 1000 had the effect of reducing the total linear displacement by about fifty percent. However, the increased damping did not reduce the peak acceleration but did reduce the width of the peak. In other words damping reduced the amount of time that the bearing was subject to high accelerations but did not reduce the maximum value of the acceleration.

Table 4.4.4-1 shows the maximum values maximum positive peak to maximum negative peak) of the accelerations $\ddot{X}$, $\ddot{Y}$, and $\ddot{\theta}$ immediately after the end of the second pulse. The sharp peak acceleration at the trailing edge of the last pulse was not considered. The maximum values are shown for each of the three weight configurations.

As expected the maximum value of the X-acceleration is not significantly affected by the configuration. Also no significant difference is seen in the Y-acceleration, but this acceleration was too small in all three cases to make a valid comparison.

From the mechanics of the configuration and from the results of the sine and step disturbances it was expected that configuration W3 would have the largest angular response with W1 and W2 having decreasing responses. However, the measured parameters are almost the same for each configuration. Within the accuracy of the measurements all three configurations behave identically.
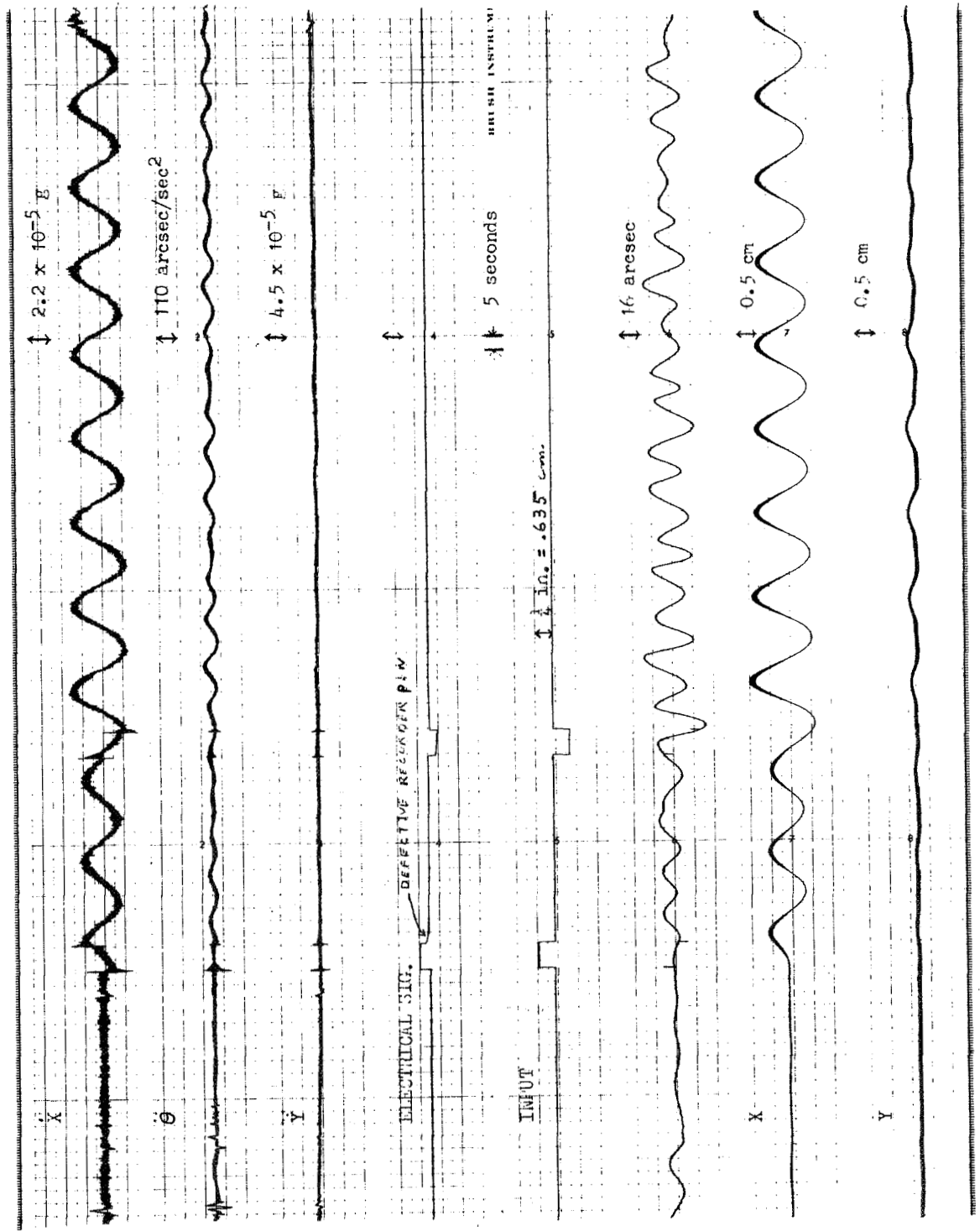
Figure 4.4.4-2, Pulse Response, No Damping, W1
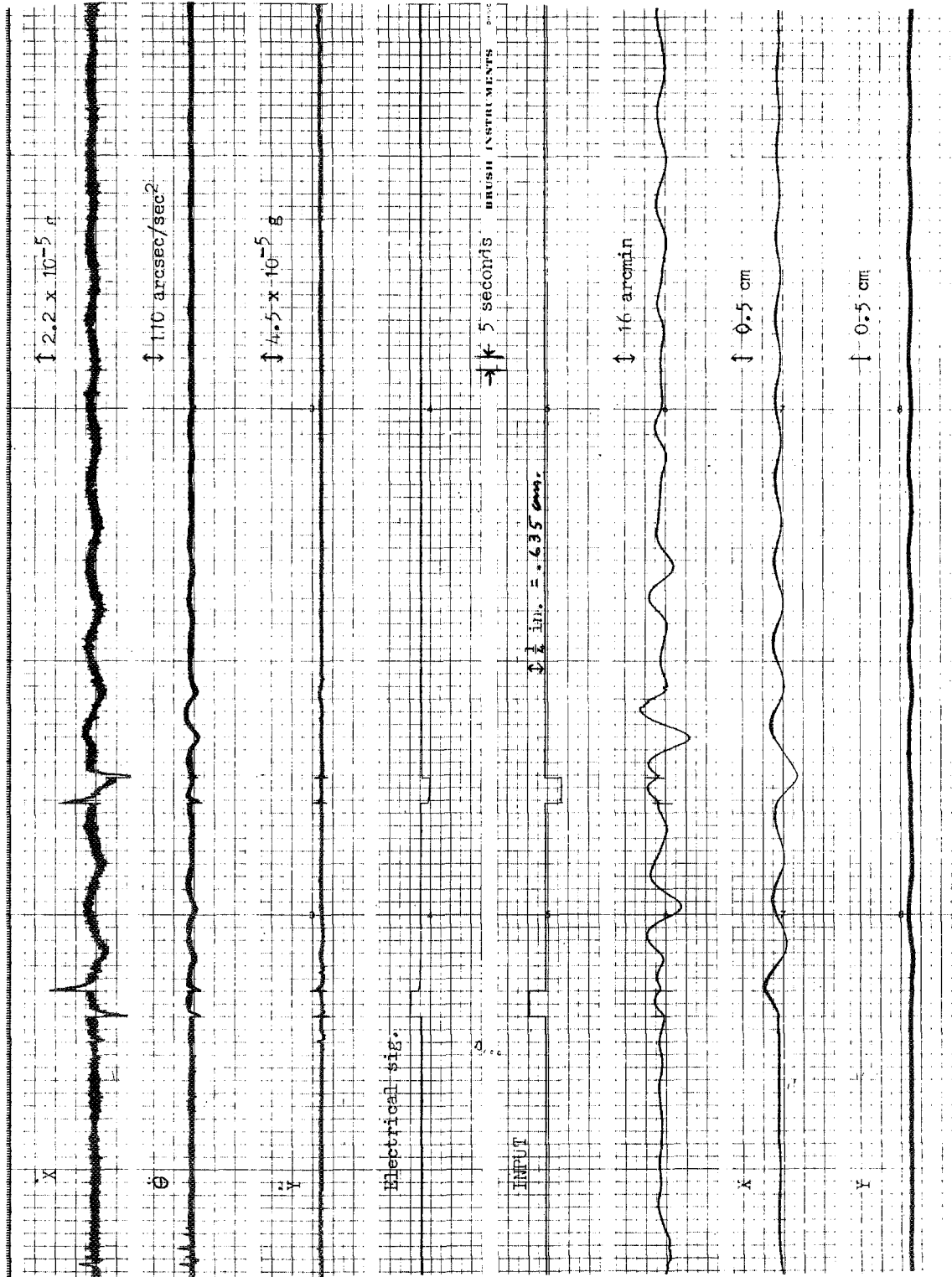
Figure 4.4.4-3, Pulse Response, DISC, '71

Table 4.4.4-1, Impulse Response of Magnetic Suspension
(see text for discription of pulses)

Damping	$\ddot{X} \times 10^{-5} g$			$\ddot{Y} \times 10^{-6} g$		
	W1	W2	W3	W1	W2	W3
D = 0	5.35	5.58	5.13	4.45	8.90	8.90
3	4.68		4.24	4.45		4.45
10	3.90		3.57	2.23		4.45
30	2.68	2.90	2.23	0.00	4.45	6.67
100	1.78	2.01	1.34	2.23	4.45	8.90
300	2.90	2.01	2.45	8.90	13.35	4.45
1000	2.45	2.23	3.35	8.90	13.35	13.35

$\ddot{\theta}$ arcsec/sec^2

Damping	W1	W2	W3
D = 0	65.0	5.0	65.0
3	43.4		32.6
10	32.6		32.6
30	27.1	21.7	32.6
100	59.7	10.9	16.3
300	97.7	86.8	65.0
1000	97.7	157.3	151.9

5.0 CONCLUDING REMARKS

5.1 EXTRANEOUS FORCES

During the course of the investigation, two sources of unwanted torques were found to be operating on the air bearing. They were:

1) Table torques due to a shifting of the table surface from horizontal.

2) Cable torques excerted by the accelerometer cables.

Table torques were eliminated by carefully leveling the table until the air bearing remained motionless when released near the center of the table. All suspension systems were disconnected during this operation. The table was found to remain level for fairly long periods of time compared to a test run. However, slight readjustments were necessary every morning, since over a twenty-four hour period the weight of the air bearing was enough to cause one side of the table to shift slightly if it were not resting exactly in the center of the table. Cable torques were eliminated by hanging the instrumentation cables from the ceiling of the test cell, such that over the normal region of travel of the air bearing during a test run, the cables exerted no measurable torque or detectable influence. The absence of table and cable torques is therefore defined as that condition in which the air bearing experiences no detectable forces or torques when placed anywhere near the center of the table.

Before each disturbance program was applied to the shaker, the air bearing was physically stopped and then carefully released so as to impart as little initial motion as possible. In all cases the initial motion of the air bearing was below the noise levels of the accelerometers. The noise levels were:

$$\ddot{X} = 2 \times 10^{-6} \, g$$

$$\ddot{Y} = 2 \times 10^{-6} \, g$$

$$\ddot{\theta} = 5 \, arcsec/sec^2$$

In the spring suspension systems the angular position sensor indicated peak to peak initial amplitudes of about 10 arcminutes. However, this reading was found to be due to an interaction between the rotation sensor and the X-position sensor. This reading represents an upper limit. It was easier to reduce the initial motion of the magnetic suspension system, due to the ability to introduce damping. The interaction between the two sensors was reduced, giving an upper limit of 1.0 arcminute for the peak to peak rotation.

It is estimated that for the magnetic suspension system with weight configurations W1 and W2, the initial rotation before the application of a disturbance was between 0.5 and 1.0 arcminutes peak to peak. However, for weight configuration W3 (largest moment of inertia and largest center of gravity offset) it became impossible to reduce the initial angular

152

rotation for the two highest values of damping constants, D300 and D1000. In fact when the control amplifiers were switched to D300 and D1000, the angular rotation increased to approximately 35 arcminutes peak to peak (there was still some interaction between sensors so that this is an upper limit). The angular acceleration also increased to approximately 4-8 arcsec/sec^2. It is believed that this increase in the minimum achievable bearing motion was due to an unusual combination of large center of gravity offset, high amplifier gain, and the saturation of the amplifiers over most of a cycle. The damping signals fed to the suspension magnets did not exactly follow the velocity of the air bearing, resulting in an amplification of bearing motion below a certain amplitude. However, larger motions were rapidly damped to this minimum amplitude.

In most cases, except for the .001 springs which represent the limit of the present equipment configuration, the response of the systems to the applied disturbance programs were at least 10 to 20 times the initial motion before the application of the disturbances. Uncertainties in the initial conditions were kept small enough so as to have a negligible effect on the experimentially derived values of transfer function, step response, and damping constant.

5.2 COMPARISON OF SYSTEMS

Any comparison or relative rating of the tested systems at this time will have to be largely subjective, since the evaluation criteria are not well defined.

The .001 springs undoubtedly showed the greatest isolation effectiveness for these particular tests. But how well would this system have reacted to a shaker displacement large enough to make contact with the platform if the platform remained stationary? All three systems displayed approximately the same transfer characteristics to X-acceleration. The hysteresis and magnetic systems showed a characteristic increase in transmissibility of a damped system to the applied sinusoidal driving function. Although the sinusoidal disturbance is not as relevant to space application as the other disturbances applied in this study, it does provide a basis for further design work and testing.

None of the systems tested showed any appreciable response to the applied ramp function, except for a possible dimunition of initial oscillatory motion.

The response of the systems to the square wave impulses was difficult to evaluate because of the effect of the relative phasing between the applied impulse and the position of the bearing at the time of application.

The response of the various systems to the step function was probably the greatest single indication of the relative effectiveness of the various systems to space applications. In this respect the magnetic suspension system is clearly superior to the hysteresis system and both, of course, are superior to the non-damped system for this purpose. Although the magnetic and hysteresis systems exhibited approximately the same overshoot characteristics, the magnetic system damped down much more rapidly. In the simplest definition of isolation system effectiveness, this would be the major factor to be considered for this function.

Several other factors must be considered in giving a final ranking to these systems. More effort during the program went into the study and optimization of the magnetic system than either of the other two systems. One reason for this was the relative ease with which the system could be modified. The effective "spring constant" can be changed in real time by merely adjusting a potentiometer.

There is some question as to whether or not the magnetic system should be termined active or passive. Since suspension or isolation is achieved by means of a magnetic field produced in a solenoid, the system is "active" in the sense that it requires a current source or power supply to activate the solenoid. If the current source should fail so would the suspension. However, unlike most other types of magnetic suspension systems, the present system is "passive" in that it requires no additional components or control loops for stability. The other common forms of magnetic suspension systems consist basically of an object suspended between two electromagnets. This configuration is basically unstable in that an infinitesimal displacement to one side or the other causes an

unbalance in the forces which in turn increases the movement away from equilib-rium, i.e., the system is in unstable equilibrium. A position sensing device and control system are needed to create a stable equilibrium. A control system malfunction therefore results in a catastrophic failure of the entire suspension.

In the present magnetic system the control system is used only to provide damping, and the suspension characteristics are only indirectly affected. In this respect the present magnetic suspension system could be termed passive, in that the suspension is independent of any control loop, and a failure in such a loop would only affect the damping characteristics of the system. (Actually the magnetic suspension coils could be replaced in two dimensions by a set of permanent magnets, in which case the system would draw no power and would be entirely passive.)

Based on results of the tests conducted under the present contract and using response to expected space disturbances as a criteria, the magnetic suspension system is the most effective of the systems, followed by the hysteresis system (if slightly modified), and the spring suspension system.

5.3 RECOMMENDATIONS FOR FUTURE STUDY

There are a number of improvements which can be made on the magnetic suspension system. Of primary importance is a redesign of the suspension magnet coil geometry. Due to the limited time available for detailed design in the present study, little optimization was done in the coil design. By properly adjusting such parameters as coil size, number of turns, current density distribution, and size and shape of the ferromagnetic disc, the magnetic field distribution can be modified to provide different shaped potential wells for the suspended object. For example, it may be desirable to have a spring constant very close to zero near the equilibrium position and extending a small distance away from equilibrium. Such a system would possess very high isolation characteristics as long as the object remained in the "flat region" of the potential well. It is also desirable to choose the optimum coil design in order to minimize power consumption. The present system, in which no attempt was made to reduce power consumption, dissipated approximately seven watts in the d.c. resistance of the suspension coils. This provided an effective spring of 0.05 lbf/in for an air bearing weight of 560 lbf.

A second area for improvement is the combining of the suspension and velocity pickup coils into one coil or into two concentric coils. Some difficulty was encountered in the present study in positioning the center of the pickup coil over the equilibrium position of the permanent magnet. An error in this positioning would tend to decrease the effectiveness of the damping and in some cases cause additional disturbances. This problem would be eliminated if the same coil could be used for both suspension and velocity sensing. However, special electronic modifications will be necessary to prevent direct interaction between the two functions due to induced voltages caused by changing magnetic fields.

The arms on which the ferromagnetic disc and the permanent magnet are mounted should be as long as possible since rotational control will increase in direct proportion to these lengths. In other words, if the arm holding the permanent magnet is made twice as long, a given angular rotation would cause the magnet to move twice the normal distance with respect to the pickup coil. This would result in a greater damping signal. The minimum value of rotational angle that could be obtained in the present investigation can be traced to the length of this arm and the sensitivity of the pickup coil.

A third, and perhaps the most significant, area for improvement is the modification of the frequency response of the control system. In this system one has the unique opportunity of studying the response of a system in which the damping is highly frequency dependent. For instance, a bandpass filter could be inserted in the control loop to provide damping only at the resonant frequency. This would be an advantage over other types of damped systems, since damping while reducing natural frequency motion also has a detrimental effect on the isolation at the higher frequencies. It is also believed that the present system could have been made much more effective by simply adding a low pass filter to remove some of the high frequency responses.

The final recommendation is the development of a two dimensional mathematical model of the system to further define capabilities and optimization

156

possibilities. An analog computer simulation would also be profitable.

APPENDIX A

Hysteresis Damping System

Continuing studies by Chrysler Corporation Space Division into the suspension/isolation requirements of manned space telescopes have indicated the requirements for some type of damping to be associated with the basic telescope suspension system. The required isolation frequency, however, is of the order of 0.01 rad/sec, which prevents the use of rate dependent damper. Therefore, an in-house study was performed to investigate the feasibility of a magnetic hysteresis damper, which is rate-independent, can be constructed to operate under a wide range of conditions and may be easily adjusted to the rate of damping required. Such a system was designed, constructed and tested in the Chrysler laboratory in 1967, and it is this system which was used in the present study.

The damper configuration is shown in Figure A-1. It consists of a vane of magnetic material suspended by a torsion wire with magnet assemblies set facing the surfaces of the disc. The poles of the magnets are arranged in a closely spaced N-S-N-S sequence. This construction provides closely spaced regions of magnetic flux reversal so that a small rotation of the disc will move material in the disc from one magnetic region to an opposing region, and thus provide hysteresis loss in that part of the disc. The torsion wire is positioned vertically and fixed to a metal frame which was bolted to the shaker for the tests.

The magnet cores and the disc are made of Armco Ingot forged steel, 99.9% Fe, Cold Rolled 50%. The magnets are Indox wafers, one inch diameter by 0.25 inches thick. There are two magnets per assembly, separated by thin iron plates and positioned with opposing poles facing. With the exception of the magnets, disc, torsion wire and pole plates, the structure is aluminum. Teflon tips are placed at either end of the guide tubes to help minimize lateral cocking of the disc due to any unbalanced force from the magnet assemblies.

Laboratory tests prior to an during this study indicate the effects of damping other than that due to hysteresis loss in the disc. The primary cause is felt to be due to friction between the torsion wire and the teflon guide tips, with material hysteresis in the torsion wire also a contributing factor.

DISC PREWOUND ON TORSION
WIRE TO KEEP CONNECTING
WIRE STRAIGHT.

CONNECTING WIRE
TO TELESCOPE MASS

TORSION
WIRE

MAGNET ASSEMBLIES

DAMPER FRAME

HOLLOW
GUIDE
TUBES

θ

DAMPING
DISC (IRON)

TEFLON
INSERT

TORSION WIRE

MAXIMUM ROTATION: ±15°

IRON CORE

PERMANENT MAGNETS
(ARROWS SHOW DIRECTION
OF FIELD)

NOTE:

MAGNET ASSEMBLIES ATTACHED TO
DAMPER FRAME. THEY DO NOT
TOUCH DISC.

MAGNET ASSEMBLY

Figure A-1, Hysteresis Damper

APPENDIX B

Magnetic Suspension System

The magnetic suspension systems investigated were based on the fact that a ferromagnetic or paramagnetic material will experience a force in a non-uniform magnetic field. The force will tend to move the material toward the region of highest magnetic field.

Two coils were used to obtain the magnetic field for the suspension system. The two coils were connected in parallel across a power supply and oriented so that the fields added. See figure below.
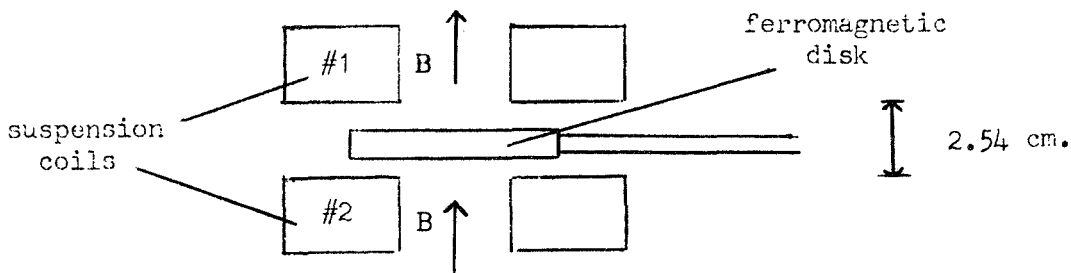

Figure B-1, Suspension Geometry

Each coil consisted of 3,910 turns of #28 AWG enamel covered copper wire. A sketch is shown in Figure B-2. The resistance of each coil was approximately 190 ohms.

The ferromagnetic disk consisted of a soft iron disk 0.7 cm thick and 5 cm in diameter. The disk was attached to the bearing by means of a small aluminum rod. An identical suspension system was placed on each side of the air bearing to prevent rotation. This provided a two axis suspension system.

Power to the two magnetic systems was initially furnished by means of a 0-130 @ 60 Hz volt variac. This provided stabilization or "suspension" with oscillation periods down to 45 seconds. However, at this time no quantitative data was taken due to a delay in the shipment of the accelerometers.

A disadvantage of this a.c. suspension was the relatively high voltage needed due to the inductance of the coils. The variac was replaced by two Kepco Model CK-36 d.c. power supplied (0-50 volts @ 1.5 amps). Each supply provided current to one of the suspension coil systems. Theoretically, the suspension system should function almost the same with a.c. or d.c. coil excitation, if the same average current is flowing in both cases. However, with d.c. excitation, the necessary current for a given "spring constant" can be reduced
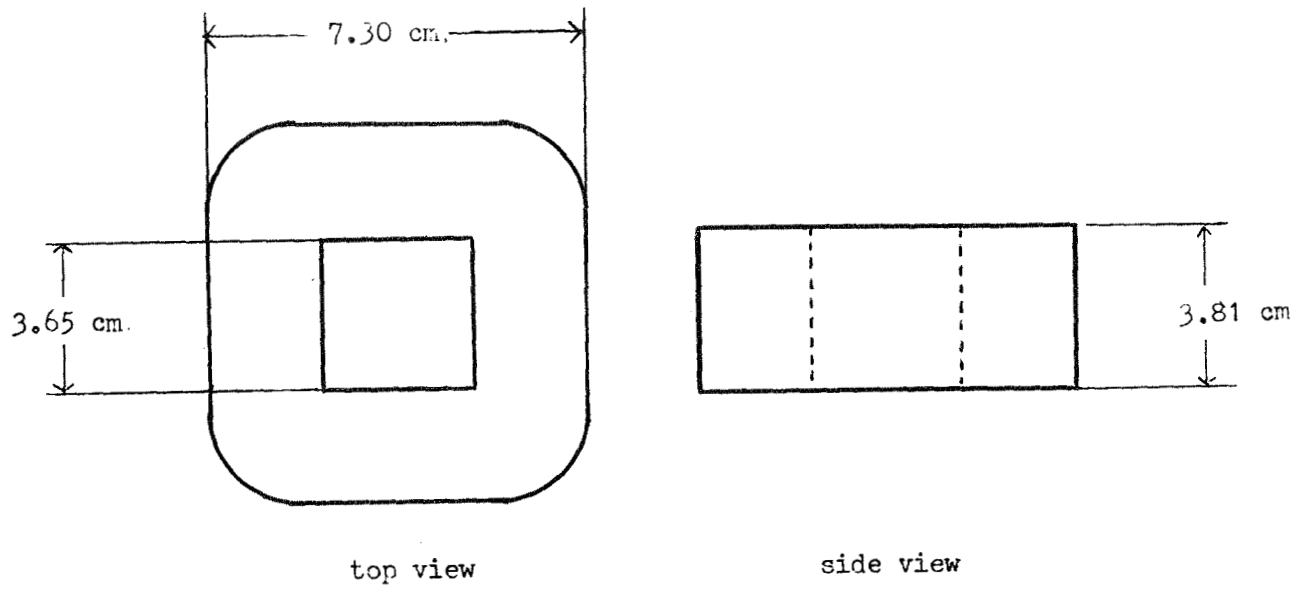
160

top view   side view

Figure B-2, Suspension Coil

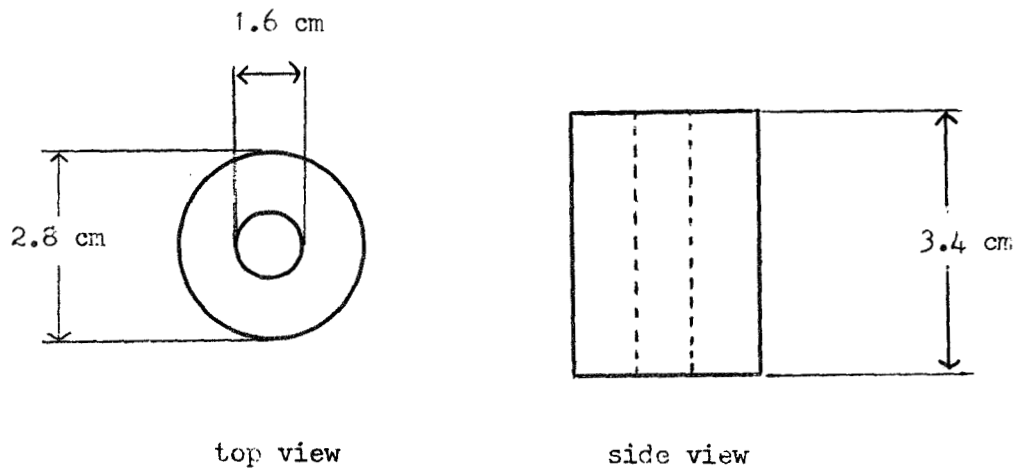top view   side view

Figure B-3, Velocity Pick-up Coil

by magnetizing the ferromagnetic disk or placing a permanent magnet on the disk. The magnetic field of the magnet should lie in the same direction as the field of the suspension coils. In the present case a small ceramic disk magnet 0.65 cm in diameter was placed on top of each ferromagnetic disk.

With the ceramic magnets and an air bearing weight of 565 pounds an effective "spring constant" of approximately 0.05 lbf/in was obtained with a power supply voltage of approximately 18 volts and 0.1 amperes through each coil. (Since the two coils are connected in parallel, the current drain from each supply is 0.2 amperes.)

Damping is introduced into the system by means of a velocity sensor which changes the current through the suspension coils with changes in the velocity of the air bearing.

The velocity is sensed by means of two pickup coils fastened to the shaker frame. The coils were obtained from a commercial solenoid valve. The dimensions are shown in Figure B-3.

A permanent magnet was then mounted on an arm whose other end was fastened to the air bearing. An identical magnet and arm was fastened to the other side of the bearing. See Figure B-4. The magnets and pickup coils were positioned so that with current going through the suspensions coils and the bearing in its equilibrium position, the small magnets in each of the arms were directly beneath the center of the pickup coils. The separation between the coils and the magnet was approximately 0.635 **centimeter.**
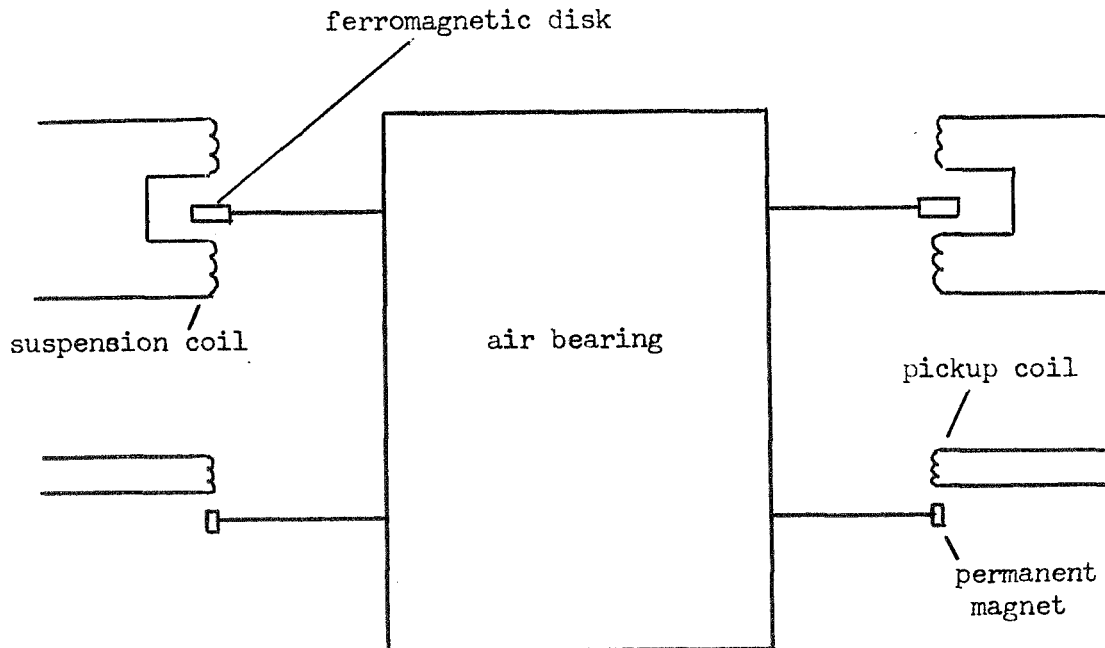

Figure 2, Suspension Geometry

With the magnets and pickup coils positioned as described, the movement of any magnet would induce a voltage in its respective pickup coil. The magnitude of the voltage is proportional to the velocity of the magnet (and hence to the velocity of that arm of the bearing). The induced voltage would have one polarity for velocities away from equilibrium and the opposite polarity for velocities toward equilibrium.

The induced voltage from each pickup coil was amplified and used as a control signal to vary the current in the suspension coils. When the air bearing was motionless, the control signal was zero, and current in the suspension coils was at its steady-state value, Io. The polarity of the control signal was such that when one arm of the air bearing was moving away from its equilibrium position, the control signal would cause the current in the suspension coils to increase in proportion to bearing velocity away from equilibrium. This increase in current creates an additional force (over and above that due to Io) tending to return the bearing to its equilibrium position. When the bearing was moving toward equilibrium the current in the suspension coils was reduced below its steady-state value, Io, creating less restoring force. The net result is a damping effect which removed energy from each oscillation, causing the amplitude to decrease with each cycle.

Figure B-5 is a schematic diagram of the damping electronics. The amount of damping is controlled by changing the gain, K, of the first amplifier or by varying the output potentiometer.
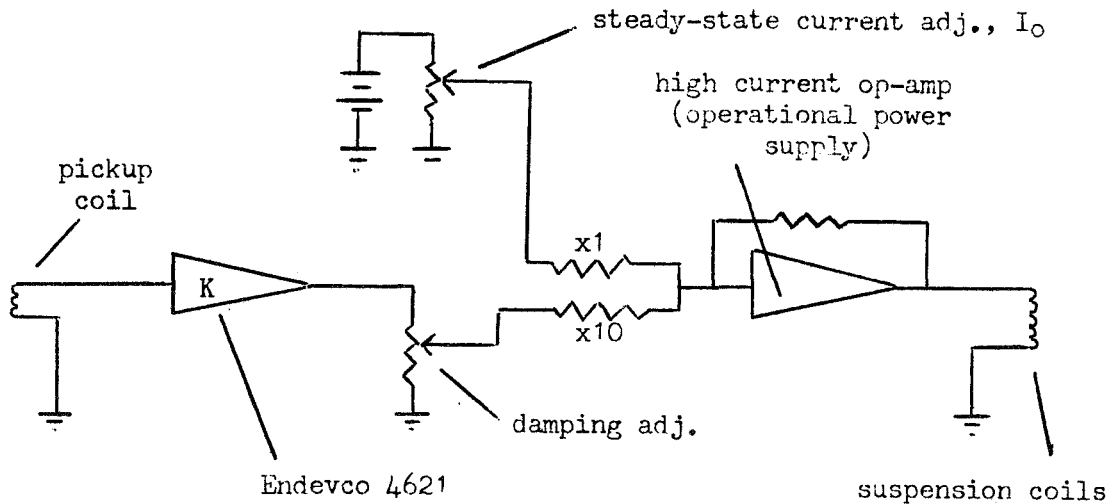

Figure 3, Damping Electronics

For actual data taking the potentiometer was left at its highest setting, and the damping was changed by adjusting the amplifier gain (a provision on the Endevo 4621). This gain setting is denoted on all of the data. For example the data labeled D30 corresponds to an amplifier gain of 30.

Figure B-6 shows some typical output voltages across the suspension coils for various velocities and damping ratios. These curves were obtained by programming the shaker to move with a constant velocity through equilibrium and recording the voltage across the suspension coils.

These curves indicate a large amount of noise introduced by the first stages of amplification and stray field pickup from the sensing coils. These signals were not recorded and the noise not discovered until late in the program. Since the noise is of a high frequency it is doubtful that it had any effect on the air bearing motion. First, the bearing itself would not respond to high frequency noise and secondly, this high frequency voltage appearing across the suspension would not produce a proportionately high noise current in the solenoids, due to the damping effect of the high inductance of the coils, i.e. the power supply and suspension coil inductance would itself act as a low pass filter. However, it is believed that better response could be obtained by inserting a low pass filter in the amplifier circuit with a cut-off frequency of approximately three cycles.

One advantage of this configuration is the capability of inserting frequency compensation networks or filters in the control signal amplifiers to modify the damping for different frequencies. In this way the damping can be increased or decreased at a selected frequency.

In the present case it would have been desirable to reduce the amplitude of the control signal for the higher frequencies, since these high frequency motions of the shaker induced a very large control signal which sometimes saturated the amplifiers.

In many applications a tendency is found to avoid the use of induction type velocity sensors, because of their susceptibility to stray pickups. However, in the present type of suspension system, with the highest frequency of interest being one or two Hz, this stray pickup can be completely eliminated with low pass filters.
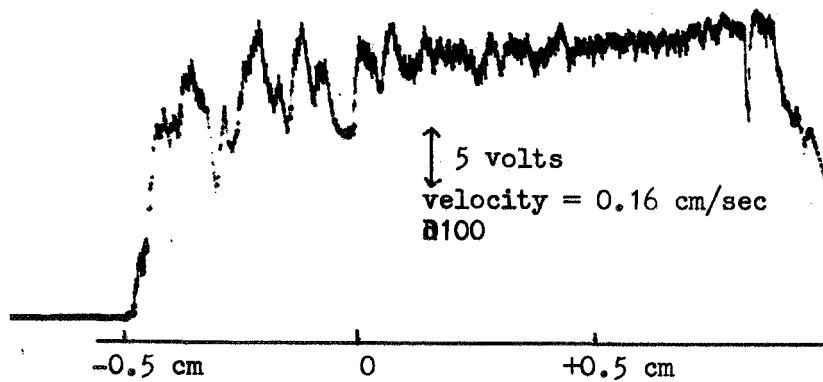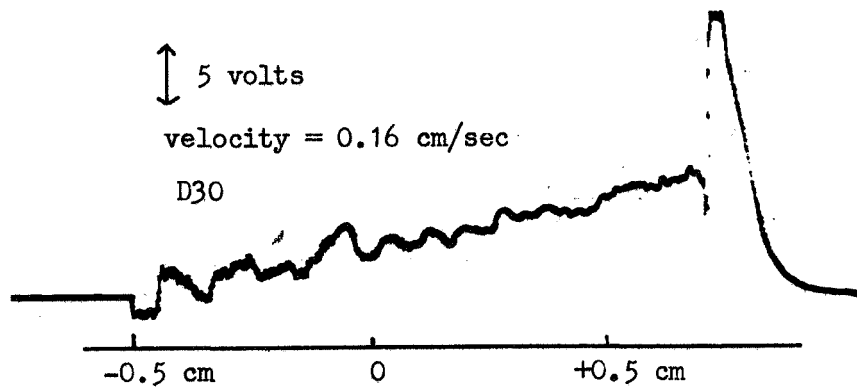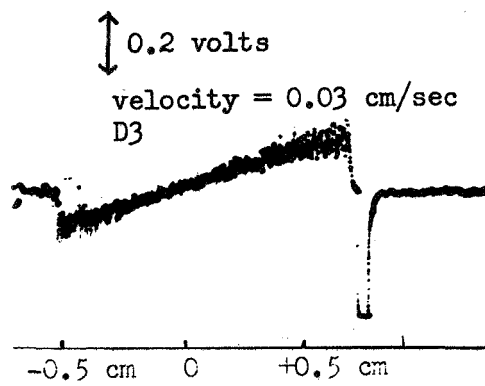
0.2 volts

velocity = 0.03 cm/sec

D3

−0.5 cm   0   +0.5 cm

5 volts

velocity = 0.16 cm/sec

D30

−0.5 cm   0   +0.5 cm

5 volts

velocity = 0.16 cm/sec

D100

−0.5 cm   0   +0.5 cm

Figure B-6, Typical Control Signals

165

APPENDIX C

Table Level Sensor

It was originally intended to investigate the isolation system for various values of table tilt (from horizontal) to simulate simple orbital forces. It was later decided not to pursue this line of investigation but a prototype optical level sensor was partially designed and tested in another laboratory.

The device consisted of an illuminated set of cross hairs placed at the focus of a collimating lens as shown in Figure C-1. The collimated beam passed through a half silvered mirror, M1, and fell on a pool of mercury. The pool of mercury is placed on the table whose tilt is to be measured. The mirror like surface of the mercury was used as an absolute horizontal reference.

A clear glass plate was placed on the dish containing the mercury, and on top of the glass plate was placed a small front silvered mirror, M2. The small mirror reflected half of the light from the collimated beam back toward the half silvered mirror, M1. The other half of the collimated beam struck the surface of the mercury and was also reflected back toward mirror M1. The result was two collimated beams reflected from M1. The two beams are separated by twice the angular difference between the surface of M2 and the surface of the mercury. These beams formed two images of the crosshairs at the focal plane of the objective lens. The seapration of these two images was measured by means of the travelling micrometer eyepiece.

From the separation distance and the focal length of the lens, the angular separation of the two beams can be determined.

$$\text{Tilt angle} = \frac{\text{Distance measured by micrometer}}{2 \times \text{focal length of objective}}$$

For the actual application it was intended to machine a fixture to hold the pool of mercury and mirror M2 so that the surface of M2 was parallel to the table surface. However, the decision not to use this sensor was made before this component could be fabricated.
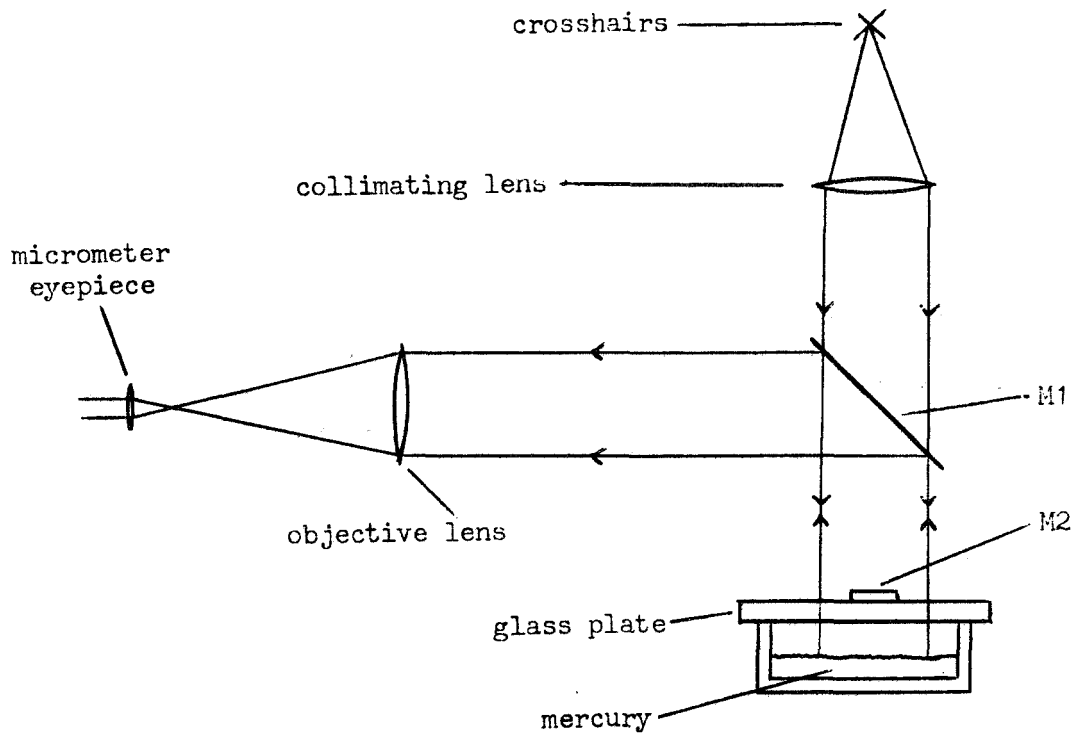
Figure C-1, Table Level Sensor

APPENDIX D

Scaling Studies

A non-dimensional analysis was performed for a linear, undamped suspension system in order to evaluate scaling techniques. The equations of motion for a free motion, two degree of freedom system are:

(1) $M\ddot{X} + K_X X + M\ell\ddot{\theta} = 0$ (2) $M\ell\ddot{X} + J\ddot{\theta} + K_\theta \theta = 0$

Where ℓ = the distance from the center of mass to a reference point on the system - in this case, the geometric center

X = displacement of the reference point in an inertial reference frame

J = moment of inertia of the system about the mass reference point

Define $W_1^2 = \dfrac{K_X}{M}$ and $W_2^2 = \dfrac{K_\theta}{J}$ and further, define a dimensionless distance, $\overline{X} = \dfrac{X}{\ell}$

and a dimensionless time $\overline{t} = w_1 t_1$

Then $\dfrac{d}{d\overline{t}} = \dfrac{1}{w_1}\dfrac{d}{dt}$ and $\dfrac{d}{d\overline{t}^2} = \dfrac{1}{w_1^2}\dfrac{d}{dt^2} = D^2$

Using these substitutions and dividing Eq. 1 by M and Eq. 2 by J, we obtain;

(3) $D^2 \overline{X} + \overline{X} + D^2 \theta = 0$

(4) $\dfrac{M\ell^2}{J} D^2 \overline{X} + D^2 \theta + \left(\dfrac{W_2}{W_1}\right)^2 \theta = 0$

Thus, mechanical systems coupled in translation and rotation by equations (1) and (2), and with the same parametric ratios of $\dfrac{M\ell^2}{J}$ and $\left(\dfrac{W_2}{W_1}\right)^2$ can all be described by the same set of equations (3) and (4).

The ratio $\left(\dfrac{W_2}{W_1}\right)^2$ is equal to $\dfrac{K_\theta/J}{K_X/M} = \dfrac{M K_\theta}{J K_X}$. Normally, $\dfrac{K_\theta}{K_X}$ can be represented

by CR^2, where CR^2, where C is a constant which depends solely upon the spring configuration geometry. Then

$$\left(\dfrac{W_2}{W_1}\right)^2 = \dfrac{M}{J} CR^2 = \dfrac{M\ell^2}{J} \cdot \dfrac{CR^2}{\ell^2} .$$

Since the condition previously cited for the use of the scaling equations is that $\dfrac{M\ell^2}{J}$ and $(W_2/W_1)^2$ be equal for both systems, then the values of $\dfrac{CR^2}{\ell^2}$ must also be equal.

As an example of the application of this analysis, consider the space telescope described by F. R. Morrell in "IEEE Transactions on Aerospace and Electronic Systems", March 1969. The value of K_θ for the telescope in the article is given by:

$$K_\theta = \frac{\delta T}{\delta \theta} = 3KR^2 \cos^2 \psi$$

and

$$K_x = \frac{\delta F}{\delta x} = 6K \cos^2 \psi$$

and

$$\frac{K_\theta}{K_x} = \frac{3KR^2 \cos^2 \psi}{6K \cos^2 \psi} = \frac{R^2}{2} \quad \text{and} \quad C = \tfrac{1}{2}$$

The telescope in the referenced article has the following parameters:

$$M = 674 \text{ slugs} = 9836 \text{ Kg}$$
$$J = 1.58 \times 10^5 \text{ slug - ft}^2 = 2.14 \times 10^5 \text{ Kg-m}^2$$
$$R = (d_3) = 7 \text{ ft.} = 2.14 \text{ m}$$
$$\ell = 0.5 \text{ ft.} = 0.152 \text{ m}$$

$$\frac{M\ell^2}{J} = \frac{9836}{2.14 \times 10^5} (.152)^2 = 106 \times 10^{-5}$$

and

$$\frac{CR^2}{\ell^2} = (\tfrac{1}{2}) \left(\frac{2.14}{.152}\right)^2 = 99.12$$

The system tested in the laboratory has the following parameters:

$$C = \tfrac{1}{2}$$
$$M \approx 250 \text{ Kg}$$
$$J \approx 25 \text{ Kg-m}^2$$
$$R = .46 \text{m}$$

Substituting in the laboratory value for the term CR^2, the value of ℓ necessary for scaling is 3.26 centimeters. This value could be attained, but would require some laboratory modification. With this value for ℓ, the required ratio of M/J to scale with the subject space telescope is approximately 1, as compared with the actual ratio of approximately 10 for the air bearing platform. Since it would be difficult to reduce the mass of the air platform significantly, the moment of inertia would have to be increased. This could be achieved by moving the air bottles to the perimeter of the platform and increasing the amounts of the added weights on the support arm, and possibly extending the length of the arm.